Role of Linoleic Acid-Derived Diol 12,13-DiHOME in Macrophage Inflammation

by

Robert Valencia

A thesis submitted in partial fulfillment of the requirements for the degree of

Master of Science

Department of Pharmacology
University of Alberta

© Robert Valencia, 2023

ABSTRACT

12,13-dihydroxy-9z-octadecenoic acid (12,13-DiHOME) is a linoleic acid-derived cardiac metabolite produced in endotoxin-induced cardiomyopathy, correlating with myocardial dysfunction, inflammation, and mitochondrial damage. The contribution of 12,13-DiHOME to inflammation in the heart is unclear. Thus, we hypothesized that 12,13-DiHOME enhances macrophage inflammation through effects on macrophage polarization and NOD-like receptor protein 3 (NLRP3) inflammasome activation.

To test this hypothesis, we used human monocytic THP1 cells differentiated into macrophage-like cells using phorbol myristate acetate (PMA). For macrophage polarization experiments, THP1 macrophages were treated for 24 hours with vehicle (remain M0 macrophages), 10 ng/mL lipopolysaccharide (LPS) + 20 ng/mL interferon-gamma (polarized into M1 macrophages), or 20 ng/mL interleukin-4 (polarized into M2 macrophages), then quantitative real-time PCR was used to measure mRNA expression of M1/M2 polarization markers. For NLRP3 inflammasome experiments, THP1 macrophages were first primed with 10 ng/mL LPS for 4.5 hours, then the NLRP3 inflammasome was activated by treatment with 10 μM nigericin for 30 minutes. NLRP3 inflammasome activation markers were measured by immunoblotting. Mitochondrial respiratory function was measured using an Oroboros-O2k respirometer. Mitophagy was assessed by live-cell microscopy in THP1 macrophages stably-expressing the pH-dependent fluorescent protein Mito-Keima. Fluorescent dyes in combination with live-cell microscopy were used to measure mitochondrial membrane potential (TMRE), mitochondrial superoxide production (MitoSOX), and cytosolic calcium (Fluo-4).

12,13-DiHOME (0.5 μM) exacerbated mRNA expression of M1-associated inflammatory cytokines in polarized THP1 macrophages. As well, 12,13-DiHOME present during lipopolysaccharide (LPS)-priming of THP1 macrophages exacerbated nigericin-induced NLRP3 inflammasome activation. LPS+12,13-DiHOME-primed macrophages exhibited mitochondrial respiratory dysfunction indicated by complex I uncoupling and reduced spare respiratory capacity. Mitophagy was also impaired in LPS+12,13-DiHOME-primed macrophages. Mitochondrial respiratory dysfunction and mitophagic defects in LPS+12,13-DiHOME-primed macrophages were correlated with an increased sensitivity to nigericin-induced mitochondrial depolarization and mitochondrial reactive oxygen species production. Exacerbated nigericin-induced mitochondrial damage and NLRP3 inflammasome activation in LPS+12,13-DiHOME-primed macrophages were blocked by the mitochondrial calcium uniporter inhibitor, Ru265.

In summary, these data demonstrate a pro-inflammatory role for 12,13-DiHOME through effects on macrophage polarization and NLRP3 inflammasome activation that could be relevant in the pathophysiology of septic cardiomyopathy.

PREFACE

This is an original work by Robert Valencia. At the time of writing, the contents of this thesis have not been previously published elsewhere. In Chapter 3, macrophage polarization data **(Figure 3.3)** were produced and analyzed by Brandon Azer. All other data in Chapter 3 were produced and analyzed by Robert Valencia. Dr. John M. Seubert was the principal investigator responsible for the study design, interpretation of data, and guidance of the project.

“And through the night, behind the wheel
The mileage clicking west
I think upon Mackenzie,
David Thompson and the rest
Who cracked the mountain ramparts
And did show a path for me
To race the roaring Fraser to the sea”

- From “Northwest Passage” by Stan Rogers

ACKNOWLEDGEMENTS

I first and foremost wish to thank my supervisor, Dr. John M. Seubert, for his guidance, support, knowledge, and most importantly, kindness. I will always cherish the experience I had in your laboratory and the memories I made throughout my program, and I will continue to look up to you as a role model for my future endeavors in research.

I also wish to express the utmost appreciation to the rest of my supervisory committee, Dr. Peter Light and Dr. Xavier Clemente-Casares, for their wisdom and helping guide me towards my graduation. Your contributions were critical to my project.

As well, I am grateful to National Sciences and Engineering Research Council of Canada and Alberta Innovates for the funding that made this research possible.

Thank you, Dr. Ahmed M. Darwesh, for training me when I was just starting in the lab, and for treating me with the friendliness you showed towards everyone else in the lab.

Thank you, Wesam Farag, for being a dependable colleague that always showed me kindness and generosity. I am grateful to have had you as a fellow research team member.

Thank you, Deanna Sosnowski. I am also happy to have had someone who shared my sense of humour, and I appreciated having you as a friend I could rely on during my graduate studies.

Thank you Ala' Yousef, for being so kind to me and often sharing treats and desserts to the rest of the lab. Any lab would be happy to have someone like you in their research group.

Thank you Joshua Kranrod, for the fun times and musical jams in the lab. It was always fun to hang out and forget about the stresses of research. I wish you the best in your future career.

Thank you, Liye Fang, for your bright attitude and humour you brought to the lab. I will always miss hearing your weird noises and reactions from across the lab room.

Thank you Andy Huang, for sharing TikToks and making me laugh daily. I promise we will eventually golf together.

Thank you Kamala Lamsal and Xiuju Li, for supporting my research through your hard work as lab technicians and for taking care of us students.

Thank you Brandon Azer, for being a star undergraduate student during your time under my mentorship. I really appreciated your hard work and patience towards me while I was figuring out how to be a better mentor!

To all the trainees I was able to work with during my time in John's lab – Jacob Korodimas, Andy Lee, Amanda Yee, Inga Olu-Jordan, Anran Zhang, Julie Yue, and Katherina Vo – it was a pleasure working with you all, getting to know you as both colleagues and as friends, and I wish you the best of luck in your future endeavors.

Thank you to all my friends, colleagues, and mentors inside and outside the Department of Pharmacology. Everyone's guidance and companionship has contributed to getting me where I am today.

My dearest thanks to my mom and dad, Catherine and Vix Valencia, and to my brother and sister, Nick and Sydney Valencia, for shaping me into who I am today and supporting me throughout my whole life journey. I am forever grateful for the effort and sacrifices you all made to make the accomplishments in my life possible.

Thank you to my second set of parents, Audrey and Stephen Fitzpatrick, and my second sister, Glory Fitzpatrick, for welcoming me into your family and for always taking care of me. There is insurmountable wisdom, experience, and memories you have given me that I will take with me forever. It is great to have another place I can call a home!

And finally, thank you to my beloved wife, Fenya Fitzpatrick. Throughout all the joys, lulls, victories, and hardships of my Master's degree, it was a constant comfort to know you were there with me the whole way, and that whatever my future holds, I'll have my best friend there with me.

I love you all!

TABLE OF CONTENTS

LIST OF TABLES

LIST OF FIGURES

LIST OF ABBREVIATIONS AND SYMBOLS

AA	Arachidonic acid
ADP	Adenosine diphosphate
AIM2	Absent in melanoma 2
ALA	Alpha-linolenic acid
ANOVA	Analysis of variance
ARDS	Adult respiratory distress syndrome
ASC	Apoptosis-associated speck like protein containing a CARD
ATCC	American Type Culture Collection
ATP	Adenosine triphosphate
BAT	Brown adipose tissue
BDI-II	Beck Depression Inventory 2nd Edition
BSA	Bovine serum albumin
c	Cytochrome *c*
Ca^{2+}	Calcium
CARD	Caspase activation and recruitment domain
CaSR	Calcium-sensing receptor
CCK-8	Cell counting kit 8
CCR2	C-C motif chemokine receptor 2
CD	Cluster of differentiation
cDNA	Complementary deoxyribonucleic acid
CFA	Complete Freund's Adjuvant
cGMP	Cyclic GMP

CHO	Chinese hamster ovarian cells
CLP	Cecal ligation and puncture
CLR	C-type lectin receptor
COVID-19	Coronavirus disease 2019
COX	Cyclooxygenase
Ct	Threshold cycle
CYP	Cytochrome P450
DAMP	Damage-associated molecular pattern
ddH_2O	Double-distilled H_2O
DHA	Docosahexaenoic acid
DiHOME	Dihydroxyoctadecenoic acid
DMSO	Dimethylsulfoxide
DNA	Deoxyribonucleic acid
D-PBS	Dulbecco's phosphate-buffered saline
dsDNA	Double-stranded DNA
dUTP	Deoxyuridine triphosphate
ECAR	Extracellular acidification rate
EDP	Epoxydocosapentaenoic acid
EEQ	Epoxyeicosatetraenoic acid
EET	Epoxyeicosatrienoic acid
ELISA	Enzyme-linked immunosorbent assay
EPA	Eicosapentaenoic acid
EpOME	Epoxyoctadecenoic acid

ER	Endoplasmic reticulum
ESCRT	Endosomal sorting complex required for transport-III
$ET / _E$	Maximum mitochondrial electron transport capacity
FADD	Fas-associated death domain
FATP1	Fatty acid transport protein 1
FCCP	Carbonyl cyanide-p-trifluoromethoxyphenylhydrazone
G	Glutamate
GAPDH	Glyceraldehyde 3-phosphate dehydrogenase
GDF3	Growth differentiation factor 3
G_i	G-protein inhibitory
GLA	Gamma-linoleic acid
GMP	Guanosine monophosphate
GSDMD	Gasdermin-D
H/R	Hypoxia-reoxygenation
H^+	Proton
H_2O	Water
HLA-DRA	HLA class II histocompatibility antigen, DR alpha chain
HMGB1	High mobility group box 1
HRP	Horseradish peroxidase
I/R	Ischemia-reperfusion
IDT	Integrated DNA Technologies
IFNγ	Interferon-gamma
IL-10	Interleukin-10

IL-13	Interleukin-13
IL-1β	Interleukin-1 beta
IL-4	Interleukin-4
IL-6	Interleukin-6
IL-8	Interleukin-8
IP_3	Inositol trisphosphate
IP_3R	Inositol trisphosphate receptor
IRF	Interferon regulatory factor
K^+	Potassium
LA	Linoleic acid
LDH	Lactate dehydrogenase
LEAK / $_L$	Leak respiration / State 4 / ATP-independent respiration
LOX	Lipoxygenase
LPS	Lipopolysaccharide
M	Malate
MAM	Mitochondria-associated endoplasmic reticulum membranes
MAVS	Mitochondrial antiviral signalling protein
MCU	Mitochondrial calcium uniporter
mEH	Microsomal epoxide hydrolase
mHCX	Mitochondrial Ca^{2+}/H^+ exchanger
MLKL	Mixed lineage kinase domain-like pseudokinase
MOMP	Mitochondrial outer membrane permeabilization
mPTP	Mitochondrial permeability transition pore

MRC1	Mannose receptor C-type 1
MSR1	Macrophage scavenger receptor 1
MSU	Monosodium urate
mtDNA	Mitochondrial DNA
MTT	3-(4,5-dimethylthiazol-2-yl)-2,5-diphenyltetrazolium bromide
n	Sample size
Na^+	Sodium
NAIP	NLR family of apoptosis inhibitory proteins
NCLX	Na+-Ca2+-Li+ exchanger
NF-κB	Nuclear factor kappa B
N-GSDMD	N-terminal fragment of gasdermin-D
NHE	Na+-H+ exchanger
NLR	NOD-like receptor
NLRP3	NOD-like receptor protein 3
NO	Nitric oxide
NOS	Nitric oxide synthase
Nrf2	Nuclear factor erythroid 2-related factor 2
O_2	Molecular oxygen
OCR	Oxygen consumption rate
OLIGO	Oligomycin
OXPHOS / P	Oxidative phosphorylation respiration / State 3 / ATP-dependent respiration
P	Pyruvate

PAMP	Pathogen-associated molecular pattern
PBMC	Peripheral blood mononuclear cell
PCR	Polymerase chain reaction
PGC-1α	Peroxisome proliferator-activated receptor-gamma coactivator
PI3K	Phosphoinositide 3-kinases
PINK1	PTEN-induced putative kinase protein 1
PKC	Protein kinase C
PMA	Phorbol 12-myristate 13-acetate
pmF	Proton motive force
PPARγ	Peroxisome proliferator-activated receptor gamma
PRR	Pattern recognition receptor
PTM	Post-translational modification
PUFA	Polyunsaturated fatty acid
PYD	Pyrin domain
qPCR	Quantitative real-time polymerase chain reaction
RCR	Respiratory control ratio / State 3 to State 4 ratio / OXPHOS to LEAK ratio
rhIL1RA	Recombinant human IL-1β receptor antagonists
RIPA	Radioimmunoprecipitation assay
RIPK	Receptor-interacting protein kinase
RNA	Ribonucleic acid
ROS	Reactive oxygen species
ROX	Residual oxygen consumption

RyR	Ryanodine receptor
S	Succinate
SCM	Septic cardiomyopathy
SDS-PAGE	Sodium dodecyl sulfate polyacrylamide gel electrophoresis
sec	Second
sEH	Soluble epoxide hydrolase
SEM	Sampling error of the mean
SIRT	Sirtuin
SOFA	Sepsis-related Organ Failure Assessment
SR	Scavenger receptor
SRC	Spare respiratory capacity
STAT	Signal transducers and activators of transcription
SUIT	Substrate-uncoupler-inhibitor titration
t-AUCB	trans-AUCB
TBST	Tris-buffered saline tween
TCA	Tricarboxylic acid cycle
Tfam	Transcription factor A, mitochondrial
TLR	Toll-like receptor
TMB	3,3',5,5'-Tetramethylbenzidine
TMRE	Tetramethylrhodamine ethyl ester, perchlorate
TNFα	Tumor necrosis factor alpha
TRAF	TNF receptor associated factor
TREM	Triggering receptor expressed on myeloid cells 2

TRP	Transient receptor potential
TRPA1	Transient receptor potential ankyrin 1
TRPV1	Transient receptor potential vanilloid 1
TRPV3	Transient receptor potential vanilloid 3
TUNEL	Terminal deoxynucleotidyl transferase dUTP nick end labeling
TXNIP	Thioredoxin-interacting protein
VDAC	Voltage-dependent anion channel

CHAPTER 1. INTRODUCTION

1.1 Septic cardiomyopathy

1.1.1 Overview of septic cardiomyopathy

The American Medical Association defines sepsis as "life-threatening organ dysfunction caused by a dysregulated host response to infection" and septic shock as "a subset of sepsis in which particularly profound circulatory, cellular, and metabolic abnormalities are associated with a greater risk of mortality than with sepsis alone" [1]. Despite these general definitions, there is no gold-standard diagnostic test to identify an individual having sepsis or septic shock, although recommendations for clinical definitions have been put forward**.** For instance, metrics for multi-organ dysfunction such as the Sepsis-related Organ Failure Assessment score (SOFA) defines sepsis patients having a SOFA score ≥ 2 resulting from infection, while septic shock patients have the additional requirement for vasopressors, hyperlactemia, and the absence of hypovolemia [1,2]. In 2017, 120 to 200 sepsis cases per 100 000 were reported in Canada, while sepsis was estimated to cause 20% deaths globally [3]. Although the proportion of deaths that were attributed to sepsis were relatively low in North America (0-8%), some countries in Sub-Saharan Africa experienced upward of 50-65% of all deaths being attributed to sepsis [3]. Sepsis treatment generally targets the infection itself (antibiotics) plus hemodynamic management to sustain adequate organ perfusion [4]. However, the pathophysiology leading to multiple organ failure in sepsis is still incompletely understood, limiting improvement of treatment options.

Septic cardiomyopathy (SCM) is cardiac dysfunction caused by a dysregulated host immune response to systemic pathogen infection [5]. SCM was first described by Parker et al. in 1986, where the majority of septic patients in their cohort presented with decreased ejection fraction <40% that was reversible by 7-10 days in survivors [6]. SCM was

additionally found not to be caused by coronary ischemia [7], and, like sepsis, SCM also does not have a gold-standard diagnostic test [5]. This is reflected by the wide range of estimated prevalence (10-70%) in septic patients, likely due to different physiological definitions for SCM used across different clinical studies [8]. SCM has been independently associated with disease severity and mortality risk in sepsis patients, depending on the definitions used. Studies have historically defined SCM as sepsis patients with left ventricular systolic dysfunction [6], although cardiac functional parameters measuring left ventricular diastolic dysfunction [9] and right ventricular dysfunction [10] along with cardiac injury biomarkers such as serum cardiac troponins [11] and B-type natriuretic peptide [12] have all been associated with disease severity and mortality risk in sepsis patients. For instance, 24-hour improvement of cardiac function was associated with a reduced 90-day mortality risk in sepsis patients (47% down to 17%) [13]. Overall, specifically targeting SCM in sepsis patients has been considered as an additional measure that could improve disease outcomes and survivability in sepsis patients.

1.1.2 Pathophysiology of septic cardiomyopathy

The physiological innate immune response to pathogen infection requires a balance between sufficient pathogen killing and clearance while maintaining tissue integrity, followed by a prompt return to homeostasis [14]. Pathogen infection prompts host recognition of pathogen-associated molecular patterns (PAMPs), which include but are not limited to pathogen cell wall components, pathogen-derived nucleic acids, pathogen-specific proteins, and pore-forming toxins. As part of the innate immune response, PAMPs are recognized by germline-encoded pattern recognition receptors (PRRs) such as toll-like

receptors (TLRs), C-type lectin receptors (CLRs), scavenger receptors (SRs), or NOD-like receptors (NLRs) expressed on resident tissue immune cells such as macrophages, dendritic cells, and mast cells, circulating leukocytes, and even parenchymal cells such as cardiomyocytes [15,16]. Damage-associated molecular patterns (DAMPs), which include extracellular ATP, endogenous proteins such as histones and high mobility group box 1 (HMGB1), mis-localized host nucleic acids, and other signals are associated with tissue injury and can also be recognized by certain PRRs [17]. Recognition of PAMPs and DAMPs by sentinel immune cells and parenchymal cells in tissues invokes events such as pro-inflammatory cytokine production, chemokine production, and vascular permeability aimed to promote the recruitment of leukocytes to the site of infection [18]. Neutrophils are early responders to infection, specialized at pathogen phagocytosis, trapping, and killing [19]. Recruited monocytes from the circulation are also crucial to the early innate immune response, mainly by differentiating into macrophages involved in phagocytosis and pro-inflammatory propagation as well as dendritic cells largely responsible for antigen presentation (along with macrophages) for the long-term adaptive immune response [20]**.** With sufficient pathogen killing and clearance, latter phases of the innate immune response involve inflammatory resolution, tissue maintenance, and a return to homeostasis orchestrated by re-programmed immune cells such as macrophages which produce anti-inflammatory cytokines, pro-resolving mediators, and tissue reparative factors [21].

The complete pathophysiology of SCM is incompletely understood but generally involves a dysregulated response to host infection leading to cardiac dysfunction [5]. How the physiological response to pathogen infection in the heart becomes dysregulated leading to cardiac dysfunction is still unclear, but hyper-inflammation and exacerbated tissue damage

are thought to be the main manifestations of this dysregulated response [22]. Likewise, the downstream effects of a dysregulated innate immune response on the heart are multifaceted and involves multiple molecular targets. Importantly, it should be noted that cardiomyocyte cell death is relatively low in the acute phases of SCM despite reduced myocardial contractile function and increased cardiac injury markers such as serum cardiac troponins being present [23], differing from other inflammatory cardiac injuries such as ischemia-reperfusion injury. Early studies sought to identify molecular factors which could directly mediate cardiodepressive effects. It was found that tumor necrosis factor alpha (TNFα) and interleukin-1β (IL-1β) were necessary factors which reduced contractility *in vitro* in cardiomyocytes incubated with sera from sepsis patients [24]. Similarly, nitric oxide (NO) and cyclic GMP (cGMP) also induced depressive effects on cardiomyocyte contractility and were likely the downstream mechanisms involved in TNFα and IL-1β-induced cardiodepression [25]. Later, cytokines such as interleukin-6 (IL-6), interleukin-8 (IL-8), and interleukin-10 (IL-10) were also found to be circulating factors with similar cardiodepressive effects [26]. Other cytokines like macrophage migration inhibitory factor act as myocardial depressants *in vitro* and in animal models [27], and in sepsis patients macrophage migration inhibitory factor is elevated in plasma relative to healthy controls [28]. DAMPs such as high-HMGB1 induce TLR-mediated reactive oxygen species (ROS) generation leading to calcium (Ca^{2+}) dysregulation to cause downstream contractile depression in cardiomyocytes [29]. Another DAMP, oxidized mitochondrial DNA (mtDNA), is well-known to activate innate immune pathways [30], and circulating mtDNA is also a predictor of mortality in sepsis patients [31]. In general, myocardial depressant factors, mitochondrial dysfunction, oxidative stress, calcium handling perturbations, adrenergic downregulation, and coronary

microvascular changes are all thought to contribute to SCM pathophysiology [5]. However, how these pathological events are interrelated and may cause one another is poorly understood.

1.1.3 Therapeutic targeting of septic cardiomyopathy

Currently, there is no gold-standard treatment which specifically targets improvement of SCM in sepsis [5]. Current treatments are focused on preventing global hypoperfusion by fluid resuscitation, vasopressor support, mechanical ventilation, and positive inotropic agents. However, additional therapies aside from antibiotics which aim to directly target the pathophysiological mechanisms causing SCM are not clinically used. Several therapies have been investigated in preclinical studies or animal models [22]. For instance, agents targeting specific pro-inflammatory cytokines have been pursued both to reduce the hyper-inflammation associated with SCM but also to limit the effects of myocardial-depressive cytokines. Early studies found that anti-TNFα antibody could transiently rescue cardiac function when administered to patients within 24 hours of septic shock [32]. A meta-analysis by Lv et al. suggests that patients with sepsis or septic shock treated with anti-TNFα had improved overall mortality [33]. Therapies targeting IL-1β, another cardiodepressive pro-inflammatory cytokine, using recombinant human IL-1β receptor antagonists (IL1RAs) have shown low effects on improving mortality in early studies, but stratification by initial serum levels of endogenous IL1RA may improve their effect [34]. Similarly, individuals with macrophage activation syndrome, an acute condition associated with excessive expansion of T lymphocytes and hemophagocytic macrophages and presenting with both hepatobiliary dysfunction and disseminated intravascular

coagulation, appeared to benefit more in terms of 28-day mortality in sepsis when given rhIL1RA [35]. Although early studies suggested that nitric oxide synthase (NOS) inhibitors could be used to target the myocardial-depressive and oxidative stress-inducing effects of nitric oxide [36,37], it was found that NOS inhibitors may increase mortality in septic shock patients [38]. Levosimendan, a calcium-sensitizing agent, was proposed as a therapeutic agent which could inhibit ROS production by polymorphonuclear leukocytes and oxidative stress in the hearts of septic shock patients [39] meanwhile improving systemic hemodynamics [40]. However, a subsequent large scale double-blinded randomized controlled trial demonstrated that levosimendan did not improve disease severity or mortality in sepsis patients, meanwhile levosimendan was associated with reduced success of weaning from mechanical ventilation and increased risk of supraventricular tachyarrhythmia [41]. Overall, as SCM is inconsistently defined in the clinic and there is a limited understand of its pathophysiology, successful therapeutic agents directly targeting SCM to improve disease severity and mortality risk in septic patients are scarce. Investigating novel molecular pathways involved in SCM-associated events, such as hyper-inflammation and innate immune cell activation, may uncover novel therapeutic targets.

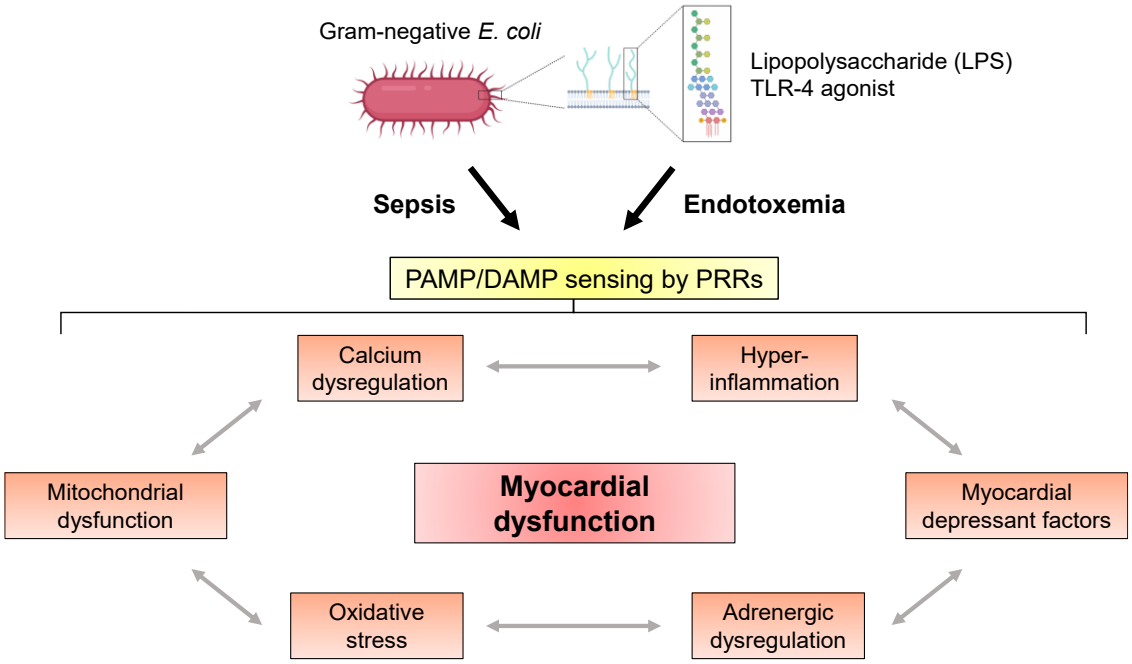

Figure 1.1 *Septic cardiomyopathy and its pathophysiological factors.* Septic cardiomyopathy can be induced experimentally by injection of exogenous whole-bacteria or by endogenous barrier disruption *in vivo* (e.g. cecal ligation and puncture). Septic cardiomyopathy can also be modelled by endotoxin (e.g. *E. coli*-derived cell wall component lipopolysaccharide) injection *in vivo*. Sepsis or endotoxemia leads to sensing of pathogen-associated molecular patterns (PAMPs) and/or damage-associated molecular patterns (DAMPs) by innate immune receptors called pattern recognition receptors (PRRs) such as toll-like receptor 4 (TLR-4). PAMP/DAMP sensing by PRRs mediates multiple interrelated pathophysiological events that ultimately result in myocardial dysfunction. Adapted using [5] and [8].

1.2 Macrophages and septic cardiomyopathy

1.2.1 Overview of cardiac macrophage biology

Macrophages are leukocytes of the innate immune system which are unique in their high degree of plasticity, having essential roles both at homeostasis and throughout all stages of the response to infectious or sterile disease [42]. Macrophages are seeded in tissues during embryonic development by yolk sac and fetal liver-derived progenitor cells, leading to distinct populations of resident tissue macrophages with self-renewal capacity to replenish themselves throughout adulthood. As well, hematopoietic stem cell-derived monocytes are recruited to tissues and become differentiated into macrophages with both overlapping and unique functions to embryonic-derived tissue macrophages. Broadly, macrophages maintain tissue homeostasis through roles in both normal tissue function and host-defense against pathogen infection and tissue injury. These functions include phagocytosis of pathogens and host cells, antigen presentation, immunomodulation of other innate/adaptive immune cells, pro-inflammatory and pro-resolving mediator secretion, extracellular matrix remodeling, protein turnover, iron homeostasis, metabolic restructuring, and many others [43]. Macrophages are found in virtually all tissues at homeostasis, displaying distinct gene expression profiles, cell-surface markers, and functions specific to a given tissue, including liver Kupffer cells, brain microglia, peritoneal macrophages, bone osteoclasts, cardiac macrophages, alveolar macrophages, and others [44]. Despite tissue-specific differences, tissue macrophages retain an overall intrinsic macrophage phenotype. By expressing a variety of cytokine/chemokine receptors as well as PRRs like TLRs, SRs, CLRs, and NLRs, tissue macrophages are capable of sensing changes to the *in situ* tissue microenvironment to appropriately differentiate into phenotypes appropriate to those changes (e.g. sensing of

bacterial PAMPs or tissue injury-derived DAMPs), a term commonly coined as "polarization" [45,46]. As well, changes in the tissue macrophage population can occur through local expansion of resident self-renewing macrophages [47] or through recruitment of circulating monocytes which differentiate into macrophages, the latter of which is important for a sufficient but transient response to infection and tissue injury [48]. The combination of polarization, local expansion, recruitment, and eventually cell death dictates how the tissue macrophage population is shaped according to tissue-specific roles in homeostasis and disease.

The mammalian heart contains embryonic-derived self-renewing macrophages (mainly $CCR2^-$) as well as circulating monocyte-derived macrophages (mainly C-C Motif Chemokine Receptor 2 $(CCR2)^+$) with distinct physiological and pathophysiological roles [49,50]. Macrophages are the dominant cardiac immune cell and consist 7-8% of all non-cardiomyocyte cells in the heart [51], and $CCR2^-$ cardiac macrophages predominate over $CCR2^+$ [52]. On average, 5 cardiac macrophages associate with each cardiomyocyte in the murine heart, and each cardiac macrophage can associate with up to 5 cardiomyocyte [53]. At homeostasis, cardiac macrophages are known to be involved in coronary vasculature development [49], myocardial tissue surveillance [54], and facilitate electrical conduction of cardiomyocytes [55]. During myocardial tissue injury or infection, expansion of monocyte-derived macrophages, which are more pro-inflammatory [56], promote the initial pro-inflammatory propagation through cytokine and chemokine production, enhance the recruitment of other phagocytes such as neutrophils [57], and contribute largely to pathogen and cell debris clearance [56]. Self-renewing tissue resident macrophages eventually dominate during latter phases of infection or tissue injury to promote the return to

homeostasis by anti-inflammatory and tissue reparative programmes. Interestingly, recent studies have shown that resident cardiac macrophages are also responsible for cardiomyocyte mitochondrial homeostasis, where cardiomyocytes extruded damaged mitochondria in "exophers" which are subsequently phagocytosed in a Mertk-dependent manner by resident cardiac macrophages [53]. Cardiomyocytes, which are less-fit for endogenous mitophagy because of dense-packing of mitochondria and constant energetic demand for contraction, off-load clearance of damaged mitochondria to macrophages. This process is upregulated in myocardial tissue injury to prevent the accumulation of inflammogenic material and to preserve cardiomyocyte function [53]. Overall, cardiac macrophages possess important roles at both homeostasis and disease, and how these roles are modulated or dysregulated, such as in the hyper-inflammation state of septic cardiomyopathy, may uncover novel mechanisms for disease pathophysiology.

1.2.2 Macrophage polarization

Macrophage polarization is a broadly defined biological process, but most generally can be described as, by Murray, "how macrophages have been activated at a given point in space and time" [46]. More specifically, macrophage polarization is the process where macrophages sense and respond to specific signals by differentiating into a phenotype appropriate to those signals. These signals include extrinsic factors such as extracellular PAMPs/DAMPs, cytokines, and chemokines, but macrophage polarization signals also include other factors from the tissue microenvironment, such as oxygen and nutrient availability and overall metabolic state (ie. glycolytic or mitochondrial oxidative) [46]. As well, intrinsic factors unique to specific ontological origins such as embryonic or

hematopoietic stem cell-derived macrophage lineages or the specific organ/tissues in which a macrophage resides in can affect how macrophages polarize [58].

Macrophages are popularly characterized to be naïve or non-polarized "M0" macrophages, classically-activated or "M1"-polarized macrophages, or alternatively-activated or "M2"-polarized macrophages [46,59]. M1 macrophages are associated with functions such as pro-inflammatory cytokine production, cytolysis, phagocytosis, and antigen presentation, and are involved in intracellular pathogen immunity [46]. M2 macrophages are associated with functions such as anti-inflammatory cytokine production, tissue maintenance, and wound-healing, and are involved in anti-helminth and fungal immunity. The "M1/M2 paradigm" comes from *in vitro* characterizations of primary macrophages in their response to prototypical signals of a type-1 immune response against intracellular pathogens or a type-2 immune response against helminth infection, where treatment with lipopolysaccharide (LPS) as a bacterial PAMP plus interferon-gamma (IFNγ) as a T_H1 cell-derived cytokine induced M1 macrophage polarization while treatment with interleukin-4 (IL-4) or interleukin-13 (IL-13) as T_H2 cell-derived cytokines to induce M2 macrophage polarization [59]. mRNA transcript levels, cell surface markers, and functional parameters like cytokine secretion, phagocytosis capacity, and nitric oxide production are all used as markers of M1 versus M2-polarized macrophages [46,60]. Eventually, other polarized macrophages subtypes such as M2a, M2b, M2c, and others have been defined with the inclusion of other stimuli such as immune complexes, glucocorticoids, or anti-inflammatory cytokine IL-10 [61]. More recent studies utilizing high content methods such as transcriptomics have accepted that the nature of macrophage polarization, especially *in vivo*, is spectral and multidimensional, where macrophages can present with mixed

phenotypes that do not neatly fit into M1 or M2-polarized subtypes [62]. This is likely due to the complex tissue microenvironment and temporal dynamics *in vivo* (e.g. different phases of infection or injury) which cannot be easily modelled *in vitro* [46]. Nevertheless, "M1/M2" classification of macrophages is still a useful concept due to the well-studied nature of signalling pathways associated with M1 and M2 polarization stimuli. Improvements on the standardization of nomenclature, stimuli, and markers used to define macrophage polarization has also allowed appreciation the functional heterogeneity where macrophages might have both "M1" or M2"-like characteristics [63]. The utility of the M1/M2 paradigm is more realized through *in vitro* experiments with more control over experimental conditions and less confounding extrinsic factors, although *in vivo* studies often report M1 or M2 macrophages in tissues which can still be useful in characterizing a general "hyper-inflammatory" or "inflammation-resolved" tissue state without the nuances of specific macrophage functions and subpopulation phenotyping [64,65]. Overall, although the simplified M1/M2 macrophage paradigm cannot fully describe macrophage polarization and its roles in physiology or pathophysiology *in vivo*, M1/M2-polarized macrophages are still powerful tools to understand and modulate polarization *in vitro.*

1.2.3 Role of macrophages in septic cardiomyopathy

Interestingly, apart from essential roles in pathogen clearance, inflammation, and tissue maintenance in sepsis, certain subpopulations of cardiac macrophages have unique roles in the response to SCM. Extensive cardiac macrophage subpopulation remodeling occurs throughout all phases of SCM, and the majority of this is governed by local tissue expansions of cardiac macrophages rather than recruitment from circulating monocytes [66].

This contrasts with other inflammatory cardiac diseases that prompts extensive recruitment of circulating monocyte-derived macrophages in response to injury like myocardial infarction [54]. Zhang et al. demonstrated that, although the cardiac neutrophil and monocyte population expands while total macrophage numbers slightly decrease early in sepsis (3 days post cecal ligation and puncture (CLP)), latter stages of SCM involve expansion of a subpopulation of cardiac macrophages with TREM2^{hi} expression and self-renewing capacity that was associated with reversibility of myocardial dysfunction in a murine sepsis model (7-28 days post CLP) [23]. Early stages of sepsis (3 days after CLP) also showed specific expansion of resident cardiac macrophage subpopulations more specialized in antigen presentation and inflammation. It should be noted that Zhang et al. reported that cardiomyocyte death was not extensive in early phases of SCM despite reduced myocardial contractile function and increased injury markers, differing from other studies [67]. Nevertheless, this TREM2^{hi} population of cardiac macrophages limited the inflammatory response and promoted cardiomyocyte mitochondrial homeostasis through the clearance of cardiomyocyte-derived exophers containing damaged mitochondria during latter phases of SCM. This clearance of cardiomyocyte-derived exophers was also shown to be important at homeostasis and in response to other cardiac diseases like myocardial infarction [53].

Aside from cardiac macrophages mediating the physiological response to sepsis by promoting tissue homeostasis [23] and direct pathogen clearance [54], most other studies have focused on how cardiac macrophages may exacerbate SCM by contributing to pathological hyper-inflammation in the heart. Macrophages secrete pro-inflammatory cytokines and extracellular DAMPs which promote cardiomyocyte apoptosis and cardiomyocyte-derived inflammation [68]. Importantly, pro-inflammatory cytokines such as

TNFα and IL-1β secreted by cardiac macrophages [56] are also known myocardial depressant factors contributing to reduced contractile function in SCM [24]. Interestingly, heme oxygenase-1 induction within infiltrating cardiac macrophages prevents lysosomal degradation of inducible nitric oxide synthase, leading to downstream nitric oxide-derived oxidative stress and cardiomyocyte dysfunction and apoptosis in endotoxemic mice [69]. This macrophage-specific heme oxygenase-1 effect appears to be independent of changes in infiltrating macrophage numbers and pro-inflammatory cytokine production. Additionally, M2 macrophages have been shown to secrete exosomes containing miR-24-3p, directly downregulating expression of TNF superfamily member 10 and thus reducing downstream cardiomyocyte apoptosis, myocardial and systemic inflammation, and myocardial dysfunction in SCM [70]. In general, an increased ratio of M1 to M2 macrophages in the myocardium is associated with worse injury through exacerbated inflammation, but M2-associated functions may also contribute to worsened SCM prognosis through immunosuppression or "immune paralysis" which increases the risk for secondary infections [71]. Wang et al. demonstrated that treatment with recombinant growth differentiation factor 3 (GDF3) of the transforming growth factor beta superfamily in SCM mice promoted M2 and inhibited M1 macrophage polarization, prevented M1-like macrophage infiltration in the heart, reduced myocardial and systemic inflammation, improved myocardial function, and reduced mortality in mice [72]. However, the researchers also found that GDF3 in plasma was correlated with increased disease severity and worse 28-day mortality in human sepsis patients. Although this is more likely due to intrinsic differences between human patients and mouse models for sepsis [73], this study may also highlight the importance of M1-associated macrophage functions in the physiological response to SCM.

Overall, the importance of cardiac macrophages in SCM beyond their canonical roles in innate immune defence is complex and poorly understood. How specific cardiac macrophage subpopulations contribute to or prevent SCM pathophysiology is only recently becoming recognized. Much knowledge about mammalian cardiac macrophage subsets obtained using mouse models still requires adequate translation to humans, as not all murine cardiac macrophage subsets have a human equivalent [74]. Furthermore, the factors governing how cardiac macrophages polarize during SCM and the mechanistic consequences of M1- or M2-associated macrophage functions in SCM are still unclear. Understanding cardiac macrophages such as by investigating pathways related to polarization and macrophage-derived inflammation will enlighten the events which transform a physiological response to pathogen infection in the heart into a dysregulated pathophysiological process leading to SCM.

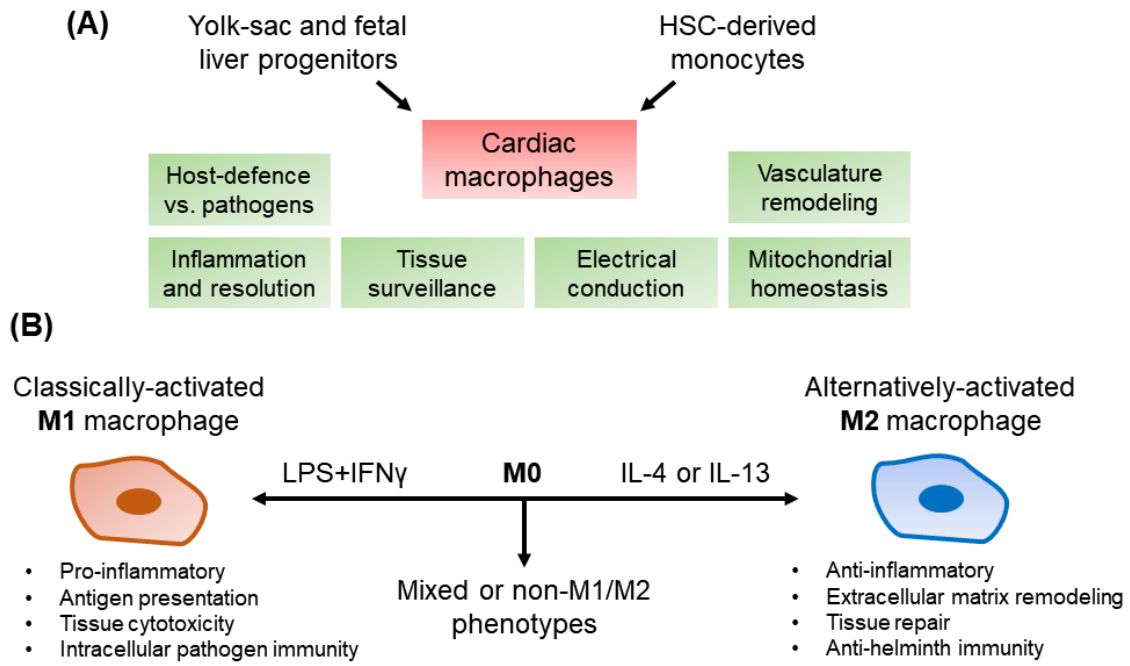

Figure 1.2. *Cardiac macrophage roles and M1/M2 paradigm of macrophage polarization.* **(A)** The heart contains tissue macrophages seeded from embryonic progenitors (yolk-sac or fetal liver-derived) which replenish themselves through self-renewal, as well as hematopoietic stem cell (HSC)-derived monocytes which are recruited to the heart and differentiate into macrophages throughout adulthood. Roles of cardiac macrophages as discussed in Section 1.2 are shown. **(B)** The M1/M2 macrophage polarization paradigm involves treatment of naïve non-polarized M0 macrophages with lipopolysaccharide (LPS) plus interferon-gamma (IFNγ) induce M1 macrophage polarization or IL-4 or IL-13 to induce M2 macrophage polarization. M1 and M2 macrophages have unique phenotypes, generally associated with type 1 and type 2 immunity, respectively. Mixed or non-M1/M2 macrophage polarization phenotypes are also possible by more complex polarization stimuli treatments. Adapted using [50,75,76].

1.3 NLRP3 inflammasome

1.3.1 Overview of inflammasomes

Inflammasomes are cytosolic multi-protein complexes which act as both PRRs and scaffolds for the activation of inflammatory effector caspases [77]. Specifically, inflammasomes mediate autoproteolytic activation of caspase-1, a protease which processes interleukin-1 family inflammatory cytokines IL-1β [78] and interleukin-18 (IL-18) [79]. Caspase-1 also mediates cleavage of cytosolic gasdermin-D (GSDMD) which forms plasma membrane pores consisting of oligomerized N-terminal fragment of GSDMD (N-GSDMD), leading to a necrotic cell death called pyroptosis and thus further promoting the release of pro-inflammatory DAMPs [80]. Importantly, N-GSDMD pores mediate the secretion of mature IL-1β, which can occur in viable cells that are "hyperactived" but not yet pyroptotic through electrostatically-favorable selective secretion of IL-1β through N-GSDMD pores, but fully pyroptotic cells can additionally release IL-1β through the non-selective process of cytolysis [81-83]. Inflammasome subtypes differ according to the individual protein subunits forming the inflammasome complex, but inflammasomes are similar in their roles for inflammatory propagation and pyroptotic cell death through a caspase-1 activation cascade [77]. Generally, inflammasomes consist of oligomerized, prion-like complexes of (i) a scaffolding protein which either directly acts as a PRR or integrates signals from other PRRs, (ii) apoptosis-associated speck like protein containing a CARD (ASC), an adapter protein that interacts with the scaffolding protein through N-terminal pyrin domain (PYD)-PYD interactions, and (iii) pro-caspase-1, the zymogen form of caspase-1 which interacts with ASC through caspase activation and recruitment domain (CARD)-CARD interactions [84]. Oligomerization of pro-caspase-1 during inflammasome complex assembly mediates its

autoproteolytic activation, leading to the formation of active caspase-1 p10/p20 dimers [85]. Notably, it is the associated scaffolding protein which dictates the PAMP/DAMP recognition specificity for a particular inflammasome subtype [77].

While many PRRs are more selective in the PAMPs and DAMPs which activate them, the NOD-like receptor protein 3 (NLRP3) inflammasome is unique in that it integrates detection of a much wider variety of PAMPs and DAMPs than other inflammasomes [77,86]. Other inflammasomes only have a few PAMPs or DAMPs which trigger activation. The absent in melanoma 2 (AIM2) inflammasome, containing the PRR and scaffolding protein AIM2, directly binds cytosolic double-stranded DNA (dsDNA) fragments which might be derived from intracellular pathogens or mis-localized mtDNA [87,88]. The NLRC4 inflammasome, which relies on NLRC4 as a scaffolding protein and the NLR family of apoptosis inhibitory proteins (NAIPs) as PRRs, is activated in response to only a few bacterial proteins such as bacterial type III secretion system needle protein [89]. The NLRP3 inflammasome, which utilizes the NLRP3 scaffolding protein, does not appear to depend on a few specific ligands for its activation, but rather multiple PRR- and non-PRR-dependent mechanisms for sensing PAMPs, DAMPs, and general "cell stress" can activate the NLRP3 inflammasome [86].

1.3.2 Mechanisms for priming and activation of the NLRP3 inflammasome

Activation of the NLRP3 inflammasome is generally a two-phase process: an initial "priming" phase followed by an "activation" phase. The NLRP3 inflammasome is primed by signals which converge at *de novo* expression of inflammasome-related proteins NLRP3 and the pro-forms of IL-1β and IL-18, commonly through activation of the transcription

factor nuclear factor kappa B (NF-κB) [90]. In addition, necessary post-translational modifications such as de-ubiquitination of NLRP3 [91] and ubiquitination and phosphorylation of ASC [92,93] occur during the priming phase. Localization of individual NLRP3 inflammasome components to the outer mitochondrial membrane may also occur during the priming phase through interactions with externalized mitochondrial cardiolipin in an mtROS-dependent manner [94]. NLRP3 inflammasome priming can be initiated by TLR agonists such as the gram-negative bacterial cell wall component LPS (a TLR-4 agonist) [90], TNF receptor agonists [95], and IL-1 receptor agonists [86]. Inflammasome priming could be interpreted as a concurrent process during an acute but transient innate immune response, whereby PRRs recognize PAMPs and/or DAMPs to respond to infection or tissue injury with later resolution and a return to homeostasis. Importantly, priming alone generally does not lead to formation of active NLRP3 inflammasome complexes and caspase-1 activation, although some exceptions such as alternative NLRP3 inflammasome activation pathways in human monocytes by treatment with LPS-alone are known [96].

The NLRP3 inflammasome activation phase is less understood, despite the identification of a wide variety of seemingly non-related PAMPs and DAMPs which can trigger formation of active NLRP3 inflammasome complexes and subsequent caspase-1 activation [86]. However, these activation signals could be considered to converge on induction of severe and/or irreversible “cellular stress” which occurs during extreme cellular perturbation during infection and tissue injury. As such, inflammasome activation signals trigger events like plasma membrane permeabilization, extensive intracellular ion dysregulation, and multiple organellar disruption [86,97]. In these cases, a “point of no return” may be crossed whereby increased inflammatory propagation and termination of the

injured cell might be necessary, mediated through NLRP3 inflammasome activation and pyroptotic cell death. This broad nature of NLRP3 inflammasome activation is likely what allows its involvement in most diseases with an inflammatory component, including almost all cardiovascular diseases [98]. Despite this broad notion of "cellular stress", NLRP3 inflammasome activation signals still have overlapping mechanisms. In particular, potassium (K^+) efflux is a potent activation signal, and although downstream consequences of K^+ efflux are still not fully understood, K^+ efflux likely induces necessary conformational changes to NLRP3 which mediate its oligomerization [99] as well as mitochondrial damage [100] and Ca^{2+} mobilization [101]. Bacterial toxins such as the K^+/H^+ ionophore nigericin and extracellular ATP-mediated $P2X_7$ and TWIK2 channel activation have been used as potent K^+ efflux inducers to activate the NLRP3 inflammasome [102,103]. Other activation stimuli such as particulate matter like monosodium urate (MSU) crystals or silica which cause lysosomal rupture also drive NLRP3 inflammasome activation through K^+ efflux-dependent mechanisms [103]. Importantly, K^+ efflux, mitochondrial damage, mitophagy, calcium mobilization, and other events have been shown to have crucial involvement in the triggering or regulation of NLRP3 inflammasome activation, but how these events interrelate with one another still requires further research.

1.3.2.1 Mitochondrial damage

Generally, damaged mitochondria act as platforms for NLRP3 inflammasome activation through a variety of interconnected pathways. The most well-recognized mitochondrial damage-derived signals which promote NLRP3 inflammasome activation are mtROS generation and mtDNA release into the cytosol, which are both associated as

consequences of mitochondrial damage-associated events such as mitochondrial depolarization, respiratory uncoupling or inhibition, oxidative stress, and mitochondrial permeability pore transition (mPTP) opening [104]. Other mitochondria-derived signals have also been recognized to contribute to NLRP3 inflammasome activation; however, the essentiality of certain mitochondrial damage-derived signals is contested.

mtROS generation derived from pharmacological inhibition of mitochondrial respiratory complexes I, II, or III can act as a trigger for NLRP3 inflammasome activation in primed macrophages [100]. mtROS also oxidizes thioredoxin to release thioredoxin-interacting protein (TXNIP), leading to stabilization and binding of TXNIP to NLRP3 to promote NLRP3 inflammasome assembly and activation [105]. Events downstream of NLRP3 inflammasome activation such as lysosomal membrane permeabilization and IL-1β secretion are also exacerbated by mtROS production [106]. Conversely, several canonical activation stimuli such as nigericin and extracellular ATP can still activate the NLRP3 inflammasome despite mtROS scavenging [103]. These data suggest that mtROS may not be necessary for NLRP3 inflammasome activation, but mtROS could be involved in potentiating the initial triggering of NLRP3 inflammasome activation as well as its downstream effects. Aside from being an NLRP3 inflammasome activator, mtROS generation is induced by priming stimuli such as those which activate TLRs [107] and may be necessary for NLRP3 inflammasome priming in macrophages [108]. Interestingly, mtROS is also involved in the *de novo* generation of oxidized mtDNA. mtDNA from damaged mitochondria is released into the cytosol and directly binds to NLRP3 to mediate inflammasome activation, while non-oxidized mtDNA in the cytosol is involved in AIM2 inflammasome activation [109-111]. Cardiolipin, which is found on the inner mitochondrial

membrane in healthy mitochondria but becomes externalized in damaged mitochondria [112], binds directly to NLRP3 to promote its scaffolding to the outer mitochondrial membrane and to promote NLRP3 inflammasome complex assembly during the activation phase [113]. The mitochondrial antiviral signalling protein (MAVS) on the mitochondrial outer membrane can also integrate viral RNA detection into NLRP3 inflammasome activation by directly interacting with NLRP3 [114]. Intriguingly, while many studies have appreciated the role of mitochondrial damage in contributing to NLRP3 inflammasome activation, other studies have also demonstrated that mitochondrial damage can occur downstream of caspase-1 activation by NLRP3 or AIM2 inflammasomes, leading to amplification of mitochondrial swelling, depolarization, mtROS production, and fragmentation [115]. Parkin, a key mitophagy protein, is also directly cleaved by caspase-1 to inhibit mitophagy [115]**.** Likewise, N-GSDMD pores can also form on mitochondrial membranes, leading to mitochondrial permeabilization and the release of factors which further promote inflammation and cell death [116]. Thus, the distinction between mitochondrial damage associated with the initial triggering of NLRP3 inflammasome activation versus mitochondrial damage downstream of NLRP3 inflammasome activation should be carefully considered.

Although mitochondrial damage is considered to promote (if not essential for) NLRP3 inflammasome activation, a recent study by Billingham et al. highlights an important role for the functional mitochondrial respiratory chain in potentiating NLRP3 inflammasome activation [117]. Independent of mtROS generation or changes in mitochondrial membrane potential, the mitochondrial respiratory chain complexes I, II, III, and V all contribute to the activation of the NLRP3 inflammasome by generating phosphocreatine, a high-energy

phosphate donor that can rapidly regenerate ATP. NLRP3 oligomerization during activation is ATPase-dependent, and although a shift to glycolytic generation of ATP occurs during the LPS-induced priming phase in macrophages, phosphocreatine-dependent ATP generation is still required for sufficient ATP supply to NLRP3 during the activation phase. As well, Ichinohe et al. demonstrated that, in contexts of RNA virus infection, NLRP3, mitofusin-2, and MAVS form a complex on the outer mitochondrial membrane that is dependent upon preserved mitochondrial membrane potential, where depolarization of mitochondria blunted NLRP3 inflammasome activation in response to RNA virus sensing [118]. Overall, multiple mitochondrial damage-associated signals are known to trigger or promote NLRP3 inflammasome activation, but this does not necessarily nullify the roles of functional mitochondria during the activation phase. In addition, how mitochondrial damage-derived signals are modulated (or perhaps "fine-tuned") in different pathophysiological contexts to affect NLRP3 inflammasome activation requires further elucidation.

1.3.2.2 Mitophagy and NLRP3 inflammasome activation

Macro-autophagy is the degradation of intracellular cargoes like whole organelles or individual proteins through their capture within autophagosomes followed by their degradation by fusion with lysosomes [119]. Specifically, macro-autophagy is the process of: (i) isolation membrane elongation in the cytosol, (ii) the recruitment of intracellular cargo to the expanding isolation membrane, (iii) the maturation of the isolation membrane into an enclosed autophagosome containing the intracellular cargo, (iv) the fusion of lysosomes with autophagosomes to form autolysosomes, and (v) the degradation of intracellular cargo to recycle macromolecules [119]. Macro-autophagy can occur as a non-selective process,

which is more important in contexts of nutrient starvation [120], meanwhile targeting of specific intracellular cargoes like whole-organelles toward autophagy can occur through multiple pathways. Mitochondria can be degraded through both non-selective bulk macro-autophagy and targeted forms of autophagy, collectively known as mitophagy. PTEN-induced putative kinase protein 1 (PINK1) can accumulate on the surface of damaged or dysfunctional mitochondria undergoing inner membrane depolarization, promoting the recruitment of an E3 ubiquitin ligase called Parkin [121]. Parkin ubiquitinates mitochondrial outer membrane proteins which are recruited to ubiquitin receptors like p62 directly associated with lipidated LC3 on the developing autophagosome, thus recruiting mitochondria marked by PINK1/Parkin toward autophagic degradation [122]. Other routes of selectively targeting mitochondria to autophagy include Parkin-independent ubiquitination of mitochondrial outer membrane proteins and ubiquitin-receptor mediated recruitment to autophagosomes, the direct binding of mitochondrial outer membrane proteins with autophagosomal proteins, or the binding of mitochondrial membrane lipids like externalized cardiolipin to autophagosomal proteins [112].

Importantly, mitophagy inhibits NLRP3 inflammasome activation through multiple mechanisms [123]. First, damaged mitochondria can be degraded by autophagy to recycle macromolecules used for *de no* mitochondrial biogenesis that maintains the healthy pool of mitochondria. Second, encapsulation of mitochondria within autophagosomes physically sequesters them from NLRP3 inflammasome components that directly bind externalized cardiolipin or mitochondrial outer membrane proteins which promote inflammasome assembly and prevents NLRP3 inflammasomes from being spatially oriented to receive oxidized mtDNA that promotes its activation [110,111,123]. Third, individual NLRP3

inflammasome components and downstream cytokines targeted by caspase-1 can be degraded through autophagic pathways to repress the NLRP3 inflammasome pathway [123,124]. Although mitophagy is well-understood to inhibit NLRP3 inflammasome activation, how mitophagy is modulated to exert control over the degree of NLRP3 inflammasome activation, and how this process becomes dysfunctional, remains a significant challenge. The complexity of mitophagy's role in NLRP3 inflammasome activation can be highlighted by a recent study by Dagvadorj et al. [125]. As known in previous studies [123], the researchers reported that externalized mitochondrial cardiolipin associates with lipidated LC3b to promote recruitment of damaged mitochondria and co-localized NLRP3 inflammasomes to autophagosomes, hampering NLRP3 inflammasome activation [125]. Interestingly, they also found that the pro-form of the interleukin-1 family cytokine IL-1α can compete with lipidated LC3 for binding mitochondrial cardiolipin, blocking the selective recruitment of damaged mitochondria to autophagosomes and thus enhancing NLRP3 inflammasome activation. Overall, the factors governing the balance between mitochondrial damage and mitophagy in a "controlled" NLRP3 inflammasome response versus a dysregulated response requires further study.

1.3.2.2 Calcium mobilization

In general, the NLRP3 inflammasome could be interpreted to sense intracellular ion perturbations as part of NLRP3 inflammasome activation [126]. Aside from K^+ efflux, numerous studies have also demonstrated calcium mobilization-dependent mechanisms downstream of canonical NLRP3 inflammasome activation stimuli, including extracellular ATP, nigericin, and lysosomal destabilizing particulates, as well as less-characterized stimuli

such as complement membrane attack complexes [127,128]. Seemingly, calcium mobilization depends on extracellular as well as intracellular stores of calcium such as the endoplasmic reticulum [127], mitochondria [129], and lysosomes [130]. Conversely, some literature suggest that cytosolic calcium increases associated with NLRP3 inflammasome activation stimuli are a secondary consequence of NLRP3 inflammasome activation downstream of caspase-1 activities [131]. These researchers suggest that previous studies which used calcium-scavenging agents or calcium channel antagonists to report that increased cytosolic calcium *via* mobilization of extracellular or intracellular calcium stores promotes NLRP3 inflammasome activation may have been confounded by off-target calcium-independent effects. However, this study did not account calcium mobilizations (e.g. between organelles or within cytosolic microdomains) that are not visible by measuring bulk cytosolic calcium levels. Recently, it has been shown that several canonical inflammasome activation stimuli including extracellular ATP, nigericin, MSU crystals, and alum all induce mitochondrial calcium overload mediated by mitochondrial calcium uptake by the mitochondrial calcium uniporter (MCU) [129,132]. MCU is the main mitochondrial calcium uptake channel [133]. Xian et al. demonstrated that MCU-dependent mitochondrial calcium overload leads to downstream mPTP opening at the inner mitochondrial membrane and VDAC oligomerization at the outer membrane, allowing the escape of oxidized mtDNA into the cytosol for binding NLRP3 to promote inflammasome activation [132]. Mitochondrial calcium overload could also be dissociated from changes in bulk cytosolic calcium levels in this study. Additionally, mitochondria-associated endoplasmic reticulum membranes (MAMs) are known to be important in NLRP3 inflammasome activation, but the specific mechanisms mediated by MAMs are still unclear [134]. MAMs serve as critical

junctions for direct calcium transport between endoplasmic reticulum (ER) and mitochondria through the increased localization of inositol trisphosphate receptor (IP_3R) on endoplasmic reticulum, increased voltage-dependent anion channel (VDAC) and MCU on mitochondrial membranes, and co-localization of other calcium transport and anchoring proteins. NLRP3 inflammasomes also co-localize with MAMs during the activation phase [100]. Hence, MAMs likely mediate MCU-dependent mitochondrial calcium overload and serve as hotspots for mitochondrial DAMPs like mtROS and mtDNA which promote NLPR3 inflammasome activation, but how MAMs are modulated by extrinsic factors to affect NLRP3 inflammasome activation is still unclear [134]. Overall, the role of calcium mobilization in NLRP3 inflammasome activation has been well-demonstrated, although the complex nature of calcium transport between different interdependent cellular calcium stores still suggests much is to be understood about how calcium is regulated – or dysregulated – during NLRP3 inflammasome activation.

1.3.3 Role of NLRP3 inflammasome in septic cardiomyopathy

NLRP3 inflammasome activation is a crucial pathway for generating inflammation related to the physiological innate immune response to pathogen infection [135]. NLRP3 inflammasome activation also mediates specific anti-infective mechanisms, such as the trapping of pathogens in pore-induced intracellular traps within pyroptotic macrophages to promote pathogen clearance by phagocytes [136]. Although these physiological innate immune functions of the NLRP3 inflammasome are assumed, the NLRP3 inflammasome is mostly considered in the literature to contribute to the hyper-inflammatory and tissue-damaging state leading to sepsis-associated organ dysfunction [135]. Furthermore, specific

roles for the NLRP3 inflammasome in the septic heart are also only becoming recently appreciated.

Global knockout of NLRP3 in mice protects against SCM-associated cardiomyocyte dysfunction and cardiac hyper-inflammation directly caused by IL-1β [137]. As well, pharmacological inhibition of the NLRP3 inflammasome can block myocardial dysfunction in SCM mouse models [138]. However, despite overall NLRP3 inflammasome activation markers in cardiac tissues following SCM [137], the specific contribution of individual cardiac cell types to NLRP3 inflammasome activation in the septic heart is an ongoing subject of research. As macrophages are the dominant cell cardiac immune cell type [51], they are the assumed source of the majority of NLRP3 inflammasome-derived inflammation in SCM. In particular, $CCR2^{+}$ cardiac macrophages, almost entirely derived from circulating monocytes, have been shown to be more inflammatory compared to their $CCR2^{-}$ embryonic-derived cardiac macrophage counterparts in that isolated $CCR2^{+}$ cardiac macrophages produce abundant IL-1β when treated with NLRP3 inflammasome priming and activation stimuli [56]. Accordingly, macrophage NLRP3 inflammasome activation contributes to SCM severity, whereas targeting macrophage NLRP3 inflammasome activation can be protective by blocking cardiomyocyte oxidative stress and apoptosis induced by inflammation [139]. Whether NLRP3 inflammasome-mediated pyroptosis contributes to the observed large-scale macrophage cell death and subsequent population remodeling that occurs during sepsis is unclear [66]. Overall, cardiac macrophage-specific NLRP3 inflammasome activation most likely contributes to SCM-related hyper-inflammation and myocardial dysfunction, but the NLRP3 inflammasome almost certainly has physiological roles in the innate immune response to cardiac pathogen infection.

NLRP3 inflammasome activation in non-immune cells in the septic heart is an exciting aspect to SCM that is only recently becoming appreciated. In cardiac diseases other than SCM, cardiomyocytes have been shown to undergo NLRP3 inflammasome activation to promote atrial fibrillation [140] and myocardial ischemia-reperfusion injury [141] through pyroptotic cell death or inflammatory cytokine production. Cardiomyocyte-specific NLRP3 inflammasome activation likely contributes to SCM pathophysiology as shown by the capability of cardiomyocytes to undergo NLRP3 inflammasome activation *in vitro* [23,142,143]. However, whether cardiomyocyte-specific NLRP3 inflammasome activation contributes to SCM pathophysiology *in vivo* is still unclear, especially in regards to some studies where potent cardiomyocyte cell death is not observed in some SCM models [23,66]. Other cells such as isolated cardiac fibroblasts are also capable of NLRP3 inflammasome activation *in vitro* and might contribute to hyper-inflammatory state of SCM and a reduced response in cardiomyocytes to therapeutic beta agonists like dobutamine [138].

Overall, the cell-specific contribution of NLRP3 inflammasome activation in the septic heart requires further research. Although NLRP3 inflammasome activation in cardiac macrophages during SCM pathophysiology is assumed, how macrophage NLRP3 inflammasome activation is controlled and dysregulated to contribute to SCM requires further research. Furthermore, the non-immune cell contribution of NLRP3 inflammasome activation is more widely researched in other cardiac pathologies, but roles in SCM is still unclear.

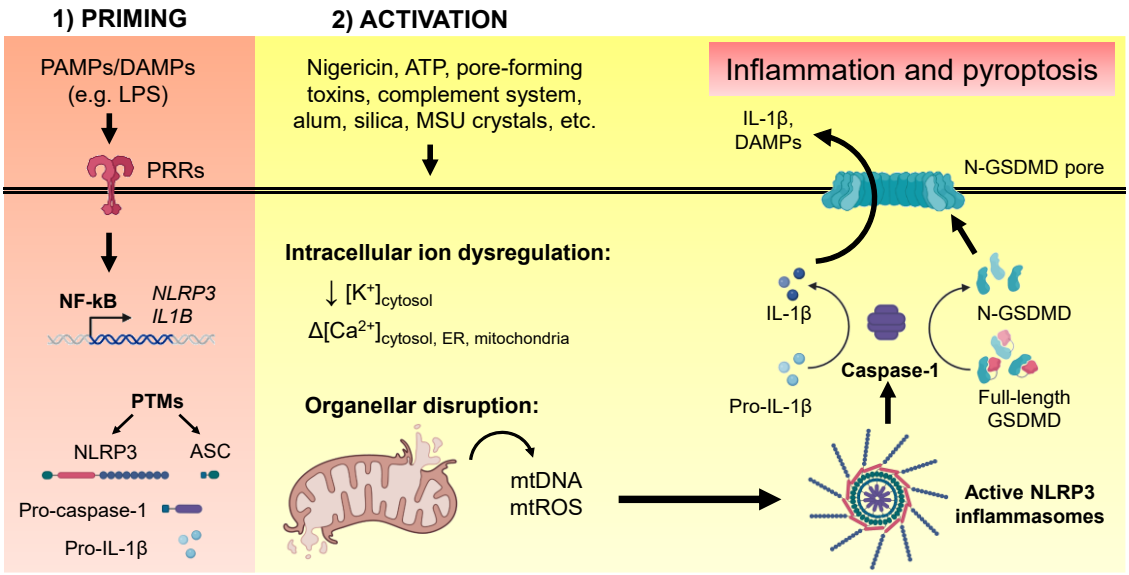

Figure 1.3. *Priming and activation of the NLRP3 inflammasome.* **(1)** Priming of the NLRP3 inflammasome involves detection of pathogen-associated molecular patterns (PAMPs) or damage-associated molecular patterns (DAMPs) by innate immune sensors called pattern recognition receptors (PRRs). A prototypical priming stimulus is the Gram-negative bacterial cell wall component lipopolysaccharide (LPS), a toll-like receptor-4 agonist. Priming involves *de novo* transcription *NLRP3* and *IL1B* downstream of nuclear factor-kappa B (NF-kB) activation, leading to increased protein levels of NLRP3 and pro-IL-1β. Essential post-translational modifications (PTMs) on NLRP3 and ASC also occur during priming. **(2)** Activation of the NLRP3 inflammasome can be induced by a variety of cell stress stimuli (prototypical examples shown) which tend to converge on intracellular ion dysregulation (K^+ efflux and Ca^{2+} mobilization depicted) and organellar disruption (mitochondrial damage depicted), leading to formation of active NLRP3 inflammasome complexes. Active NLRP3 inflammasomes mediate autoproteolytic activation of caspase-1, a protease which processes pro-IL-1β and full-length gasdermin-D (GSDMD) into their mature and functional forms. N-GSDMD oligomerizes into a plasma membrane pore which mediates inflammatory IL-1β and DAMP secretion as well as pyroptotic cell death. Adapted using [77,86,97].

1.4 12,13-DiHOME

1.4.1 Cytochrome P450 epoxygenase and soluble epoxide hydrolase metabolism of dietary N-3/N-6 polyunsaturated fatty acids in the heart

Cytochrome P450s (CYPs) are a superfamily of monooxygenases involved in the oxidative metabolism of many endogenous and xenobiotic substrates [144]. Humans have 57 genes encoding CYP isoforms, each with their own unique substrate and product selectivity, tissue-distribution, and biological roles. Historically, CYPs have been recognized as important hepatic enzymes involved in xenobiotic detoxification; however, there is now an increasing recognition for the importance of CYPs in the metabolism of endogenous substrates to produce secondary messengers, and the role of CYPs expressed in extrahepatic tissues has also garnered new research interest.

N-3 and N-6 polyunsaturated fatty acids (PUFAs) are fatty acids containing more than one double bond along the aliphatic chain, with N-3 and N-6 denoting the carbon of the first double bond relative to the terminal carbon of the aliphatic chain [145]. Major N-3 PUFAs include α-linolenic acid (ALA), docosahexaenoic acid (DHA), and eicosapentaenoic acid (EPA), while major N-6 PUFAs include linoleic acid (LA), γ-linolenic acid (GLA), and arachidonic acid (AA). N-3 and N-6 PUFAs are subject to metabolism by oxidative enzymes such as cyclooxygenases (COX) or lipoxygenases (LOX), producing well-studied lipid mediators such as thromboxanes, prostaglandins, prostacyclins, and leukotrienes with well-recognized bioactivities on inflammation, vasoconstriction, pain, and other processes at homeostasis and disease [146]. However, a third branch of N-3 and N-6 PUFA metabolism, mediated by CYPs, is only recently becoming recognized, and the bioactive effects of CYP-derived N-3 and N-6 PUFA metabolites are less clear.

Of recent importance are the CYP epoxygenase-derived metabolites of N-3 and N-6 PUFAs in the heart [147]. The major human cardiac CYP epoxygenase isoforms, CYP2J2, CYP2C8, and CYP2C9 mediate epoxidation at the double bonds of N-3 and N-6 PUFAs, creating PUFA epoxide products. These PUFA epoxides differ according to the N-3 and N-6 PUFA parent substrate, regioisomeric configuration of the epoxide moiety (N-3, N-6, N-9, etc.), and stereochemistry (R,S or S,R), with all these factors mainly determined by the selectivity of the particular CYP epoxygenase isoform in question [148]. Importantly, PUFA epoxides are labile to soluble epoxide hydrolase (sEH)-mediated hydrolysis to produce PUFA vicinal diol metabolites, as sEH is ubiquitously expressed in tissues also expressing CYP epoxygenases [149]. Hence, a "CYP epoxygenase-sEH axis" of PUFA metabolism has been suggested to mediate a significant portion of the biological effects of N-3 and N-6 PUFAs through the production of a large family of PUFA epoxides and diols [147].

In the heart, N-3 and N-6 PUFA epoxides and diols have been shown to have roles in a variety of disease models such as myocardial ischemia-reperfusion injury, hypertension-induced hypertrophy, conduction disorders, and sepsis [150]. CYP2J2 is the predominant CYP epoxygenase isoform in human cardiomyocytes, CYP2C9 appears to predominate in cardiac endothelial cells, and sEH is expressed in both [149]. Generally, N-3 PUFA epoxides like DHA-derived 19,20-epoxydocosapentaenoic acid (19,20-EDP) and the EPA-derived 17,18-epoxyeicosatetraenoic acid (17,18-EEQ) have been shown to mediate at least part of the cardioprotective effects observed by dietary supplementation of N-3 PUFAs [151]. For instance, in models of *ex vivo* myocardial ischemia-reperfusion injury, rescue of post-ischemic function by DHA can be blocked by co-treatment with the CYP epoxygenase inhibitor MSPPOH and re-capitulated by treatment with 19,20-EDP alone [152]. On the

other hand, certain N-6 PUFA epoxides are thought to be either cardioprotective or deleterious in certain conditions. Similar to N-3 PUFA epoxides, the arachidonic acid-derived epoxyeicosatrienoic acids (EETs) are known to be cytoprotective and anti-inflammatory mediators in a variety of cardiac diseases [153], but EETs are also known to be pro-cancer agents [154]. Interestingly, 19,20-EDP and 17,18-EEQ have been shown to mediate both more potent cardioprotective effects compared to EETs [148,155], in addition to anti-cancer effects [156,157]. Additionally, the LA-derived PUFA epoxides and diols have been historically known as potent cytotoxic agents in the lung, heart, and kidneys, but emerging roles in physiological processes in other tissues such as brown fat and skeletal muscle have questioned whether they are generally cytotoxic [158]. As N-3 and N-6 PUFA epoxides are readily subject to sEH-mediated hydrolysis, these metabolites are relatively short-lived before they are converted into PUFA diols. Importantly, while PUFA diols are generally considered less potent or inactivated metabolites of PUFA epoxides, PUFA diols like those derived from LA epoxides can mediate unique bioactivities or are responsible for the cardiotoxicity previously attributed to the PUFA epoxides alone [147].

Increasing the dietary ratio of N-3 to N-6 PUFAs has been thought to promote the production of cardioprotective N-3 PUFA epoxides meanwhile reducing the production of less potent or cardiotoxic N-3 PUFA diols and N-6 PUFA epoxides and diols [151]. In addition, pharmacological inhibition of sEH to prevent degradation of the relatively short-lived PUFA epoxides has also been shown to be cardioprotective in multiple disease models [142,159,160]. However, for both these clinically-viable approaches which target the CYP epoxygenase-sEH axis, the specific N-3 and N-6 PUFA epoxides or diols that are increased and decreased respectively to mediate overall cardioprotection are poorly understood, and

whether this holds true in other diseases where some biological effects associated with cardioprotection (e.g. cytoprotection, anti-inflammation) might exacerbate other diseases in different tissues (e.g. cancer) requires further research. Although tissue-specific and disease-specific functions for individual PUFA epoxides and diols are increasingly becoming appreciated, recommending changes to dietary N-3 and N-6 PUFA intake or administering sEH inhibitors to cardiac disease patients must be preceded by an improved mechanistic understanding of these metabolites in multiple cell types and multiple disease contexts, where in some cases the same metabolite could have opposing effects in different tissues and diseases.

1.4.2 Overview of EpOMEs and DiHOMEs

LA is the most abundant PUFA in the Western diet, obtained from dietary sources such as meats, eggs, vegetable oils, nuts, and seeds [161]. LA can become epoxidated through a CYP epoxygenase-dependent mechanism, which is the most likely route of biosynthesis in cells such as cardiomyocytes [142], endothelial cells [162], renal proximal tubule cells [163], and hepatocytes [163], but LA can also become epoxidated by reacting with hydroxyl radicals formed during the neutrophil-associated respiratory burst [164]. The two LA epoxide regioisomers which can form are 9,10-epoxyoctadecenoic acid (9,10-EpOME) and 12,13-epoxyoctadecenoic acid (12,13-EpOME), although 12,13-EpOME is the preferred product by most CYP epoxygenases [163]. Subsequently, their epoxide hydrolase-mediated hydrolysis, preferentially by sEH as opposed to the membrane-associated microsomal epoxide hydrolase (mEH) [165], leads to the formation of 9,10-

dihydroxy-12z-octadecenoic acid (9,10-DiHOME) and 12,13-dihydroxy-9Z-octadecenoic acid (12,13-DiHOME) [158].

From the original studies of the 1980s to 1990s, 9,10-EpOME and 12,13-EpOME were widely thought to be toxic metabolites while the hydrolyzed DiHOMEs were "de-toxified" metabolites, as was generally thought for most epoxide-containing bioactive molecules [165]. Yokoo et al. isolated 9,10-EpOME and 12,13-EpOME from the skin of severe burn victims to identify putative cytotoxic lipid mediators with toxic effects on mitochondria [166]. Later, 9,10-EpOME and 12,13-EpOME were found to be produced by leukocyte (specifically neutrophil) fractions from the lung lavages of rats treated with hyperoxia, hence they were named "leukotoxin" and "isoleukotoxin", respectively [167,168]. EpOMEs were the proposed endogenous factors mediating the "late death" observed in severe burn victims who, despite overcoming the initial primary shock, generally died of pulmonary edematous injury presenting as adult respiratory distress syndrome (ARDS), renal and cardiac failure, and an overall systemic hyper-inflammatory state [169]. Hypothetically, neutrophils invading burned skin as an anti-infective mechanism would produce EpOMEs that would be enter the circulation and mediate multiple organ failure due to EpOME-induced cytotoxic damage, and neutrophils invading these other damaged tissues would further exacerbate EpOME production and systemic inflammatory tissue damage. In case studies of a few patients presenting with >50% body surface area being severely burned, plasma concentrations of EpOMEs were 11.4 - 37 μM [169]. Strikingly, in patients with septicemia or diabetes mellitus-related circulatory shock, both presenting with disseminated intravascular coagulation and leukocytosis, plasma levels of EpOMEs reached 580 μM and 880 μM and were associated with cardiac, renal, and respiratory failure [170]. As such, these

high-micromolar concentrations served as the reference for "physiologically relevant" concentrations of EpOMEs to be used in most early studies, where high-micromolar EpOME concentrations induced cytotoxicity [171], mitochondrial uncoupling [167], pulmonary edematous injury [172], cardiac failure [173], and disseminated intravascular coagulation [174].

Later studies attempting to further define the bioactive mechanisms of EpOMEs found that their apparently toxic effects were more convoluted than initially thought. An important finding was that both LA diol metabolites, 9,10- and 12,13-DiHOME, were found to be the sole mediators of cytotoxicity in Sf21 insect cells, while 9,10- and 12,13-EpOME were only cytotoxic in the presence of sEH, contradicting the general assumption that epoxide hydrolysis was a detoxification mechanism against EpOMEs but rather mediated their cytotoxicity [165]. These findings prompted a re-analysis of previous studies which did not take EpOME to DiHOME conversion by sEH into account. For instance, *in vivo* EpOME-induced pulmonary edematous injury was dependent upon sEH-mediated conversion into DiHOMEs [175]. The effects of EpOMEs and DiHOMEs were also found to be much more species-, tissue-, concentration-, regioisomer-, and sEH-dependent, and sometimes contradictory. As low as 10 nM 9,10-DiHOME could induce potent chemotaxis in human neutrophils with no cytotoxic effects observed up to 10 μM [176], but both 9,10-DiHOME and 12,13-DiHOME inhibited the neutrophil respiratory burst at 20 μM [177]. 1000 μM 9,10-EpOME and 12,13-EpOME in an equimolar mixture could not induce cytotoxicity in renal proximal tubule cells but the same concentration of DiHOMEs could [178]. As well, 10 μM 9,10-EpOME could induce pulmonary edematous injury in isolated *ex vivo* perfused rat lungs without causing mitochondrial dysfunction, suggesting

mitochondrial dysfunction was not the sole cytotoxic mechanism of these metabolites [179]. 180 μM 9,10-DiHOME could cause mitochondrial permeability pore transition-induced damage in Sf21 insect cells, while the same concentration of 9,10-EpOME could not [180]. 12,13-DiHOME was four-times more potent than 9,10-DiHOME in irreversibly inhibiting overall electron transport chain activity of Sf21 cells, while EpOMEs and LA induced reversible mitochondrial uncoupling effects [181]. Strikingly, in a renal proximal tubule cell hypoxia-reoxygenation (H/R) injury model, pre-treatment with 12,13-EpOME (1 to 10 μM) protected these cells from H/R-induced mitochondrial respiratory dysfunction, whereas 12,13-DiHOME at equimolar concentrations had no effect [182]. These studies highlight the heterogeneity observed in the literature regarding the cellular targets of EpOMEs and DiHOMEs, their roles as solely "toxic" mediators, what constitutes "physiologically-relevant" concentrations of EpOMEs and DiHOMEs, and the relative importance between the 9,10- and 12,13- regioisomers. More recent literature has mainly focused on 12,13-DiHOME, as a wide range of physiological and pathophysiological roles for this metabolite not shared with 12,13-EpOME and 9,10-EpOME/DiHOME have been uncovered.

1.4.3 Physiological and pathophysiological roles of 12,13-DiHOME

1.4.3.1 Immune system

Early studies originally identified 12,13-DiHOME as the downstream metabolite of 12,13-EpOME, which could be isolated from neutrophils incubated with linoleic acid [168]. EpOMEs and DiHOMEs were shown to potently induce neutrophil chemotaxis without affecting the expression of adhesion molecules, acting *via* G_i-dependent, PI3K-dependent, and tyrosine kinase and protein kinase C-independent pathways [176]. These concentrations

were astonishingly low (10 nM) for maximally inducing chemotaxis, compared to the concentrations found in patients with severe burn injuries [169] or sepsis [170] who presented with high-micromolar plasma concentrations. However, it was later shown that both DiHOME regioisomers at high concentrations (10-200 μM) inhibited the neutrophil respiratory burst [177]. This pair of studies suggests that, potentially, low concentrations of DiHOMEs may be stimulatory of the acute inflammatory response in neutrophils, while higher concentrations of DiHOMEs over time may act as a negative feedback signal to regulate the response. A plasma lipidomics screen of animals infected with a highly pathogenic influenza strain identified that 12,13-DiHOME levels were associated with infection-induced lung damage [183]. Importantly, Levan et al. demonstrated that fecal levels of 12,13-DiHOME in human neonates were associated with an increased risk of childhood atopy, eczema, or asthma [184]. Gut bacteria-derived epoxide hydrolases were likely responsible for 12,13-DiHOME production as opposed to host-derived sEH or microsomal epoxide hydrolase (mEH). In mice, 12,13-DiHOME treatment led to enhanced allergic lung inflammation induced by cockroach antigen challenge and reduced the number of T_{reg} cells in lungs of these mice. *In vitro*, 12,13-DiHOME (75-200 μM) induced a pro-allergic response in dendritic cells, where dendritic cells had reduced IL-10 secretion and the number of T_{reg} cells resulting from dendritic cell and autologous T cell co-culture was reduced [184]. The authors suggested that 12,13-DiHOME's effects were due to peroxisome proliferator-activated receptor gamma (PPARγ) activation, as the concentrations used could stimulate a PPARγ-luciferase reporter expressed in RAW264.7 murine macrophages. Additionally, the same research group recently published abstract claiming that 12,13-DiHOME promotes inflammatory macrophage polarization by increasing the number of IL-

1β+ cells [185]. Lastly, Bergmann et al. reported that 12,13-DiHOME promoted maturation and activation in LPS or IFNγ-stimulated neutrophils, meanwhile inhibiting acidification and antigen presentation in monocytes and macrophages and IL-6 and TNFα secretion of splenic cell suspensions [186]. Overall, 12,13-DiHOME appears to be associated with multiple immune-related processes, but concentration-dependent immune cell-specific functions of 12,13-DiHOME requires further elucidation.

1.4.3.2 Cardiac homeostasis and disease

Although 12,13-DiHOME has been historically studied as a cardiotoxic metabolite, the literature consists of conflicting data regarding its effects on the heart. Elevated myocardial 12,13-DiHOME levels appear to be ubiquitous in many cardiac diseases, including dilated cardiomyopathy in humans (3.6-fold increase) [187], *ex vivo* cardiac ischemia-reperfusion injury (3.2-fold increase) [188], and endotoxin-induced septic cardiomyopathy in mice (3.7-fold increase) [159]. Despite these observed increases in myocardial tissue levels of 12,13-DiHOME, the precise cellular effects induced by 12,13-DiHOME have been contentious, as well as whether 12,13-DiHOME production is deleterious itself or rather is an adaptive mechanism. Early studies demonstrating that 12,13-DiHOME induced mitochondrial respiratory dysfunction [181] were supported in later studies showing that as low as 100 nM 12,13-DiHOME induces mitochondrial uncoupling in cardiomyocytes associated with increased inflammatory cytokine secretion and cytotoxicity [159]. However, a recent study by Pinckard et al. reported that 10 μM 12,13-DIHOME led to stimulation of basal respiration and maximal respiratory capacity in cardiomyocytes by increasing fatty acid uptake and oxidation, and 12,13-DiHOME

treatment also increased *in vivo* heart contractility through improved cardiomyocyte Ca^{2+} handling [189]. An earlier study by Mitchell et al. also demonstrated that perfusion with 12,13-DiHOME at 30 μM led to sustained increases in contractility in *ex vivo* rat hearts with no changes in blood pressure, heart rate, or electrocardiogram parameters observed *in vivo*, suggesting that 12,13-DiHOME could have positive inotropic effects [190]. However, Bannehr et al. demonstrated that 100 nM 12,13-DiHOME perfused during ischemia-reperfusion injury in *ex vivo* mouse hearts reduced post-ischemic functional recovery, suggesting that 12,13-DiHOME may have differential or concentration-dependent effects at cardiac homeostasis versus disease [191].

More recent studies have used CYP overexpression and/or sEH inhibition to study the effects that could be related to 12,13-DiHOME in cardiac disease models. 12,13-DiHOME levels were associated with exacerbated ischemia-reperfusion (I/R) injury in *ex vivo* perfused hearts from mice with endothelium-specific CYP2C8 epoxygenase overexpression, suggesting that endothelial cells might contribute cardiotoxic DiHOME production during I/R injury [162]. Likewise, increased myocardial 12,13-DiHOME levels were associated with a loss of cardioprotection offered by cardiomyocyte-specific CYP2J2 epoxygenase overexpression in aged mice compared to young mice against *ex vivo* cardiac I/R injury [188]. In young mice, cardiomyocyte-specific CYP2J2 overexpression is cardioprotective due to the increased formation of cardioprotective PUFA epoxides like EETs, EDPs, and EEQs. However, cardiomyocyte-specific CYP2J2 overexpression appears have a deleterious effect in aged mice, where these mice exhibit exacerbated cardiac I/R injury correlated with enhanced 12,13-DiHOME production despite no changes in CYP2J2 or sEH activity. As well, cardiomyocyte-specific ablation of sEH improved post-ischemic

function in *ex vivo* isolated mouse hearts, which correlated with reduced myocardial 12,13-DiHOME levels [192]. In these myocardial I/R injury studies, a specific role cannot be ascribed to 12,13-DiHOME alone, as other CYP epoxygenase or sEH-derived metabolites might also be affected by overexpression or pharmacological targeting of these enzymes. Overall, 12,13-DiHOME's effects in the heart are likely concentration-, species-, and, disease-specific, but its dynamic biosynthesis correlating with perturbations in the heart and observed toxic effects on cardiomyocytes effects *in vitro* suggests a potentially important role for 12,13-DiHOME in cardiac disease. However, the specific molecular targets and cell-specific effects through which 12,13-DiHOME may act as a cardiotoxic autocrine and/or paracrine lipid mediator requires further elucidation.

1.4.3.3 Nervous system

Interestingly, 12,13-DiHOME has been shown to modulate ion channel and transporter activities both *in vitro* and *in vivo*. With the observation that 9,10-DiHOME but not linoleic acid or 9,10-EpOME affected rat ventricular myocyte action potentials [193], Ha et al. investigated the role of EpOMEs and DiHOMEs in N20.1 mouse oligodendrocyte electrical activity, in which they showed that 10 μM 12,13-DiHOME inhibited Na^+/K^+ ATPase current through effects independent on changes in membrane fluidity [194]. Other ion channels, such as the transient receptor potential (TRP) channel family, appear to be modulated by 12,13-DiHOME. Green et al. demonstrated that increased 12,13-DiHOME levels were observed in the spinal cord tissues of mice with burn injury [195]. Additionally, 12,13-DiHOME (100 μM) could activate whole-cell currents of Chinese hamster ovarian (CHO) cells expressing exogenous TRP vanilloid 1 (TRPV1), TRP vanilloid 3 (TRPV3), or

TRP ankyrin 1 (TRPA1), and 12,13-DiHOME injection directly into the spines of mice reduced pain thresholds versus mechanical and thermal pain-inducing stimuli in a TRPV1 and TRPA1-dependent manner [195]. Later, Zimmer et al. demonstrated that 12,13-DiHOME levels were increased in dorsal root ganglia and spinal dorsal horn tissues following zymosan-induced acute inflammatory pain or Complete Freund's Adjuvant (CFA)-induced chronic inflammatory pain in mice, which could be blocked by an sEH inhibitor [196]. It was found that 10 μM 12,13-DiHOME could induce spontaneous calcium currents in sensory neurons in a TRPV1-dependent manner, and 0.25-1 μM 12,13-DiHOME could sensitize TRPV1 channels to capsaicin-induced calcium currents in a protein kinase C-dependent manner. Importantly, injection of 10 μM 12,13-DiHOME into the hind paws of mice led to a reduction in thermal pain threshold in a time-dependent manner *in vivo*. Interestingly, 12,13-DiHOME could decrease axonal outgrowth in primary cortical neuron-glial cell co-cultures from male but not female rats, suggesting sex-dependent neuronal effects by 12,13-DiHOME that should be considered [197]. As well, an increased 12,13-DiHOME to 12,13-EpOME ratio was associated with higher scores measured by the Beck Depression Inventory 2nd Edition score (BDI-II), suggesting a positive association between 12,13-DiHOME and depression [198]. Overall, 12,13-DiHOME-mediated changes in ion channel and transporter activities have been well-observed, but connecting these molecular effects to biological pathways associated with thermal or inflammatory pain and potentially depression requires further research.

1.4.3.4 Obesity, brown fat activation, and exercise

12,13-DiHOME has recently become recognized as an important physiological "lipokine" derived from brown adipose tissue (BAT) that modulates fatty acid metabolism in a variety of tissues. Lynes et al. performed a lipidomics screen to identify novel metabolites associated with cold-induced BAT-mediated thermogenesis, as BAT-mediated fuel consumption could an interesting approach to treat metabolic disorders [199]. Interestingly, 12,13-DiHOME was a novel hit for elevated plasma metabolites following cold exposure in human volunteers and correlated with thermogenic BAT activity. 12,13-DiHOME plasma levels were also negatively correlated with body mass index, insulin resistance, fasting plasma insulin and glucose concentrations, circulating triglycerides, and leptin levels in this cohort. In a cold-induced BAT thermogenesis mouse model, it was found that BAT mediates 12,13-DiHOME production in response to thermogenic stimuli, increasing expression of both soluble and microsomal epoxide hydrolase. Importantly, a target plasma concentration of 30-50 nM 12,13-DiHOME being administered into mice could promote thermogenesis in cold-challenged mice without the presence of tachycardia and hypertension, protected against diet-induced obesity, and stimulated fatty acid uptake into BAT *in vivo*. *In vitro*, 12,13-DiHOME induced translocation of the fatty acid transporters cluster of differentiation 36 (CD36) and fatty acid transport protein 1 (FATP1) to brown adipocyte membranes and stimulated fatty acid oxidation without changes in mitochondrial maximal respiratory capacity or respiratory uncoupling. Following this foundational study identifying 12,13-DiHOME as a pro-thermogenic "lipokine", Stanford et al. demonstrated that BAT-derived 12,13-DiHOME was also stimulated by moderate intensity exercise in human volunteers and resting plasma levels of 12,13-DiHOME correlated with skeletal

muscle respiratory function [200]. In a mouse model, 12,13-DiHOME administration could enhance fatty acid uptake and oxidation of skeletal muscle *in vivo* and stimulated fatty acid oxidation, uptake, and the basal and maximal oxygen consumption rate of myotube cells but not white adipocyte cells *in vitro*. Pinckard et al. also demonstrated that BAT transplantation in mice increased physiological systolic and diastolic function which correlated with 12,13-DiHOME in plasma [189]. Administration of 12,13-DiHOME also increased systolic and diastolic function in mice and protected heart function in high-fat diet-challenged mice. Interestingly, 10 μM 12,13-DiHOME enhanced basal, maximal, and non-mitochondrial respiration in isolated cardiomyocytes from adult mice. These effects were associated with increased fatty acid uptake (like in BAT and skeletal muscle), enhanced Ca^{2+} handling, as well as improved contractile function in cardiomyocytes *in vitro*. These effects were dependent upon nitric oxide synthase 1 and ryanodine receptor. In humans, Vasan et al. observed that 12,13-DiHOME plasma levels were associated with lower fasting plasma insulin and lower plasma triacylglycerols but not associated with changes in body mass index, fasting hyperinsulinemia, or elevated lipid levels [201]. Wolfs et al. found that 12,13-DiHOME was present in human milk and 12,13-DiHOME abundance in milk was correlated with higher body-mass index in infants at birth, but lower weight-for-length score at birth, lower fat mass in 1 month-old infants, lower overall infant adiposity, and lower gains in weight-for-length and body-mass index from 0 months to 6 months after birth [202]. Interestingly, the levels of 12,13-DiHOME in milk could be increased by a bout of exercise in mothers, suggesting that 12,13-DiHOME could be an adipose remodeling signal transferred from mothers to infants through breast feeding. Overall, 12,13-DiHOME appears to have a physiological role in thermogenesis, exercise, and adipose tissue remodelling, but

the clinical implications of these findings have yet to be contextualized with previous studies demonstrating its cytotoxic, mitochondrial toxic, and cardiotoxic effects. Thus, further studies investigating 12,13-DiHOME's species-, tissue-, and concentration-dependent effects across different (or superimposed) disease models are necessary prior to therapeutic targeting of 12,13-DiHOME in metabolic disease.

1.4.4 Putative role for 12,13-DiHOME in septic cardiomyopathy

The original body of work focusing on 12,13-DiHOME, its regioisomer 9,10-DiHOME, and the PUFA epoxide precursors to these diols, EpOMEs, centred on a dogma that these metabolites were "leukotoxins" derived from neutrophils and potentially other leukocytes. Although these metabolites were studied more in the context of severe burn victims' "late death" and multiple organ failure, the foundational hypothesis where systemic EpOME (and subsequent DiHOME) production was a result of leukocytosis implies that these metabolites could also be involved in other hyper-inflammatory disorders involving the innate immune response, such as SCM. Intriguingly, myocardial neutrophil numbers increase in the same phases associated with myocardial dysfunction in septic mice [23], suggesting that 12,13-DiHOME could be contributed by the influx of neutrophils, but the contribution of 12,13-DiHOME from cardiomyocytes [142], endothelial cells [162], and other cardiac cell types which express CYP epoxygenases and sEH is unclear. As well, associations between EpOME levels and cardiac failure observed in animal models [173] and sepsis and severe burn patients [169,170], plus their *in vitro* mitochondrial toxic effects [159,181], have since then established a cardiotoxic role to EpOMEs and DiHOMEs that could be extrapolated to SCM pathophysiology. Recent studies measuring 12,13-DiHOME

specifically have also supported 12,13-DiHOME's role in infection and hyper-inflammation, as plasma 12,13-DiHOME was observed in sepsis patients and associated with a sepsis-related mortality [203]. In another study, increased 12,13-DiHOME plasma levels were associated with severe coronavirus disease 2019 (COVID-19) infection [204]. However, with recent studies suggesting physiological and even cardioprotective roles for 12,13-DiHOME in tissues such as BAT, skeletal muscle, and cardiomyocytes [189,199], contextualizing these foundational studies claiming a cardiotoxic role for 12,13-DiHOME with these newer studies claiming the opposite has yet to be fully demonstrated. However, this does not mean that these contrasting observations have no applicability to each other. Presumably, 12,13-DiHOME likely has species-, tissue-, concentration-, and most importantly, disease-specific effects, and the same 12,13-DiHOME-mediated biological effects may be "therapeutic" or "deleterious" depending on the physiological context. For instance, mitochondrial respiratory depression induced by 12,13-DiHOME could be involved in a metabolic "hibernation" state in cardiomyocytes, theorized to be an adaptive mechanism in SCM [205], but this same mitochondrial dysfunction may have roles in prompting inflammation (and hyper-inflammation) from innate immune cells in the septic heart [206].

Although large clinical studies associating 12,13-DiHOME and SCM have not been performed, a few recent studies utilizing animal models have attempted this. Samokhvalov et al. demonstrated that protection against endotoxin-induced cardiomyopathy was conferred by global sEH knockout in mice, and this was correlated with ablation of myocardial 12,13-DiHOME levels [159]. *In vitro*, 12,13-DiHOME mediated potent cytotoxicity, mitochondrial uncoupling, and pro-inflammatory cytokine and chemokine secretion in cardiomyocytes.

However, whether 12,13-DiHOME could directly affect innate immune cell-derived inflammation and other functions was not investigated. Strikingly, Sosnowski et al. demonstrated that cardiomyocyte-specific sEH ablation was sufficient to protect mice from endotoxin-induced cardiomyopathy, correlating with inhibition of myocardial NLRP3 inflammasome activation, monocyte/macrophage invasion into the myocardium, and systemic innate immune activation [142]. *In vitro*, cardiomyocyte NLRP3 inflammasome was found to play a potential role, as pharmacological sEH inhibition or treatment with the PUFA epoxide 19,20-EDP could prevent LPS-induced NLRP3 inflammasome activation in neonatal rat cardiomyocytes. These data suggest that cardiomyocyte-specific PUFA epoxide and downstream sEH-derived diol biosynthesis could be crucial in modulating cardiac hyper-inflammation and innate immune activation in SCM. However, whether cardiomyocyte-specific sEH ablation also reduced 12,13-DiHOME levels in the myocardium was not assessed, and the direct effects of PUFA epoxide treatment or sEH inhibition on immune cell-derived inflammation was not measured. Although other studies have pursued the roles of cardiotherapeutic PUFA epoxides such as EETs on cardiomyocyte [207] and innate immune cell function [208] in SCM models, the role of putatively cardiotoxic PUFA diols, such as 12,13-DiHOME, were not assessed in these studies.

Intriguingly, many other studies have shown that sEH ablation can ameliorate sepsis-associated perturbations in other tissues but did not assess cardiomyopathy in their models. Pharmacological sEH inhibition has anti-pyretic effects against LPS-induced fever in rats [209]. Dong et al. reported that endothelial CYP2J2 overexpression or pharmacological sEH inhibition almost completely rescued mice from LPS-induced mortality, and these effects correlated with ablation of LPS-induced lung vascular hyperpermeability [210]. Zhang et al.

found that a novel sEH inhibitor called wedelolactone could prevent LPS-induced acute lung injury through anti-oxidative and anti-inflammatory effects by repressing macrophage inflammation and preventing pulmonary infiltration of macrophages and neutrophils [211]. Similarly, Chen et al. found that pharmacological sEH inhibition blunted mortality in septic mice treated with cecal ligation and puncture, correlating with reduced multiple organ dysfunction, lower systemic inflammation, and anti-inflammatory effects in macrophages [212]. As well, pharmacological sEH inhibition improved phagocytic capacity of macrophages, potentially promoting pathogen clearance. Luo et al. showed that pharmacological sEH inhibition or treatment with EETs could block LPS-induced acute lung injury in mice [213]. *In vitro*, pharmacological sEH inhibition or treatment with EETs could inhibit NLRP3 inflammasome activation in peritoneal macrophages [213].

Overall, the role of 12,13-DiHOME in SCM is poorly understood. While many studies have shown 12,13-DiHOME may be cardiotoxic in SCM and non-SCM disease models, more recent data suggesting physiological roles of 12,13-DiHOME in other tissues suggests concentration-, tissue-, species- and disease-specific effects of 12,13-DiHOME. It is likely that the same molecular targets of 12,13-DiHOME have opposing effects depending on the physiological or disease context. As well, the immune and non-immune cell-specific effects of 12,13-DiHOME in the context of SCM have not been investigated. Understanding the full breadth of biological effects of 12,13-DiHOME in different contexts is required prior to targeting its biosynthesis for therapeutic outcomes in SCM.

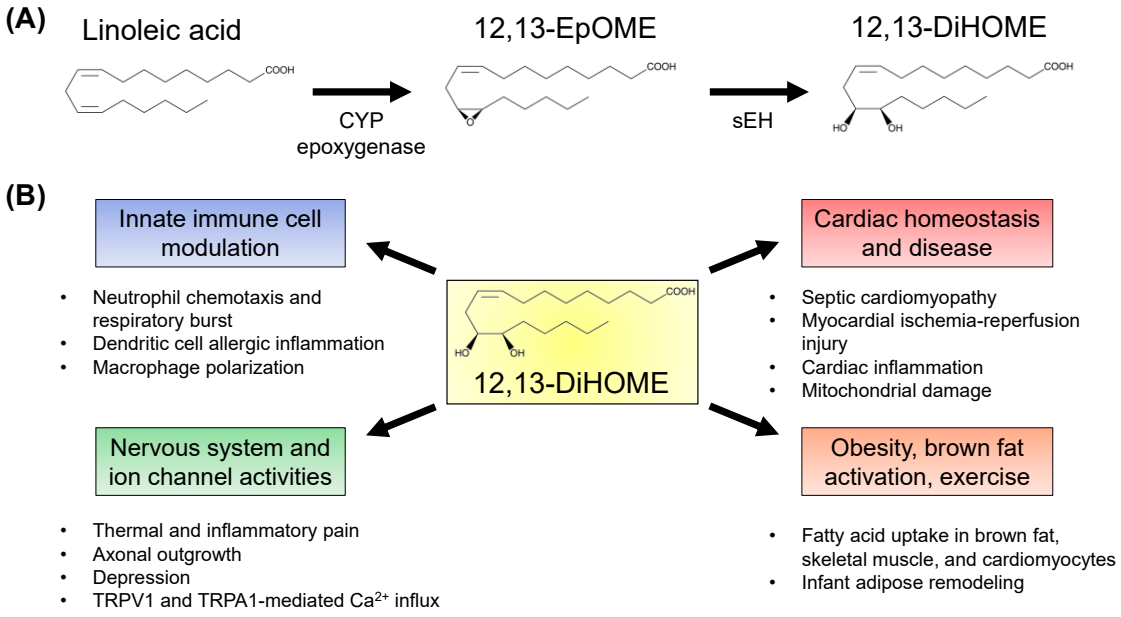

Figure 1.4. *Biosynthesis and biological roles of 12,13-DIHOME.* **(A)** Biosynthetic pathway for 12,13-dihydroxy-9z-octadecenoic acid (12,13-DIHOME). Linoleic acid is an n-6 polyunsaturated fatty acid (PUFA) derived from dietary sources like vegetables, meats, eggs, and seed oils. It is the most abundant PUFA in the Western diet. Linoleic acid can be epoxidated by cytochrome P450 (CYP) epoxygenase enzymes, including CYP2J or CYP2C isoforms. The dominant regioisomer product is (±)12,13-epoxy-9z-octadecenoic acid (12,13-EpOME). 12,13-EpOME is labile to soluble epoxide hydrolase (sEH)-mediated hydrolysis to form the vicinal diol metabolite, 12,13-DiHOME. **(B)** Biological roles of 12,13-DiHOME as discussed in Section 1.4 and using [158].

1.5 Thesis overview

1.5.1 Rationale

SCM, which is highly prevalent in sepsis patients, could be targeted therapeutically to reduce the burden conferred by sepsis-related hospitalizations and mortality. However, SCM pathophysiology is ill-defined, poorly understood, and lacks effective treatment. While macrophages, the dominant cardiac immune cell, have essential roles in the physiological response to pathogen infection, how macrophage-related functions contribute to the hyper-inflammatory and injured state in SCM has not been fully elucidated. Macrophage inflammation pathways already associated with SCM pathophysiology, such as M1-like macrophage polarization or NLRP3 inflammasome activation, lack a complete mechanistic understanding regarding the factors which lead to their dysregulation in SCM.

We have recently demonstrated the protective effects of cardiomyocyte-specific sEH inhibition in murine SCM models. Our initial hypothesis was that sEH inhibition led to the preservation of cardioprotective PUFA epoxides in the heart, but an alternative hypothesis where sEH inhibition prevents cardiotoxic PUFA diol production has only recently been appreciated. Of these PUFA diols, 12,13-DiHOME levels in myocardial tissues are associated with endotoxin-induced cardiomyopathy in mice. 12,13-DiHOME directly mediates potent pro-inflammatory and mitochondrial damaging effects on cardiomyocytes, supporting previous studies observing its cytotoxic effects. However, the direct effects of 12,13-DiHOME on immune cells of the septic heart, specifically macrophages, has not been explored previously. Additionally, whether 12,13-DiHOME exacerbates macrophage inflammation pathways such as pro-inflammatory M1-like macrophage polarization and NLRP3 inflammasome activation is unclear.

1.5.2 Hypothesis

We hypothesize that 12,13-DiHOME enhances macrophage inflammation through effects on macrophage polarization and NLRP3 inflammasome activation.

1.5.3 Objectives

1) Investigate the effects of 12,13-DiHOME on macrophage polarization and NLRP3 inflammasome activation.
2) Determine the mechanisms by which 12,13-DiHOME modulates macrophage inflammation.

1.6 Condensed introduction and thesis outline

Septic cardiomyopathy (SCM) is cardiac dysfunction caused by a dysregulated host immune response to systemic pathogen infection [5]. Although SCM is highly prevalent and increases mortality risk in septic patients, its poorly understood pathophysiology limits effective treatment of SCM. Inflammation, oxidative stress, mitochondrial dysfunction, perturbed Ca^{2+} handling, and other pathways are well-associated with SCM, but how these cellular events relate to one another and the role of specific cells in SCM requires further exploration. In this regard, macrophages are innate immune cells essential in the physiological response to pathogen infection through roles in acute inflammatory propagation, pathogen recognition and clearance, and subsequent inflammation resolution and tissue maintenance [214]. However, dysregulation of macrophage-derived inflammation exacerbates septic tissue injury, so improving our understanding macrophage inflammation will aid in identifying novel therapeutic targets in SCM.

The NLRP3 inflammasome is a cytosolic multiprotein complex that functions as a PRR for a variety of PAMPs and DAMPs [86]. PAMPs and DAMPs are signals associated with infection or tissue injury, respectively. PAMPs include (but are not limited to) bacterial cell wall components, bacterial pore-forming toxins, and pathogen-derived nucleic acids, while DAMPs include inflammatory cytokines, extracellular ATP, intracellular ion perturbations, and mitochondrial damage. Activation of the NLRP3 inflammasome is a two-phase process: an initial "priming" signal followed by a secondary "activation" signal, where either PAMPs and/or DAMPs can act as priming or activation signals. NLRP3 inflammasome priming signals converge at upregulating expression of NLRP3 inflammasome-related proteins and necessary post-translational modifications. NLRP3 inflammasome activation signals converge at events such as plasma membrane permeabilization, intracellular ion perturbation (e.g. cytosolic K^+ depletion or Ca^{2+} mobilization), and/or multiple organellar disruption (e.g. mitochondrial damage), leading to formation of active NLRP3 inflammasome complexes (NLRP3, ASC, and zymogen pro-caspase-1). Active NLRP3 inflammasomes mediate inflammatory autoproteolytic caspase-1 activation, caspase-1-mediated cleavage of pro-IL-1β followed by mature IL-1β secretion, and caspase-1-mediated cleavage of GSDMD into plasma membrane pore-forming N-GSDMD followed by a lytic cell death pathway called pyroptosis. Although NLRP3 inflammasome activation can limit pathogen infection, it may contribute to the dysregulated host response and inflammatory tissue injury in sepsis [135]. Importantly, macrophages are major sources of NLRP3 inflammasome-derived inflammation in sepsis [56,135], and mitochondrial damage and intracellular Ca^{2+} perturbations promote macrophage NLRP3 inflammasome activation [86]. As inhibiting NLRP3 inflammasome activation is protective

in SCM [137], identifying the factors which influence NLRP3 inflammasome priming and activation will improve our mechanistic understanding and treatment of SCM.

The CYP superfamily of monooxygenases are most often associated with liver metabolism and xenobiotic clearance, but there is increasing interest in extrahepatic CYP metabolism and endogenous CYP substrates. Interestingly, CYP epoxygenases expressed in the heart can metabolize essential dietary N-3/N-6 long-chain PUFAs at double bonds along the aliphatic chain, leading to the formation of bioactive PUFA epoxides with relevant roles in cardiac homeostasis and disease, including SCM [150]. Importantly, these PUFA epoxides are readily labile *via* cardiac sEH metabolism to form PUFA diol metabolites with unique bioactivities in the heart. 12,13-DiHOME is a PUFA diol derived from LA, an N-6 PUFA and the most abundant PUFA in the Western diet, found in foods such as vegetable oils, cereals, meats, and eggs [158]. LA is metabolized by CYP epoxygenases to form 12,13-EpOME which is hydrolyzed by sEH into 12,13-DiHOME. In a murine SCM model, we have shown that 12,13-DiHOME is produced in the myocardium in response to LPS-induced endotoxemic cardiac injury correlating with myocardial inflammation, mitochondrial damage, and dysfunction [159]. We have also recently reported that cardiac sEH inhibition protects against LPS-induced endotoxemic cardiac injury in part by limiting NLRP3 inflammasome activation in the heart [142]. Whether specific sEH-derived metabolites like 12,13-DiHOME directly promote NLRP3 inflammasome activation has not been demonstrated. Also, whether 12,13-DiHOME targets other cell types present in the myocardium, such as macrophages, to mediate its pro-inflammatory effects is unclear.

In the present thesis, we hypothesized that 12,13-DiHOME is pro-inflammatory in macrophages. Using an *in vitro* THP1 cell-derived macrophage model, we found that 12,13-

DiHOME present during macrophage polarization increased mRNA expression of M1-associated pro-inflammatory cytokines. Additionally, 12,13-DiHOME present during NLRP3 inflammasome priming led to exacerbated NLRP3 inflammasome activation. 12,13-DiHOME present during priming induced mitochondrial respiratory dysfunction and mitophagic defects prior to NLRP3 inflammasome activation. These mitochondrial effects were correlated with an increased sensitivity to mitochondrial damage during the inflammasome activation phase which could be effectively blocked by the MCU inhibitor, Ru265. MCU inhibition could similarly block NLRP3 inflammasome activation in LPS+12,13-DiHOME-primed macrophages. Overall, these data provide evidence for a novel pro-inflammatory role for 12,13-DiHOME in macrophages that could be relevant in SCM pathophysiology.

CHAPTER 2. METHODS

2.1 Reagents

Stock solutions of nigericin, rotenone, antimycin A, and FCCP were prepared in absolute ethanol. Stock solutions of phorbol myristate acetate (PMA), trans-AUCB (t-AUCB), oligomycin, digitonin, tetramethylrhodamine ethyl ester perchlorate (TMRE), MitoTracker Green FM, MitoSOX Red, and Fluo-4-AM were prepared in dimethylsulfoxide (DMSO). Stock solutions of LPS, recombinant human interferon-gamma, and recombinant human interleukin-4 were prepared in Dulbecco's phosphate-buffered saline (D-PBS). Stock solutions of pyruvate (freshly prepared on day of experiment), puromycin, and Ru265 were prepared in sterile cell culture-grade water (H_2O). Drugs were treated such that vehicle concentrations did not exceed 1% v/v in media. A list of materials and reagents used in the present thesis are provided in **Table 1**.

Table 1. List of materials and reagents used.

Reagent	**Supplier**	**Catalogue #**
THP1 cells	ATCC	TIB-202
HEK293T cells	ATCC	CRL-3216
Water, cell culture grade (Endotoxin-Free)	Fisher Scientific	SH3052902
Methyl acetate, anhydrous	Sigma Aldrich	296996
Dimethylsulfoxide (DMSO), Sterile/Filtered,	Sigma Aldrich	D2650
RPMI 1640	Thermo Fisher Scientific	11875093
Trypan Blue (0.4%)	Thermo Fisher Scientific	15250061
DPBS, no calcium, no magnesium	Thermo Fisher Scientific	14190144
Fetal Bovine Serum (FBS)	Thermo Fisher Scientific	12483-020
Accutase	Stempro	A1110501

10000U Penicillin-Streptomycin	Thermo Fisher Scientific	15140122
Phorbol 12-myristate 13-acetate (PMA)	Millipore Sigma	P8139
Lipopolysaccharides from Escherichia coli O111:B4 (LPS)	Millipore Sigma	L4391
(+/-) 12,13-DiHOME	Cayman Chemical	10009832
(+/-) 12,13-EpOME	Cayman Chemical	52450
t-AUCB	Cayman Chemical	16568
Recombinant human interferon-gamma	PeproTech	300-02
Recombinant human interleukin-4	PeproTech	200-04
Nigericin (sodium salt)	Cayman Chemical	11437
NLRP3 (D4D8T) Rabbit antibody	Cell Signaling Technology	15101
Pro-Caspase-1 and caspase-1 p10/p12 antibody	Abcam	CAD526
Interleukin-1β antibody	Abcam	ab9722
Beta-actin antibody	Cell Signaling Technology	4967
GAPDH (D16H11) XP Rabbit mAb	Cell Signaling Technology	5174
ASC antibody	Adipogen	AL177
Gasdermin-D Ab Monoclonal mouse Ab	Santa Cruz	sc-393581
Anti-rabbit HRP-conjugated antibody	Cell Signaling Technology	7074
Anti-mouse HRP-conjugated antibody	Cell Signaling Technology	7076
ELISA MAX™ Deluxe Set Human IL-1 beta	BioLegend	437004
TMRE	Thermo Fisher Scientific	T669
MitoTracker Greem FM	Thermo Fisher Scientific	M7514
MitoSOX Red	Thermo Fisher Scientific	M36008
Fluo-4-AM	Thermo Fisher Scientific	F14201
Hoecsht 33342	Thermo Fisher Scientific	62249

2,4-dinitrophenol (2,4-DNP)	Sigma Aldrich	D198501
CoralHue® Mitochondria-targeted mKeima-Red (pMT-mKeima-Red)	MBL Life Science	AM-V0251M
pLJM1-eGFP plasmid	Addgene	19319
pCMV-dR8.2 dvpr plasmid	Addgene	8455
pCMV-VSV-G plasmid	Addgene	8454
Digitonin	Sigma Aldrich	D141
Sodium pyruvate	Sigma Aldrich	P5280
Glutamate (L-Glutamic acid potassium salt monohydrate)	Sigma Aldrich	G1501
Malate (L-(-)-Malic acid)	Sigma Aldrich	M1000
ADP (Adenosine 5'-diphosphate sodium salt)	Sigma Aldrich	A2754
Cytochrome c (cytochrome c from equine heart)	Sigma Aldrich	C2506
Succinate (sodium succinate dibasic)	Sigma Aldrich	14160
Oligomycin	New England Biolabs	9996L
FCCP	Abcam	ab147482
Rotenone	Sigma Aldrich	R8875
Antimycin A	Sigma Aldrich	A8674
MiR05-Ki	Oroboros Instruments	60101-01
10 cm plastic tissue culture dishes	Sarstedt	83.3902
35 mm glass-bottom dishes	Mattek	P35G-1.0-14-C
TRIZol RNA isolation reagent	Thermo Fisher Scientific	15596026
High capacity cDNA reverse transcriptase kit	Thermo Fisher Scientific	4368814
Puromycin	Sigma Aldrich	P8833
Lipofectamine 2000	Thermo Fisher Scientific	11668019
Bradford Protein Dye Concentrate	Bio-Rad	5000006
Immun-Blot® PVDF Membrane	Bio-Rad	1620177
Opti-MEM reduced serum media	Thermo Fisher Scientific	31985070

Ru265	Sigma Aldrich	SML2991
PowerTracker SYBR Green Master Mix	Thermo Fisher Scientific	A46109

2.2 THP1 cell culture and PMA-induced macrophage differentiation

Human THP1 monocytic cells were purchased from the American Type Culture Collection (ATCC). THP1 monocytic cells were maintained between $2*10^5$ to $1*10^6$ cells/mL in RPMI 1640 supplemented with 10% FBS and 100U/mL penicillin and streptomycin (RPMI 1640-complete medium) in a 37°C and 5% CO_2 humidified cell culture incubator. THP1 cells were used for experiments with <5 passages and >95% viability. We found that THP1 cell lines which exceeded confluency or were over-passaged had variable responses to drug treatments (data not shown). To differentiate THP1 monocytic cells to macrophage-like cells, THP1 monocytic cells were plated with 50 nM PMA on 10 cm plastic tissue culture dishes (9*10^6 cells/dish) for all experiments except microscopy experiments, where THP1 cells were plated on 35 mm glass-bottom dishes (9*10^5 cells/dish). THP1 cells were incubated with PMA for 48 hours, PBS washed twice, then incubated for an additional 24 hours in fresh PMA-free RPMI 1640-complete medium prior to being treated with NLRP3 inflammasome priming (signal 1). After inflammasome priming, cells were washed twice with phenol red-free and FBS-free RPMI 1640 medium before adding inflammasome activation (signal 2) stimuli in phenol red-free and FBS-free RPMI 1640.

2.3 Trypan blue exclusion assay

THP1 monocytes or PMA-differentiated THP1 macrophages in 12-well plates (1 mL culture volume) were treated with vehicle or the indicated concentrations of 12,13-EpOME

or 12,13-DiHOME for 24 hours, with cells 90% confluent at harvest. To harvest THP1 monocytes for trypan blue exclusion assay, media containing cells was collected, and a 0.5 mL PBS wash was collected in the same tube. For THP1 macrophages, 0.2 mL Accutase was added after PBS washing to dissociated THP1 macrophages, then media+PBS wash was used to wash down and collect dissociated THP1 macrophages. 100 uL of Trypan blue solution was added to THP1 monocytes or macrophages, then trypan blue exclusion assay was performed by hemocytometer. Viable cells were trypan blue-negative while non-viable cells were trypan blue-positive. "Cell viability" was calculated as (viable cells / viable + non-viable cells). Gross number of viable cells indicated "proliferation".

2.4 Lentivirus infection and stable Mito-Keima expression in THP1 cells

The mito-Keima open reading frame from the CoralHue® Mitochondria-targeted mKeima-Red plasmid was subcloned into a pLJM1 empty vector backbone to make the pLJM1-mito-Keima transfer plasmid. Transfection complexes were formed by incubating 15000 ng pLJM1-mito-Keima plasmid, 6000 ng pCMV-dR8.2 dvpr packaging plasmid, 3000 ng pCMV-VSV-G envelope plasmid plus Lipofectamine 2000 Transfection Reagent in 750 µL Opti-MEM at room temperature for 30 minutes. Transfection complexes were incubated with wild-type HEK293T cells in T75 flasks with 10 mL DMEM supplemented with 10% FBS and 100U/mL each of penicillin and streptomycin (DMEM-complete) for 24 hours at 37°C, 5% CO_2. Thereafter, transfection complex-containing media was aspirated and cells were incubated in fresh DMEM-complete for an additional 24 hours to allow sufficient lentivirus production. Lentivirus-containing DMEM was collected, centrifuged at 500 x *g* for 5 minutes, then run through 0.45 µm PES syringe filters to remove all HEK293T

cells. THP1 monocytic cells were plated in 6-well tissue culture plates and grown to 40% confluency on the day of lentivirus infection, where cells were centrifuged and resuspended in 3 mL lentivirus-containing DMEM. THP1 monocytic cells were spinfected by centrifuging 6-well plates at 1000 x *g* for 45 minutes at 37°C, followed by 24 hour incubation. Infected THP1 cells were then centrifuged and resuspended in fresh RPMI 1640-complete medium and grown for another 24 hours before selecting for successfully transduced cells with 2 μg/mL puromycin. THP1 cells were transferred to T75 flasks after reaching 80-90% confluency and puromycin-selected for at least 4 days. THP1 Mito-Keima cells were then assessed for stable mito-Keima expression by fluorescence microscopy before growing several stocks for cryostorage and subsequent experiments.

2.5 Live-cell epifluorescence microscopy

For the last 30 minutes of inflammasome priming, THP1 macrophages were incubated with 0.5 μM Hoechst 33342 (nuclei), 50 nM TMRE (mitochondrial membrane potential), 100 nM MitoTracker Green FM (mitochondria independent of membrane potential), 2 μM MitoSOX Red (mitochondrial superoxide), or 2 μM Fluo-4-AM (cytosolic calcium) dyes at 37°C, 5% CO_2. Cells were subsequently washed twice and imaged in phenol red-free and FBS-free RPMI 1640 medium. For some experiments, 30 nM TMRE and/or 12.5 nM MitoTracker Green were included in the imaging medium to maintain consistent signal over time. For other experiments, Ru265 (25 μM) was added for the last 30 minutes of priming to sufficiently pre-load macrophages [215], then Ru265 was maintained in medium during the activation phase. Images were acquired using a Zeiss Axio Observer Z1

widefield epifluorescence microscope fitted with a microincubator (37°C, 5% CO2) and using a 40X/1.3NA oil DIC objective lens.

2.6 Macrophage polarization and quantitative real-time polymerase chain reaction

THP1 macrophages were treated for 24 hours with vehicle (M0 macrophages), 10 ng/mL LPS + 20 ng/mL interferon gamma (M1 macrophages), or 20 ng/mL interleukin-4 (M2 macrophages) in the absence or presence of 0.5 μM 12,13-DiHOME. Following macrophage polarization, media was aspirated from cells and 750 μL of TRIZol RNA isolation reagent was added directly to tissue culture dishes. Cells were scraped down in TRIZol while on ice, and transferred to a new microcentrifuge tube. Cells were homogenized in TRIZol by pipetting up and down until becoming a uniform suspension then incubating at room temperature for 10 minutes. 150 μL of chloroform was added to each tube and shaken vigorously by hand until becoming a uniform white-opaque suspension. TRIZol-chloroform cell mixture was incubated for 3 minutes at room temperature prior to phase separation by centrifugation at 12 000 x *g* for 15 minutes at 4°C. Subsequent steps were performed in RNase/DNase-free conditions. The upper aqueous layer was transferred to a new tube, then RNA was precipitated by adding 375 μL of room-temperature isopropanol and mixing by 10 inversions followed by incubation at room temperature for 10 minutes. RNA was pelleted by centrifugation at 12 000 x *g* for 10 minutes at 4°C, supernatant was discarded, and then the pellet was washed twice with 1 mL 75% ethanol. The RNA pellet was air dried for 15 minutes at room temperature prior to adding 80 μL of nuclease-free water for solubilization in a 55°C water bath for 15 minutes. 1 μg RNA was used for cDNA production using the High Capacity cDNA Reverse Transcriptase Kit. qPCR primers were designed with the

Integrated DNA Technologies (IDT) online quantitative real-time polymerase chain reaction (qPCR) Primer Design Tool (https://www.idtdna.com/scitools/Applications/RealTimePCR/default.aspx) and confirmed for specificity using Primer-BLAST (https://www.ncbi.nlm.nih.gov/tools/primer-blast/) [216]. Primer pairs were designed to either span exon-exon junctions or be separated by large introns to prevent non-specific DNA amplification. 10 µL qPCR reactions containing 1X PowerTrack™ SYBR Green Master Mix, 0.4 µM forward primer, 0.4 µM reverse primer, and 1 µL of 5X-diluted complementary DNA (cDNA) product were added to 96-well qPCR plates in triplicate. Real-time qPCR experiments were performed in a QuantStudio™ 3 Real-Time PCR System. cDNA was PCR amplified by 1 cycle of 95°C for 2 minutes followed by 40 cycles of 5-second 95°C denaturation and 30-second 60°C annealing/extension. PCR products were assessed for non-specific products by melt curve analysis (95°C denaturation for 15 seconds, 60°C annealing for 1 minute, then 0.075°C/second melt curve from 60°C to 95°C). Threshold cycle (Ct) values were obtained using QuantStudio™ data analysis software. Fold-RNA expression levels were calculated using the comparative Ct method relative to M0 macrophage Ct values and using *ACTB* as a housekeeping transcript control. Primer sequences are listed in **Table 2**.

Table 2. List of sequences for primers pairs used for macrophage polarization experiments.

Gene	**Refseq ID**	**Forward primer (5'-3')** **Reverse primer (5'-3')**
ACTB	NM_001101	CATTGGCAATGAGCGGTTC CTTTGCGGATGTCCACGT

HLA-DRA	NM_019111	CCTGGAAATCATGACAAAGCG AAACAGATGAGGACGTTGGG
TNF	NM_000594	ACTTTGGAGTGATCGGCC GCTTGAGGGTTTGCTACAAC
IL1B	NM_000576	ATGCACCTGTACGATCACTG ACAAAGGACATGGAGAACACC
NLRP3	NM_001079821	GTGTTTCGAATCCCACTGTG TCTGCTTCTCACGTACTTTCTG
CD163	NM_004244	GAGTCCCTTCACCATTACTGTG GACTTTCACTTCCACTCTCCC
IL10	NM_000572	CGCATGTGAACTCCCTGG TAGATGCCTTTCTCTTGGAGC
MRC1	NM_002438	GCAAAGTGGATTACGTGTCTTG CTGTTATGTCGCTGGCAAATG
MSR1	NM_002445	ACTGATTGCCCTTTACCTCC TCCTTTTCCCGTGAGACTTTG

2.7 High-resolution mitochondrial respirometry

An Oroboros-O2k high-resolution respirometer (OROBOROS Instruments, Innsbruck, Austria) was used to measure mitochondrial respiratory function in THP1 macrophages [217]. After treating THP1 macrophages with NLRP3 inflammasome priming stimuli (4.5 hours), cells were washed once with PBS and incubated with 2 mL Accutase Cell Dissociation Reagent for 10 minutes at 37°C. Cells were then washed down with 8 mL RPMI 1640-complete medium and centrifuged at 200 x *g* for 3 minutes. Cell pellets were PBS washed, re-centrifuged, then resuspended in mitochondrial respiration medium MiR05 (pH = 7.1, 0.5 mM EGTA, 3 mM $MgCl_2$, 60 mM potassium lactobionic acid, 20 mM taurine,

10 mM KH_2PO_4, 20 mM HEPES, 110 mM D-sucrose, 1 g/L fatty acid-free bovine serum albumin (BSA), dissolved in double-distilled H_2O (ddH_2O)). Cells were counted and $1.5*10^6$ cells were added to a total volume of 2 mL MiR05 within closed chambers at 37°C and 750 RPM stirrer speed. Cells were equilibrated in chambers for 15 minutes then respiration rate was recorded (basal respiration state). Cytosolic membranes were selectively permeabilized by adding 2 µM digitonin and incubated for 20 minutes prior to substrate-uncoupler-inhibitor titration (SUIT) protocol 008 [218] and measuring oxygen consumption rates (OCRs) at each respiratory state in the following order: (i) addition of 5 mM pyruvate and 2 mM malate (PM_L); (ii) addition of 2.5 mM adenosine diphosphate (ADP) to stimulate oxidative phosphorylation (OXPHOS) (PM_P); (iii) addition of 10 µM cytochrome *c* (c) to assess integrity of the mitochondrial outer membrane (PMc_P); (iv) addition of 10 mM glutamate to assess saturation of complex I pathway-mediated OXPHOS by pyruvate+malate (PMG_P); (v) addition of 10 mM succinate to stimulate maximum complex I+II-mediated OXPHOS ($PMGS_P$); (vi) 0.1 µM step-wise titrations with FCCP until reaching a maximal non-coupled respiration rate ($PMGS_E$); (vii) addition of 0.5 µM rotenone to inhibit complex I and induce maximum complex II-mediated non-coupled respiration (S_E); (viii) addition of 2.5 µM antimycin A to achieve residual oxygen consumption (ROX) respiration state. Reported O_2 flux values were obtained by subtracting ROX respiration from all respiration values and normalizing to cell count ([pmol O_2] / [sec * million cells]).

2.8 Immunoblotting

Following inflammasome priming and/or activation, media was collected in centrifuge tubes, cleared by centrifugation for 10 minutes at 500 x *g* and 4°C, then media

supernatants were aliquoted for storage at -80°C. THP1 macrophage cells were harvested by PBS washing cells prior to scraping cells in radioimmunoprecipitation assay (RIPA) cell lysis buffer (50 mM Tris (pH = 7.6), 150 mM NaCl, 1% Triton X-100, 0.5% sodium deoxycholate, 0.1% SDS plus Pierce Protease and Phosphatase Inhibitor Mini Tablet) before transferring to a new microcentrifuge tube. Cells were lysed by incubating with lysis buffer on ice for 40 minutes, vortexing for 5 seconds every 10 minutes. Insoluble cell debris was cleared by centrifugation at 18 000 x *g* for 10 min at 4°C, and supernatant was collected as whole-cell lysate. For some experiments, cell debris pellets were washed in RIPA buffer and further solubilized with RIPA + 8M urea buffer. Media supernatants (pre-cleared by centrifugation at 500 x *g* for 5 minutes at 4°C) were prepared for immunoblotting by methanol/chloroform precipitation [219]. Briefly, 500 µL media, 500 µL methanol, and 125 µL chloroform were vortexed for 30 seconds then phase separated by centrifugation at 13 000 x *g* for 5 minutes at room temperature. The upper aqueous phase was discarded and 500 µL methanol was added again to the microcentrifuge tube and vortexed for 10 seconds. Precipitated protein was pelleted by centrifugation at 13 000 x *g* for 5 minutes at room temperature. The supernatant was discarded, the protein pellet was air-dried for 10 minutes under chemical fume-hood flow, then pellets were reconstituted and boiled in 80 µL 1X Laemmli Sample Buffer. Whole-cell lysates and solubilized cell debris fractions were measured for protein concentration by Bradford assay, boiled in 1X Laemmli Sample Buffer, and 20 µg protein was loaded onto 4-20% gels for sodium dodecyl sulfate polyacrylamide gel electrophoresis (SDS-PAGE). For media supernatant fractions, equal volumes of sample were loaded onto SDS-PAGE gels. Samples were resolved by SDS-PAGE at room temperature prior to electrophoretic transfer onto Immun-Blot PVDF Membranes (0.2 µm

pore size). Membranes were blocked in tris-buffered saline tween solution (TBST; 50 mM Tris-HCl (pH = 7.6), 150 mM NaCl, 0.1% Tween-20) with 5% bovine serum albumin, then primary antibodies made in TBST + 5% BSA were incubated overnight (16-20 hours). Membranes were washed in TBST then incubated with secondary antibodies were made in TBST + 5% skim milk power. Primary and secondary antibodies used are listed in **Table 1**. Membranes were then washed prior to chemiluminescent detection using SuperSignal West Pico PLUS ECL reagent. Membranes were re-probed by incubation with stripping buffer (1.5% glycine, 0.1% SDS, 1% Tween-20, pH = 2.2) followed by 1 hour re-blocking before proceeding with further immunoblotting. Images were acquired using a ChemiDoc MP Imaging System, and densitometric analysis was conducted using ImageJ software.

2.9 Interleukin-1β enzyme-linked immunosorbent assay

Enzyme-linked immunosorbent assay (ELISA) for IL-1β was performed according to kit protocol. Briefly, the ELISA MAX™ Deluxe Set Human IL-1 beta kit (BioLegend), a sandwich ELISA kit, was used. All incubations were conducted with rotary shaking at 500RPM with a 0.3 cm circular orbit. 96-well plates were coated the capture antibody overnight, washed, and blocked for 1 hour at room temperature. The same media supernatant samples used for immunoblotting were prepared with assay buffer diluent and an IL-1β standard curve was prepared. Samples and IL-1β standards were incubated for 2 hours at room temperature, washed, then incubated with biotinylated detection antibody for 1 hour at room temperature. After washing, avidin horseradish peroxidase (avidin-HRP) was incubated for 30 minutes at room temperature, then, after a final wash, 3,3',5,5'-

tetramethylbenzidine (TMB) substrate was added and incubated for 10 minutes. Stop solution was added, then absorbance at 450 nm was immediately read thereafter.

2.10 Statistical analysis

Statistical analyses were conducted using GraphPad Prism software. Data was graphed as mean +/- sampling error of the mean (SEM) and statistical tests and parameters used are stated in figure legends. Briefly, one-sample t-tests were used to assess if means, expressed as fold-changes relative to a control set to "1", were significantly different from a hypothetical mean of 1.0. Two-sample unpaired t-tests were used to assess if two means were significantly different. One-way analysis of variance (ANOVA) with Dunnett's post-hoc test was used to compare two or more means to a control mean. *$P<0.05$ was considered statistically significant. Individual data points on graphs represent independent experiments conducted on separate days.

CHAPTER 3. RESULTS

3.1 PMA-differentiated THP1 macrophage model

First, we established an *in vitro* macrophage model using the immortalized human monocytic leukemia-derived cell line, THP1. THP1 monocytic cells can be differentiated into macrophage-like cells using the protein kinase C-activator, PMA. A minimal PMA concentration (50 nM) was used to treat THP1 monocytic cells for 48 hours, followed by a 24-hour PMA-free rest incubation to minimize a basal pro-inflammatory macrophage phenotype **(Figure 3.1A)** [220]. 50 nM PMA induced complete adherence of THP1 cells after 48-hour treatment **(Figure 3.1B)** and was the minimum concentration required to prevent cells from detaching from tissue culture plates after the 24-hour PMA-free rest incubation (**Figure 3.1C**). As well, 50 nM PMA-differentiated macrophages expressed monocyte-to-macrophage differentiation markers *CD14* and *CD36* [221], and these markers were not further enhanced with a higher PMA concentration **(Figure 3.1D-E)**.

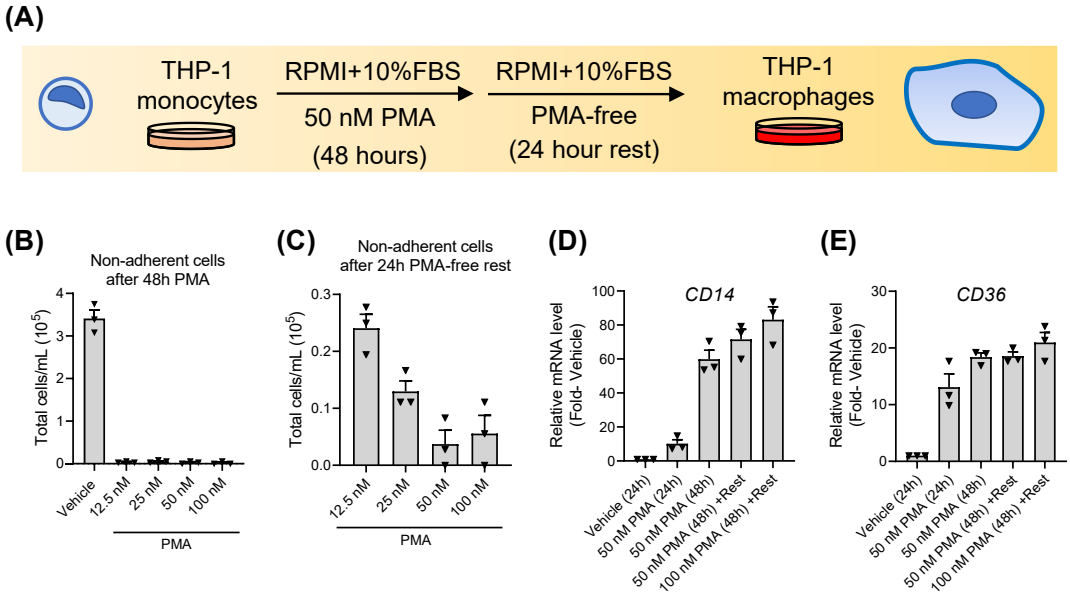

Figure 3.1. *PMA-differentiated THP1 macrophage model.* Human monocytic THP1 cells were differentiated into macrophage-like cells using phorbol myristate acetate (PMA). **(A)** Standard PMA-differentiation protocol used to produce THP1 macrophages throughout this study. **(B)** Total non-adherent cells in media plus one PBS wash were counted by hemocytometer following 48-hour treatment with the indicated PMA concentrations. **(C)** Non-adherent cells treated with the indicated PMA concentration for 48-hours plus a 24-hour PMA-free rest incubation were counted as in **(B)**. Monocyte-to-macrophage differentiation markers **(D)** *CD14* and **(E)** *CD36* mRNA expression was measured by qPCR after the indicated PMA-differentiation treatments. All graphs represent mean+/-SEM (n=3).

3.2 12,13-EpOME and 12,13-DiHOME do not affect THP1 cell viability or proliferation

Previously, we found that 12,13-DiHOME was cytotoxic to cardiomyocyte cells at concentrations as low as 10 nM, and 12,13-EpOME's apparent cytotoxicity at 10 nM was attributed to its conversion into 12,13-DiHOME [159]. We decided to measure the effects of 12,13-EpOME and 12,13-DiHOME on cell viability and proliferation of undifferentiated THP1 monocytes **(Figure 3.2A)** or PMA-differentiated THP1 macrophages **(Figure 3.2B)** by trypan blue exclusion assay. Interestingly, 12,13-EpOME at concentrations from 500 nM to 2000 nM did not induce changes in trypan blue-negative cells **(Figure 3.2C)** nor the gross number of viable cells **(Figure 3.2D**), indicating that 12,13-EpOME does not affect THP1 monocyte cell viability nor proliferation by treatment at these concentrations for 24 hours. Furthermore, 24-hour treatment with 10 nM to 2000 nM 12,13-DiHOME also did not affect THP1 monocyte cell viability **(Figure 3.2E)** or proliferation **(Figure 3.2F)**. Similar observations were made when treating PMA-differentiated THP1 macrophages with 12,13-EpOME **(Figure 3.2G-H)** or 12,13-DiHOME **(Figure 3.2I-J)**. Overall, these data suggest that 12,13-EpOME or 12,13-DiHOME, at concentrations up to 2 μM, do not have cytotoxic or anti-proliferative effects on THP1 monocytes or macrophages. These data also aid to the observation that 12,13-EpOME and 12,13-DiHOME have a wide variety or even opposite bioactivities that are seemingly cell-, tissue-, and concentration-dependent [158].

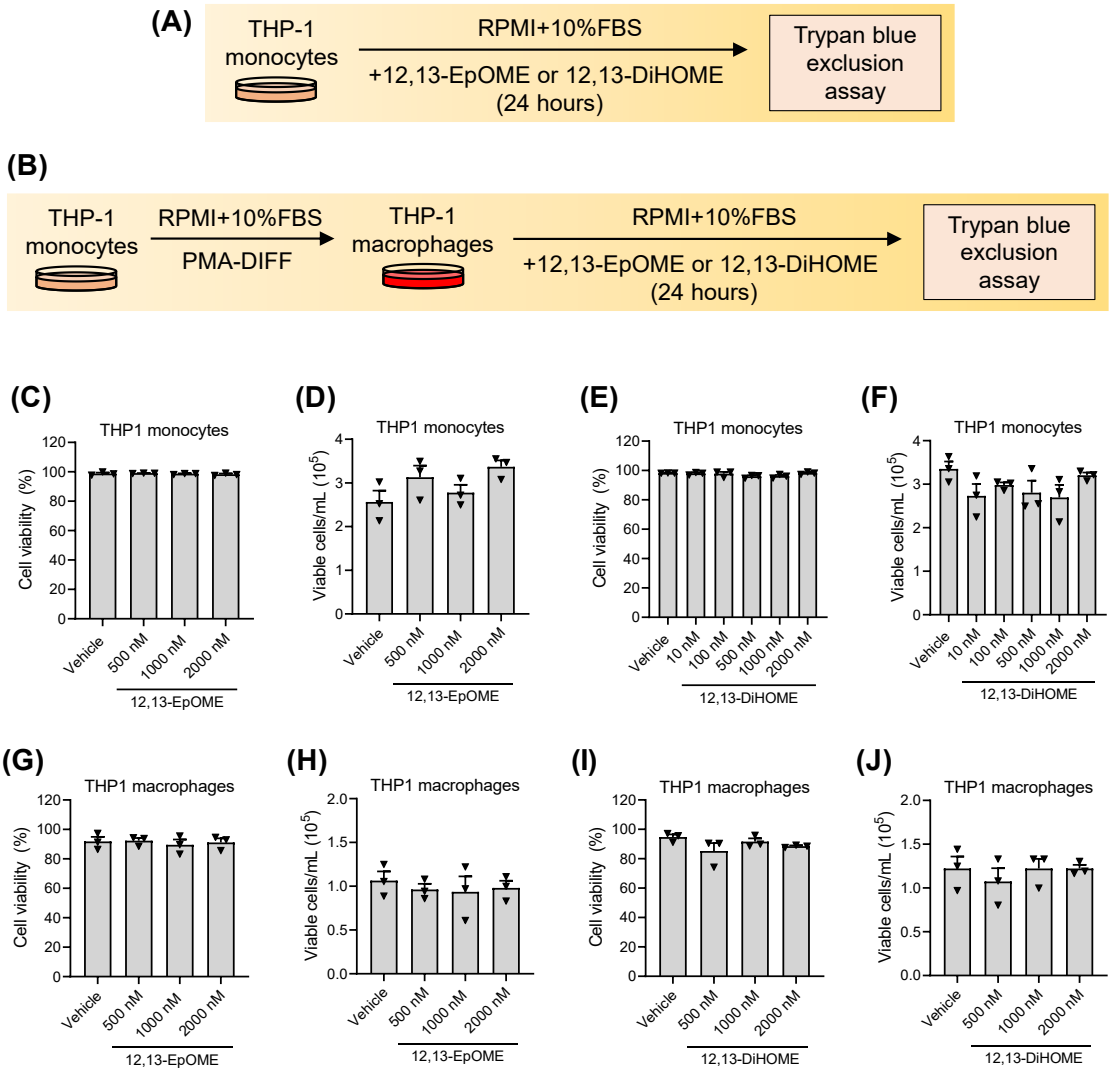

Figure 3.2. *12,13-EpOME and 12,13-DiHOME do not affect THP1 cell viability or proliferation.* Undifferentiated THP1 monocytes **(A, C-F)** or PMA-differentiated THP1 macrophages **(B, G-J)** were treated with the indicated concentrations of 12,13-EpOME **(C-D, G-H)** or 12,13-DiHOME **(E-F, I-J)** for 24 hours then assessed for changes in cell viability (% trypan blue-negative cells) **(C,E,G,I)** or proliferation (viable cells/mL) **(D,F,H,J)**. Graphs represent means+/-SEM (n=3). *P<0.05 compared to vehicle using one-way ANOVA with Dunnett's post-hoc test.

3.3 12,13-DiHOME exacerbates inflammatory cytokine expression in polarized macrophages

Macrophages characteristically differentiate (or "polarize") into a phenotype appropriate for a given stimuli [46]. For instance, macrophages may polarize into a pro-inflammatory/tissue-damaging "M1" macrophage phenotype or an anti-inflammatory/tissue-reparative "M2" macrophage phenotype depending on the phase of inflammatory tissue injury [214]. We tested whether 12,13-DiHOME had effects on macrophage polarization in our THP1-derived macrophage model **(Figure 3.3A)**. THP1 macrophages were treated with prototypical M0 (vehicle), M1 (10 ng/mL LPS + 20 ng/mL IFNγ), or M2 (20 ng/mL IL-4) polarization stimuli in the absence or presence of 0.5 μM 12,13-DiHOME for 24 hours, then we measured mRNA expression levels of classical M1- and M2-associated polarization markers by qPCR [221,222]. As expected, we observed strong induction of M1-associated antigen presentation genes (*HLA-DRA*) **(Figure 3.3B)** and inflammatory cytokine genes (*IL1B, TNF*) **(Figure 3.3C-D)** and a small induction of *NLRP3* of the NLRP3 inflammasome pathway (shown to be upregulated in LPS- and IFNγ-treated M1 macrophages [222]) relative to M0 macrophages, although this trend was non-significant **(Figure 3.3E)**. Unexpectedly, we did not observe upregulation of typical M2-associated markers (*CD163, IL10, MRC1, MSR1*) in M2-polarized macrophages compared to M0 macrophages **(Figure 3.3F-I)**. Indeed, THP1 macrophages have been observed to respond to M1 polarization stimuli similarly to more physiological models like *in vitro* human monocyte-derived macrophages, but these two models responded differently to treatment with M2 polarization stimuli [223]. This is further supported by the observation that M1-polarized THP1 macrophages had reduced expression of all M2-associated markers **(Figure**

3.3F-I), but M2-polarized macrophages did not have reduced expression of all M1-associated markers except for *NLRP3* **(Figure 3.3B-E)**.

12,13-DiHOME co-treatment with polarization stimuli did not induce further changes in *HLA-DRA* **(Figure 3.3B)**, *NLRP3* **(Figure 3.3E)**, *CD163* **(Figure 3.3F)**, *IL10* **(Figure 3.3G)**, or *MRC1* **(Figure 3.3H)** expression in M0, M1, or M2-polarized macrophages. Intriguingly, *TNF* was exacerbated by 12,13-DiHOME co-treatment in M0, M1, and M2-polarized macrophages **(Figure 3.3C)**, as was and *IL1B* in M0 and M2-polarized macrophages **(Figure 3.3D)**. This was in line with a recent abstract suggesting that 12,13-DiHOME mediated changes in pro-inflammatory macrophage polarization by increasing the number of IL-1β^+ cells [185]. Furthermore, 12,13-DiHOME increased expression of the phagocytic receptor and M2 marker *MSR1* in M1 polarized macrophages **(Figure 3.3I)**. Overall, these data suggest that 12,13-DiHOME could be pro-inflammatory in THP1 macrophages by exacerbating pro-inflammatory cytokine and phagocytic receptor gene expression during macrophage polarization. As well, THP1 macrophages may not be suitable as a classical M2 macrophage polarization model.

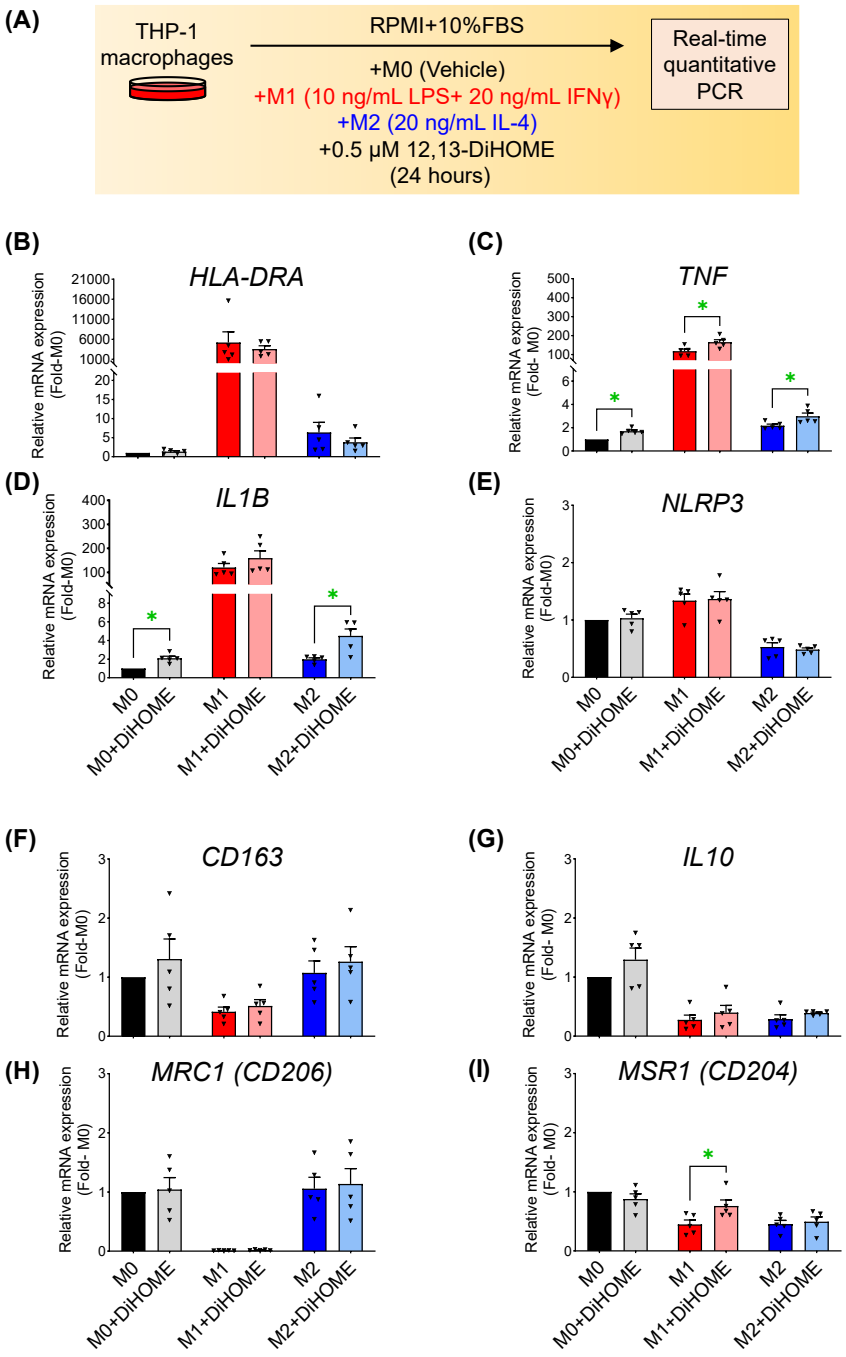

Figure 3.3. *12,13-DiHOME exacerbates inflammatory cytokine expression in polarized macrophages*. THP1 macrophages were subjected to the indicated polarization treatments **(A)** for 24 hours, with or without the presence of 0.5 μM 12,13-DiHOME. M1 macrophage markers **(B-E)** and M2 macrophage markers **(F-I)** were measured by qPCR. Bars represent mean+/-SEM. *P<0.05 vs. the indicated treatment group using one-sample t-test compared to a hypothetical mean of "1.0" or using unpaired t-test (n=5).

3.4 NLRP3 inflammasome priming and activation model in THP1 macrophages

Modelling the NLRP3 inflammasome in THP1 macrophages has been successfully performed in other studies [224,225]. To prime the NLRP3 inflammasome, we used the Gram-negative bacterial cell wall component LPS, a common treatment in systemic endotoxemia/sepsis models and a TLR4 ligand which leads to downstream NF-κB-controlled gene induction and post-translational events necessary for NLRP3 inflammasome priming [86,214]. We chose 10 ng/mL LPS treatment (4.5 hours), which was the maximal concentration that did not reduce cell viability indicated by trypan blue exclusion assay in 50 nM PMA-differentiated THP1 macrophages **(Figure 3.4A)**. After priming THP1 macrophages with LPS, we treated cells with 10 μM of the bacterial toxin nigericin (30 minutes), a known K^+/H^+ ionophore that leads to cytosolic K^+ efflux and potent NLRP3 inflammasome activation [103]. The combination of 10 ng/mL LPS-priming (4.5 hours) and 10 μM nigericin-activation (30 minutes) consists of the complete NLRP3 inflammasome activation protocol, and NLRP3 inflammasome activation markers can be assessed by immunoblotting cell lysates and media supernatants **(Figure 3.4B)**. As expected, immunoblots of non-primed and non-activated THP1 macrophage cell lysates exhibited constitutively expressed NLRP3 and pro-caspase-1 **(Figure 3.4C)**. However, there was no detectable mature caspase-1 (indicated by the caspase-1 p10 subunit) or pro-IL-1β in cell lysates, nor mature IL-1β or mature caspase-1 detected in media supernatants of these cells. NLRP3 inflammasome activation by nigericin treatment in non-primed THP1 macrophages led to no detectable pro-IL-1β in cell lysates or mature IL-1β in media supernatants but did induce some mature caspase-1 in cell lysates and media supernatants. This suggests that PMA-differentiated THP1 macrophages are basally primed for low levels of NLRP3

inflammasome activation but lack release of mature IL-1β in this manner. This is further supported by the release of cytosolic glyceraldehyde 3-phosphate dehydrogenase (GAPDH) into media supernatant fractions by nigericin treatment alone, indicative of lytic cell death likely induced by pyroptosis downstream of NLRP3 inflammasome activation. THP1 macrophages treated with LPS-priming alone led to robust NLRP3 and pro-IL-1β expression but did not induce caspase-1 cleavage in cell lysates nor release of mature IL-1β, caspase-1, or GAPDH into media supernatants. Lastly, the combination of LPS-priming and nigericin-induced NLRP3 inflammasome activation led to induction of NLRP3, pro-IL-1β, and mature caspase-1 in cell lysates, increased release of mature IL-1β into media supernatants, as well as severe cell lysis indicated by mature caspase-1 and GAPDH released into media supernatants. It is important to note that mature IL-1β was only detected in media supernatant fractions and not cell lysate fractions (data not shown), suggesting that once processed by caspase-1, mature IL-1β is rapidly secreted. Overall, LPS-priming induces NLRP3 and pro-IL-1β protein expression without changes in pro-caspase-1, then nigericin treatment leads to robust proteolytic processing of pro-caspase-1 into its mature and active form (indicated by the caspase-1 p10 subunit), proteolytic processing of pro-IL-1β into mature IL-1β (likely mature caspase-1-mediated), and release of cytosolic proteins indicating cell lysis (presumably due to pyroptosis). Thus, the combination of LPS-priming and subsequent nigericin treatment led to the presence of canonical markers for NLRP3 inflammasome activation in THP1 macrophages, most importantly by the induction of mature caspase-1 in cell lysates and mature IL-1β in media supernatants.

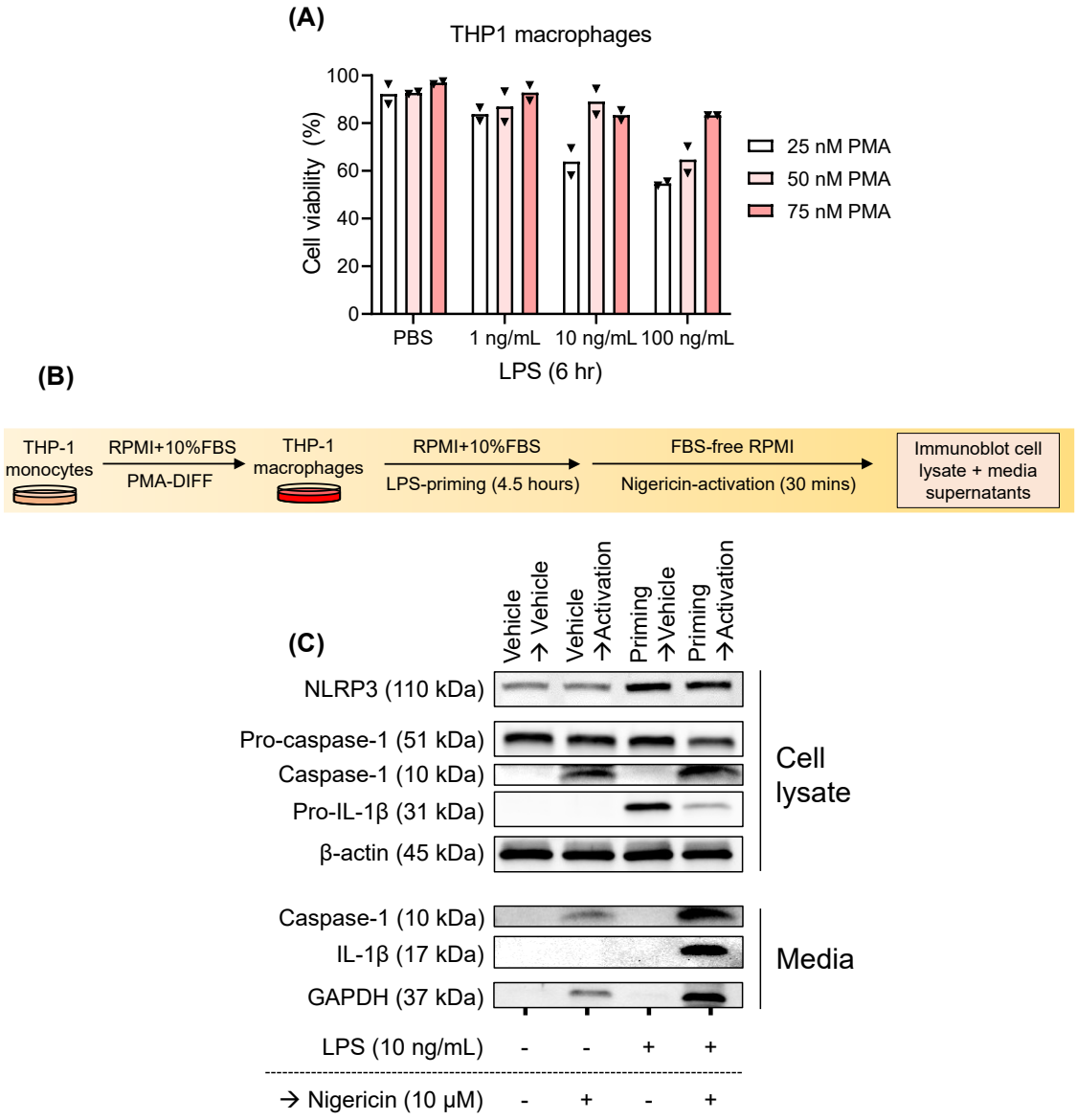

Figure 3.4. *NLRP3 inflammasome priming and activation model in THP1 macrophages.* **(A)** THP1 macrophages were subjected to the indicated PMA concentrations for differentiation and subsequent lipopolysaccharide (LPS) treatments to first establish a non-cytotoxic concentration to use during inflammasome priming. Bars represent mean (n=2). **(B)** The full NLRP3 inflammasome priming and activation protocol. **(C)** Representative immunoblots of cell lysates and media supernatants from THP1 macrophages treated with different combinations of the indicated LPS-priming and/or activation stimuli, probing for indicators of NLRP3 inflammasome activation (caspase 1 p10 in cell lysates, IL-1β p17 in media, and GAPDH in media).

3.5 12,13-DiHOME present during LPS-priming exacerbates nigericin-induced NLRP3 inflammasome activation

We next sought to investigate whether 12,13-DiHOME could modulate NLRP3 inflammasome activation in THP1 macrophages. Considering that low nanomolar concentrations of 12,13-DiHOME have visible effects on myocardial inflammation, cardiomyocyte cytotoxicity, and mitochondrial damage on the time scale of hours [159], we decided to treat THP1 macrophages with increasing concentrations of 12,13-DiHOME during the 4.5 hour-long LPS-priming phase **(Figures 3.5.1A-B and 3.5.2A)**. Interestingly, co-treating with increasing concentrations of 12,13-DiHOME (10 nM to 2 μM) during LPS-priming led to exacerbated nigericin-induced NLRP3 inflammasome activation in a concentration-dependent manner. As low as 0.5 μM 12,13-DiHOME led to significantly increased cleavage of caspase-1 in cell lysates **(Figure 3.5.1C)** as well as release of mature IL-1β into media supernatants **(Figure 3.5.1D)**. Furthermore, immunoblots of mature IL-1β in media supernatants were corroborated by measuring IL-1β in media supernatants by ELISA, which showed an identical trend to the immunoblots (**Figure 3.5.1E)**. Increasing concentrations of 12,13-DiHOME with LPS-priming did not exacerbate protein levels of NLRP3 **(Figure 3.5.2B)**, pro-caspase-1 **(Figure 3.5.2C)**, or pro-IL-1β **(Figure 3.5.2D)** in cell lysates. Additionally, inflammasome priming with a maximal concentration of 2 μM 12,13-DiHOME alone without LPS and nigericin treatment did not lead to NLRP3 **(Figure 3.5.2B),** pro-caspase-1 **(Figure 3.5.2C)**, or pro-IL-1β induction **(Figure 3.5.2D)** in cell lysates, suggesting that 12,13-DiHOME is not an inflammasome priming stimulus by promoting inflammasome protein expression. 12,13-DiHOME-priming alone without nigericin treatment also did not lead to detectable mature caspase-1 p10 subunit in cell

lysates **(Figure 3.5.1C)** nor release of mature IL-1β into media supernatants **(Figure 3.5.1D-E)**, indicating that 12,13-DiHOME alone is not a sufficient activator of the NLRP3 inflammasome in THP1 macrophages. As 0.5 μM 12,13-DiHOME present during LPS-priming was the lowest concentration we tested that significantly increased NLRP3 inflammasome activation markers, we used this concentration in all subsequent experiments.

From the insoluble pellet obtained after lysing THP1 macrophages with conventional RIPA buffer, we reconstituted an this "cell debris" fraction using RIPA buffer supplemented with 8M urea **(Figure 3.5.3A-B)**. We speculated that NLRP3 and ASC, as part of the large and more-insoluble multimeric NLRP3 inflammasome complexes, as well as pyroptotic pores formed by the N-terminal product of cleaved GSDMD (N-GSDMD) targeted to plasma membrane, would be enriched in cell debris fractions following nigericin-induced NLRP3 inflammasome activation and pyroptosis. Indeed, NLRP3 **(Figure 3.5.3C)** was significantly increased and ASC **(Figure 3.5.3D)** and N-GSDMD **(Figure 3.5.3E)** were only detectable in cell debris fractions from cells treated with the combination of LPS-priming and nigericin-induced NLRP3 inflammasome activation. Supporting our observations in cell lysates and media supernatant fractions **(Figure 3.5.1 - 3.5.2)**, by priming macrophages with both LPS and 0.5 μM 12,13-DiHOME, NLRP3 in cell debris fractions were not increased **(Figure 3.5.3C)**, but nigericin-induced levels of ASC **(Figure 3.5.3D)** and N-GSDMD **(Figure 3.5.3E)** in cell debris fractions were exacerbated compared to macrophages primed with LPS alone. Overall, 12,13-DiHOME present during LPS-priming exacerbated nigericin-induced NLRP3 inflammasome activation, as indicated by multiple markers in different protein fractions.

We then asked whether 12,13-EpOME, the LA epoxide precursor of 12,13-DiHOME, would have similar effects to 12,13-DiHOME on NLRP3 inflammasome activation, and if so, whether this activity would be dependent upon hydrolysis of 12,13-EpOME into 12,13-DiHOME by sEH. To investigate this, we treated THP1 macrophages with different combinations of a maximal concentration of 12,13-EpOME (2 μM), a minimal concentration of 12,13-DiHOME (0.5 μM), and the sEH inhibitor t-AUCB (200 nM) during the LPS-priming phase **(Figure 3.5.4 - 3.5.5)**. t-AUCB has been used in previous studies to negate endogenous sEH-mediated conversion of 12,13-EpOME to 12,13-DiHOME, demonstrating that 12,13-DiHOME is the dominantly bioactive metabolite [159,165]. sEH inhibitors have also been assessed in clinical trials targeting obesity and pre-diabetes [226]. As before, 0.5 μM 12,13-DiHOME present during LPS-priming exacerbated nigericin-induced mature caspase-1 levels in cell lysates **(Figure 3.5.4C)** and mature IL-1β in media supernatants **(Figure 3.5.4D)**. Surprisingly, 12,13-EpOME treatment alone, sEH inhibition with t-AUCB alone, or t-AUCB co-treated with 12,13-EpOME during LPS-priming had no effects on nigericin-induced NLRP3 inflammasome activation, and 12,13-DiHOME was also not affected by sEH inhibition with t-AUCB **(Figure 3.5.4C-D)**. Likewise, no treatment exacerbated NLRP3 **(Figure 3.5.5A)**, pro-caspase-1 **(Figure 3.5.5B)**, or pro-IL-1β **(Figure 3.5.5C)** expression in cell lysates. In summary, these data suggest that (1) 12,13-DiHOME is the predominantly bioactive linoleic acid metabolite of the CYP epoxygenase-sEH-pathway in exacerbating NLRP3 inflammasome activation compared to 12,13-EpOME, (2) that 12,13-DiHOME-enhanced NLRP3 inflammasome activation is not sEH-dependent, and (3) that THP1 macrophages do not convert 12,13-EpOME into sufficiently bioactive levels of 12,13-DiHOME *via* endogenous sEH-mediated hydrolysis.

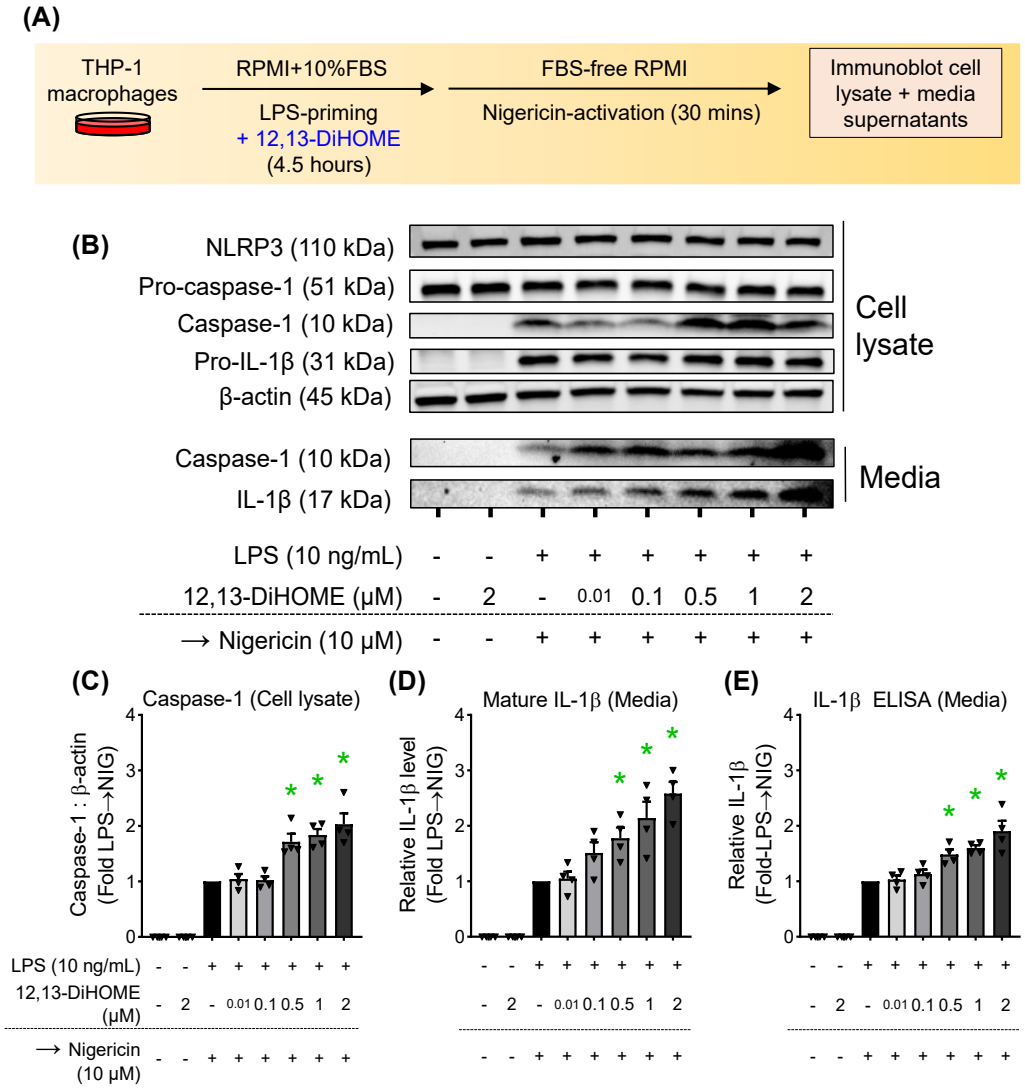

Figure 3.5.1. *12,13-DiHOME present during LPS-priming exacerbates nigericin-induced NLRP3 inflammasome activation*. **(A)** Simplified NLRP3 inflammasome priming (with or without 12,13-DiHOME) and activation protocol. **(B)** Representative immunoblots of cell lysates and media supernatants from THP1 macrophages subjected to the indicated priming stimuli (above dashed line) and subsequent NLRP3 inflammasome activation stimuli (below dashed line). Densitometric analysis of active caspase-1 (p10) in cell lysates **(C)**, mature IL-1β (p17) in media **(D)**, and confirmatory enzyme-linked immunosorbent assay (ELISA) measuring IL-1β in media **(E)** were performed. Bars represents mean+/-SEM. *P<0.05 vs. black bar using one-way ANOVA with Dunnett's post-hoc test (n=4).

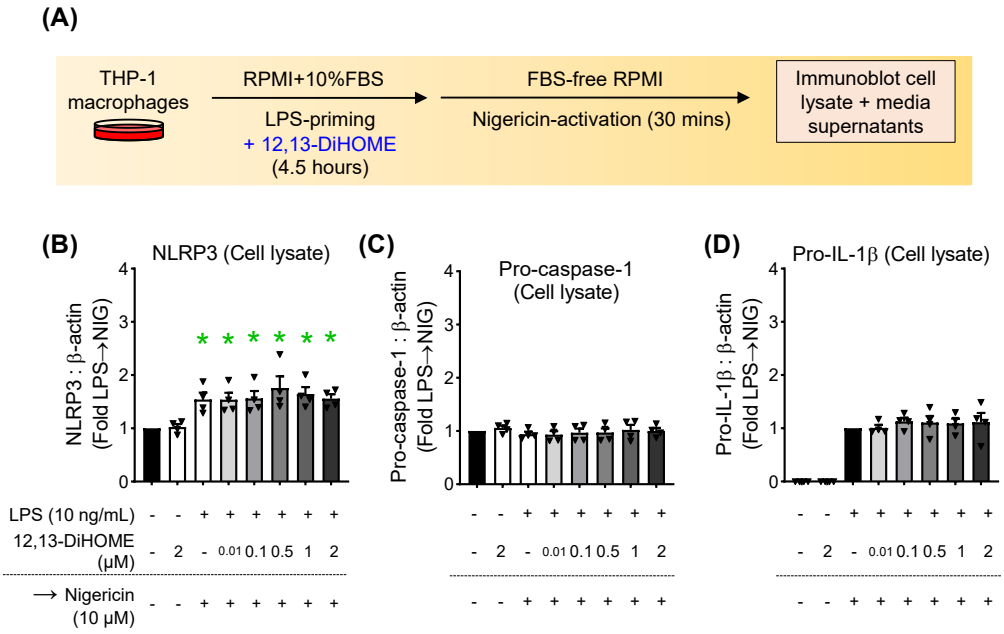

Figure 3.5.2. *Additional densitometric analyses of samples from Figure 3.5.1.* The same samples from the experiment in Figure 3.5.1 **(A)** were subjected to additional immunoblotting. Densitometric analyses of NLRP3 **(B)**, pro-caspase-1 (p51) **(C)**, and pro-IL-1β (p31) **(D)** in cell lysates were performed. Bars represent mean+/-SEM. *P<0.05 vs. black bar using one-way ANOVA with Dunnett's post-hoc test (n=4).

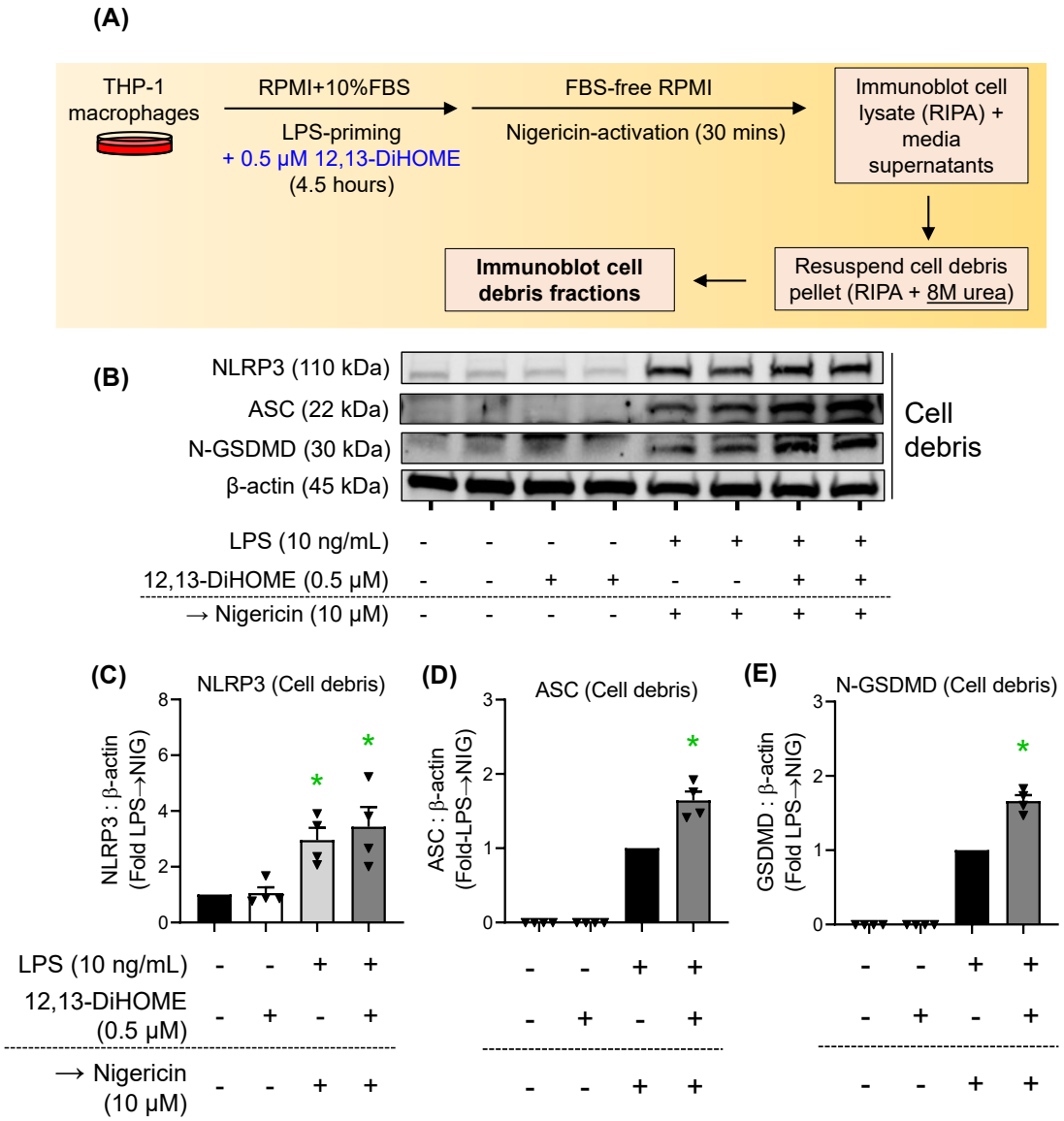

Figure 3.5.3. *Immunoblotting cell debris fractions of samples from Figure 3.5.1.* **(A)** Cell debris fractions from the indicated treatment groups **(B)** from the experiment in Figure 3.5.1 were subjected to immunoblotting (loaded onto SDS-PAGE gels as pairs of individual replicates per treatment group). Densitometric analyses of NLRP3 **(C)**, ASC **(D)**, and N-terminal product of cleaved gasdermin-D (N-GSDMD) **(D)** in cell debris fractions were performed. Bars represent mean+/-SEM.*P<0.05 vs. black bar using one-way ANOVA with Dunnett's post-hoc test (n=4).

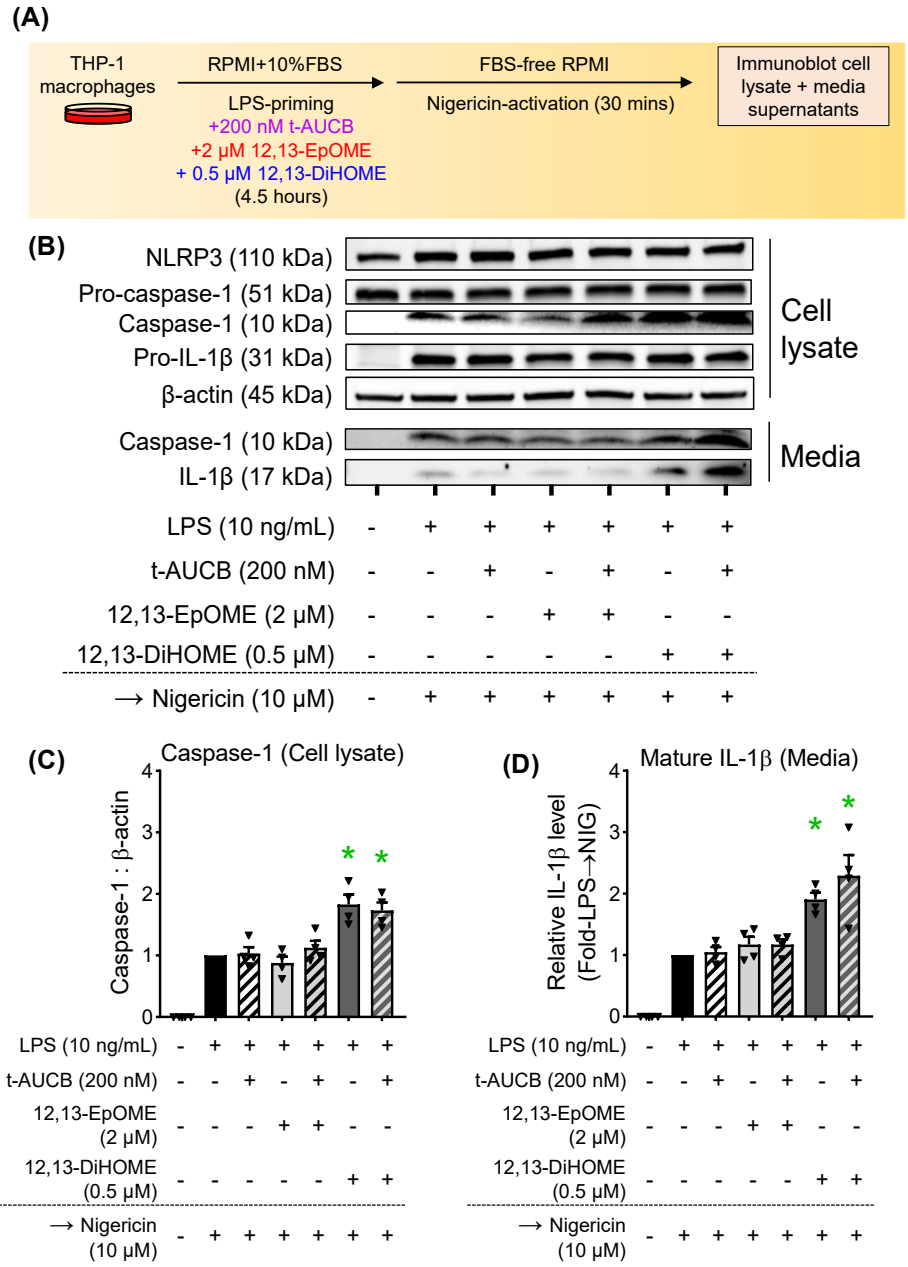

Figure 3.5.4. *12,13-DiHOME is the bioactive metabolite in exacerbating NLRP3 inflammasome activation.* **(A)** Soluble epoxide hydrolase inhibitor, t-AUCB, 12,13-EpOME, or 12,13-DiHOME were included during LPS-priming prior to NLRP3 inflammasome activation. **(B)** Representative immunoblots of cell lysate and media fractions from THP1 macrophages treated with the indicated priming (above dashed line) and activation (below dashed line) stimuli. Densitometric analyses of caspase-1 (p10) in cell lysates **(C)** and IL-1β (p17) in media **(D)** were performed. Bars represent mean+/-SEM. *P<0.05 vs. black bar using one-way ANOVA with Dunnett's post-hoc test (n=4).

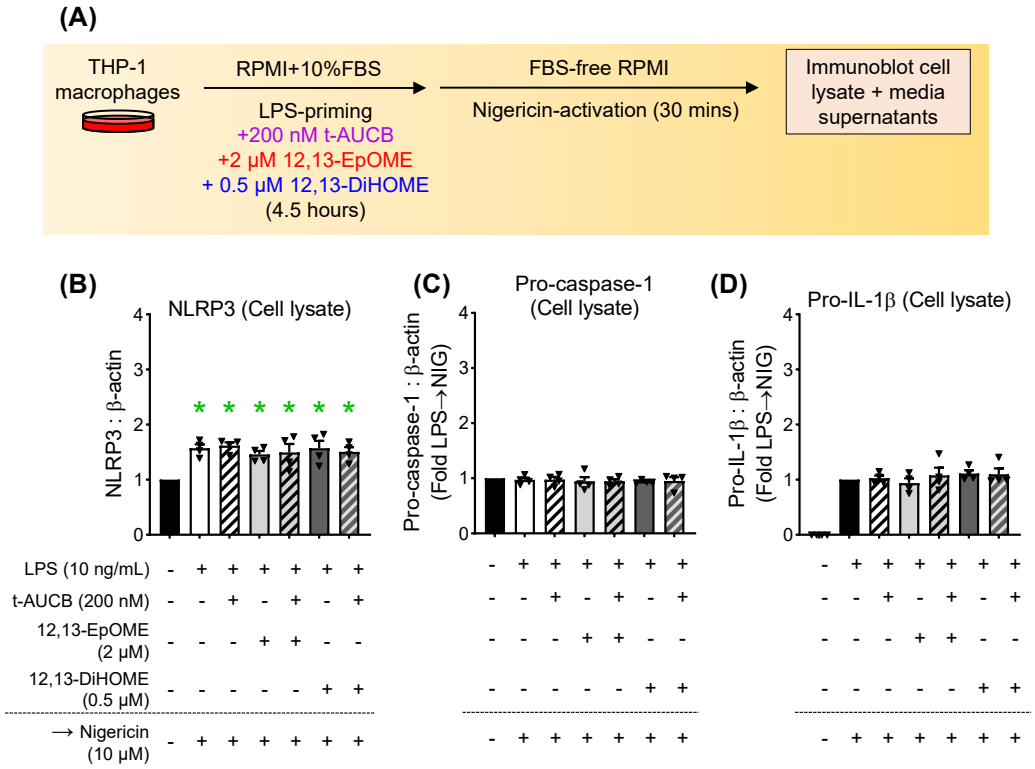

Figure 3.5.5. *Additional densitometric analyses of samples from Figure 3.5.4.* The same samples from the experiment in Figure 3.5.4 **(A)** were subjected to additional immunoblotting. Densitometric analyses of NLRP3 **(B)**, pro-caspase-1 (p51) **(C)**, and pro-IL-1β (p31) **(D)** in cell lysates were performed. Bars represent mean+/-SEM. *P<0.05 vs. black bar using one-way ANOVA with Dunnett's post-hoc analysis (n=4).

3.6 12,13-DiHOME induces mitochondrial uncoupling and reduces spare respiratory capacity during LPS-priming

As 12,13-DiHOME present during LPS-priming exacerbated nigericin-induced NLRP3 inflammasome activation, we asked what cellular effects 12,13-DiHOME might induce during inflammasome priming but prior to the addition of the NLRP3 inflammasome activator nigericin. First, we assessed NLRP3 inflammasome protein expression immediately after priming **(Figure 3.6.1A-B)**. Supporting our observations **(Figure 3.5.2 and 3.5.5)**, priming with 0.5 μM 12,13-DiHOME alone did not induce significant differences in the protein expression of NLRP3 **(Figure 3.6.1C)**, ASC **(Figure 3.6.1D)**, pro-caspase-1 **(Figure 3.6.1E)**, nor pro-IL-1β **(Figure 3.6.1F)** in cell lysates relative to vehicle-primed THP1 macrophages. Similarly, LPS+12,13-DiHOME-primed THP1 macrophages did not have exacerbated expression of these proteins relative to cells primed with LPS alone. These data suggest that 12,13-DiHOME does not affect NLRP3 inflammasome priming *via* changes in NLRP3 inflammasome protein expression prior to nigericin-induced inflammasome activation.

Damaged mitochondria are well-known to promote NLRP3 inflammasome activation through effects during both inflammasome priming and activation. Damaged mitochondria are involved *via* mechanisms such as release of intracellular DAMPs like mtROS and mtDNA, as well as through physical interactions between NLRP3 and externalized mitochondrial cardiolipin or mitochondrial outer membrane proteins [86]. As 12,13-DiHOME induced marked mitochondrial respiratory dysfunction in cardiomyocytes [159], we hypothesized that 12,13-DiHOME present during LPS-priming might mediate these effects in THP1 macrophages to promote nigericin-induced NLRP3 inflammasome

activation. After priming THP1 macrophages with vehicle, 12,13-DiHOME, LPS, or LPS+12,13-DiHOME, we measured mitochondrial respiratory function using an Oroboros-O2k high-resolution respirometry system and mitochondrial substrate-uncoupler-inhibitor titrations to attain oxygen consumption rates (OCRs) at different mitochondrial respiratory states **(Figure 3.6.2A-C and 3.6.3A-B)**.

After treating THP1 macrophages with priming stimuli, adding these cells directly into the chamber allows measurement of basal respiration. In this respiration state, THP1 macrophages have fully intact mitochondrial respiratory pathways and are reliant on endogenous substrates and basal respiratory demand [217]. Here, we observed no differences in basal respiration rates by 12,13-DiHOME, LPS, nor LPS+12,13-DiHOME **(Figure 3.6.3Bi)**.

Digitonin is added to the chamber to selectively permeabilize the cytosolic membrane without permeabilizing mitochondrial membranes. This allows (i) the depletion of endogenous mitochondrial respiratory substrates, (ii) the direct access of exogenously-added substrates to the mitochondria, and (iii) preservation of *in situ* intracellular interactions of mitochondria [217]. Following digitonin permeabilization, saturating concentrations of complex I substrates pyruvate (P) and malate (M) were added to chambers to induce the complex I-mediated LEAK state, or "PM_L" state. In this respiratory state, oxygen consumption is dependent mainly on ATP synthesis-independent complex I substrate oxidation, due to downstream processes such as proton "slip" and "leak" or electron leak resulting in mtROS formation, as there is no endogenous ADP available for conversion into ATP by ATP synthase once cells are permeabilized by digitonin [217]. THP1 macrophages

primed with LPS had increased PM_L respiration, but no further changes were mediated by 12,13-DiHOME present during inflammasome priming **(Figure 3.6.3Bii)**.

Next, exogenous ADP at a saturating concentration was added to induce a maximal state of oxidative phosphorylation (OXPHOS) *via* complex I, called the "PM_P" respiratory state. Interestingly, 12,13-DiHOME-primed THP1 macrophages had reduced PM_P respiration compared to vehicle-primed macrophages, and LPS-primed macrophages had significantly higher PM_P respiration compared to vehicle-treated cells **(Figure 3.6.3Biii)**. The latter observation may be surprising, as LPS treatment is traditionally thought to induce mitochondrial respiratory dysfunction and a shift from mitochondrial OXPHOS reliance toward aerobic glycolysis in macrophages [227]. However, LPS-induced mitochondrial respiratory enhancement in THP1 macrophages has been observed in other studies [228], and we used a relatively low concentration (10 ng/mL) of LPS that did not significantly reduce cell viability **(Figure 3.4A)**. As well, the proportion of total OXPHOS capacity (**see Figure 3.6.3Bvi**) used by basal respiration in LPS-primed THP1 macrophages (basal / $PMGS_P$) was lower relative to vehicle-primed cells, suggesting that LPS-primed THP1 macrophages do not basally utilize OXPHOS capacity as much as vehicle-treated cells **(Figure 3.6.3C)**. Nevertheless, 12,13-DiHOME-priming reduced PM_P respiration relative to vehicle-treated THP1 macrophages, and the LPS-induced increase in PM_P was attenuated by co-treatment with 12,13-DiHOME, suggesting that 12,13-DiHOME present during priming leads to defects in complex I OXPHOS in macrophages **(Figure 3.6.3Biii)**. Importantly, we obtained the complex I-mediated respiratory control ratio (RCR), which is the ratio between complex I-mediated OXPHOS (PM_P) and complex I-mediated LEAK respiration (PM_L) ($RCR = PM_P / PM_L$). RCR is an indicator for the coupling between mitochondrial respiration

and ATP synthesis, and lower RCR may suggest the propensity for mtROS generation resulting from uncoupling of these two processes [217]. We observed that 12,13-DiHOME-primed and LPS+12,13-DiHOME-primed macrophages had significantly reduced complex I RCR relative to vehicle-primed cells **(Figure 3.6.2D)**. LPS-primed macrophages also showed a slight trend toward reduced RCR, but this was not significantly different compared to vehicle-primed macrophages.

After measuring complex I-mediated OXPHOS capacity (PM_P), we added exogenous cytochrome *c* (c) to the chambers to induce the "PMc_P" respiratory state **(Figure 3.6.3Biv)**. If mitochondrial outer membrane permeabilization (MOMP) was present, such as in cells undergoing apoptosis or artifactually by an excessive digitonin concentration used during cytosolic membrane permeabilization, PMc_P respiration would be strongly stimulated relative to PM_P respiration, as exogenous cytochrome *c* would replace endogenous cytochrome *c* lost during MOMP [217]. This cytochrome *c*-stimulated respiration is calculated as the "cytochrome *c* control efficiency" ratio (PMc_P / PM_P**)**. However, we saw no differences in the cytochrome *c* control efficiency among any of the inflammasome priming treatment groups, and all groups' respiration rates were stimulated no more than 8% by addition of exogenous cytochrome *c* **(Figure 3.6.3D)**. Thus, 12,13-DiHOME, LPS, or LPS+12,13-DiHOME likely did not trigger significant apoptosis during inflammasome priming, corroborating our cell viability data **(Figure 3.1**), nor did we use an excessive digitonin concentration during cytosolic membrane permeabilization that could produce artifacts. Additionally, we added glutamate (G), another complex I substrate, to measure if complex I-mediated respiration was not saturated by pyruvate and malate alone [217], but we observed no further increase in respiration (PMG_P) **(Figure 3.6.3Bv)**.

The complex II substrate succinate (S) was subsequently added to measure complex I plus complex II-mediated OXPHOS respiration, which is an approximate measure for total OXPHOS capacity of mitochondria ("$PMGS_P$" respiration) [217]. Like the PM_P respiration data, LPS-primed macrophages had greater $PMGS_P$ respiration compared to vehicle-treated cells, while macrophages primed with LPS+12,13-DiHOME did not **(Figure 3.6.3Bvi)**. However, unlike the PM_P respiration rates, macrophages primed with 12,13-DiHOME alone did not have significantly lower $PMGS_P$ respiration compared to vehicle-primed macrophages. This could be explained by complex II-mediated OXPHOS compensating for dysfunctional complex I-mediated OXPHOS **(Figure 3.6.3Biii)**, as complex II-mediated respiration did not appear to be affected by 12,13-DiHOME present during priming (**see Figure 3.6.3Bvii)**. This compensation for 12,13-DiHOME-induced complex I dysfunction by complex II might be sufficient in macrophages not primed with LPS, but this may not occur to a sufficient degree in combination with LPS-priming. Overall, LPS+12,13-DiHOME-priming significantly impaired total mitochondrial OXPHOS capacity.

Next, mitochondrial respiration was uncoupled from ATP synthesis by additions of the protonophore carbonyl cyanide-p-trifluoromethoxyphenylhydrazone (FCCP). With both complex I and complex II substrates present, the rapid FCCP-mediated transport of protons back into the matrix independent of translocation *via* ATP synthase prompts a state of maximum mitochondrial electron transport (ET) capacity to maintain the proton gradient ("$PMGS_E$" respiration state). Here, we observed that 12,13-DiHOME-primed macrophages had significantly lower $PMGS_E$ respiration compared to vehicle-primed cells **(Figure 3.6.3Bvii)**. In addition, LPS-primed cells had a higher $PMGS_E$ respiration compared to vehicle-primed cells, but this increase was completely ablated in LPS+12,13-DiHOME-

primed macrophages. These data suggest that 12,13-DiHOME reduces maximum ET transport capacity in THP1 macrophages independent of rate limitation by OXPHOS capacity **(Figure 3.6.3Bvi)**, which also aids to the postulation that complex II OXPHOS could compensate for complex I OXPHOS in a rate-limited state in 12,13-DiHOME-primed macrophages. This observation is also complemented by measurement of the spare respiratory capacity (SRC), which is the leftover proportion of maximum ET capacity ($PMGS_E$) that is not used by the maximum OXPHOS capacity ($PMGS_P$) (SRC = [1 – ($PMGS_P$ / $PMGS_E$)]). Importantly, SRC reflects the "reserve" capacity that is available to mitochondria for maintaining proton motive force (pmF) under respiratory stress conditions or the capacity available for pmF-coupled processes other than ATP synthesis, such as proton-coupled ion transport [217]. In this regard, 12,13-DiHOME-primed and LPS+12,13-DiHOME-primed macrophages had lower SRC compared to vehicle-primed macrophages, while LPS-primed macrophages did not **(Figure 3.6.2E)**.

Finally, maximum ET capacity *via* complex II was measured following addition of the complex I inhibitor rotenone ("S_E" respiration). Interestingly, there was no significant difference in S_E respiration between vehicle-primed and 12,13-DiHOME-primed macrophages, suggesting that the large reduction in $PMGS_E$ respiration in macrophages primed with 12,13-DiHOME was likely attributed to selective complex I dysfunction **(Figure 3.6.3Bviii)**. Likewise, S_E respiration was equivalent between LPS-primed and LPS+12,13-DiHOME-primed THP1 macrophages while both were significantly higher compared to vehicle-primed cells. In summary, these data suggest that 12,13-DiHOME present during NLRP3 inflammasome priming leads to mitochondrial respiratory

dysfunction, indicated by increased uncoupling, ablation of SRC, and limitations in OXPHOS and maximum ET capacities, primarily due to effects at complex I.

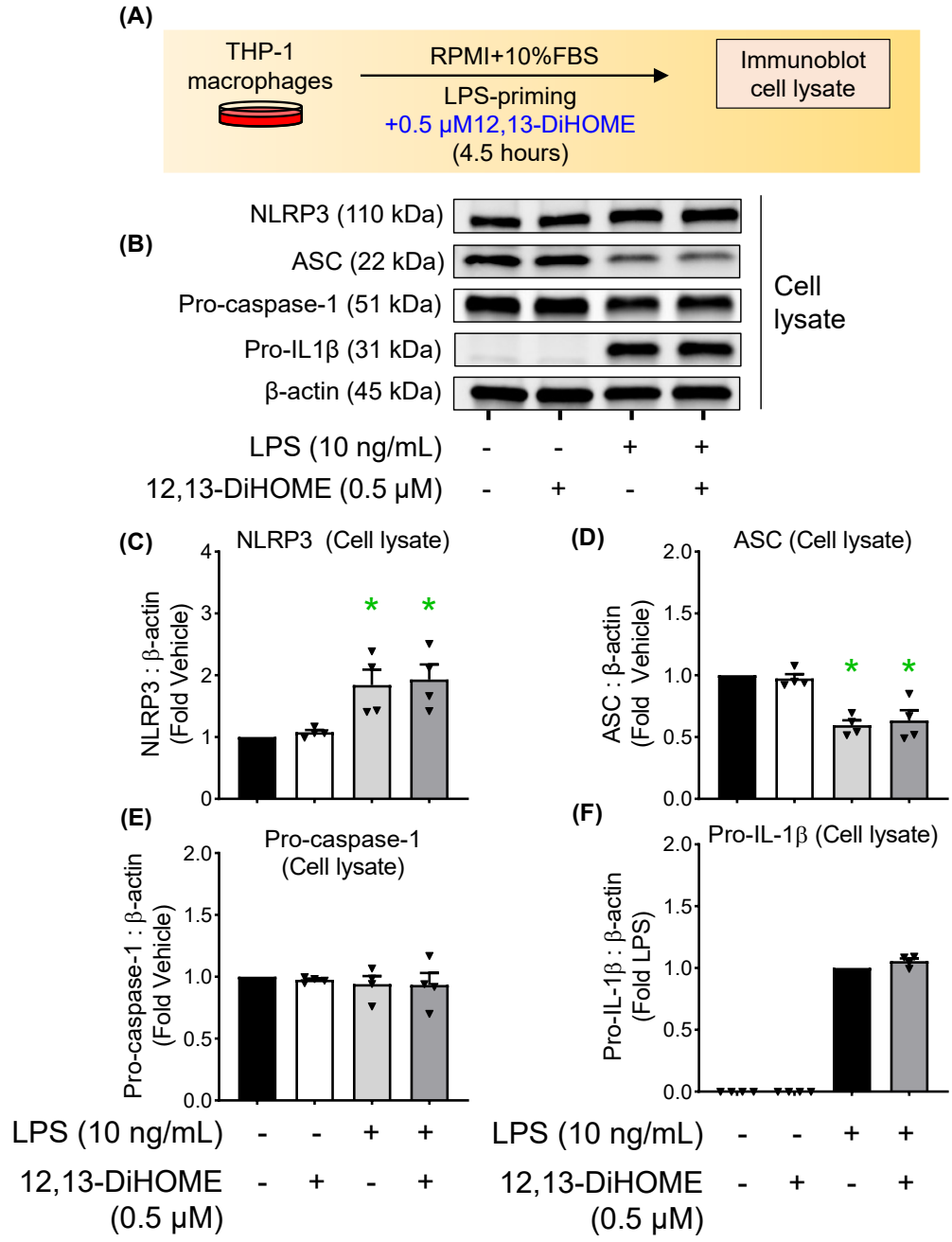

Figure 3.6.1. *12,13-DiHOME present during priming does not affect NLRP3 inflammasome protein expression.* **(A)** THP1 macrophages were treated only with priming stimuli prior to immunoblotting. **(B)** Representative immunoblots of cell lysates from THP1 macrophages treated with the indicated priming stimuli. Densitometric analyses of NLRP3 **(C)**, ASC **(D)**, pro-caspase-1 (p51) **(E)**, and pro-IL-1β (p31) **(F)** in cell lysates were performed. Bars represent mean+/-SEM. *P<0.05 vs. black bar using one-way ANOVA with Dunnett's post-hoc test (n=4).

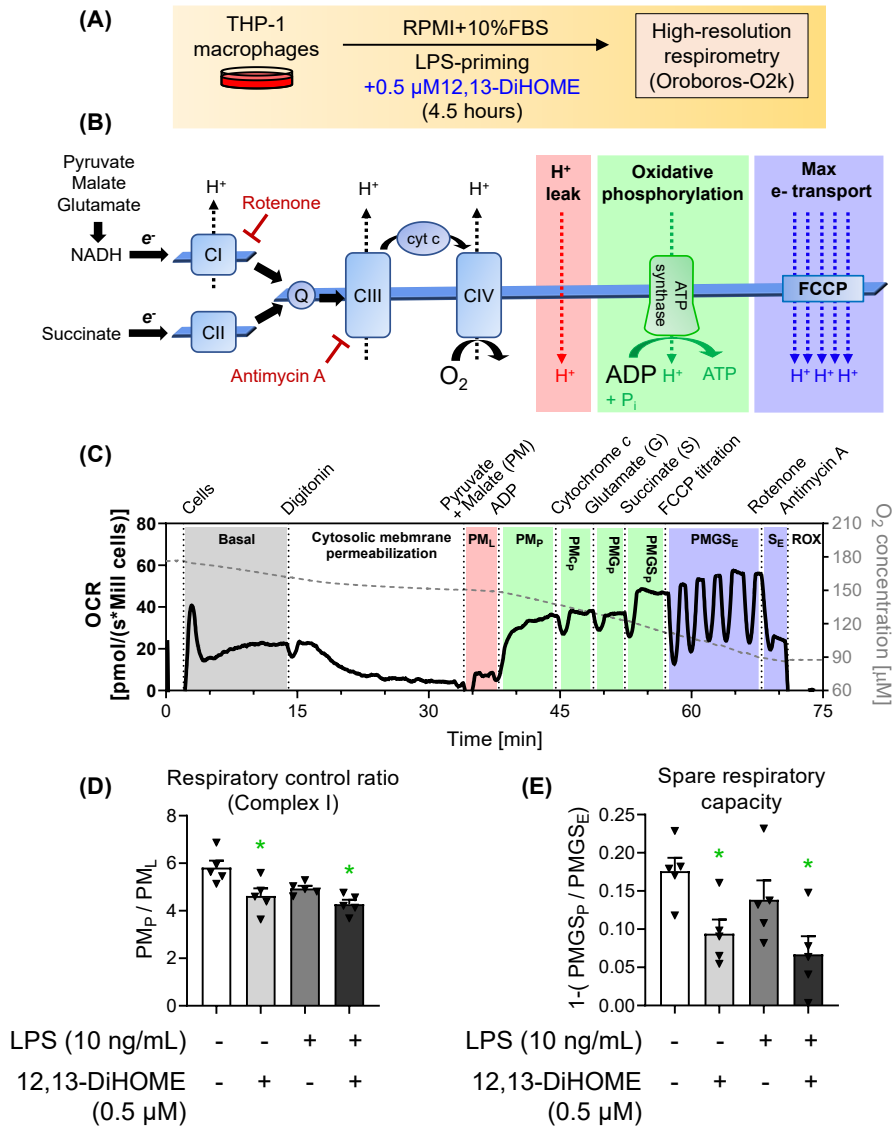

Figure 3.6.2. *12,13-DiHOME induces mitochondrial uncoupling and reductions in spare respiratory capacity during LPS-priming*. **(A)** THP1 macrophages were treated with the priming stimuli prior to high-resolution respirometry (Oroboros-O2k). **(B)** Simplified mitochondrial electron transport chain schematic, with respiratory complexes I-IV (CI-IV), Q-junction (Q), cytochrome c (cyt c), CI and CII substrates, CI and CIII inhibitors (rotenone and antimycin A), and general respiratory states. e^- flow is indicated by solid black arrows, and H^+ flow by dashed arrows. **(C)** Representative experiment, where oxygen consumption rates (OCRs) were measured at different respiratory states induced by the substrate, uncoupler, and inhibitor titrations indicated, and used to calculate **(D)** and **(E)** for the indicated priming treatments. Bars in **(D)** and **(E)** represent mean+/-SEM. *P<0.05 vs. vehicle using one-way ANOVA with Dunnett's post-hoc test (n=5).

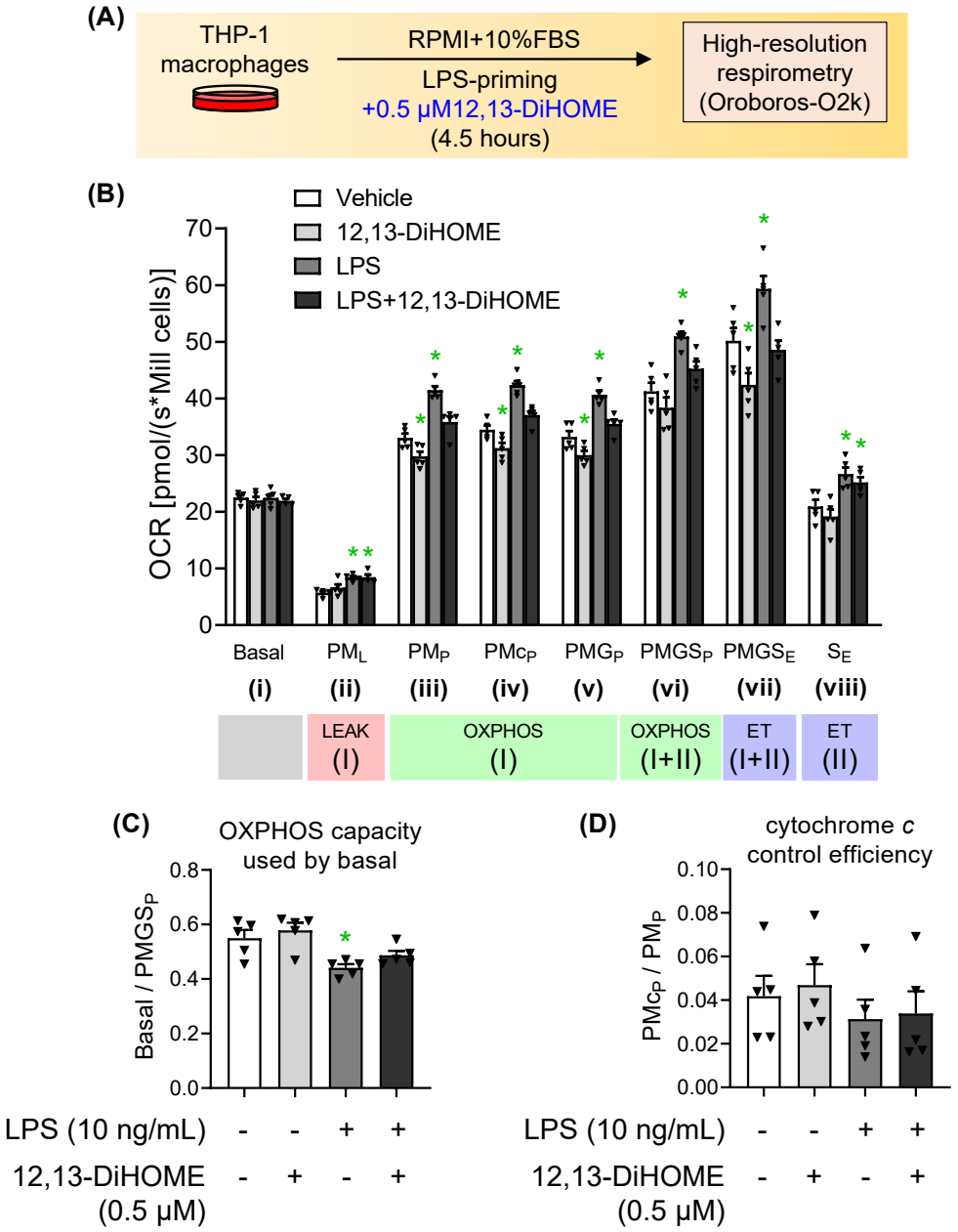

Figure 3.6.3. *Raw oxygen consumption rates and additional respiratory parameters measured in THP1 macrophages treated with priming stimuli.* **(A)** Simplified experimental protocol indicating the same experiment from Figure 3.6.2. **(B)** Raw oxygen consumption rates (OCRs) for each respiratory state **(i-viii)** used to calculate **(C)** and **(D)** for the indicated priming treatments. Bars represent mean+/-SEM. *P<0.05 vs. vehicle using one-way ANOVA and Dunnett's post-hoc analysis (n=5). See Figure 3.6.2 for respiratory state abbreviations.

3.7 Mitophagy is inhibited in LPS+12,13-DiHOME-primed macrophages

As mitochondrial dysfunction was apparent by respirometry **(Figure 3.6.2 – 3.6.3)**, we asked whether the mitophagic response was affected by 12,13-DiHOME present during inflammasome priming. Mitophagy is the selective targeting of mitochondria to autophagy, where damaged mitochondria can be recruited to autophagosomes and eventually degraded *via* fusion with lysosomes [123]. This allows recycling of macromolecules for mitobiogenesis and prevents accumulation of inflammogenic and pro-cell death stimuli derived from damaged mitochondria. Notably, mitophagy is known to strongly inhibit NLRP3 inflammasome activation, either by maintaining a healthy mitochondrial pool, physical blockade of damaged mitochondria which act as a scaffold for the NLRP3 inflammasome complex, or by sequestration of individual NLRP3 inflammasome proteins [123]. To assess mitophagy, we used THP1 macrophages stably-expressing lentivirus-transduced Mito-Keima, a mitochondrial targeting sequence-tagged fluorescent protein with a pH-dependent excitation spectra and resistance to lysosomal degradation [229]. This allows differentiation of mitochondria present in a neutral pH environment (ie. cytosol) as opposed to an acidic pH environment (ie. autophagosomes/autolysosomes) **(Figure 3.7A-B)**. Strikingly, priming THP1 macrophages with 12,13-DiHOME alone or LPS alone significantly increased the acidic-to-neutral mito-Keima ratio above levels detected in vehicle-primed macrophages, but LPS+12,13-DiHOME-priming did not **(Figure 3.7C)**. This may suggest that 12,13-DiHOME- or LPS-primed macrophages might induce mitophagy in response to mitochondrial damage while LPS+12,13-DiHOME-primed macrophages cannot, potentially exacerbating NLRP3 inflammasome activation in LPS+12,13-DiHOME-primed macrophages.

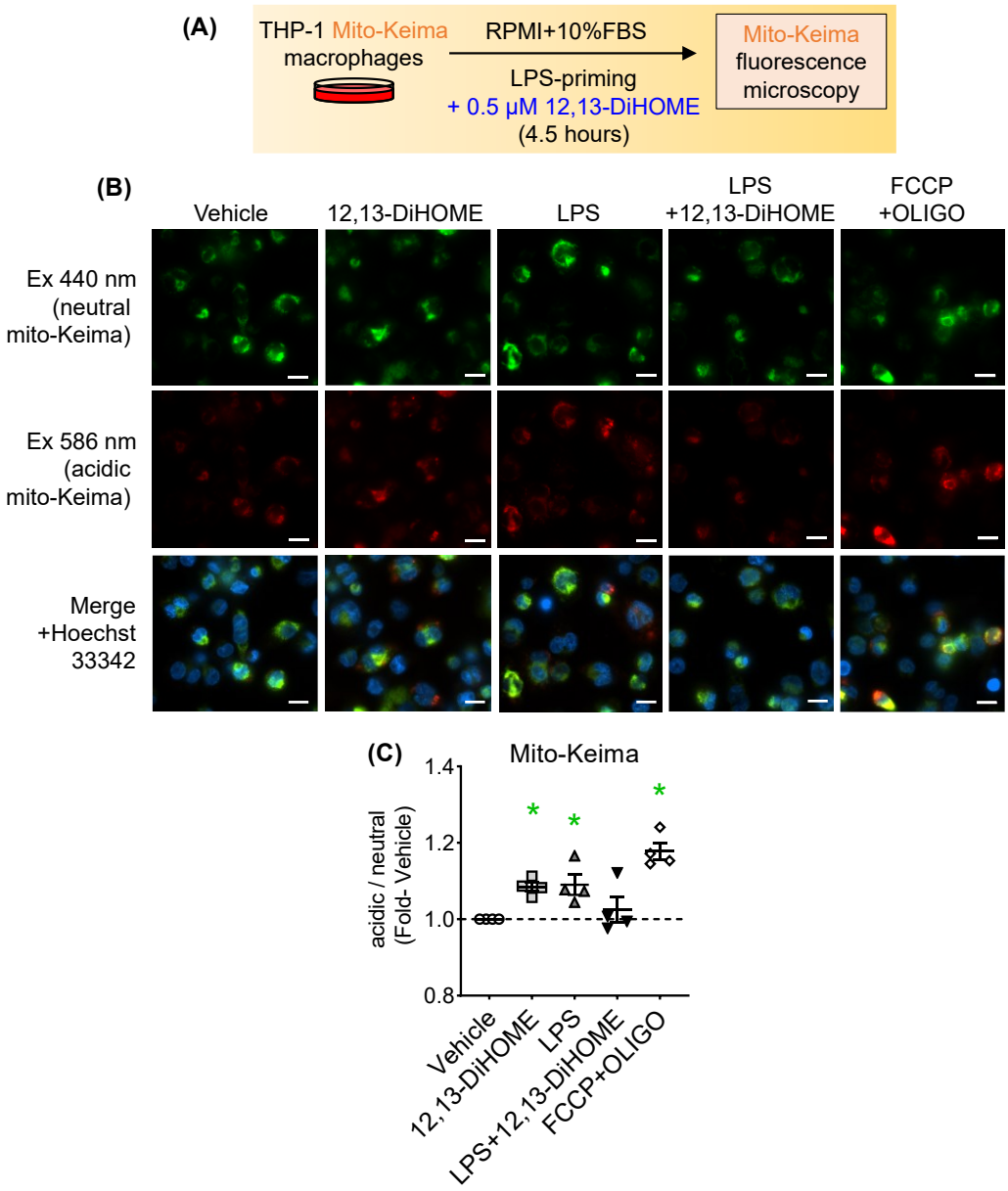

Figure 3.7. *Mitophagy is inhibited in LPS+12,13-DiHOME-primed macrophages.* **(A)** THP1 macrophages stably-expressing the mitochondria-targeted and pH-sensitive fluorescent protein Mito-Keima were treated with priming stimuli and assessed by live-cell epifluorescence microscopy. **(B)** Representative images, white bar = 20 µm. Vehicle, 12,13-DiHOME (0.5 µM), LPS (10 ng/mL), LPS+12,13-DiHOME, or positive control FCCP (10 µM)+oligomycin (OLIGO) (10 µM) were used as priming stimuli **(C)** Acidic to neutral mito-Keima ratio was measured (Average of 5 random fields' whole-field fluorescence represents each data point). Line represents mean+/-SEM. *P<0.05 vs. vehicle using one-way ANOVA with Dunnett's post-hoc test (n=4).

3.8 Exacerbated nigericin-induced mitochondrial damage in LPS+12,13-DiHOME-primed macrophages is blocked by mitochondrial calcium uniporter inhibition

With evidence of 12,13-DiHOME-induced mitochondrial dysfunction and alterations of mitophagy during inflammasome priming, we began to assess how other measures of mitochondrial damage are affected during NLRP3 inflammasome priming and activation. Tetramethylrhodamine ethyl ester (TMRE), a mitochondria-targeted potentiometric dye that indicates mitochondrial membrane potential, was used in combination with live-cell fluorescence microscopy to assess mitochondrial membrane potential immediately after the inflammasome priming phase **(Figure 3.8.1A-B)**. Interestingly, we observed no differences in mitochondrial membrane potential between vehicle-, 12,13-DiHOME-, LPS, or LPS+12,13-DiHOME-primed THP1 macrophages **(Figure 3.8.1C)**. This supports our observation that basal respiration was not affected by any priming treatment **(Figure 3.6.3Bi)** despite 12,13-DiHOME-induced mitochondrial respiratory dysfunctions being present prior to NLRP3 inflammasome activation, such as complex I uncoupling **(Figure 3.6.2D)** and SRC reduction **(Figure 3.6.2E)**.

We postulated that 12,13-DiHOME-induced mitochondrial dysfunction during priming would manifest during the subsequent nigericin-induced NLRP3 inflammasome activation phase. Indeed, nigericin induces acute mitochondrial respiratory stress [103] as well as mitochondrial depolarization and mtROS production in macrophages during NLRP3 inflammasome activation [115]. To investigate this hypothesis, we first primed THP1 macrophages with vehicle, 12,13-DiHOME, LPS, or LPS+12,13-DiHOME, then tracked whole-field TMRE fluorescence changes induced by nigericin throughout the NLRP3 inflammasome activation phase using live-cell epifluorescence microscopy to monitor

mitochondrial membrane potential **(Figure 3.8.2A and 3.8.3)**. In a separate experiment, we also monitored mtROS production using the superoxide-reactive mitochondrial dye, MitoSOX. Nigericin-induced mitochondrial depolarization (loss of TMRE fluorescence) was absent in vehicle-primed macrophages **(Figure 3.8.2B)**, but mild mtROS production (increased MitoSOX fluorescence) **(Figure 3.8.2C)** was observed in this same treatment group. Interestingly, both 12,13-DiHOME-primed and LPS-primed macrophages displayed greater nigericin-induced mitochondrial depolarization and mtROS production relative to vehicle-primed cells. Meanwhile, LPS+12,13-DiHOME-primed macrophages exhibited the most extensive nigericin-induced mitochondrial depolarization and mtROS production compared to all other priming treatments. Overall, 12,13-DiHOME present during LPS-priming increased the sensitivity of THP1 macrophages to mitochondrial damage during nigericin-induced NLRP3 inflammasome activation.

This data could be explained by our observation that 12,13-DiHOME-primed macrophages have increased uncoupling at complex I (ie. increased propensity for mtROS formation) **(Figure 3.6.2D)** and reduced SRC (ie. reduced ability to preserve pmF under respiratory stress) **(Figure 3.6.2E)** due to defects in mitochondrial OXPHOS and ET capacities **(Figure 3.6.3Biii-viii)**. However, we wondered whether 12,13-DiHOME-induced mitochondrial dysfunction during priming affected mitochondrial pmF-coupled processes other than ATP synthesis to mediate enhancement of nigericin-induced mitochondrial damage. It has been suggested that NLRP3 inflammasome activation stimuli can mobilize Ca^{2+} to exacerbate activation of the NLRP3 inflammasome, mediated partly by mitochondrial Ca^{2+} overload leading to events such as mitochondrial uncoupling, mitochondrial depolarization, mtROS production, permeability transition pore (mPTP)

opening, and release of mitochondrial DAMPs [230]. With this knowledge, we made several hypotheses: (i) 12,13-DiHOME could hamper mitochondrial Ca^{2+}-transport, a pmF-coupled process, leading to increased susceptibility to nigericin-induced mitochondrial Ca^{2+} overload and subsequent damage; (ii) 12,13-DiHOME exacerbates nigericin-induced perturbations in cytosolic Ca^{2+}, leading to enhanced Ca^{2+}-mediated mitochondrial damage [127]; or (iii) 12,13-DiHOME mediates a combination of these effects. These hypotheses were interesting in that 12,13-DiHOME is already known to modulate Ca^{2+} handling *via* activities dependent upon transient receptor potential (TRP) family channels [196] and ryanodine receptors (RyRs) [189].

To begin investigating these hypotheses, we used the cytosolic Ca^{2+} indicator dye, Fluo-4, co-incubated with the mitochondrial membrane potential indicator dye, TMRE, and tracked whole-field fluorescence at a higher temporal resolution (every minute **(Figure 3.8.2D)** compared to every 5 minutes **(Figure 3.8.2A)**) to monitor overall cytosolic Ca^{2+} changes in relation to nigericin-induced mitochondrial depolarization during the NLRP3 inflammasome activation phase. We saw an identical trend as before **(Figure 3.8.2B)**, where vehicle-primed macrophages exhibited no mitochondrial depolarization, while nigericin-induced mitochondrial depolarization was present in 12,13-DiHOME- or LPS-primed macrophages **(Figure 3.8.2E-G)**. Likewise, LPS+12,13-DiHOME-primed macrophages had the most extensive nigericin-induced mitochondrial depolarization compared to all other priming treatments **(Figure 3.8.2H)**. Notably, we observed no nigericin-induced increases in cytosolic Ca^{2+} in vehicle-primed macrophages until approximately 15 minutes post-nigericin addition **(Figure 3.8.2E)**. This nigericin-induced cytosolic Ca^{2+} increase does not appear to precede mitochondrial depolarization indicated by loss of TMRE fluorescence.

Interestingly, some reports suggest that nigericin-induced increases in cytosolic Ca^{2+} are a secondary effect downstream of NLRP3 inflammasome activation [131], which PMA-differentiated THP1 macrophages appear to be slightly basally primed for **(Figure 3.4C)**. Conversely, the temporal resolution and methodology (minute-long timepoints with widefield epifluorescence microscopy) may not have been sensitive enough to detect early nigericin-induced changes in cytosolic Ca^{2+} (<15 minutes post-nigericin) exhibited in other studies [127,132]. Thus, whether changes in cytosolic Ca^{2+} mediate mitochondrial depolarization during NLRP3 inflammasome activation is unclear in our study. Furthermore, it should be noted that this nigericin-induced cytosolic Ca^{2+} increase (>15 minutes post-nigericin) observed in vehicle-primed and 12,13-DiHOME-primed macrophages was not observed in cells with LPS present during priming **(Figures 3.8.2G-I)**. This can likely be explained by the observation that LPS-priming plus nigericin treatment leads to extensive NLRP3 inflammasome activation-mediated pyroptosis in these cells **(Figures 3.4C and 3.8.4B)**, and pyroptosis-induced plasma membrane rupture could lead to loss of cytosolic Fluo-4 retention that negates observable increases in cytosolic Ca^{2+} compared to macrophages not primed with LPS **(Figures 3.8.2E-F)**.

Interestingly, 12,13-DiHOME-priming or LPS+12,13-DiHOME priming did not lead to obvious changes in cytosolic Ca^{2+} dynamics during nigericin-induced NLRP3 inflammasome activation compared to vehicle-primed or LPS-primed macrophages, respectively **(Figures 3.8.2F and 3.8.2H)**. These data suggest that 12,13-DiHOME-sensitized mitochondrial depolarization is likely not associated with visible changes in cytosolic Ca^{2+} levels throughout the activation phase. Nevertheless, we predicted that mitochondria Ca^{2+}-overload could still play a role in 12,13-DiHOME-sensitized

mitochondrial damage without affecting the levels of bulk cytosolic Ca^{2+}. For instance, mitochondria-associated endoplasmic reticulum (ER) membranes (MAMs) act as physical connections between mitochondria and ER for calcium transport between organelles [231], and MAMs appear to be important for NLRP3 inflammasome activation [232]. Thus, we tested whether pharmacologically inhibiting mitochondrial Ca^{2+} uptake using the mitochondrial calcium uniporter (MCU) inhibitor, Ru265 (25 μM) [233], could block exacerbated nigericin-induced mitochondrial depolarization in LPS+12,13-DiHOME-primed macrophages. Remarkably, mitochondrial membrane potential appeared to be completely preserved in LPS+12,13-DiHOME-primed macrophages treated with nigericin plus Ru265 without changes to cytosolic Ca^{2+} dynamics (**Figure 3.8.2I)**, suggesting that 12,13-DiHOME-mediated sensitization to nigericin-induced mitochondrial damage during NLRP3 inflammasome activation is likely MCU-dependent. Moreover, these data suggest that macrophages primed with LPS+12,13-DiHOME could be more sensitive to mitochondrial Ca^{2+}-overload induced damage throughout the activation phase.

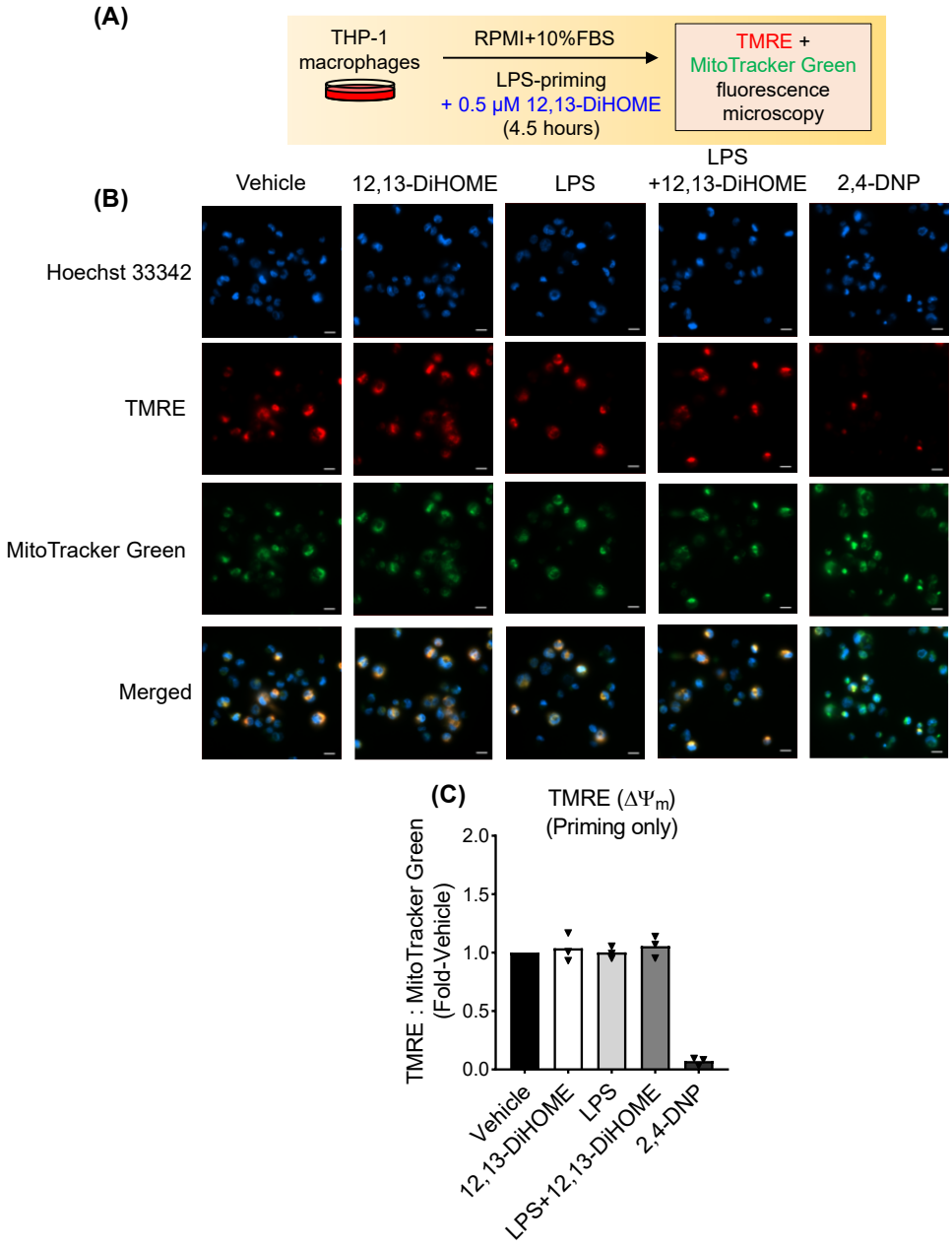

Figure 3.8.1. *Priming with 12,13-DiHOME does not induce changes in mitochondrial membrane potential.* **(A)** THP1 macrophages were treated with priming stimuli prior to staining with mitochondrial membrane potential indicator TMRE plus non-potentiometric mitochondrial dye, MitoTracker Green then live-cell epifluorescence microscopy. **(B)** Representative images, white bar = 20 μm. Vehicle, 12,13-DiHOME (0.5 μM), LPS (10 ng/mL), LPS+12,13-DiHOME, or positive control 2,4-dinitrophenol (2,4-DNP) (10 mM) were used as priming stimuli. **(C)** 5 random fields' average for whole-field TMRE to MitoTracker Green fluorescence ratio represents each data point. *P<0.05 vs. black bar using one-way ANOVA with Dunnett's post-hoc test (n=3).

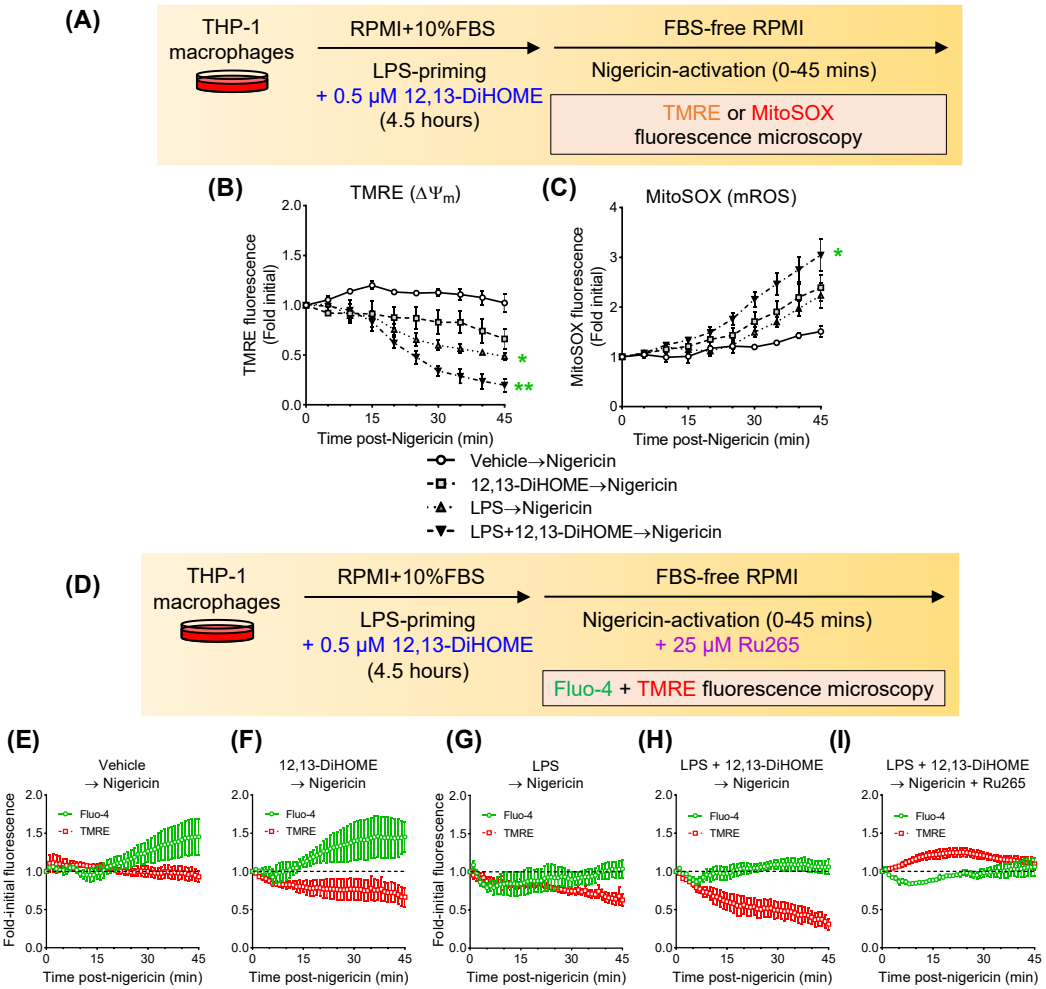

Figure 3.8.2. *Exacerbated nigericin-induced mitochondrial damage in LPS+12,13-DiHOME-primed macrophages is blocked by mitochondrial calcium uniporter inhibition.* **(A)** THP1 macrophages were primed wtih vehicle, 12,13-DiHOME (0.5 μM), LPS (10 ng/mL), or LPS+12,13-DiHOME followed by nigericin (10 μM)-induced NLRP3 inflammasome activation. Mitochondrial membrane potential or mitochondrial reactive oxygen species (ROS) production were monitored throughout the activation phase with either TMRE **(B)** or MitoSOX **(C)**, respectively, then using live-cell fluorescence microscopy. **(D)** THP1 macrophages were subject to the same priming and activation treatments in **(A)** expect in **(I)** where the mitochondrial calcium uniporter inhibitor Ru265 (25 μM) was pre-loaded for the last 30 minutes of priming and present throughout the activation phase. **(E-I)** Cytosolic Ca^{2+} and mitochondrial membrane potential were monitored throughout the activation phase by co-staining with both Fluo-4 and TMRE, respectively. All data points represent means of single fields' whole-field fluorescence relative to time = 0 min +/- SEM. *P<0.05, **P<0.01 vs. Vehicle→Nigericin at t=45 mins using one-way ANOVA with Dunnett's post-hoc test (n=3-4).

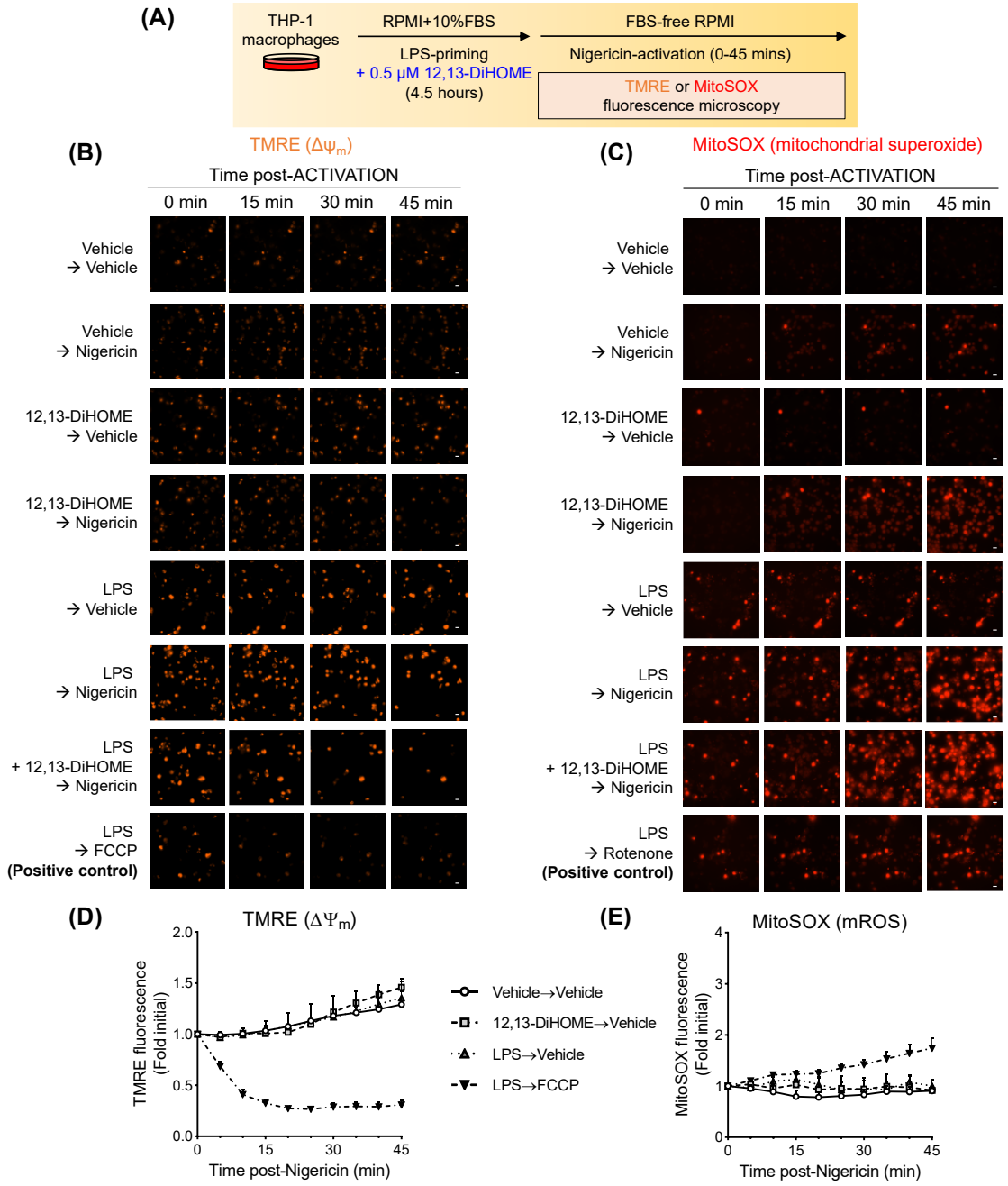

Figure 3.8.3. *Representative images and control treatment groups for Figures 3.8.2A-C.* **(A)** The same experiment design as in Figure 3.8.2A is shown. Representative images for Figure 3.8.2B **(B)** and Figure 3.8.2C **(C)** plus additional treatment groups are shown, white bar = 20 μm). Quantification was performed for control treatment groups for TMRE **(D)** and MitoSOX **(E)**. FCCP (10 μM) or rotenone (10 μM) were used as positive controls for TMRE and MitoSOX, respectively. All data points represent means of single fields' whole-field fluorescence relative to time = 0 min +/- SEM (n=3-4).

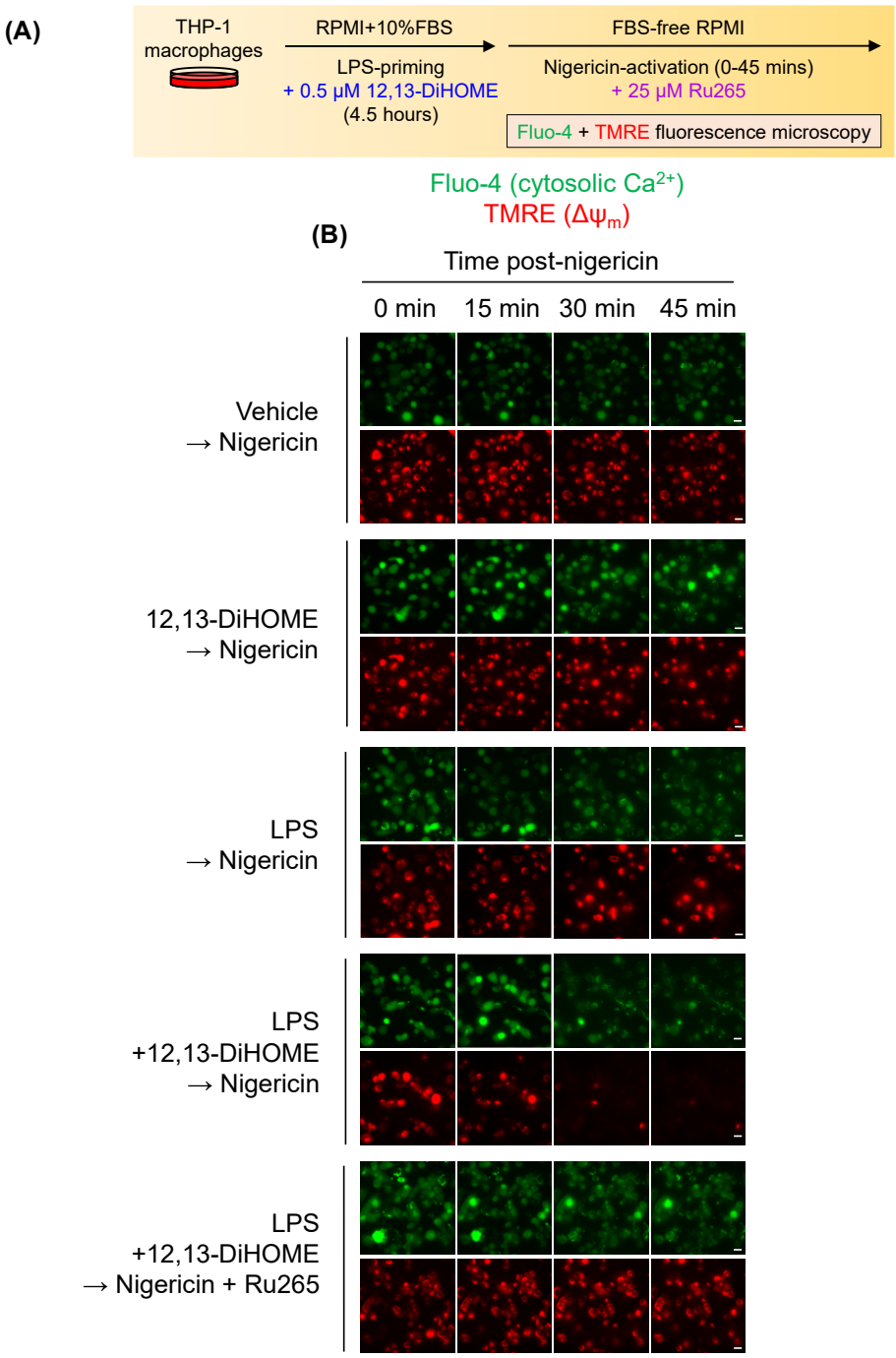

Figure 3.8.4. *Representative images for Figures 3.8.2D-I.* **(A)** THP1 macrophages were subjected to the same experimental protocol in Figure 3.8.2D. **(B)** Representative images for each treatment group for Figures 3.8.2E-I. White bar = 20 μm.

3.9 Exacerbated NLRP3 inflammasome activation in LPS+12,13-DiHOME-primed macrophages is blocked by mitochondrial calcium uniporter inhibition

Lastly, we tested whether Ru265-mediated protection from nigericin-induced mitochondrial damage in 12,13-DiHOME-primed macrophages translated to ablation of 12,13-DiHOME-enhanced NLRP3 inflammasome activation **(Figure 3.9A-B)**. Indeed, Ru265 treatment during nigericin-induced NLRP3 inflammasome activation blocked exacerbation of mature caspase-1 in cell lysates **(Figure 3.9C)** and mature IL-1β in media supernatants **(Figure 3.9D)** from LPS+12,13-DiHOME-primed cells. As well, LPS-primed macrophages co-treated with nigericin and Ru265 had mildly reduced mature IL-1β release into media, although this trend was non-significant. Overall, these data suggest that 12,13-DiHOME-mediated sensitization to nigericin-induced mitochondrial damage and NLRP3 inflammasome activation are both MCU-dependent, likely due to blocking mitochondrial Ca^{2+} uptake and Ca^{2+}-overload induced damage.

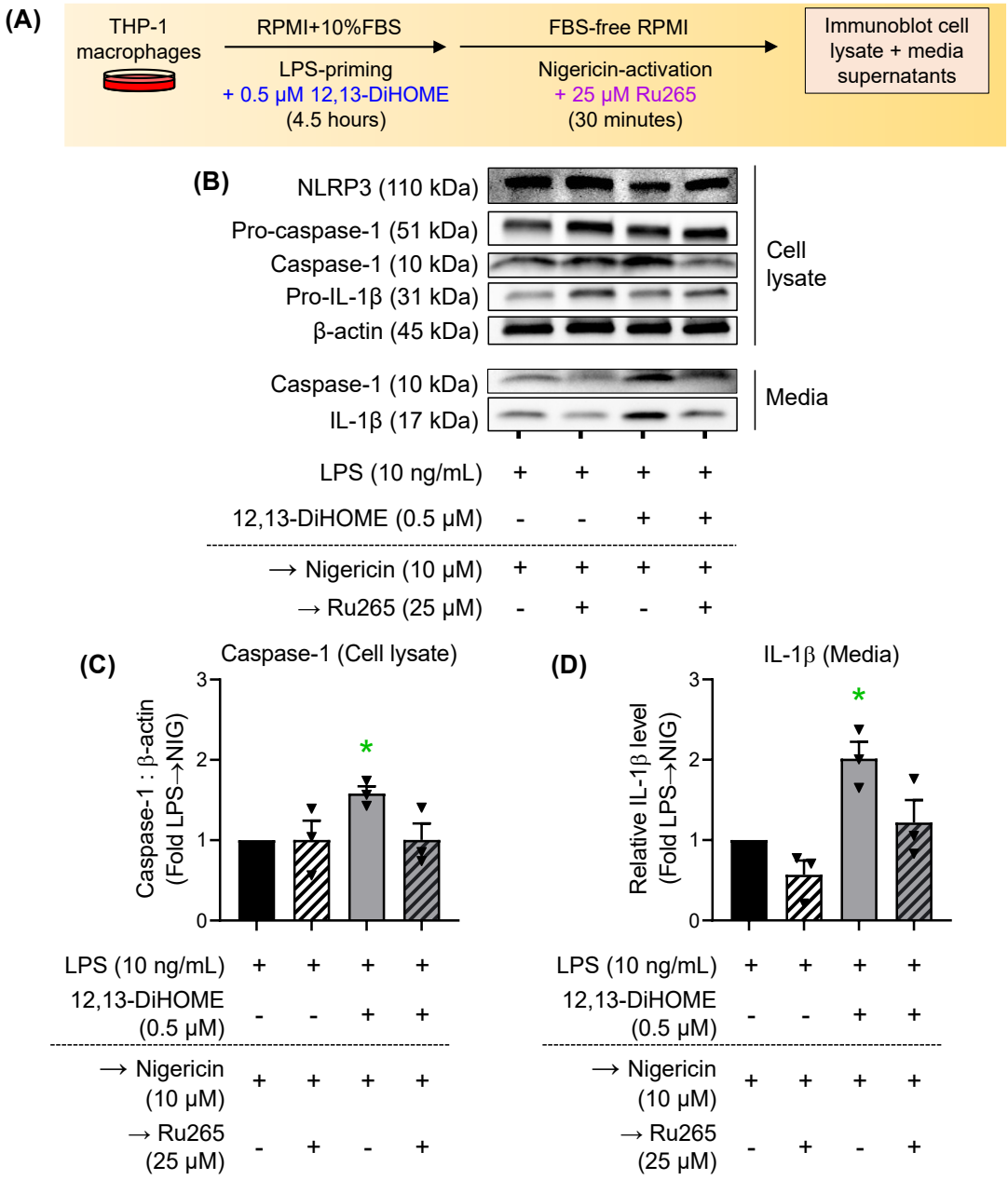

Figure 3.9. *Exacerbated NLRP3 inflammasome activation in LPS+12,13-DiHOME-primed macrophages is blocked by mitochondrial calcium uniporter inhibition.* **(A)** The effect of mitochondrial calcium uniporter inhibition with Ru265 on NLRP3 inflammasome activation was assessed by adding Ru265 for the last 30 minutes of priming (pre-loading) and throughout the activation phase. **(B)** Representative immunoblots of cell lysate and media supernatant fractions from THP1 macrophages treated with the indicated priming and activation stimuli. Densitometric analyses for caspase-1 (p10) in cell lysates **(C)** and IL-1β (p17) in media **(D)** were performed. Bars represent mean+/-SEM. *P<0.05 vs. black bar using one-way ANOVA with Dunnett's post-hoc test (n=3).

CHAPTER 4. DISCUSSION

4.1 Results summary

In the present thesis, we demonstrated that the linoleic acid-derived metabolite, 12,13-DiHOME, is pro-inflammatory in a THP1-derived macrophage model **(Figure 3.1)**. Our initial experiments demonstrated that 24-hour treatment with 12,13-EpOME (500 nM – 2 μM) or 12,13-DiHOME (10 nM – 2 μM) alone was not cytotoxic or anti-proliferative to THP1 monocytes or macrophages **(Figure 3.2)**. However, we observed that 12,13-DiHOME increased the expression of M1-associated pro-inflammatory cytokine genes *IL1B* and *TNF* in polarized macrophages **(Figure 3.3)**. Thereafter, 12,13-DiHOME present during LPS-priming was found to exacerbate nigericin-induced NLRP3 inflammasome activation, as indicated by enhanced caspase-1 cleavage, mature IL-1β secretion, and increased levels of pyroptotic pore-forming protein N-GSDMD **(Figures 3.5.1 – 3.5.3)**. Additionally, these effects were specific to 12,13-DiHOME and not inducible by its PUFA epoxide precursor, 12,13-EpOME, nor were these effects dependent upon sEH **(Figures 3.5.4 – 3.5.5)**. We then sought to investigate the effects mediated by 12,13-DiHOME during LPS-priming that promotes subsequent NLRP3 inflammasome activation. Inflammasome priming with 12,13-DiHOME did not lead to changes in NLRP3 inflammasome-related protein expression **(Figure 3.6.1)**. Rather, 12,13-DiHOME present during inflammasome priming led to mitochondrial respiratory dysfunction *via* respiratory uncoupling, reduced SRC, and lower OXPHOS and maximum ET capacities, likely through selective complex I dysfunction **(Figures 3.6.2 – 3.6.3)**. LPS+12,13-DiHOME-priming also did not prompt a protective mitophagic response that was observed with LPS-priming or 12,13-DiHOME-priming alone **(Figure 3.7)**. Intriguingly, mitochondrial respiratory dysfunction and mitophagy defects in LPS+12,13-DiHOME-primed macrophages were did not affect basal mitochondrial function

prior to NLRP3 inflammasome activation **(Figures 3.6.3 and 3.8.1)**, but this correlated with an increased sensitivity to nigericin-induced mitochondrial depolarization and mtROS production during the activation phase in LPS+12,13-DiHOME-primed macrophages **(Figures 3.8.2 – 3.8.3)**. Apparently, 12,13-DiHOME present during priming did not affect nigericin-induced cytosolic Ca^{2+} fluxes during the NLRP3 inflammasome activation phase **(Figure 3.8.2 and 3.8.4)**. However, inhibiting the mitochondrial Ca^{2+} uptake channel MCU by treatment with Ru265 during the activation phase prevented nigericin-induced mitochondrial depolarization in LPS+12,13-DiHOME-primed macrophages, independent of effects on cytosolic Ca^{2+} dynamics **(Figure 3.8.2)**. These data suggest that mitochondrial Ca^{2+} uptake and increased sensitivity to Ca^{2+} overload-related damage could mediate enhancement of nigericin-induced mitochondrial damage observed in LPS+12,13-DiHOME-primed macrophages. Finally, Ru265-mediated MCU inhibition also blocked exacerbation of nigericin-induced NLRP3 inflammasome activation in LPS+12,13-DiHOME-primed macrophages **(Figure 3.9)**. A graphical results summary is shown in **Figure 4.1**.

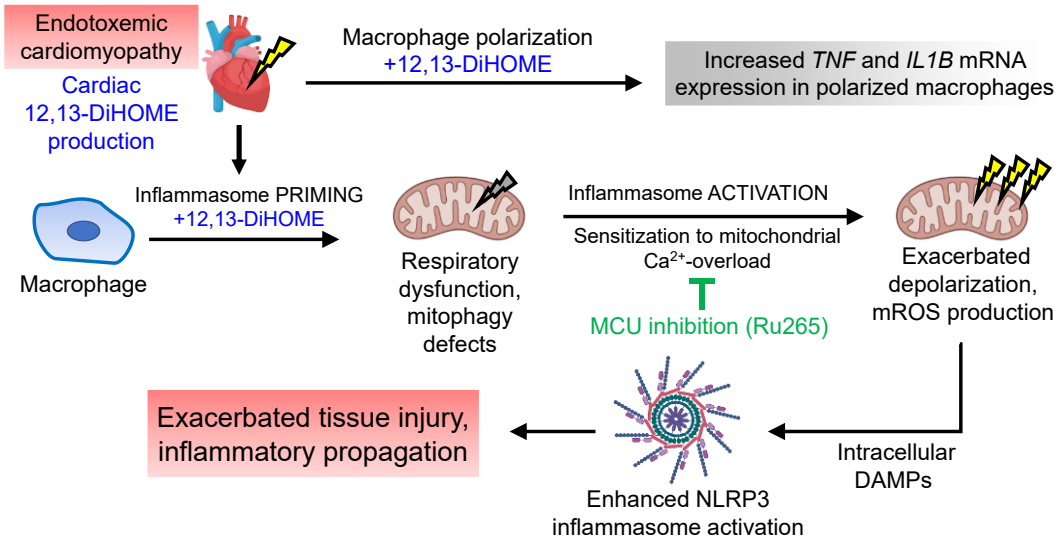

Figure 4.1. *Graphical results summary.*

4.2 PMA-differentiated THP1 macrophages as a physiological macrophage model

The human monocytic THP1 cell line has been widely used as an affordable and versatile *in vitro* model for monocytes and macrophages [234]. The advantages of using THP1 cells are like using any other immortalized cell line for biological research, for instance: (i) low cost and fast doubling time allow for large sample availability, (ii) better reproducibility due to genetic homogeneity across passages and avoiding inter-individual donor variability, and (iii) easy cell culture and genetic manipulation [234]. Upon treatment with a minimal concentration of the PKC-activator PMA followed by a sufficient rest incubation (at least 24 hours), THP1 cells acquire macrophage-like traits while avoiding a basal M1-like phenotype [220,235,236]. In addition to being a general "tissue macrophage" model, PMA-differentiated THP1 macrophages have been used in co-culture models to resemble tumor-associated macrophages [237], foam cells in atherosclerosis [238], inflammatory adipose tissue macrophages [239], and even microglia [240]. Similarly, THP1 macrophages have been used to model functions such as macrophage polarization [236], NLRP3 inflammasome activation [241], and microbe phagocytosis [242]. THP1 monocytes and macrophages have also been used to screen for immunomodulatory compounds [243,244]. Despite these data, their malignant background, being derived from the blood of a 1-year old boy with acute monocytic leukemia [245], and other factors have scrutinized the ability of THP1 cells to serve as a physiologically relevant monocyte and macrophage model.

In a study comparing human blood monocyte-derived macrophages and PMA-differentiated THP1 macrophages and their response to *in vitro Mycobacterium tuberculosis* infection, Madhvi et al. demonstrated that both macrophage models had similar uptake rates of several *M. tuberculosis* strains, cell viability in response to infection, and pro- and anti-

inflammatory cytokine expression and secretion across different *M. tuberculosis* strains [242]. Similarly, Shiratori et al. demonstrated that THP1 macrophages and peripheral blood mononuclear cell (PBMC)-derived macrophages have similar responses to LPS+IFNγ-induced M1 macrophage polarization, and that THP1 macrophages are able to appropriately model phagocytic capacities of macrophages at different polarization states [246]. However, these researchers also found that THP1 macrophages and PBMC-derived macrophages greatly diverged in terms of mRNA expression, cell surface markers, and secreted cytokines in response to M2 polarization stimuli. Schildberger et al. found that THP-1 monocytes could secrete similar amounts of TNFα compared to PBMCs and isolated human monocytes in response to *Pseudomonas aeruginosa* or *E. coli* -derived LPS treatment, but THP1 cells differed in IL-8, IL-6, and IL-10 secretion levels [247]. This correlated with differences in the ability of THP1 cell-conditioned media to activate cytokine secretion in human umbilical vein endothelial cells compared to PBMC-conditioned media. Using a gene expression approach, Kohro et al. observed that PMA-differentiated THP1 macrophages have similar macrophage-associated gene expression markers such as apolipoprotein-E, matrix metalloproteinase 9, and α2 macroglobulin when compared to PBMC-derived macrophages, but the overall gene expression profiles between THP1 macrophages and PBMC-derived macrophages do not correlate well [248]. Conversely, a more recent study by Riddy et al. comparing the genotypic and phenotypic profiles of PBMCs compared to a number of monocyte-like cell lines, including THP1, HL-60, and U-937, suggested that THP1 cells were the most similar to PBMCs [249]. Lastly, THP1 monocytes appear to have differences in LPS-stimulated expression of PRRs such as TLRs when compared to PBMCs [250].

Importantly, the ability of PMA-differentiated THP1 macrophages to appropriately model physiological macrophage responses is likely dependent upon the PMA differentiation protocol used. Baxter et al. found that a minimal concentration of PMA, enough to induce irreversible adherence, plus a sufficient PMA-free rest incubation (at least 24 hours) are both required to prevent a basal M1-like phenotype and to improve their response to M2 stimuli [236]. Similar PMA concentrations and incubations also promote the ability for THP1 macrophages to effectively respond to all polarization stimuli in terms of classical polarization markers [251]. Interestingly, persistent high-confluency culturing of THP1 cells leads to a more heterogenous and generally pro-inflammatory population in response to PMA-differentiation [252]. These data suggest that protocols for PMA-induced differentiation of THP1 cells into macrophages should be standardized to improve reproducibility across multiple studies. In our model, we found that 50 nM PMA was the minimum concentration required to prevent THP1 macrophage dis-adherence following the 24-hour PMA-free rest period (**Figure 3.1B-C)**, and this PMA concentration correlates well with other studies aimed at optimizing macrophage differentiation of THP1 cells [234]. Although we have successfully used PMA-differentiated THP1 macrophages to model macrophage polarization **(Figure 3.3)** and NLRP3 inflammasome activation **(Figure 3.4)**, as has been done by others previously [236,241], we only assessed adherence and mRNA expression of *CD14* and *CD36* as monocyte-to-macrophage differentiation markers that have been confirmed elsewhere in the literature [221,235,253]. In future studies, these should be complemented by a more diverse panel of mRNA markers, cell-surface markers, and functional assays to confirm that THP1 cells were fully differentiated into macrophage-like cells and to improve the reproducibility of our data. Importantly, the macrophage

differentiation state and the basal inflammatory state are known to affect macrophage polarization and NLRP3 inflammasome activation [222,236]. Comparing 12,13-DiHOME's effects on the same pathways in more physiological macrophage models is also necessary to confirm the relevance of our observations made in THP1 macrophages.

4.2 Effect of 12,13-EpOME and 12,13-DiHOME on cell viability and proliferation

We observed that 24-hour treatment with 12,13-EpOME (500-2000 nM) or 12,13-DiHOME (10-2000 nM) were tolerated in both THP1 monocytes and PMA-differentiated macrophages, where no visible effects on cell viability (trypan blue-negative cells) or proliferation (gross number of viable cells/mL) were observed **(Figure 3.2)**. We chose our concentrations according to a previous study, wherein 24-hour treatment of cardiomyocytes with either 12,13-EpOME or 12,13-DiHOME (as low as 10 nM in HL-1 cells and as low as 100 nM in neonatal rat cardiomyocytes) produced profound reductions in cell viability, as represented by oxidative metabolism using the formazan formation-based assay, CCK-8 [159]. The discrepancy between the observed "cytotoxicity" in cardiomyocytes and not in THP1 cells upon treatment with equal concentrations of 12,13-EpOME or 12,13-DiHOME might be attributed to the fact we used cytosolic membrane integrity (ie. necrosis) as our cell viability metric, measured as % trypan blue-negative cells, as opposed to oxidative metabolism by cell counting kit 8 (CCK-8) used by Samokhvalov et al. [159]. However, any irreversible 12,13-EpOME or 12,13-DiHOME-induced inhibition of oxidative metabolism, undetectable by trypan blue exclusion assay, did not have any apparent consequence on THP1 monocyte or macrophage proliferation **(Figure 3.2D,E,H,J)**. As well, our mitochondrial respiration data **(Figure 3.6.3)** and TMRE fluorescence after priming data

(Figure 3.8.1) suggests that 4.5-hour treatment with 0.5 μM 12,13-DiHOME had no visible effect on THP1 macrophage basal respiration rate **(Figure 3.6.3Bi)** or mitochondrial membrane potential **(Figure 3.8.1)** (ie. at unstressed conditions), despite complex I-dependent uncoupling **(Figure 3.6.2D)** and reduced spare respiratory capacity **(Figure 3.6.2E)** being present. These data could suggest that THP1 macrophages might tolerate mitochondrial toxic effects induced by 12,13-EpOME and 12,13-DiHOME better than a more mitochondria-dependent cell type such as cardiomyocytes. Interestingly, the foundational studies which identified that EpOMEs must be converted into DiHOMEs to mediate mitochondrial toxicity and cytotoxicity demonstrated this both through measuring oxidative metabolism by 3-(4,5-dimethylthiazol-2-yl)-2,5-diphenyltetrazolium bromide (MTT) assay in Sf21 insect cells [165] as well as cell necrosis measured by lactate dehydrogenase (LDH) release in renal proximal tubule cells [178]. Notably, these studies only observed cytotoxicity at much higher concentrations of 12,13-EpOME and 12,13-DiHOME, where at least 100 μM was required to profoundly reduce viability in Sf21 cells and at least 1 mM required in renal proximal tubule cells. HL-60-derived neutrophilic cells treated with 200 μM 12,13-DiHOME for 5 hours [177], human PBMC-derived dendritic cells treated with 130 μM 12,13-DiHOME for 5 days [184], and RAW264.7 murine macrophages treated with 200 μM for 24 hours [184] appeared to have no reported cytotoxic effects, further supporting 12,13-DiHOME's cardiomyocyte-selective cytotoxicity at sub-micromolar to low-micromolar concentrations. A limitation of our study is the relatively low concentration of 12,13-EpOME and 12,13-DiHOME we used relative to other studies, as the stock formulations of 12,13-EpOME and 12,13-DiHOME (Cayman Chemical) utilized in our experiments were only 337 μM and 318 μM, respectively. This limited the amount of

12,13-EpOME and 12,13-DiHOME we could add without vehicle (methyl acetate) concentrations in media from exceeding 1% v/v. As such, future studies assessing a greater concentration range of 12,13-EpOME and 12,13-DiHOME are necessary to fully interrogate these concentration- and cell type-specific cytotoxic effects. These data must also be corroborated by orthogonal approaches for measuring overall "cell viability", such as plasma membrane integrity (e.g. trypan blue exclusion, propidium iodide staining, LDH release), oxidative metabolism (formazan formation-based assays like MTT or CCK-8), nuclear DNA damage (terminal deoxynucleotidyl transferase dUTP nick end labeling (TUNEL)), caspase activity assays, cell death complex formation assays, and other measures [254].

4.3 12,13-DiHOME and macrophage polarization

Our data suggests that 0.5 μM 12,13-DiHOME present during macrophage polarization can exacerbate the expression of M1-associated cytokines such as *TNF* **(Figure 3.3C)** and *IL1B* **(Figure 3.3D)**. Supporting these data, Lin et al. reported in a recently published abstract that, through epigenetic modulations, 12,13-DiHOME increases the number of IL-1β+ polarized macrophages, reduces phagocytic function, and enhances allergic stimuli-induced inflammation [185]. A major limitation of our polarization data is that we only tested a single 12,13-DiHOME concentration (0.5 μM) and timepoint (24 hours), as well as single concentrations of polarization stimuli, so whether 12,13-DiHOME had concentration- or time-dependent effects on the expression of certain macrophage polarization markers is unclear. We also utilized a very limited panel of macrophage polarization markers that should be complemented in future studies by other marker genes encoding cytokines and chemokines, scavenger receptors, matrix metalloproteinases, amino

acid metabolism proteins, and the receptors and transcription factors associated with upstream control of these genes [63]. Measures for the protein expression and function of these genes, including cell surface marker expression, cytokine and chemokine secretion, glycolytic and mitochondrial metabolism, migration and motility, phagocytic ability, and other functional measures are also necessary to fully understand the degree that 12,13-DiHOME affects macrophage polarization.

M1/M2 macrophage polarization is determined by the activation of key transcriptional factors by M1 and M2-associated stimuli. M1 (LPS+IFNγ) polarization treatments are associated with activation of nuclear factor kappa B (NF-κB), activated protein-1 (AP-1), signal transducers and activators of transcription-1 (STAT1), and interferon regulatory factor-5 (IRF5) [255]. M2 (IL-4 or IL-13) polarization treatment is most associated with STAT6, IRF4, and PPARγ activation [255]. These and a multitude of other transcription factors co-regulate macrophage polarization, often through cross-talk and complementary activation and inhibition. PPARγ activation, through PPARγ binding endogenous ligands such as arachidonic acid-derived prostaglandin D2, is essential for both promoting M2-like macrophage polarization and repressing M1-like macrophage polarization [256]. These effects are mediated by inhibition of NF-κB, AP-1, and STAT1 downstream of PPARγ activation. Notably, 12,13-DiHOME was suggested by Levan et al. to be a PPARγ agonist in human PBMC-derived dendritic cells due to its structural similarity to other endogenous PPARγ ligands, and they used RAW264.7 murine macrophages expressing a PPARγ-luciferase reporter to demonstrate the 12,13-DiHOME had PPARγ agonist activity [184]. At first glance, these data contradict the observations in the current thesis, as we observed M1-associated cytokine expression to be enhanced by 12,13-

DiHOME **(Figure 3.3)**. However, PPARγ activation by 12,13-DiHOME in RAW264.7 macrophages was only observed at concentrations exceeding 75 μM [184], much greater than the 0.5 μM 12,13-DiHOME we used to treat THP1 macrophages during M1/M2 polarization. Aside from intrinsic differences between *in vitro* macrophage models, it is an interesting postulation that exogenous 12,13-DiHOME at low concentrations (e.g. 0.5 μM utilized in this study) could have partial agonist activity that antagonizes endogenous PPARγ agonists, leading to overall reduced PPARγ activity that promotes M1-associated pro-inflammatory cytokine expression **(Figure 3.3)**. Other CYP epoxygenase/sEH-derived PUFA metabolites that are structurally similar to 12,13-DiHOME, such as the arachidonic acid-derived epoxyeicosatrienoic acids (EETs), are potent PPARγ activators that can skew M1-polarized macrophages towards an M2 phenotype at 1 μM [208]. Other potential 12,13-DiHOME receptors like TRPV1 and TRPA1 [195,196] have also been demonstrated to inhibit M1 macrophage polarization at the transcriptional level. Wang et al. demonstrated that TRPA1 activation promoted polycomb repressive complex 2-mediated chromatin remodeling, leading to inhibition of M1 macrophage genes and activation of M2 macrophage genes [257]. Lv et al. observed that TRPV1 activation mediated calcium/calmodulin-dependent protein kinase phosphorylation and downstream nuclear factor-erythroid 2-related factor 2 (Nrf2)-mediated repression of M1 macrophage polarization genes [258]. Again, concentrations of 12,13-DiHOME necessary for activation of TRPA1 and TRPV1 currents (100 μM and 10 μM, respectively) greatly exceed the 0.5 μM concentration utilized in the present thesis [195,196]. Whether 12,13-DiHOME displays partial agonist activity by competing with endogenous agonists for PPARγ, TRPA1, TRPV1 or other unidentified 12,13-DiHOME-binding receptors could be an interesting subject of further research.

It is known that remodeling cellular metabolism is crucial for M1 and M2 macrophage polarization, whereby M1 macrophages tend to have enhanced glycolytic metabolism and repressed mitochondrial OXPHOS while M2 macrophages are more dependent on the latter [259]. This metabolic rewiring is mediated by complex shifts in metabolite biosynthesis pathways. Interestingly, changes in cellular nutrient uptake mechanisms by 12,13-DiHOME could participate in metabolic shifts during macrophage polarization. Expression of *MSR1*, which encodes macrophage class A scavenger receptor (also known as CD204), was enhanced by 12,13-DiHOME co-treatment in M1-polarized macrophages **(Figure 3.3I)**. Although MSR1 is a known macrophage phagocytic receptor with roles in the host response to pathogen infection and M2 macrophage polarization [260], MSR1 can also mediate saturated fatty acid uptake leading to downstream pro-inflammatory effects in foamy macrophages [261]. Analogously, 12,13-DiHOME treatment promotes fatty acid uptake and oxidation in brown adipose tissue [199], skeletal muscle [200], and cardiomyocytes [189]. In BAT and skeletal muscle, this enhanced fatty acid uptake was mediated by increasing plasma membrane translocation of fatty acid transporters FATP1 and CD36. Although *MSR1* is a recognized M2 marker gene associated with changes in arginine and proline metabolism [260], whether *MSR1* has different roles in M1 macrophages is unclear. *MSR1* upregulation could act as an additional fatty acid uptake pathway induced by 12,13-DiIHOME in other studies, but the functional consequence of increased *MSR1* expression in M1 or M2 polarized macrophages should be a subject of future studies. We also did not assess how 12,13-DiHOME-mediated mitochondrial respiratory dysfunction, including complex I uncoupling **(Figure 3.6.2D)** and reduced SRC **(Figure 3.6.2E)**, might also have consequences on macrophage polarization. Complex I dysfunction has been

previously associated with pro-inflammatory macrophage activation [262], exacerbated LPS-induced inflammation [263], and mtROS-mediated enhancement of M1 macrophage polarization [264]. Meanwhile, M2 macrophages display increased mitochondrial OXPHOS function and enhanced spare respiratory capacity [265,266]. Mitochondrial respiratory dysfunction also reduces the ability of M1 macrophages to "re-polarize" into an M2 macrophages [266]. Overall, investigating the relationship between M1/M2 marker gene expression, macrophage function, and putative molecular targets of 12,13-DiHOME will provide a clearer picture of 12,13-DiHOME's mechanisms of action leading to pro-inflammatory effects on macrophage polarization.

4.4 12,13-DiHOME and NLRP3 inflammasome activation

Our data demonstrates that as low as 0.5 μM 12,13-DiHOME present during the 4.5-hour LPS-priming phase could exacerbate nigericin-induced NLRP3 inflammasome activation, as measured by multiple markers in cell lysates, media supernatants, and cell debris fractions **(Figures 3.5.1-3.5.3)**. An important limitation is that we only used a single prototypical priming stimulus (LPS) to model NLRP3 inflammasome activation in THP1 macrophages. LPS (a TLR-4 agonist) and other priming stimuli such as cytokines TNFα (acting through TNF receptor) and IL-1β (acting through IL-1 receptor) are generally understood to converge at NF-κB-mediated *de novo* transcription and translation of NLRP3 and pro-IL-1β as well as necessary PTMs of inflammasome proteins, but this may not be universal for all priming stimuli [86]. Xing et al. demonstrated that TNF receptor associated factor 6 (TRAF6) was important for transcription-independent and PTM-dependent priming of the NLRP3 inflammasome downstream of TLR and IL-1R agonists but not TNFα [267].

12,13-DiHOME present during LPS-priming did not modulate NLRP3 inflammasome protein expression **(Figure 3.6.1**), potentially ruling out that 12,13-DiHOME exacerbates NF-κB activation and transcription of inflammasome proteins (though we did not measure NF-κB activity or mRNA transcripts directly). Conversely, we demonstrated that 12,13-DiHOME might potentiate nigericin-induced NLRP3 inflammasome activation through mitochondrial respiratory dysfunction **(Figure 3.6.2 – 3.6.3)** and mitophagy defects **(Figure 3.7)** during LPS-priming. It is unclear whether 12,13-DiHOME exacerbates other priming-associated events, such as essential PTMs on NLRP3 [91] or ASC [92] or externalized cardiolipin-mediated mitochondrial NLRP3 scaffolding during priming [94] leading to exacerbated NLRP3 inflammasome activation. Externalized cardiolipin may be relevant to 12,13-DiHOME's effects during priming. Elliott et al. observed that cardiolipin was externalized on outer mitochondrial membranes in an mtROS-dependent manner during priming [94], and we observed 12,13-DiHOME induced mitochondrial uncoupling during priming **(Figure 3.6.2D)** that could be associated with enhanced mtROS production. In future studies, it is necessary to fully characterize both transcription-dependent and transcription-independent effects by 12,13-DiHOME during inflammasome priming and whether these are universal for all priming stimuli.

Similarly, we only used a single prototypical activation stimulus, the K^+/H^+ ionophore nigericin, to determine 12,13-DiHOME's role in NLRP3 inflammasome activation. Relative to priming-associated events, the downstream pathways associated with NLRP3 inflammasome activation stimuli are more complex and less understood [86]. As previously mentioned, while inflammasome priming might be concurrent with an acute but transient innate immune response that returns to homeostasis, inflammasome activation

could be associated with severe "cellular stress" associated with extreme perturbations like plasma membrane permeabilization, intracellular ion dysregulation, and multiple organellar disruption that might occur in an exacerbated innate immune response [86]. In our THP1 macrophage model, 12,13-DiHOME present during LPS-priming appeared to sensitize mitochondria to nigericin-induced damage, indicated by mitochondrial depolarization **(Figure 3.8.2B)** and mtROS production **(Figure 3.8.2C)** during the activation phase. Importantly, blocking nigericin-induced mitochondrial damage with the MCU inhibitor Ru265 in LPS+12,13-DiHOME-primed macrophages (**Figure 3.8.2I)** was associated with reduced NLRP3 inflammasome activation but not less than macrophages primed with LPS-alone **(Figure 3.9)**. Thus, mitochondrial damage may not be necessary for NLRP3 inflammasome activation in our THP1 macrophage model, but enhanced NLRP3 inflammasome activation by priming with 12,13-DiHOME may depend on activation stimuli which mediate mitochondrial damage. While nigericin, extracellular ATP, and MSU crystals induce mitochondrial damage which exacerbates NLRP3 inflammasome activation [100,103], the bacterial pore-forming toxin gramicidin appears to activate the NLRP3 inflammasome without profound mitochondrial perturbation [103]. Hence, whether 12,13-DiHOME can similarly enhance NLRP3 inflammasome activation elicited by extracellular ATP [268], silica and alum [269], MSU crystals [270], complement membrane attack complex [128], viral nucleic acids [271], or other inflammasome activation stimuli should be tested in parallel in future studies.

Whether the canonical NLRP3 inflammasome pathway alone fully accounts for exacerbated caspase-1 activation and IL-1β secretion by 12,13-DiHOME was not determined in our study. The combination of priming and activation triggers assembly of the

NLRP3 inflammasome complex, consisting of the scaffolding protein and PRR NLRP3, the adaptor protein ASC, and the effector pro-caspase-1 [86]. NLRP3 inflammasomes mediate autoproteolytic caspase-1 activation, caspase 1-mediated cleavage of IL-1β into its mature and secreted form, and GSDMD cleavage leading to N-GSDMD pore formation, IL-1β secretion, and eventual pyroptosis [86]. Collectively, this is the "canonical" NLRP3 inflammasome pathway, but there are also "non-canonical" pathways through which the NLRP3 inflammasome is also activated. Murine caspase-11 and the human homologues caspase-4 and caspase-5 are classified as inflammatory caspases alongside caspase-1 [272]. Caspases-4/5/11 can function as both PRRs and effector caspases, forming "non-canonical inflammasomes" which are activated by sensing intracellular LPS derived from invading or phagocytosed Gram-negative bacteria [273]. In addition to directly cleaving GSDMD to induce pyroptosis [274], caspase-4/5/11 inflammasomes can induce downstream activation of the canonical NLRP3 inflammasome through N-GSDMD pore-mediated K^+ efflux, leading to amplification of caspase-1 autoproteolytic activation, IL-1β secretion, and pyroptosis [275-277]. As we did not observe changes in necrosis-associated cytotoxicity **(Figure 3.4A)** nor caspase-1 cleavage **(Figure 3.4C)** in THP1 macrophages treated with LPS-priming alone, LPS-induced caspase-4/5/11 inflammasome activation upstream of canonical NLRP3 inflammasome activation was likely not present in our model, although this should be confirmed in future experiments. These data also suggest that "one-step" NLRP3 inflammasome activation by LPS-priming alone, observed in human monocytes, was also not present in THP1 macrophages [278]. Additionally, AIM2 inflammasomes (consisting of the scaffold protein and PRR AIM2 instead of NLRP3, plus ASC and pro-caspase-1) can be activated by AIM2-mediated sensing of cytosolic DNA derived from

intracellular pathogens [279]. AIM2 inflammasomes also mediate caspase-1 activation and caspase 1-dependent cytokine secretion and pyroptosis independent of NLRP3 inflammasomes [280]. However, AIM2 and NLRP3 inflammasomes have been shown to extensively crosstalk. In response to *Legionella* infection and cytosolic DNA sensing, AIM2 inflammasomes can induce pore-mediated K^+-efflux through a non-cleaved pro-caspase-1-dependent pathway [281]. In combination with caspase-11-dependent K^+ efflux, these events lead to downstream NLRP3 inflammasome activation and amplified caspase-1 cleavage and IL-1β secretion [281]. Although we utilized a simple LPS-priming and nigericin-induced NLRP3 inflammasome activation model **(Figure 3.4)** without the presence abundant pathogen-derived cytosolic DNA required for AIM2 inflammasome activation, recent literature may suggest that AIM2 inflammasome can also be activated by mis-localized cytosolic mtDNA [88,282]. As 12,13-DiHOME exacerbated nigericin-induced mitochondrial damage during NLRP3 inflammasome activation **(Figure 3.8.2)**, future studies should test whether this mitochondrial damage prompts mtDNA release into the cytosol to simultaneously activate NLRP3 and AIM2 inflammasomes, together amplifying caspase-1 cleavage, IL-1β release, and pyroptosis in macrophages. Importantly, oxidized mtDNA preferentially activates NLRP3 over AIM2 inflammasomes compared to non-oxidized mtDNA [110], so 12,13-DiHOME might selectively enhance NLRP3 inflammasome activation by exacerbating nigericin-induced production of mtROS **(Figure 3.8.2C)** that reacts with mtDNA during the activation phase [110]. Overall, investigating if 12,13-DiHOME can promote the activation of other inflammasomes, either directly or through cross-talk, may further our understanding of 12,13-DiHOME's pro-inflammatory effects in macrophages and disease.

Lastly, whether enhanced NLRP3 inflammasome activation and pyroptosis in LPS+12,13-DiHOME-primed macrophages involves other programmed cell death pathways was not tested in our study. In addition to pyroptosis, the most well-characterized programmed cell death pathways are apoptosis and necroptosis [283]. Apoptosis is mediated through intrinsic (mitochondrial outer membrane permeabilization-mediated) or extrinsic (TNF receptor- or Fas-mediated) pathways which activate initiator caspases-8/9/10 and downstream executioner caspases-3/6/7, leading to events such as nuclear condensation and fragmentation, membrane blebbing, and cell fragmentation generally without plasma membrane rupture [283]. Necroptosis is mediated by TNF-, Fas-, or TLR-receptor activation leading to downstream receptor-interacting protein kinase 1 (RIPK1) and/or RIPK3-dependent phosphorylation of mixed lineage kinase domain-like pseudokinase (MLKL) [283]. Phosphorylated MLKL forms pores that disrupt the plasma membrane and induce necrotic cell death that may act as a "failsafe" in contexts of apoptotic caspase inhibition [283]. Indeed, both apoptosis and necroptosis are known to be activated by LPS in macrophages [284,285]. We did not directly determine whether apoptosis or necroptosis were activated upon LPS-priming of THP1 macrophages. However, LPS treatment alone did not induce significant plasma membrane permeabilization characteristic of necroptosis or apoptosis-induced secondary necrosis (or pyroptosis) **(Figure 3.2A**, trypan blue exclusion assay). We also did not observe apoptosis-associated mitochondrial outer membrane permeabilization in THP1 macrophages treated with priming stimuli, indicated by mitochondrial retention of cytochrome *c* **(Figure 3.6.3D,** cytochrome *c* control efficiency) and the absence of changes in mitochondrial membrane potential following priming **(Figure 3.8.1**, TMRE/MitoTracker Green microscopy). We demonstrated LPS-priming plus nigericin

induced multiple markers of pyroptosis, including caspase-1 cleavage in cell lysates **(Figure 3.4C)**, pyroptotic pore-forming N-GSDMD in cell debris **(Figure 3.5.3E)**, and the release of cytosolic proteins such as GAPDH into media indicative of cell lysis **(Figure 3.4C)**. However, apoptosis may be activated downstream or in addition to NLRP3 inflammasome-mediated pyroptosis [283]. LPS plus nigericin-induced NLRP3 inflammasome and caspase-1 activation can mediate direct proteolytic activation of the apoptosis executioner caspase-7 [286]. In GSDMD-deficient cells such as mast cells and cortical neurons, NLRP3 inflammasome and caspase-1 activation leads to caspase 3-dependent apoptosis rather than pyroptosis [287]. Nigericin treatment in LPS-primed wild-type bone marrow-derived macrophages leads to rapid NLRP3-dependent pyroptosis as expected, but LPS-priming plus nigericin treatment induces caspase 8-dependent apoptosis in caspase 1-deficient macrophages [288]. Conversely, under certain priming and activation conditions associated with enteropathogenic infection, caspase-1 activation is dependent upon apoptosis proteins Fas-associated death domain (FADD) and caspase-8, where caspase-8 may promote *NLRP3* and *IL1B* transcription during priming and directly cleave caspase-1 during activation [289]. In human primary blood monocytes, Gaidt et al. demonstrated that LPS-priming alone induces TLR4-TRIF-RIPK1-FADD-caspase-8-dependent "alternative" NLRP3 inflammasome activation which occurs independently of K^+ efflux, ASC oligomerization, and pyroptosis while still mediating caspase-1 activation and cleavage of IL-1β [96]. However, these researchers also found that THP1 cells were not capable of this pathway [96]. Future studies investigating 12,13-DiHOME's potential role in other programmed cell death pathways and their crosstalk will provide a greater understanding of 12,13-DiHOME's

role in cytotoxicity or pro-inflammatory effects in macrophages or other cell types relevant to inflammatory disease.

4.5 12,13-DiHOME and mitochondrial respiratory dysfunction during inflammasome priming

We demonstrated that 0.5 μM 12,13-DiHOME present during LPS-priming led to mitochondrial respiratory dysfunction in THP1 macrophages, indicated by (i) a greater degree of uncoupling between complex I respiration and OXPHOS (lower RCR; PM_P/PM_L) **(Figure 3.6.2D)** and (ii) reduced SRC ($PMGS_P/PMGS_E$) **(Figure 3.6.2E)** [217]. 12,13-DiHOME-induced complex I uncoupling was not caused by changes in LEAK respiration (PM_L) **(Figure 3.6.3Bii)** but rather due to reduced complex I OXPHOS capacity (PM_P) **(Figure 3.6.3Biii)**. Reduced SRC by 12,13-DiHOME-priming was attributed to reduced complex I+II ET capacity ($PMGS_E$) **(Figure 3.6.3Bvii)** in combination with less profound reductions in complex I+II OXPHOS capacity ($PMGS_P$) **(Figure 3.6.3Bvi)**, likely due to compensation by complex II-mediated OXPHOS in the latter. As complex II ET capacity (S_E) was unchanged by 12,13-DiHOME-priming **(Figure 3.6.3Bviii)**, 12,13-DiHOME-induced reduction of complex I-mediated ET capacity (ie. inhibition of complex I-mediated respiration), although not directly measured, likely explains this reduction in complex I+II-mediated maximum ET capacity ($PGMS_E$). As well, inhibition of complex I-mediated respiration by 12,13-DiHOME could also explain reductions in complex I-mediated OXPHOS (PM_P) **(Figure 3.6.3Biii)** and complex I+II OXPHOS ($PMGS_P$) **(Figure 3.6.3Bvi)** irrespective of rate-limitation by ATP synthase or phosphate transporters [217]. Although inhibition of intrinsic complex I activity could explain this effect, it is important to note that

differences in mitochondrial respiratory substrate transport pathways and/or tricarboxylic acid cycle (TCA) enzyme activities upstream of complex I could also account for reduced complex I-dependent respiration in our study [217]. However, we demonstrated that an additional complex I substrate (glutamate), which supplies NADH through a separate transport pathway, did not further stimulate complex I OXPHOS (PMG_P) **(Figure 3.6.3Bv)**, suggesting that complex I substrates pyruvate and malate were sufficient to saturate complex I-mediated OXPHOS in the absence or presence of 12,13-DiHOME during priming. Therefore, how 12,13-DiHOME mediates selective dysfunction of the complex I pathway is an interesting topic for future studies. We only primed THP1 macrophages with 12,13-DiHOME prior to washing off 12,13-DiHOME-containing media, followed by dissociating cells from tissue culture plates and adding them into respiration chambers. Whether 12,13-DiHOME mediates similar mitochondrial respiratory defects when directly administered into respiration chambers was not tested; it is unclear whether (i) residual 12,13-DiHOME present during respiration experiments or (ii) lasting effects on upstream pathways mediated mitochondrial respiratory dysfunction induced by 12,13-DiHOME. Complementary experiments assessing the activities of substrate transporter pathways, individual TCA enzymes, and respiratory complexes I-IV are necessary to elucidate these mechanisms. Whether 12,13-DiHOME also affects other mitochondrial oxidative pathways such as fatty acid oxidation (which is complex I-dependent) or glycerophosphate oxidation (supplied directly to the Q-junction) should also be tested. 12,13-DiHOME treatment has been shown to promote fatty acid uptake and oxidation in BAT [199], skeletal muscle [200], and cardiomyocytes [189], but whether this occurs in macrophages is unknown. Overall, these data will provide a clearer picture for how 12,13-DiHOME induces mitochondrial

respiratory dysfunction relevant to inflammatory disease pathophysiology in macrophages and other cells of the heart.

12,13-DiHOME appears to have cell-type and concentration-specific effects on mitochondrial function, and different experimental methodologies assessing "mitochondrial function" further complicates these observations. Our lab has previously demonstrated that 24-hour pre-treatment with 100 nM 12,13-DiHOME induced prominent mitochondrial uncoupling in permeabilized HL-1 cells utilizing complex I substrates glutamate and malate and polarographic Clark-type O_2 electrode respirometry [159]. As well, 12,13-DiHOME inhibited the TCA cycle enzyme citrate synthase and inhibited mitochondrial biogenesis, suggesting that perturbation of multiple mitochondrial respiration, metabolism, and maintenance pathways may explain overall respiratory dysfunction in these cells. Moran et al. used isolated rabbit renal cortical mitochondria to assess the direct effects of linoleic acid, 12,13-EpOME, and 12,13-DiHOME on mitochondrial function, also using glutamate and malate as complex I substrates and polarographic O_2 electrode respirometry [290]. While no treatment affected FCCP-stimulated (ie. max ET capacity) respiration, they found that 50 μM but not 0.5 μM of linoleic acid or 12,13-EpOME was sufficient to profoundly increase State 4 (LEAK) respiration, reduce State 3 (OXPHOS) respiration, and led to mitochondrial depolarization. In contrary to our findings **(Figure 3.8.2 – 3.8.3)**, they observed that both 0.5 μM and 50 μM 12,13-DiHOME could not mediate mitochondrial respiratory dysfunction, so the researchers suggested that hydrolysis of 12,13-EpOME was a detoxification pathway to prevent mitochondrial uncoupling and other toxic effects leading to downstream cytotoxicity. However, both 12,13-EpOME and 12,13-DiHOME at these high concentrations are cytotoxic in renal proximal tubule cells [163]. Interestingly, this group later found that

pre-treatment with lower concentrations of 12,13-EpOME (1-10 μM) could protect primary cultured renal proximal tubular cells from hypoxia/reoxygenation (H/R) injury by maintaining mitochondrial respiratory function and preventing mitochondrial hyperpolarization induced by H/R, thus promoting recovery of ATP synthesis during reoxygenation. A low concentration of 12,13-DiHOME (5 μM) could not mediate such protection but also did not exacerbate mitochondrial respiratory dysfunction in combination with H/R injury [182]. However, supporting our data, this group observed that 1 hour treatment with 5 μM 12,13-DiHOME alone reduced basal oxygen consumption, reduced OXPHOS-dependent respiration, lowered maximum ET capacity, reduced ATP levels, reduced ATP synthase activity, appearing to lead to mitochondrial hyperpolarization and reduced respiration-dependent Na^+/K^+ ATPase activity in intact primary renal proximal tubular cells [182]. Thus, 12,13-DiHOME-induced mitochondrial dysfunction likely depends on multiple pathways, including those extrinsic to the mitochondrial respiratory chain itself. Future experiments comparing different cell types in parallel are required to understand the concentration- and tissue-specific effects of 12,13-DiHOME on mitochondrial respiration.

More recent studies utilizing the Seahorse Extracellular Flux Analyzer have reported that 12,13-DiHOME promotes mitochondrial respiration by increasing fatty acid uptake in multiple cell types. 15-minute pre-treatment with 1 μM 12,13-DiHOME increased fatty acid uptake and oxidation, correlating with increased basal respiration but with no reported effects on FCCP-stimulated maximal respiratory capacity or uncoupling in brown adipocytes [199]. In C2C12 myotube cells, 15-minute pre-treatment with 1.5 μM 12,13-DiHOME increased basal respiration and FCCP-stimulated respiration, correlating with increased fatty acid

uptake and oxidation [200]. In isolated adult mouse cardiomyocytes, 1-hour pre-treatment with 10 μM 12,13-DiHOME led to increased basal respiration, FCCP-stimulated maximal respiration, and increased non-mitochondrial respiration dependent on NOS1 [189]. Whether these studies reflect cell type- or concentration-dependent effects of 12,13-DiHOME or differences between mitochondrial respirometry methods (ie. polarographic oxygen electrodes versus Seahorse) is unclear. The Oroboros-O2k, utilized in the present thesis **(Figures 3.6.2 – 3.6.3)**, uses an electrochemical polarographic oxygen sensor to monitor O_2 concentration in chambers containing a suspended and constantly-stirred biological sample [217]. By permeabilizing cells with digitonin, saturating concentrations of respiratory complex-specific substrates, inhibitors, and uncouplers can be exogenously added with direct access to mitochondria. This allows assessment of different aspects of mitochondrial respiratory chain function while maintaining *in situ* interactions of mitochondria. On the other hand, the Seahorse Extracellular Flux analyzer utilizes optical sensors to monitor oxygen consumption of intact and adhered cells on multi-well tissue culture plates [291]. Usually, a "mito-stress test" is performed in Seahorse experiments by (i) measuring baseline oxygen consumption rate (OCR) of intact cells, (ii) subsequently adding FCCP to stimulate "maximal" uncoupled OCR, then (iii) completed by the addition of the ATP synthase inhibitor oligomycin to attain ATP synthesis-independent (or "LEAK") respiration [291]. Although Seahorse offers high-throughput OCR measurements in addition to extracellular acidification rate (ECAR) as a metric for glycolysis, Seahorse is limited by (i) a maximum of 4 exogenous compound injections, (ii) lower temporal resolution of oxygen fluxes (minutes as opposed to seconds), and (iii) the inability to measure specific aspects of mitochondrial respiratory chain function using substrate-uncoupler-inhibitor titrations in

permeabilized cells or isolated mitochondria [217]. Intact cells' mitochondrial respiration can be rate-limited by endogenous substrate supply/demand that (i) does not necessarily depend on intrinsic mitochondrial respiratory chain function (e.g. extracellular nutrient uptake and transport pathways) and (ii) may not be sufficient to drive maximal mitochondrial respiratory capacities. Thus, saturating concentrations of complex-specific mitochondrial respiratory substrates (ie. in Oroboros experiments with permeabilized cells) can reveal mitochondrial respiratory chain-specific pathologies that may not be observable in intact cell experiments using Seahorse. Indeed, these enhanced fatty acid uptake by increased translocation of fatty acid transporters FATP1 and CD36 may underly 12,13-DiHOME's stimulatory effects on mitochondrial respiration [199], but whether 12,13-DiHOME still limits absolute maximal respiratory capacities (ie. in the present study) or mediates respiratory dysfunction not visible using intact cells and Seahorse is unclear. Ideally, respirometry using permeabilized cells (Oroboros-O2k) and intact cells (Seahorse) should be complementary methods to understand overall mitochondrial and glycolytic metabolism as well as mitochondrial respiratory chain function in cells. Future studies should utilize a variety of cell and tissue models, 12,13-DiHOME treatment concentrations and timepoints, and mitochondrial respirometry methodologies in parallel to clarify these discrepancies in 12,13-DiHOME's effects on mitochondrial respiration.

4.6 12,13-DiHOME and effects on mitophagy during inflammasome priming

Mitophagy inhibits NLRP3 inflammasome activation through multiple pathways, such as: (i) physically sequestering damaged mitochondria from NLRP3 inflammasomes to prevent molecular scaffolding and complex formation, (ii) promoting the overall healthy

mitochondrial pool by recycling damaged mitochondria for *de novo* mitochondrial biogenesis, or (iii) physically sequestering and degrading individual NLRP3 inflammasome proteins [123]. In the present study, we demonstrated that priming with 12,13-DiHOME- or LPS-alone led to an increased acidic to neutral Mito-Keima fluorescence in THP1 macrophages, suggestive of mitophagy induction in these cells **(Figure 3.7)**. However, acidic to neutral Mito-Keima fluorescence in LPS+12,13-DiHOME-primed macrophages was not significantly different from vehicle-primed cells, suggesting that mitophagy is not induced in LPS+12,13-DiHOME-primed macrophages. These data could partially account for how nigericin-induced NLRP3 inflammasome activation is exacerbated in LPS+12,13-DiHOME-primed cells **(Figure 3.5.1 – 3.5.3)**. However, it is important to note that our mitophagy data (using Mito-Keima) may be confounded by changes in mitochondrial biogenesis (ie. changes in the number of "neutral" mitochondria) rather than mitophagy (ie. changes in the number of "acidic" mitochondria). Indeed, 24-hour treatment with 100 nM 12,13-DiHOME inhibited mitochondrial biogenesis in HL-1 cells [159]. However, we qualitatively observed that there is an increased presence of punctate "acidic" mitochondria, indicative of mitophagy **(Figure 3.7)**. Assessing different aspects mitochondrial biogenesis would complement our data well (e.g. MitoTracker Green time-courses, mtDNA to nuclear DNA ratios, levels of mitochondrial proteins, or activities of mitobiogenesis-controlling factors such as PGC-1α, SIRTs, Tfam) [292]. As well, the specific pathways related to 12,13-DiHOME's effects on mitophagy (e.g. non-selective bulk macro-autophagy versus mitochondria-specific and receptor-dependent mitophagy) is unclear from our data [293]. Assessing specific mitophagy-associated molecular events (e.g. immunoblotting for mitochondrial localization of mitophagy proteins like PINK1/Parkin, lipidated LC3b, p62)

and more robust microscopy methods (single-field time courses, electron or confocal microscopy, autophagy protein co-localization with mitochondria, etc.) [294] could be used in future studies.

How 12,13-DiHOME-priming alone induces mitophagy but LPS+12,13-DiHOME-priming does not is unclear. Evidently, 12,13-DiHOME-primed and LPS+12,13-DiHOME-primed THP1 macrophages display mitochondrial respiratory dysfunction **(Figure 3.6.2 – 3.6.3)** which may prompt recruitment to mitophagy [295,296]. The degree of mitochondrial respiratory uncoupling **(Figure 3.6.2D)** and reductions in SRC **(Figure 3.6.2E)** were not different between 12,13-DiHOME and LPS+12,13-DiHOME-primed cells, but raw OCRs related to OXPHOS and maximal ET capacities were lower in 12,13-DiHOME-primed macrophages compared to LPS+12,13-DiHOME-primed macrophages **(Figure 3.6.3B)**. Additionally, depolarized mitochondria are specifically targeted to mitophagy [296], although we observed no changes in mitochondrial membrane potential by any priming treatment **(Figure 3.8.1)**. It is possible that changes in mitochondrial membrane potential during priming were time-dependent as we only measured TMRE fluorescence at the end of priming, or our methods (wide-field epifluorescence microscopy) were not sensitive enough to detect changes in mitochondrial membrane potential. As well, changes to mitochondrial fission and fusion dynamics can lead to differential recruitment to mitophagy [297]. The structurally-related regioisomer 9,10-DiHOME can induce mitochondrial fragmentation in HL-1 cells [159], an event which precedes mitophagy [295,297], but alterations in mitochondrial fission/fusion by 12,13-DiHOME were not assessed in our study. Mitochondrial calcium transport may also mediate recruitment to mitophagy. Interestingly, small mitochondrial calcium oscillations appear to initiate mitophagy through the

PINK1/Parkin pathway [298], and increased MCU expression and MCU-dependent mitochondrial calcium uptake can stimulate mitophagy [299,300]. It is unclear whether calcium transport is modulated by 12,13-DiHOME through TRPA1 [195], TRPV1 [195,196], RyRs [189], MCU-dependent effects (**Figures 3.8.2 and 3.9**), or other mechanisms during inflammasome priming, leading to effects on mitochondrial Ca^{2+}-dependent mitophagy. As LPS is known mobilize calcium important for inflammation in macrophages [301-303], 12,13-DiHOME could modulate LPS-induced calcium mobilization during priming that leads to different effects on mitophagy compared to priming with 12,13-DiHOME alone. Intriguingly, Balderas et al. have recently demonstrated that complex I dysfunction leads to reduced turnover of MCU, increasing mitochondrial calcium uptake that promotes preservation of mitochondrial respiratory function [304]. Whether 12,13-DiHOME-induced complex I dysfunction **(Figure 3.6.2 – 3.6.3)** similarly leads to increased MCU levels in THP1 macrophages was not assessed in the present study, and whether increased MCU levels mediated enhanced mitochondrial damage during NLRP3 inflammasome activation **(Figure 3.8.2)** is unclear. Overall, determining the precise mechanisms through which 12,13-DiHOME alone promotes mitophagy and LPS+12,13-DiHOME inhibits it will be an interesting subject for future experiments.

4.7 12,13-DiHOME-sensitized mitochondrial damage during inflammasome activation

We observed that THP1 macrophages primed in the presence of 0.5 μM 12,13-DiHOME did not have functionally-relevant mitochondrial damage prior to inflammasome activation. Basal mitochondrial respiration **(Figure 3.6.3)** and mitochondrial membrane

potential **(Figure 3.8.1)** were not perturbed in LPS+12,13-DiHOME-primed macrophages prior to inflammasome activation, despite mitochondrial uncoupling **(Figure 3.6.2D),** reductions in SRC **(Figure 3.6.2E)**, reduced OXPHOS and maximal ET capacities (**Figure 3.6.3B)**, and hampered mitophagy **(Figure 3.7)** being present. However, 12,13-DiHOME's effects on mitochondria during priming appeared to manifest during the NLRP3 inflammasome activation phase, where LPS+12,13-DiHOME-primed macrophages were more sensitive to nigericin-induced mitochondrial depolarization **(Figure 3.8.2B)** and mtROS production **(Figure 3.8.2C)** compared to macrophages primed with LPS alone. Furthermore, we demonstrated that nigericin-induced mitochondrial depolarization in LPS+12,13-DiHOME-primed macrophages could be blocked by pharmacological inhibition of MCU using Ru265 during the activation phase **(Figure 3.8.2I)**, and this correlated with blunted NLRP3 inflammasome activation in LPS+12,13-DiHOME-primed macrophages **(Figure 3.9)**.

Although nigericin has been shown to mediate mitochondrial damage during NLRP3 inflammasome activation in multiple models, the mechanisms underlying this process are not fully understood. Nigericin is a toxin derived from *Streptomytces hygroscopicus* that acts as a K^+/H^+ ionophore [305]. Because the extracellular concentration of K^+ in media is normally lower than the intracellular K^+ concentration, nigericin mediates efflux of K^+ and influx of H^+, leading to broad cellular effects including cytosolic membrane depolarization, acidification of the cytosol, lysosomal disruption and hampered autophagy, and, importantly, effects on the mitochondria [306]. Along with acting at cytosolic membranes, nigericin can also act at the mitochondrial inner membrane, allowing H^+ influx from the intermembrane space back into the matrix and K^+ efflux in the opposite direction. This leads to dissipation

of the pH gradient and a compensatory rise in mitochondrial membrane potential causing hyperpolarization to maintain the proton-motive force meanwhile also uncoupling mitochondrial respiration from ATP synthesis [306]. However, the effect of nigericin on isolated mitochondria appears to differ in whole-cells. In isolated mitochondria [307] or at low concentrations of nigericin in whole-cells (e.g. 100 nM) [308], sustained mitochondrial hyperpolarization appears to be the main effect of nigericin, but treating whole-cells with sufficiently high concentrations of nigericin (e.g. 10 μM utilized in the present study) leads to transient mitochondrial hyperpolarization followed by mitochondrial depolarization, particularly in LPS-primed macrophages during NLRP3 inflammasome activation [230]. Likewise, high concentrations of nigericin immediately stimulates mitochondrial respiration in LPS-primed macrophages [103] but inhibits respiratory function at later timepoints [110]. Nigericin also prompts rapid mtROS production (**Figure 3.8.2)** [100,110] and the release of mitochondrial DAMPs like mtDNA through mitochondrial permeability pore transition [132] that, altogether, promotes NLRP3 inflammasome activation. The full breadth of mechanisms in whole-cells by which nigericin causes mitochondrial damage are not completely understood, but mobilization of Ca^{2+} may also play a role (discussed in subsequent sections). We demonstrated that blocking MCU with Ru265 could block nigericin-induced mitochondrial depolarization in LPS+12,13-DiHOME-primed macrophages **(Figure 3.8.2I)**, suggesting that MCU-mediated mitochondrial Ca^{2+} transport (and overload) might mediate mitochondrial damage downstream of nigericin K^+/H^+ antiporter activities, either at the cytosolic or mitochondrial membrane. Confirming these data by demonstrating mitochondrial Ca^{2+} overload, mPTP, mtDNA release into the cytosol,

and other measures for mitochondrial damage will be necessary to fully elucidate the nature of nigericin-induced mitochondrial damage and how 12,13-DiHOME exacerbates it.

The role of mitochondrial damage as an exacerbator of the NLRP3 inflammasome is well-recognized, but whether it is essential to NLRP3 inflammasome activation is unclear. Foundational studies have found that mtROS is sufficient to activate the NLRP3 inflammasome in LPS-primed macrophages [100]. mtROS is involved in oxidizing mtDNA that directly interacts with NLRP3 inflammasome to promote its activation [110], and mtROS may be involved in oxidizing other components of the pyroptosis pathway such as GSDMD [309]. By treating with a diverse range of inflammasome activators such as nigericin, ATP, MSU crystals, and alum, oxidized mtDNA is released through a mitochondrial Ca^{2+}-overload and mitochondrial permeability transition pore-dependent process that allows its cytosolic interaction with the NLRP3 inflammasome [132]. Thus, mitochondrial damage has been thought to be an upstream signal universal to NLRP3 inflammasome activation stimuli; however, other studies appear to complicate this theory. NLRP3 inflammasome activation stimuli such as the pore-forming toxin gramicidin can induce K^+ efflux without significant mitochondrial perturbation during the initiation of NLRP3 inflammasome activation [103]. Interestingly, Billingham et al. demonstrated that inhibition of mitochondrial respiratory complexes I and III blocked NLRP3 inflammasome activation, but reconstituting these respiration pathways with exogenous oxidases that do not produce mtROS still rescued NLRP3 inflammasome activation [117]. Allam et al. showed that mitochondrial apoptosis executioners Bax and Bak and mitochondrial permeability transition pore component cyclophilin D, involved in the release of mitochondrial DAMPs such as mtDNA downstream of extracellular ATP or nigericin, were dispensable for NLRP3

inflammasome activation [310]. Importantly, mitochondrial damage also occurs downstream of NLRP3 inflammasome activation. Caspase-1 inhibition could blunt mitochondrial swelling, depolarization, fragmentation, and mtROS production during NLRP3 inflammasome activation [115]. In this study, caspase-1 cleaved the mitochondrial apoptosis protein Bid to initiate mitochondrial outer membrane permeabilization and mPTP, and Parkin was also cleaved to inhibit mitophagy during the activation phase [115]. As well, Rogers et al. found that N-GSDMD pores produced during NLRP3 inflammasome activation could form on mitochondrial membranes in addition to cytosolic membranes, releasing cytochrome *c* and activating caspase-3 to initiate apoptosis [116]. In our study, although mitochondrial damage (indicated by mitochondrial depolarization) was completely blocked in LPS+12,13-DiHOME-primed macrophages treated with nigericin plus the MCU inhibitor Ru265 **(Figure 3.8.2I)**, NLRP3 inflammasome activation markers (caspase 1 p10 in cell lysates and mature IL-1β in media) were still present and approximately equivalent to LPS-primed macrophages activated with nigericin alone **(Figure 3.9).** These data suggest that mitochondrial damage may not be necessary for NLRP3 inflammasome activation in THP1 macrophages. However, enhanced mitochondrial damage could be involved in amplifying NLRP3 inflammasome activation in LPS+12,13-DiHOME-primed macrophages. Future studies testing whether mitochondrial damage initiates, modulates, or is consequence of NLRP3 inflammasome activation are necessary to understand how 12,13-DiHOME exacerbates NLRP3 inflammasome activation in macrophages.

4.8 12,13-DiHOME and calcium perturbations during inflammasome activation

The role of calcium mobilization during NLRP3 inflammasome activation is somewhat contested in the literature. A general but popular theory is that NLRP3 inflammasome activators mobilize extracellular and intracellular Ca^{2+} stores to promote Ca^{2+}-dependent mitochondrial damage and the release of DAMPs (ie. mtROS, mtDNA) which promote NLRP3 inflammasome activation [230]. However, the absolute necessity for Ca^{2+} transport and the specific stores of Ca^{2+} mobilized to enact mitochondrial damage and/or NLRP3 inflammasome activation are unclear. As well, the nature of Ca^{2+} mobilization appears to be specific to the inflammasome activator (ATP, nigericin, etc.) utilized. Murakami et al. demonstrated that inflammasome activators ATP, nigericin, and MSU increase cytosolic Ca^{2+} during the activation phase, and that calcium chelation or pharmacological block of store-operated calcium entry, phospholipase C activity, or IP_3 receptor activation leads to reduced mitochondrial damage and inhibition of the NLRP3 inflammasome [127]. NLRP3 inflammasome activation by extracellular ATP depends on TWIK2-mediated K^+ efflux to mobilize Ca^{2+} influx through ATP-activated P2X7 for effective NLRP3 inflammasome activation in macrophages while nigericin does not [102,311]. Additionally, NLRP3 inflammasome activation by increased extracellular Ca^{2+} or ATP occurs partly through activation of the Ca^{2+}-sensing receptor (CaSR) protein, which can further increase intracellular Ca^{2+} through activation of phospholipase C-mediated IP_3 production and Ca^{2+} release from the ER [311]. Activated CaSR also inhibits adenylate cyclase to reduce intracellular cyclic AMP, which can directly interact with the nucleotide-binding domain of NLRP3 to prevent NLRP3 inflammasome complex assembly. However, the researchers did not determine whether nigericin also utilizes this pathway. Importantly,

findings by Katsnelson et al. contradict this presumed role for increases in bulk cytosolic Ca^{2+} during NLRP3 inflammasome activation [131]. They found that changes in bulk cytosolic Ca^{2+} levels were not necessary for ATP, nigericin, or lysosome-destabilizing agent-induced activation of the NLRP3 inflammasome. They also demonstrated that extracellular ATP immediately induced cytosolic Ca^{2+} increase prior to NLRP3 inflammasome activation, but nigericin-induced cytosolic Ca^{2+} occurs as a secondary event either simultaneous with or downstream of pyroptosis induced by NLRP3 inflammasome activation. On the other hand, mitochondrial Ca^{2+} changes were not directly measured in these studies which might explain how nigericin could induce Ca^{2+}-dependent mitochondrial damage without observable changes to bulk cytosolic Ca^{2+}. Thus, whether nigericin increases bulk cytosolic Ca^{2+} like extracellular ATP during NLRP3 inflammasome activation to mediate Ca^{2+}-induced mitochondrial damage is unclear from the literature.

In the present thesis, we measured cytosolic Ca^{2+} changes during nigericin-induced NLRP3 inflammasome activation in relation to mitochondrial depolarization **(Figure 3.8.2)**. As 12,13-DiHOME is known to modulate cytosolic Ca^{2+} transport through cation channels such as TRPA1 [195], TRPV1 [195,196], and RyRs [189], we theorized that 12,13-DiHOME-priming could promote nigericin-induced NLRP3 inflammasome activation by increasing bulk cytosolic Ca^{2+} levels during the activation phase to promote mitochondrial Ca^{2+} uptake and Ca^{2+} overload-induced damage. In our study, we did not observe immediate increases in bulk cytosolic Ca^{2+} induced by nigericin, but cytosolic Ca^{2+} increased at later timepoints (>15 minutes post-nigericin) during the activation phase of vehicle-primed macrophages **(Figure 3.8.2E)**. As vehicle-primed macrophages were capable of low levels of NLRP3 inflammasome activation **(Figure 3.4C)**, our observations are more in line with

Katsnelson et al. who demonstrated that bulk cytosolic Ca^{2+} increases are a simultaneous or secondary result of nigericin-induced NLRP3 inflammasome activation [131]. Although lytic cell death (likely pyroptosis) during the activation phase prevented us from observing bulk cytosolic Ca^{2+} increases at later timepoints in all LPS-primed macrophage groups **(Figure 3.8.4G-I)**, 12,13-DiHOME present during priming did not change cytosolic Ca^{2+} levels during the inflammasome activation phase despite exacerbating mitochondrial depolarization **(Figure 3.8.2F)**. Thus, MCU-dependent mitochondrial damage, exacerbated by 12,13-DiHOME-priming, is likely independent from changes to cytosolic Ca^{2+} levels. Future experiments using more sensitive Ca^{2+}-imaging techniques with higher spatial and temporal resolution (e.g. quantitative Ca^{2+} indicators such as Fura-2 in combination with spinning-disk confocal microscopy) plus complementary methods (e.g. calcium transport antagonists or genetic knockouts) are required to confirm that changes in bulk cytosolic Ca^{2+} levels are not involved in 12,13-DiHOME-exacerbated NLRP3 inflammasome activation.

Another major limitation is that we did not directly measure whether mitochondrial Ca^{2+} was affected by 12,13-DiHOME priming, or how changes in mitochondrial Ca^{2+} dynamics related to mitochondrial damage. Xian et al. demonstrated that mitochondrial Ca^{2+} is immediately increased within the first 30-60 seconds of adding inflammasome activators ATP, nigericin, alum, or MSU crystals in an MCU- but not IP_3 receptor-dependent manner [132]. MCU inhibition but not IP_3R inhibition blocked ATP or nigericin-induced mitochondrial Ca^{2+} influx and prevented mPTP opening, VDAC oligomerization, and the release of oxidized mtDNA fragments concomitant with mtROS production and mitochondrial depolarization which enhanced NLRP3 inflammasome activation. As well, ATP-induced mitochondrial Ca^{2+} overload could be dissociated from changes in bulk

cytosolic Ca^{2+}[132]. As we did not measure mitochondrial Ca^{2+} during nigericin-induced NLRP3 inflammasome activation, it is unclear whether: (i) 12,13-DiHOME increases the sensitivity of mitochondria to Ca^{2+} overload-induced damage, (ii) 12,13-DiHOME increases mitochondrial Ca^{2+} levels through increased influx through channels such as MCU or by hampered calcium efflux, or (iii) 12,13-DiHOME mediates a combination of these effects. We theorize that 12,13-DiHOME-induced respiratory dysfunction during priming **(Figures 3.6.2 – 3.6.3)** might hamper mitochondrial Ca^{2+} handling to promote Ca^{2+}-overload induced damage. Indeed, mitochondrial respiratory function and mitochondrial calcium handling are interdependent processes. Mitochondrial Ca^{2+} transport is a proton motive force-coupled process that competes with proton-driven ATP synthesis [133], so defects in respiratory chain function, such as uncoupling **(Figure 3.6.2D)** and reduced spare respiratory capacity **(Figure 3.6.2E)**, may lead to dysregulation of mitochondrial Ca^{2+} transport that could exacerbate Ca^{2+}-induced mitochondrial damage downstream of nigericin-induced mitochondrial respiratory stress. Hypothetically, uncoupling of the H^+ gradient from ATP synthesis by nigericin acting at the inner mitochondrial membrane (K^+ efflux and H^+ influx into the matrix) in combination with nigericin-induced mitochondrial Ca^{2+} influx due to upstream extramitochondrial effects may dissipate the H^+ gradient and lead to stimulation of mitochondrial respiration to maintain it. As a result, H^+-coupled Ca^{2+} efflux is challenged, and 12,13-DiHOME-primed macrophages with respiratory dysfunction struggle to maintain both the H^+ gradient, ATP synthesis, and sufficient mitochondrial Ca^{2+} efflux to prevent Ca^{2+} overload-induced damage (increased mitochondrial Ca^{2+} might first promote mitochondrial respiration [312] but eventually reach mtROS-exacerbating or mPTP-triggering levels [313,314]). Whether 12,13-DiHOME has additional effects on MCU-mediated Ca^{2+}

transport will be discussed in the next section. More elaborate experiments assessing the relationship between 12,13-DiHOME's effects during priming (ie. mitochondrial respiratory dysfunction, mitophagy defects), mitochondrial, cytosolic, ER, or other organellar Ca^{2+} transport dynamics, and the nature of Ca^{2+}-induced mitochondrial damage are required to elucidate the mechanisms by which 12,13-DiHOME exacerbates NLRP3 inflammasome activation.

4.9 12,13-DiHOME and mitochondrial calcium uniporter-dependent effects on NLRP3 inflammasome activation

Although other mitochondrial Ca^{2+} import mechanisms exist, MCU is the major channel involved in mitochondrial Ca^{2+} uptake [133]. The gene encoding the pore-forming subunit of MCU was only recently identified simultaneously by Baughman et al. and Stefani et al. [315,316]. While VDAC confers non-selective cation permeability to the outer mitochondrial membrane that is not rate-limiting, MCU is a multiprotein complex located on the inner mitochondrial membrane that mediates selective Ca^{2+} transport from the intermembrane space into the matrix [317,318]. The main MCU complex consists of the pore-forming MCU protein itself (targeted by the inhibitor ruthenium red as well as its derivatives Ru360 and Ru265) [233,316,319], as well as other channel-forming subunits with essential or regulatory functions [320]. Importantly, MCU is a low-affinity Ca^{2+} channel; although bulk cytosolic Ca^{2+} concentrations only fluctuate between 0.1 – 5 μM, the K_d for Ca^{2+} binding to MCU was at least 25 μM, initially questioning its functional relevance to mitochondrial Ca^{2+} import [321]. However, direct mitochondria and endoplasmic reticulum contacts called mitochondria-associated endoplasmic reticulum membranes

(MAMs) exist which contain high concentrations of MCU and VDAC1 on mitochondrial membranes, IP_3R on ER membranes, and other anchoring or regulatory proteins linking both organelles [322]. Ca^{2+} exiting the ER at MAMs creates transient cytosolic Ca^{2+} "hotspots" which allow sufficient mitochondrial Ca^{2+} import through MCU despite its low Ca^{2+} binding affinity [321,323,324]. Importantly, mitochondrial Ca^{2+} transport is coupled to both the H^+ gradient and the electrochemical gradient at the inner membrane; Ca^{2+} influx is driven by the large mitochondrial membrane potential (-150 to -180 mV), and Ca^{2+} efflux is dependent upon H^+-coupled transporters such as the putative mitochondrial Ca^{2+}/H exchanger (mHCX) and the Na^+-Ca^{2+}-Li^+ exchanger (NCLX) coupled to the Na^+-H^+ exchanger (NHE) [133]. Together, these processes maintain mitochondrial Ca^{2+} homeostasis, but various stimuli can lead to transient increases or decreases in mitochondrial Ca^{2+}, new "setpoints" for basal mitochondrial Ca^{2+}, or total mitochondrial collapse caused by Ca^{2+} depletion (e.g. bioenergetic crisis due to lack of Ca^{2+}-stimulated TCA cycle or respiratory chain activity) or Ca^{2+} overload (e.g. due to Ca^{2+}-induced mtROS production and/or mPTP opening [317]. Thus, MCU has been implicated in multiple physiological and pathophysiological processes, including cardiovascular disease, neurodegenerative disease, skeletal muscle disorders [320], and more recently, NLRP3 inflammasome activation. MCU appears to largely mediate Ca^{2+}-induced mitochondrial damage that exacerbates NLRP3 inflammasome activation [230]. NLRP3 inflammasome activation by complement membrane attack complex was shown to stimulate IP_3R-mediated Ca^{2+}-release from the ER, leading to MCU-dependent mitochondrial Ca^{2+} accumulation and damage that promoted NLRP3 inflammasome activation [128]. Interestingly, Dong et al. demonstrated that MCU deletion did not blunt NLRP3 inflammasome activation by ATP or nigericin but appeared to blunt phagocytosis-

mediated NLRP3 inflammasome activation by particulates silica and alum [129]. Upon particulate phagocytosis, MCU-dependent buffering of cytosolic Ca^{2+} inhibited endosomal sorting complex required for transport-III (ESCRT), a protein involved in phagolysosomal repair, leading to increased phagolysosomal destabilization and downstream NLRP3 inflammasome activation. Conversely, Xian et al. demonstrated that ATP, nigericin, MSU, and alum-induced NLRP3 inflammasome activation were blunted by pharmacological inhibition of MCU with ruthenium red [132]. In this study, these NLRP3 inflammasome activators induced MCU-dependent mitochondrial Ca^{2+} influx that led to mPTP opening at the inner mitochondrial membrane and VDAC oligomerization at the outer mitochondrial membrane, allowing the escape of oxidized mtDNA fragments which bind and activate the NLRP3 inflammasome in the cytosol. Interestingly, the pharmacological IP_3R inhibitor xestospongin C inhibited the ATP-induced increase in bulk cytosolic Ca^{2+} but not mitochondrial Ca^{2+} influx, suggesting increases in bulk cytosolic Ca^{2+} can be dissociated from changes in mitochondrial Ca^{2+}. Whether xestospongin C completely blocked IP_3R at the concentration and timepoint used, especially at MAMs, was not confirmed. Overall, the role of MCU in NLRP3 inflammasome activation appears to be multifaceted and dependent upon the activation stimulus utilized, although MCU-dependent Ca^{2+} overload-induced mitochondrial damage is at least modulatory for NLRP3 inflammasome activation.

We demonstrated that nigericin-induced mitochondrial damage in LPS+12,13-DiHOME-primed macrophages could be blocked by MCU inhibition with Ru265 present during the activation phase **(Figure 3.8.2I)**. However, this only reduced NLRP3 inflammasome activation in LPS+12,13-DiHOME-primed macrophages to levels comparable to macrophages primed with LPS-alone **(Figure 3.9)**. MCU inhibition also did

not block NLRP3 inflammasome activation in macrophages primed with LPS-alone. These data suggest that MCU-dependent mitochondrial damage is not necessary for NLRP3 inflammasome activation in THP1 macrophages, but 12,13-DiHOME, through effects on mitochondria during priming, may enhance MCU-dependent mitochondrial damage to exacerbate NLRP3 inflammasome activation. As we did not measure mitochondrial Ca^{2+} levels in our experiments, it is unclear how 12,13-DiHOME might exacerbate MCU-dependent mitochondrial damage or if this truly depends on changes in mitochondrial Ca^{2+}. As mentioned previously, 12,13-DiHOME could increase the sensitivity of mitochondria to Ca^{2+}-induced damage through mitochondrial respiratory dysfunction that abrogates H^{+}-coupled mitochondrial Ca^{2+} efflux. Interestingly, the N-terminal domain of MCU located in the mitochondrial matrix can be S-glutathionylated in response to mtROS-induced oxidative stress, inducing conformational changes which promote MCU opening [325]. As LPS+12,13-DiHOME-primed macrophages displayed enhanced nigericin-induced mtROS production during NLRP3 inflammasome activation **(Figure 3.8.2C)**, S-glutathionylation of MCU could be increased in these cells during the activation phase, increasing mitochondrial Ca^{2+} influx and Ca^{2+} overload-induced damage. Intriguingly, Balderas et al. have shown that MCU expression is regulated by complex I respiratory function [304]. The researchers demonstrated that MCU and complex I physically interact, and reduced complex I respiratory function leads to reduced MCU protein turnover. Thus, complex I dysfunction promotes accumulation of MCU that enhances mitochondrial Ca^{2+} uptake. Balderas et al. suggest this is a homeostatic mechanism that promotes Ca^{2+}-stimulated mitochondrial ATP production to prevent bioenergetic crisis [304], but it is an interesting postulation that MCU accumulation downstream of complex I dysfunction could be pathological in other contexts,

such as cases where mitochondria are challenged with high Ca^{2+} influx. As such, mitochondrial respiratory dysfunction induced by 12,13-DiHOME during priming, which was complex I-selective **(Figures 3.6.2 – 3.6.3)**, could lead to an accumulation of MCU prior to NLRP3 inflammasome activation. Upon addition of nigericin, MCU-dependent Ca^{2+}-influx would be enhanced, promoting mitochondrial Ca^{2+} overload and damage that potentiates NLRP3 inflammasome activation. We did not measure MCU expression in our experiments, but this would be interesting to pursue in future studies. As well, MCU stability is dependent on direct interactions with mitochondrial cardiolipin [326] and likely overall membrane lipid composition [320]. Future studies should pursue whether 12,13-DiHOME affects mitochondrial membrane biophysical properties either by (i) directly becoming esterified into phospholipids to affect membrane fluidity and MCU function or (ii) through upstream pathways leading to lipid membrane remodeling (e.g. mtROS-dependent cardiolipin externalization to the OMM [94,112]. Complementary experiments are necessary to confirm that Ru265 abrogates mitochondrial Ca^{2+} influx and Ca^{2+}-induced mitochondrial damage at the concentration utilized (25 μM). We must also use different inhibitors or gene ablation studies to demonstrate that (i) Ru265 mediates inhibition of mitochondrial damage and NLRP3 inflammasome activation specifically through MCU rather than off-target effects, and (ii) test whether 12,13-DiHOME's effects depend on MCU function. Importantly, we must determine whether the lack of observed bulk cytosolic Ca^{2+} changes during nigericin-induced NLRP3 inflammasome activation **(Figure 3.8.2)** are either: (i) a result of our methods having insufficient sensitivity or temporal resolution to detect small or transient changes in bulk cytosolic Ca^{2+}, or (ii) due to the involvement of cytosolic Ca^{2+} microdomains at MAMs which mediate MCU-dependent Ca^{2+} entry into mitochondria and

Ca^{2+} overload-induced damage. Overall, although we demonstrated that exacerbated mitochondrial damage and NLRP3 inflammasome activation in LPS+12,13-DiHOME-primed macrophages is MCU-dependent, how MCU activities are modulated by 12,13-DiHOME is unknown and should be pursued in future studies.

4.10 Other future directions

4.10.1 Identification of molecular targets for 12,13-DiHOME in macrophage inflammation

Future studies aimed towards identifying the molecular targets of 12,13-DiHOME are necessary to understand how it may exacerbate inflammatory macrophage polarization and NLRP3 inflammasome activation. These data will improve our ability to target 12,13-DiHOME for therapeutic effects in SCM pathophysiology. 0.5 μM 12,13-DiHOME exogenously added to THP1 macrophages is likely both water-soluble in serum-containing media and will partition preferentially into cells [165]; 12,13-DHOME has a predicted water solubility of 0.036 g/L (approximately 114 μM) and log P value of 5.2 obtained from the Human Metabolome Database [327]. Free fatty acids either freely present in solution or associated with serum albumins in media, which can accommodate 300-600 μM of free fatty acids, can be delivered to plasma membranes and integrate due to their amphipathic nature [328]. Either through associations with fatty acid transporters or by spontaneously "flip-flopping" from the outer to inner leaflet due to transient protonation, free fatty acids can enter the cell and, again, either exist freely in the cytoplasm or become associated with cytoplasmic fatty acid binding protein [327]. How 12,13-DiHOME may distribute from media, into cells, and toward specific cellular compartments (e.g. mitochondria) has not been

tested. Nevertheless, 12,13-DiHOME present extracellularly, intracellularly, or in plasma membrane may act through direct interactions with extracellular or endosomal receptors, intracellular soluble receptors, or through changes on plasma membrane fluidity properties, meanwhile being subject to degradation pathways such as autooxidation, beta-oxidation, or even further oxidative metabolism by CYP, COX, or LOX enzymes [147,151]. Studies investigating how 12,13-DiHOME affects plasma membrane fluidity properties are lacking, but CYP epoxygenase/sEH-derived metabolites like 12,13-DiHOME can exist in plasma membrane in the free fatty acid form or after becoming esterified into phospholipids. Increased plasma membrane content of another structurally-related PUFA metabolite, the CYP epoxygenase-derived EPA epoxide 17,18-EEQ, has been shown increase membrane fluidity and bending stiffness in human microvascular endothelial cells to increase the number of TRPV4 channels available for activity, overall decreasing Ca^{2+} dependent desensitization of these cells [329]. Whether 12,13-DiHOME can similarly affect plasma membrane properties and how 12,13-DiHOME distributes into cells should be a subject of future studies.

To our knowledge, binding studies for how 12,13-DiHOME directly interacts with putative receptors have not been undertaken, but a few protein targets have been implied to interact with 12,13-DiHOME or at least mediate part of 12,13-DiHOME's effects. 100 μM 12,13-DiHOME could trigger spontaneous whole cell inward currents in sensory neutrons and were dependent on ligand-gated cation channels TRPA1 and TRPV1 and to a lesser extent TRPV3 [195]. Later, Zimmer et al., demonstrated that Ca^{2+} influx in sensory neutrons can be immediately stimulated by exogenously-added 12,13-DiHOME (10 μM), and this was blocked by pharmacological inhibition of TRPV1 but, contrarily, not TRPA1 [196]. In

isolated adult murine cardiomyocytes, Pinckard et al. demonstrated that 12,13-DiHOME-stimulated Ca^{2+} cycling and enhanced FCCP-stimulated respiration was dependent on NOS1 signaling and likely downstream activation of RyR [189]. Levan et al. used human PBMC-derived dendritic cells and RAW264.7 macrophages with a PPARγ-luciferase reporter to demonstrate that treatment with 12,13-DiHOME could activate PPARγ-controlled gene expression, albeit only at concentrations exceeding 75 μM [184]. It is unknown whether 12,13-DiHOME-mediated exacerbation of inflammatory macrophage polarization or NLRP3 inflammasome activation is dependent upon these putative protein interactors. TRPV1 activation has been shown to shift M1 macrophages toward an M2 state [330]. TRPV1 also promotes NLRP3 inflammasome activation through Ca^{2+} influx-induced activation of protein phosphatase 2A and resulting dephosphorylation of the NLRP3 protein [331]. PPARγ activation is well-recognized to inhibit M1 macrophage polarization and promote M2 macrophage polarization [256]. Interestingly, Yang et al. demonstrated that PPARγ may directly interact with the NLRP3 protein during the NLRP3 inflammasome activation phase, blocking interactions between NLRP3 and ASC and preventing inflammasome formation, but it is unclear whether this occurs in a ligand-binding dependent fashion [332]. Future studies should investigate whether 12,13-DiHOME directly binds and activates these protein receptors, or, alternatively, inhibit them through partial agonist activity which antagonizes endogenous ligands. Ligand-receptor binding studies and complementary pharmacological inhibitor or gene ablation studies are required to elucidate whether these proteins are direct molecular targets of 12,13-DiHOME.

The variety of protein targets and biological effects of 12,13-DiHOME may suggest a pleiotropic nature to its biological effects [158]. This appears to be a common property of

CYP epoxygenase/sEH-derived PUFA epoxides and diols [147]. For instance, although a putative 47 kDa G-protein-coupled receptor was thought to mediate the cardioprotective effects of arachidonic acid epoxides, EETs, this receptor has yet to be identified, and no single receptor seems to account for all of its broad effects such as anti-inflammation, cytoprotection, and vasoregulation [147,333]. To identify novel protein targets of 12,13-DiHOME important in macrophage inflammation, it may help to look towards the protein targets of structurally-related PUFA epoxides and diols. Perhaps 12,13-DiHOME's effects are not only dependent upon its own intrinsic ability to modulate a protein target (or plasma membrane properties), but 12,13-DiHOME's activities may also depend on competition with other CYP epoxygenase/sEH-derived PUFA epoxides and diols or their parent PUFAs. For example, 11,12-EET treatment in macrophages is known to shift M1 macrophages towards an M2 phenotype in a PPARα/γ-dependent manner [208]. As well, N-3 PUFAs DHA and EPA act as direct ligands for G-protein coupled free fatty acid receptors GPR120 and GPR40 [334]. These receptors mediate β-arrestin-2 recruitment and direct binding between NLRP3 and β-arrestin-2 to prevent NLRP3 inflammasome assembly and activation [334]. Treatment of LPS-primed macrophages with EETs 10 minutes prior to addition ATP or nigericin inhibits NLRP3 inflammasome activation in a manner which prevents ROS generation and cytosolic Ca^{2+} overload early in the activation phase [213]. The DHA epoxide 19,20-EDP can also inhibit LPS-induced NLRP3 inflammasome activation in cardiomyocytes [142]. 9,10-DiHOME, a regioisomer of 12,13-DiHOME, can induce neutrophil chemotaxis in a manner dependent upon PI3K and G_i proteins but not tyrosine kinase or PKC [176]. Overall, these studies suggest that assessing the overlap of protein-dependent effects by other structurally-related compounds may aid in identifying 12,13-DiHOME's molecular targets. Future

studies assessing the antagonistic (or synergistic) effects of 12,13-DiHOME and other PUFA epoxides or diols on macrophage inflammation, plus pharmacological inhibitor or gene ablation studies, could be extremely beneficial in identifying putative 12,13-DiHOME receptors.

4.10.2 12,13-DiHOME as an autocrine, paracrine, or endocrine factor

We have previously observed elevated myocardial levels of 12,13-DiHOME in murine models of endotoxin-induced cardiomyopathy [159], murine *ex vivo* myocardial ischemia-reperfusion injury (I/R injury) [188], and human tissues of dilated cardiomyopathy patients [187]. CYP epoxygenase and sEH-mediated 12,13-DiHOME production in the heart is mainly attributed to cardiomyocytes due to high expression of CYP epoxygenases and sEH [192], though other cardiac cell types expressing these enzymes, such as endothelial cells, could also contribute to myocardial 12,13-DiHOME production [162]. Neutrophils invading the myocardium during SCM [23] could also theoretically contribute to 12,13-DiHOME production since they are known to produce 12,13-EpOME by hydroxyl radical reacting with linoleic acid during the neutrophil respiratory burst [164,176]. However, neutrophil-derived 12,13-DiHOME has yet to be demonstrated as biologically relevant in the heart. We speculate that cardiomyocyte-derived 12,13-DiHOME could act as a paracrine lipid mediator to proximal macrophages within the myocardium to promote inflammatory macrophage polarization and NLRP3 inflammasome activation, contributing to myocardial hyper-inflammation associated with SCM. Indeed, macrophages are the dominant immune cell in the heart [51,335]. Approximately 5 cardiac macrophages directly associate with a single cardiomyocyte at resting state within murine myocardium, and this number increases

in cardiac disease [53]. Whether *in vivo* macrophages possess the ability to sufficiently utilize linoleic acid and/or 12,13-EpOME directly for 12,13-DiHOME biosynthesis has yet to be demonstrated, although endogenous CYP epoxygenase and sEH activity is important for macrophage cytokine production [336], extracellular matrix remodelling [337], phagocytosis [338], tissue invasion [211] and polarization [208]. Conversely, we observed that 2 μM 12,13-EpOME could not be sufficiently converted by THP1 macrophages into bioactive concentrations of 12,13-DiHOME (≥500 nM) during the priming phase to promote NLRP3 inflammasome activation in our model **(Figure 3.5.4)**. Additionally, as BAT produces 12,13-DiHOME that acts as an endocrine "lipokine" [199] promoting fatty acid uptake and oxidation in skeletal muscle [200] and cardiomyocytes [189], cardiac-derived 12,13-DiHOME may also act as an endocrine factor which enhances macrophage NLRP3 inflammasome activation in extracardiac tissues. Whether 12,13-DiHOME also enhances NLRP3 inflammasome activation in other cell types in SCM, such as cardiomyocytes [141], fibroblasts [138], endothelial cells [339], or dendritic cells [340] has yet to be tested. Overall, we postulate cardiac 12,13-DiHOME could be produced during early phases of SCM, promoting acute inflammation through enhanced inflammatory macrophage polarization and NLRP3 inflammasome activation in macrophages. An interesting future experiment would be to treat macrophages with cardiomyocyte-conditioned media to assess whether cardiomyocytes stressed with SCM-like stimuli (e.g. LPS) can lead to exacerbated inflammatory macrophage polarization or NLRP3 inflammasome activation in a manner dependent on CYP epoxygenase/sEH-mediated 12,13-DiHOME production. In addition, future studies should investigate 12,13-DiHOME's role in not only SCM but also septic multi-organ dysfunction.

4.10.3 Therapeutic viability of targeting 12,13-DiHOME and macrophage inflammation in septic cardiomyopathy: physiological or pathophysiological role?

Targeting 12,13-DiHOME for therapeutic effects in SCM could be approached in several ways. First, increasing the ratio of N-3 to N-6 PUFAs in the diet could reduce the levels of linoleic acid available for CYP epoxygenase/sEH-mediated production of 12,13-DiHOME (or increase other PUFA metabolites which compete with 12,13-DiHOME targets) [147]. For instance, Fan et al. found that n-3 PUFA-enrichment promoted n-3 PUFA epoxide and diol plasma levels while reducing LA epoxides and diols (including 12,13-DiHOME) in high fat diet-treated mice, correlating with attenuated M1 macrophage polarization in adipose tissues [341]. However, this approach is limited by interindividual differences in overall CYP epoxygenase-sEH metabolism, either due to environmental or genetic factors [342,343]. In addition, compounds with antagonistic effects on 12,13-DiHOME biological activities could be utilized, but the lack of specific molecular targets and binding mechanisms of 12,13-DiHOME prevents any therapeutically-viable rational drug design. Lastly, pharmacological sEH inhibition has a two-pronged effect, as cardioprotective PUFA epoxides are preserved while inactive or cardiotoxic PUFA diols (like 12,13-DiHOME) are reduced [147]. In animal models of sepsis, sEH inhibitors have anti-pyretic effects [209], reduce leukocyte infiltration and inflammation in damaged tissues [211], rescue cardiac function and prevent myocardial inflammation and oxidative stress [159] and reduce mortality [210,212]. As well, some clinical trials are testing the effect of sEH inhibitors on diseases with a sterile inflammation component, such as obesity and pre-diabetes [226]. However, it is likely that cardioprotection against SCM offered by sEH inhibitors is not solely attributed to attenuation of 12,13-DiHOME production. Overall, there are multiple

approaches which target the CYP epoxygenase-sEH axis of N-3 and N-6 PUFA metabolism for therapeutic effects in SCM, but future studies are necessary to understand the importance of attenuated 12,13-DiHOME biosynthesis and bioactivities in mediating cardioprotection by these interventions. By understanding its pathophysiological roles, 12,13-DiHOME could also be an important biomarker that could help guide stratified therapies for SCM.

Prior to therapeutically targeting 12,13-DiHOME production to reduce inflammatory macrophage polarization and NLRP3 inflammasome activation in SCM, it should be carefully considered that these processes have physiological roles in SCM. As an example, cardiac macrophage numbers are known to acutely reduce following systemic sepsis by cecal ligation and puncture [66]. The authors of this study suggest that cardiac macrophages die after uptake of bacteria to promote pathogen trapping and subsequent clearance. This is followed by a delayed proliferation phase leading to supranormal cardiac macrophage numbers correlated with roles in reversing SCM. Indeed, Zhang et al. demonstrated that early phases of SCM involve cardiac macrophage subpopulations more tailored to antigen presentation and inflammation, while $TREM2^{hi}$ cardiac macrophages expand in the myocardium during latter phases of SCM to help clear damaged mitochondria exuded from viable cardiomyocytes, correlating with restoration of cardiac function [23]. Following myocardial infarction, extensive remodeling of the cardiac macrophage population is likely mediated by a combination of cell death, circulating monocyte recruitment, and *in situ* local expansion and differentiation [54,74,344]. Regarding 12,13-DiHOME's effects on macrophages, macrophage polarization (ie. the phenotypical shift of macrophages in response to stimuli) is intrinsic to remodeling the cardiac macrophage subpopulation to respond to different phases of SCM. It is also interesting to speculate that NLRP3

inflammasome-mediated inflammation and pyroptosis contributes to cardiac macrophage population remodeling in SCM. Additionally, NLRP3 inflammasome is important in the initial recognition and pro-inflammatory response to infection [135]. NLRP3 inflammasome also mediates anti-infective mechanisms such as intracellular trapping of pathogens in pyroptotic pore-induced intracellular traps [136]. Overall, future studies investigating how 12,13-DiHOME may be involved in the physiological response to pathogen infection or maintaining homeostasis should be conducted prior to targeting its production for therapeutic effects in SCM.

Conversely, our previous studies demonstrate that inhibition of cardiomyocyte-specific sEH is protective in SCM mouse models by limiting cardiac NLRP3 inflammasome activation, IL-1β levels, inflammation, systemic innate immune activation, and macrophage/monocyte recruitment to the heart [142]. It is tempting to speculate that part of this therapeutic benefit is mediated by reducing myocardial 12,13-DiHOME and thus limiting pro-inflammatory macrophage polarization and NLRP3 inflammasome activation. Indeed, cardiac 12,13-DiHOME levels correlate with myocardial dysfunction and inflammation in endotoxin-treated mice, and 12,13-DiHOME can directly induce cardiomyocyte cytotoxicity, inflammation, and mitochondrial dysfunction [159]. However, sEH inhibition could also preserve cardiac levels of cardioprotective PUFA epoxides, including epoxyeicosatrienoic acids which have been shown to inhibit NLRP3 inflammasome activation [213] and inflammatory M1 macrophage polarization [208]. Further research is necessary to assess the viability of sEH inhibitors in treating septic cardiomyopathy and to better understand the physiological and pathophysiological responses elicited by CYP epoxygenase-sEH-mediated metabolites like 12,13-DiHOME.

4.11 Summary of future directions

The literature contains contrasting evidence for 12,13-DiHOME's effects on cytotoxicity, mitochondrial function, inflammation, and other biological functions [158]. As 12,13-DiHOME's biological effects are likely species-, tissue-, concentration-, and time-dependent, these parameters should be compared in parallel. For instance, different cell types (e.g. cardiomyocytes, skeletal muscle, brown adipocytes, macrophages), cell models (e.g. THP1 macrophages, bone marrow-derived macrophages, peritoneal macrophages, PBMC-derived macrophages), and a wider range of concentrations (nanomolar to millimolar) and treatment timepoints should be compared in the same experiments. These data will also provide a basis for the physiological relevance of 12,13-DiHOME's observed effects in THP1 macrophages.

12,13-DiHOME's effects may also be disease context-dependent. The same observed 12,13-DiHOME-induced effects (e.g. inflammation, mitochondrial uncoupling) should be tested for their relevance in different or superimposed disease models. Does cardioprotective BAT-derived 12,13-DiHOME production during high-fat diet [189] have direct deleterious effects on subsequent SCM or myocardial infarction? Does targeting 12,13-DiHOME for therapeutic benefit in SCM lead to deleterious effects in physiological processes like BAT-mediated thermogenesis? Does 12,13-DiHOME mediate similar effects on macrophage inflammation in the heart versus other failing organs in SCM?

Specific receptors which bind 12,13-DiHOME and/or effects on plasma membrane fluidity caused by 12,13-DiHOME should be defined in future studies. Although there are some putative protein receptors which mediate 12,13-DiHOME's effects, assessing how 12,13-DiHOME may antagonize or synergize with other structurally-related N-3 or N-6

PUFAs and their CYP epoxygenase-sEH-derived PUFA metabolites, or other endogenous ligands, may reveal molecular targets of 12,13-DiHOME. Does 12,13-DiHOME possibly antagonize free fatty acid receptors which mediate inhibition of NLRP3 inflammasome by DHA and EPA [334]? Does 12,13-DiHOME mediate partial agonist activity at PPARγ? These studies will also uncover the precise pathways which mediate 12,13-DiHOME's effects on cytotoxicity, mitochondrial respiration, inflammation, and other functions.

It is unclear whether 12,13-DiHOME can act as an autocrine, paracrine, or endocrine signal to affect cardiac macrophages or other tissues *in vivo*. Perhaps cell type-specific gene ablation models (e.g. cardiomyocyte-specific sEH knockout [142]) targeting 12,13-DiHOME production in the heart could be used to identify how 12,13-DiHOME is produced in the septic heart and whether 12,13-DiHOME has direct consequences on cardiac macrophages *in situ*. Data from co-culture models could also support the role of 12,13-DiHOME as either a paracrine factor itself or a signal which modulates paracrine signalling (e.g. cytokine/chemokine secretion).

12,13-DiHOME's observed effects on macrophage polarization and NLRP3 inflammasome activation have yet to be contextualized to physiological or diseased states *in vivo.* Do myocardial 12,13-DiHOME levels correlate with markers of M1 polarization and NLRP3 inflammasome activation in cardiac macrophages of the septic heart? Can experimentally blocking or promoting 12,13-DiHOME production in the heart protect against SCM pathophysiology through effects on cardiac macrophages? As well, future studies should assess whether 12,13-DiHOME has additional effects on other macrophage (or other immune cell) functions, such as phagocytosis, antigen presentation, tissue invasion, extracellular matrix remodeling, inflammatory resolution, tissue repair, and others.

4.12 Conclusion

In the present thesis, we investigated the effects of 12,13-DiHOME, a cardiotoxic linoleic acid diol metabolite with putative roles in SCM pathophysiology, on macrophage inflammation. We hypothesized that 12,13-DiHOME modulates macrophage inflammation through effects on macrophage polarization and NLRP3 inflammasome activation. Using a PMA-differentiated THP1 macrophage-like cell model, we demonstrated that 12,13-DiHOME exacerbated mRNA expression of inflammatory cytokines in polarized macrophages. As well, 12,13-DiHOME present during LPS-priming exacerbated nigericin-induced NLRP3 inflammasome activation. Mitochondrial respiratory dysfunction and mitophagic defects in LPS+12,13-DiHOME-primed macrophages correlated with increased sensitivity to nigericin-induced mitochondrial damage during NLRP3 inflammasome activation. Both nigericin-induced mitochondrial damage and exacerbated NLRP3 inflammasome activation in LPS+12,13-DiHOME-primed macrophages could be blocked by pharmacological MCU inhibition. The specific molecular targets through which 12,13-DiHOME mediates these effects are unclear. The physiological relevance of 12,13-DiHOME and its pro-inflammatory effects on macrophages must also be demonstrated in more physiological macrophage models and *in vivo* studies to determine its mechanisms of action. These studies must precede attempts to therapeutically target 12,13-DiHOME production in SCM, as 12,13-DiHOME is also known to have pleiotropic effects in both disease and homeostasis. The physiological role of macrophage inflammation in SCM should also not be underestimated. Overall, the current thesis provides important information about SCM pathophysiology. These data could aid in identifying novel therapeutic approaches to treat SCM and improve patient outcomes in sepsis.

REFERENCES

1. Singer M, Deutschman CS, Seymour CW, et al. The Third International Consensus Definitions for Sepsis and Septic Shock (Sepsis-3). JAMA. 2016 Feb 23;315(8):801-10.
2. Vincent JL, Moreno R, Takala J, et al. The SOFA (Sepsis-related Organ Failure Assessment) score to describe organ dysfunction/failure. On behalf of the Working Group on Sepsis-Related Problems of the European Society of Intensive Care Medicine. Intensive Care Med. 1996 Jul;22(7):707-10.
3. Rudd KE, Johnson SC, Agesa KM, et al. Global, regional, and national sepsis incidence and mortality, 1990-2017: analysis for the Global Burden of Disease Study. Lancet. 2020 Jan 18;395(10219):200-211.
4. Evans L, Rhodes A, Alhazzani W, et al. Surviving Sepsis Campaign: International Guidelines for Management of Sepsis and Septic Shock 2021. Crit Care Med. 2021 Nov 1;49(11):e1063-e1143.
5. Hollenberg SM, Singer M. Pathophysiology of sepsis-induced cardiomyopathy. Nat Rev Cardiol. 2021 Jun;18(6):424-434.
6. Parker MM, Shelhamer JH, Bacharach SL, et al. Profound but reversible myocardial depression in patients with septic shock. Ann Intern Med. 1984 Apr;100(4):483-90.
7. Cunnion RE, Schaer GL, Parker MM, et al. The coronary circulation in human septic shock. Circulation. 1986 Apr;73(4):637-44.
8. Beesley SJ, Weber G, Sarge T, et al. Septic Cardiomyopathy. Crit Care Med. 2018 Apr;46(4):625-634.
9. Sanfilippo F, Corredor C, Arcadipane A, et al. Tissue Doppler assessment of diastolic function and relationship with mortality in critically ill septic patients: a systematic review and meta-analysis. Br J Anaesth. 2017 Oct 1;119(4):583-594.
10. Winkelhorst JC, Bootsma IT, Koetsier PM, et al. Right Ventricular Function and Long-Term Outcome in Sepsis: A Retrospective Cohort Study. Shock. 2020 May;53(5):537-543.
11. Turner A, Tsamitros M, Bellomo R. Myocardial cell injury in septic shock. Crit Care Med. 1999 Sep;27(9):1775-80.
12. Papanikolaou J, Makris D, Mpaka M, et al. New insights into the mechanisms involved in B-type natriuretic peptide elevation and its prognostic value in septic patients. Crit Care. 2014 May 9;18(3):R94.
13. Nizamuddin J, Mahmood F, Tung A, et al. Interval Changes in Myocardial Performance Index Predict Outcome in Severe Sepsis. J Cardiothorac Vasc Anesth. 2017 Jun;31(3):957-964.
14. Raymond SL, Holden DC, Mira JC, et al. Microbial recognition and danger signals in sepsis and trauma. Biochim Biophys Acta Mol Basis Dis. 2017 Oct;1863(10 Pt B):2564-2573.
15. Turvey SE, Broide DH. Innate immunity. J Allergy Clin Immunol. 2010 Feb;125(2 Suppl 2):S24-32.
16. Fallach R, Shainberg A, Avlas O, et al. Cardiomyocyte Toll-like receptor 4 is involved in heart dysfunction following septic shock or myocardial ischemia. J Mol Cell Cardiol. 2010 Jun;48(6):1236-44.

17. Roh JS, Sohn DH. Damage-Associated Molecular Patterns in Inflammatory Diseases. Immune Netw. 2018 Aug;18(4):e27.
18. Zindel J, Kubes P. DAMPs, PAMPs, and LAMPs in Immunity and Sterile Inflammation. Annu Rev Pathol. 2020 Jan 24;15:493-518.
19. Nauseef WM, Borregaard N. Neutrophils at work. Nat Immunol. 2014 Jul;15(7):602-11.
20. Shi C, Pamer EG. Monocyte recruitment during infection and inflammation. Nat Rev Immunol. 2011 Oct 10;11(11):762-74.
21. Sugimoto MA, Sousa LP, Pinho V, et al. Resolution of Inflammation: What Controls Its Onset? Front Immunol. 2016;7:160.
22. Liu YC, Yu MM, Shou ST, et al. Sepsis-Induced Cardiomyopathy: Mechanisms and Treatments. Front Immunol. 2017;8:1021.
23. Zhang K, Wang Y, Chen S, et al. TREM2(hi) resident macrophages protect the septic heart by maintaining cardiomyocyte homeostasis. Nat Metab. 2023 Jan;5(1):129-146.
24. Kumar A, Thota V, Dee L, et al. Tumor necrosis factor alpha and interleukin 1beta are responsible for in vitro myocardial cell depression induced by human septic shock serum. J Exp Med. 1996 Mar 1;183(3):949-58.
25. Kumar A, Brar R, Wang P, et al. Role of nitric oxide and cGMP in human septic serum-induced depression of cardiac myocyte contractility. Am J Physiol. 1999 Jan;276(1):R265-76.
26. Joulin O, Petillot P, Labalette M, et al. Cytokine profile of human septic shock serum inducing cardiomyocyte contractile dysfunction. Physiol Res. 2007;56(3):291-297.
27. Garner LB, Willis MS, Carlson DL, et al. Macrophage migration inhibitory factor is a cardiac-derived myocardial depressant factor. Am J Physiol Heart Circ Physiol. 2003 Dec;285(6):H2500-9.
28. Lehmann LE, Novender U, Schroeder S, et al. Plasma levels of macrophage migration inhibitory factor are elevated in patients with severe sepsis. Intensive Care Med. 2001 Aug;27(8):1412-5.
29. Zhang C, Mo M, Ding W, et al. High-mobility group box 1 (HMGB1) impaired cardiac excitation-contraction coupling by enhancing the sarcoplasmic reticulum (SR) Ca(2+) leak through TLR4-ROS signaling in cardiomyocytes. J Mol Cell Cardiol. 2014 Sep;74:260-73.
30. West AP, Shadel GS. Mitochondrial DNA in innate immune responses and inflammatory pathology. Nat Rev Immunol. 2017 Jun;17(6):363-375.
31. Nakahira K, Kyung SY, Rogers AJ, et al. Circulating mitochondrial DNA in patients in the ICU as a marker of mortality: derivation and validation. PLoS Med. 2013 Dec;10(12):e1001577; discussion e1001577.
32. Vincent JL, Bakker J, Marecaux G, et al. Administration of anti-TNF antibody improves left ventricular function in septic shock patients. Results of a pilot study. Chest. 1992 Mar;101(3):810-5.
33. Lv S, Han M, Yi R, et al. Anti-TNF-alpha therapy for patients with sepsis: a systematic meta-analysis. Int J Clin Pract. 2014 Apr;68(4):520-8.

34. Meyer NJ, Reilly JP, Anderson BJ, et al. Mortality Benefit of Recombinant Human Interleukin-1 Receptor Antagonist for Sepsis Varies by Initial Interleukin-1 Receptor Antagonist Plasma Concentration. Crit Care Med. 2018 Jan;46(1):21-28.
35. Shakoory B, Carcillo JA, Chatham WW, et al. Interleukin-1 Receptor Blockade Is Associated With Reduced Mortality in Sepsis Patients With Features of Macrophage Activation Syndrome: Reanalysis of a Prior Phase III Trial. Crit Care Med. 2016 Feb;44(2):275-81.
36. Schulz R, Panas DL, Catena R, et al. The role of nitric oxide in cardiac depression induced by interleukin-1 beta and tumour necrosis factor-alpha. Br J Pharmacol. 1995 Jan;114(1):27-34.
37. Ferdinandy P, Danial H, Ambrus I, et al. Peroxynitrite is a major contributor to cytokine-induced myocardial contractile failure. Circ Res. 2000 Aug 4;87(3):241-7.
38. Lopez A, Lorente JA, Steingrub J, et al. Multiple-center, randomized, placebo-controlled, double-blind study of the nitric oxide synthase inhibitor 546C88: effect on survival in patients with septic shock. Crit Care Med. 2004 Jan;32(1):21-30.
39. Hasslacher J, Bijuklic K, Bertocchi C, et al. Levosimendan inhibits release of reactive oxygen species in polymorphonuclear leukocytes in vitro and in patients with acute heart failure and septic shock: a prospective observational study. Crit Care. 2011 Jul 12;15(4):R166.
40. Morelli A, De Castro S, Teboul JL, et al. Effects of levosimendan on systemic and regional hemodynamics in septic myocardial depression. Intensive Care Med. 2005 May;31(5):638-44.
41. Gordon AC, Perkins GD, Singer M, et al. Levosimendan for the Prevention of Acute Organ Dysfunction in Sepsis. N Engl J Med. 2016 Oct 27;375(17):1638-1648.
42. Williams JW, Giannarelli C, Rahman A, et al. Macrophage Biology, Classification, and Phenotype in Cardiovascular Disease: JACC Macrophage in CVD Series (Part 1). J Am Coll Cardiol. 2018 Oct 30;72(18):2166-2180.
43. Gordon S, Martinez-Pomares L. Physiological roles of macrophages. Pflugers Arch. 2017 Apr;469(3-4):365-374.
44. Epelman S, Lavine KJ, Randolph GJ. Origin and functions of tissue macrophages. Immunity. 2014 Jul 17;41(1):21-35.
45. Amarante-Mendes GP, Adjemian S, Branco LM, et al. Pattern Recognition Receptors and the Host Cell Death Molecular Machinery. Front Immunol. 2018;9:2379.
46. Murray PJ. Macrophage Polarization. Annu Rev Physiol. 2017 Feb 10;79:541-566.
47. Hashimoto D, Chow A, Noizat C, et al. Tissue-resident macrophages self-maintain locally throughout adult life with minimal contribution from circulating monocytes. Immunity. 2013 Apr 18;38(4):792-804.
48. Watanabe S, Alexander M, Misharin AV, et al. The role of macrophages in the resolution of inflammation. J Clin Invest. 2019 May 20;129(7):2619-2628.
49. Leid J, Carrelha J, Boukarabila H, et al. Primitive Embryonic Macrophages are Required for Coronary Development and Maturation. Circ Res. 2016 May 13;118(10):1498-511.

50. Lavine KJ, Pinto AR, Epelman S, et al. The Macrophage in Cardiac Homeostasis and Disease: JACC Macrophage in CVD Series (Part 4). J Am Coll Cardiol. 2018 Oct 30;72(18):2213-2230.
51. Pinto AR, Ilinykh A, Ivey MJ, et al. Revisiting Cardiac Cellular Composition. Circ Res. 2016 Feb 5;118(3):400-9.
52. Epelman S, Lavine KJ, Beaudin AE, et al. Embryonic and adult-derived resident cardiac macrophages are maintained through distinct mechanisms at steady state and during inflammation. Immunity. 2014 Jan 16;40(1):91-104.
53. Nicolas-Avila JA, Lechuga-Vieco AV, Esteban-Martinez L, et al. A Network of Macrophages Supports Mitochondrial Homeostasis in the Heart. Cell. 2020 Oct 1;183(1):94-109 e23.
54. Heidt T, Courties G, Dutta P, et al. Differential contribution of monocytes to heart macrophages in steady-state and after myocardial infarction. Circ Res. 2014 Jul 7;115(2):284-95.
55. Hulsmans M, Clauss S, Xiao L, et al. Macrophages Facilitate Electrical Conduction in the Heart. Cell. 2017 Apr 20;169(3):510-522 e20.
56. Lavine KJ, Epelman S, Uchida K, et al. Distinct macrophage lineages contribute to disparate patterns of cardiac recovery and remodeling in the neonatal and adult heart. Proc Natl Acad Sci U S A. 2014 Nov 11;111(45):16029-34.
57. Li W, Hsiao HM, Higashikubo R, et al. Heart-resident CCR2(+) macrophages promote neutrophil extravasation through TLR9/MyD88/CXCL5 signaling. JCI Insight. 2016 Aug 4;1(12).
58. Gundra UM, Girgis NM, Ruckerl D, et al. Alternatively activated macrophages derived from monocytes and tissue macrophages are phenotypically and functionally distinct. Blood. 2014 May 15;123(20):e110-22.
59. Mills CD, Kincaid K, Alt JM, et al. M-1/M-2 macrophages and the Th1/Th2 paradigm. J Immunol. 2000 Jun 15;164(12):6166-73.
60. Yao Y, Xu XH, Jin L. Macrophage Polarization in Physiological and Pathological Pregnancy. Front Immunol. 2019;10:792.
61. Mantovani A, Sica A, Sozzani S, et al. The chemokine system in diverse forms of macrophage activation and polarization. Trends Immunol. 2004 Dec;25(12):677-86.
62. Xue J, Schmidt SV, Sander J, et al. Transcriptome-based network analysis reveals a spectrum model of human macrophage activation. Immunity. 2014 Feb 20;40(2):274-88.
63. Murray PJ, Allen JE, Biswas SK, et al. Macrophage activation and polarization: nomenclature and experimental guidelines. Immunity. 2014 Jul 17;41(1):14-20.
64. Cho H, Kwon HY, Sharma A, et al. Visualizing inflammation with an M1 macrophage selective probe via GLUT1 as the gating target. Nat Commun. 2022 Oct 10;13(1):5974.
65. Kambara K, Ohashi W, Tomita K, et al. In vivo depletion of CD206+ M2 macrophages exaggerates lung injury in endotoxemic mice. Am J Pathol. 2015 Jan;185(1):162-71.
66. Hoyer FF, Naxerova K, Schloss MJ, et al. Tissue-Specific Macrophage Responses to Remote Injury Impact the Outcome of Subsequent Local Immune Challenge. Immunity. 2019 Nov 19;51(5):899-914 e7.

67. Zhang G, Dong D, Wan X, et al. Cardiomyocyte death in sepsis: Mechanisms and regulation (Review). Mol Med Rep. 2022 Aug;26(2).
68. Neu C, Thiele Y, Horr F, et al. DAMPs Released from Proinflammatory Macrophages Induce Inflammation in Cardiomyocytes via Activation of TLR4 and TNFR. Int J Mol Sci. 2022 Dec 8;23(24).
69. Jia L, Wang Y, Wang Y, et al. Heme Oxygenase-1 in Macrophages Drives Septic Cardiac Dysfunction via Suppressing Lysosomal Degradation of Inducible Nitric Oxide Synthase. Circ Res. 2018 May 25;122(11):1532-1544.
70. Sun X, Liu Y, Wang J, et al. Cardioprotection of M2 macrophages-derived exosomal microRNA-24-3p/Tnfsf10 axis against myocardial injury after sepsis. Mol Immunol. 2022 Jan;141:309-317.
71. Song C, Xu J, Gao C, et al. Nanomaterials targeting macrophages in sepsis: A promising approach for sepsis management. Front Immunol. 2022;13:1026173.
72. Wang L, Li Y, Wang X, et al. GDF3 Protects Mice against Sepsis-Induced Cardiac Dysfunction and Mortality by Suppression of Macrophage Pro-Inflammatory Phenotype. Cells. 2020 Jan 3;9(1).
73. Chen P, Stanojcic M, Jeschke MG. Differences between murine and human sepsis. Surg Clin North Am. 2014 Dec;94(6):1135-49.
74. Bajpai G, Bredemeyer A, Li W, et al. Tissue Resident CCR2- and CCR2+ Cardiac Macrophages Differentially Orchestrate Monocyte Recruitment and Fate Specification Following Myocardial Injury. Circ Res. 2019 Jan 18;124(2):263-278.
75. Zaman R, Epelman S. Resident cardiac macrophages: Heterogeneity and function in health and disease. Immunity. 2022 Sep 13;55(9):1549-1563.
76. Mosser DM, Edwards JP. Exploring the full spectrum of macrophage activation. Nat Rev Immunol. 2008 Dec;8(12):958-69.
77. Guo H, Callaway JB, Ting JP. Inflammasomes: mechanism of action, role in disease, and therapeutics. Nat Med. 2015 Jul;21(7):677-87.
78. Howard AD, Kostura MJ, Thornberry N, et al. IL-1-converting enzyme requires aspartic acid residues for processing of the IL-1 beta precursor at two distinct sites and does not cleave 31-kDa IL-1 alpha. J Immunol. 1991 Nov 1;147(9):2964-9.
79. Gu Y, Kuida K, Tsutsui H, et al. Activation of interferon-gamma inducing factor mediated by interleukin-1beta converting enzyme. Science. 1997 Jan 10;275(5297):206-9.
80. Shi J, Zhao Y, Wang K, et al. Cleavage of GSDMD by inflammatory caspases determines pyroptotic cell death. Nature. 2015 Oct 29;526(7575):660-5.
81. He WT, Wan H, Hu L, et al. Gasdermin D is an executor of pyroptosis and required for interleukin-1beta secretion. Cell Res. 2015 Dec;25(12):1285-98.
82. Evavold CL, Ruan J, Tan Y, et al. The Pore-Forming Protein Gasdermin D Regulates Interleukin-1 Secretion from Living Macrophages. Immunity. 2018 Jan 16;48(1):35-44 e6.
83. Xie WJ, Xia S, Warshel A, et al. Electrostatic influence on IL-1 transport through the GSDMD pore. Proc Natl Acad Sci U S A. 2022 Feb 8;119(6).
84. Lu A, Magupalli VG, Ruan J, et al. Unified polymerization mechanism for the assembly of ASC-dependent inflammasomes. Cell. 2014 Mar 13;156(6):1193-1206.
85. Yang X, Chang HY, Baltimore D. Autoproteolytic activation of pro-caspases by oligomerization. Mol Cell. 1998 Jan;1(2):319-25.

86. Swanson KV, Deng M, Ting JP. The NLRP3 inflammasome: molecular activation and regulation to therapeutics. Nat Rev Immunol. 2019 Aug;19(8):477-489.
87. Hornung V, Ablasser A, Charrel-Dennis M, et al. AIM2 recognizes cytosolic dsDNA and forms a caspase-1-activating inflammasome with ASC. Nature. 2009 Mar 26;458(7237):514-8.
88. Xu L, Zhou J, Che J, et al. Mitochondrial DNA enables AIM2 inflammasome activation and hepatocyte pyroptosis in nonalcoholic fatty liver disease. Am J Physiol Gastrointest Liver Physiol. 2021 Jun 1;320(6):G1034-G1044.
89. Vance RE. The NAIP/NLRC4 inflammasomes. Curr Opin Immunol. 2015 Feb;32:84-9.
90. Bauernfeind FG, Horvath G, Stutz A, et al. Cutting edge: NF-kappaB activating pattern recognition and cytokine receptors license NLRP3 inflammasome activation by regulating NLRP3 expression. J Immunol. 2009 Jul 15;183(2):787-91.
91. Juliana C, Fernandes-Alnemri T, Kang S, et al. Non-transcriptional priming and deubiquitination regulate NLRP3 inflammasome activation. J Biol Chem. 2012 Oct 19;287(43):36617-22.
92. Rodgers MA, Bowman JW, Fujita H, et al. The linear ubiquitin assembly complex (LUBAC) is essential for NLRP3 inflammasome activation. J Exp Med. 2014 Jun 30;211(7):1333-47.
93. Hara H, Tsuchiya K, Kawamura I, et al. Phosphorylation of the adaptor ASC acts as a molecular switch that controls the formation of speck-like aggregates and inflammasome activity. Nat Immunol. 2013 Dec;14(12):1247-55.
94. Elliott EI, Miller AN, Banoth B, et al. Cutting Edge: Mitochondrial Assembly of the NLRP3 Inflammasome Complex Is Initiated at Priming. J Immunol. 2018 May 1;200(9):3047-3052.
95. McGeough MD, Wree A, Inzaugarat ME, et al. TNF regulates transcription of NLRP3 inflammasome components and inflammatory molecules in cryopyrinopathies. J Clin Invest. 2017 Dec 1;127(12):4488-4497.
96. Gaidt MM, Ebert TS, Chauhan D, et al. Human Monocytes Engage an Alternative Inflammasome Pathway. Immunity. 2016 Apr 19;44(4):833-46.
97. Kelley N, Jeltema D, Duan Y, et al. The NLRP3 Inflammasome: An Overview of Mechanisms of Activation and Regulation. Int J Mol Sci. 2019 Jul 6;20(13).
98. Zheng Y, Xu L, Dong N, et al. NLRP3 inflammasome: The rising star in cardiovascular diseases. Front Cardiovasc Med. 2022;9:927061.
99. Tapia-Abellan A, Angosto-Bazarra D, Alarcon-Vila C, et al. Sensing low intracellular potassium by NLRP3 results in a stable open structure that promotes inflammasome activation. Sci Adv. 2021 Sep 17;7(38):eabf4468.
100. Zhou R, Yazdi AS, Menu P, et al. A role for mitochondria in NLRP3 inflammasome activation. Nature. 2011 Jan 13;469(7329):221-5.
101. Yaron JR, Gangaraju S, Rao MY, et al. K(+) regulates Ca(2+) to drive inflammasome signaling: dynamic visualization of ion flux in live cells. Cell Death Dis. 2015 Oct 29;6(10):e1954.
102. Di A, Xiong S, Ye Z, et al. The TWIK2 Potassium Efflux Channel in Macrophages Mediates NLRP3 Inflammasome-Induced Inflammation. Immunity. 2018 Jul 17;49(1):56-65 e4.

103. Munoz-Planillo R, Kuffa P, Martinez-Colon G, et al. K(+) efflux is the common trigger of NLRP3 inflammasome activation by bacterial toxins and particulate matter. Immunity. 2013 Jun 27;38(6):1142-53.
104. Mishra SR, Mahapatra KK, Behera BP, et al. Mitochondrial dysfunction as a driver of NLRP3 inflammasome activation and its modulation through mitophagy for potential therapeutics. Int J Biochem Cell Biol. 2021 Jul;136:106013.
105. Zhou R, Tardivel A, Thorens B, et al. Thioredoxin-interacting protein links oxidative stress to inflammasome activation. Nat Immunol. 2010 Feb;11(2):136-40.
106. Heid ME, Keyel PA, Kamga C, et al. Mitochondrial reactive oxygen species induces NLRP3-dependent lysosomal damage and inflammasome activation. J Immunol. 2013 Nov 15;191(10):5230-8.
107. West AP, Brodsky IE, Rahner C, et al. TLR signalling augments macrophage bactericidal activity through mitochondrial ROS. Nature. 2011 Apr 28;472(7344):476-80.
108. Bauernfeind F, Bartok E, Rieger A, et al. Cutting edge: reactive oxygen species inhibitors block priming, but not activation, of the NLRP3 inflammasome. J Immunol. 2011 Jul 15;187(2):613-7.
109. Nakahira K, Haspel JA, Rathinam VA, et al. Autophagy proteins regulate innate immune responses by inhibiting the release of mitochondrial DNA mediated by the NALP3 inflammasome. Nat Immunol. 2011 Mar;12(3):222-30.
110. Shimada K, Crother TR, Karlin J, et al. Oxidized mitochondrial DNA activates the NLRP3 inflammasome during apoptosis. Immunity. 2012 Mar 23;36(3):401-14.
111. Zhong Z, Liang S, Sanchez-Lopez E, et al. New mitochondrial DNA synthesis enables NLRP3 inflammasome activation. Nature. 2018 Aug;560(7717):198-203.
112. Chu CT, Ji J, Dagda RK, et al. Cardiolipin externalization to the outer mitochondrial membrane acts as an elimination signal for mitophagy in neuronal cells. Nat Cell Biol. 2013 Oct;15(10):1197-1205.
113. Iyer SS, He Q, Janczy JR, et al. Mitochondrial cardiolipin is required for Nlrp3 inflammasome activation. Immunity. 2013 Aug 22;39(2):311-323.
114. Park S, Juliana C, Hong S, et al. The mitochondrial antiviral protein MAVS associates with NLRP3 and regulates its inflammasome activity. J Immunol. 2013 Oct 15;191(8):4358-66.
115. Yu J, Nagasu H, Murakami T, et al. Inflammasome activation leads to Caspase-1-dependent mitochondrial damage and block of mitophagy. Proc Natl Acad Sci U S A. 2014 Oct 28;111(43):15514-9.
116. Rogers C, Erkes DA, Nardone A, et al. Gasdermin pores permeabilize mitochondria to augment caspase-3 activation during apoptosis and inflammasome activation. Nat Commun. 2019 Apr 11;10(1):1689.
117. Billingham LK, Stoolman JS, Vasan K, et al. Mitochondrial electron transport chain is necessary for NLRP3 inflammasome activation. Nat Immunol. 2022 May;23(5):692-704.
118. Ichinohe T, Yamazaki T, Koshiba T, et al. Mitochondrial protein mitofusin 2 is required for NLRP3 inflammasome activation after RNA virus infection. Proc Natl Acad Sci U S A. 2013 Oct 29;110(44):17963-8.
119. Mizushima N. Autophagy: process and function. Genes Dev. 2007 Nov 15;21(22):2861-73.

120. Mizushima N, Yamamoto A, Matsui M, et al. In vivo analysis of autophagy in response to nutrient starvation using transgenic mice expressing a fluorescent autophagosome marker. Mol Biol Cell. 2004 Mar;15(3):1101-11.
121. Cai Q, Jeong YY. Mitophagy in Alzheimer's Disease and Other Age-Related Neurodegenerative Diseases. Cells. 2020 Jan 8;9(1).
122. Ashrafi G, Schwarz TL. The pathways of mitophagy for quality control and clearance of mitochondria. Cell Death Differ. 2013 Jan;20(1):31-42.
123. Biasizzo M, Kopitar-Jerala N. Interplay Between NLRP3 Inflammasome and Autophagy. Front Immunol. 2020;11:591803.
124. Harris J, Hartman M, Roche C, et al. Autophagy controls IL-1beta secretion by targeting pro-IL-1beta for degradation. J Biol Chem. 2011 Mar 18;286(11):9587-97.
125. Dagvadorj J, Mikulska-Ruminska K, Tumurkhuu G, et al. Recruitment of pro-IL-1alpha to mitochondrial cardiolipin, via shared LC3 binding domain, inhibits mitophagy and drives maximal NLRP3 activation. Proc Natl Acad Sci U S A. 2021 Jan 5;118(1).
126. Paik S, Kim JK, Silwal P, et al. An update on the regulatory mechanisms of NLRP3 inflammasome activation. Cell Mol Immunol. 2021 May;18(5):1141-1160.
127. Murakami T, Ockinger J, Yu J, et al. Critical role for calcium mobilization in activation of the NLRP3 inflammasome. Proc Natl Acad Sci U S A. 2012 Jul 10;109(28):11282-7.
128. Triantafilou K, Hughes TR, Triantafilou M, et al. The complement membrane attack complex triggers intracellular Ca2+ fluxes leading to NLRP3 inflammasome activation. J Cell Sci. 2013 Jul 1;126(Pt 13):2903-13.
129. Dong H, Zhao B, Chen J, et al. Mitochondrial calcium uniporter promotes phagocytosis-dependent activation of the NLRP3 inflammasome. Proc Natl Acad Sci U S A. 2022 Jun 28;119(26):e2123247119.
130. Platt N, Shepherd D, Weng Y, et al. Release of acidic store calcium is required for effective priming of the NLRP3 inflammasome. bioRxiv. 2022.
131. Katsnelson MA, Rucker LG, Russo HM, et al. K+ efflux agonists induce NLRP3 inflammasome activation independently of Ca2+ signaling. J Immunol. 2015 Apr 15;194(8):3937-52.
132. Xian H, Watari K, Sanchez-Lopez E, et al. Oxidized DNA fragments exit mitochondria via mPTP- and VDAC-dependent channels to activate NLRP3 inflammasome and interferon signaling. Immunity. 2022 Aug 9;55(8):1370-1385 e8.
133. Finkel T, Menazza S, Holmstrom KM, et al. The ins and outs of mitochondrial calcium. Circ Res. 2015 May 22;116(11):1810-9.
134. Missiroli S, Patergnani S, Caroccia N, et al. Mitochondria-associated membranes (MAMs) and inflammation. Cell Death Dis. 2018 Feb 28;9(3):329.
135. Vigneron C, Py BF, Monneret G, et al. The double sides of NLRP3 inflammasome activation in sepsis. Clin Sci (Lond). 2023 Mar 15;137(5):333-351.
136. Jorgensen I, Zhang Y, Krantz BA, et al. Pyroptosis triggers pore-induced intracellular traps (PITs) that capture bacteria and lead to their clearance by efferocytosis. J Exp Med. 2016 Sep 19;213(10):2113-28.

137. Busch K, Kny M, Huang N, et al. Inhibition of the NLRP3/IL-1beta axis protects against sepsis-induced cardiomyopathy. J Cachexia Sarcopenia Muscle. 2021 Dec;12(6):1653-1668.
138. Zhang W, Xu X, Kao R, et al. Cardiac fibroblasts contribute to myocardial dysfunction in mice with sepsis: the role of NLRP3 inflammasome activation. PLoS One. 2014;9(9):e107639.
139. Zhou T, Qian H, Zheng N, et al. GYY4137 ameliorates sepsis-induced cardiomyopathy via NLRP3 pathway. Biochim Biophys Acta Mol Basis Dis. 2022 Dec 1;1868(12):166497.
140. Yao C, Veleva T, Scott L, Jr., et al. Enhanced Cardiomyocyte NLRP3 Inflammasome Signaling Promotes Atrial Fibrillation. Circulation. 2018 Nov 13;138(20):2227-2242.
141. Shi H, Gao Y, Dong Z, et al. GSDMD-Mediated Cardiomyocyte Pyroptosis Promotes Myocardial I/R Injury. Circ Res. 2021 Jul 23;129(3):383-396.
142. Sosnowski DK, Jamieson KL, Gruzdev A, et al. Cardiomyocyte-specific disruption of soluble epoxide hydrolase limits inflammation to preserve cardiac function. Am J Physiol Heart Circ Physiol. 2022 Oct 1;323(4):H670-H687.
143. Song C, Zhang Y, Pei Q, et al. HSP70 alleviates sepsis-induced cardiomyopathy by attenuating mitochondrial dysfunction-initiated NLRP3 inflammasome-mediated pyroptosis in cardiomyocytes. Burns Trauma. 2022;10:tkac043.
144. Nebert DW, Wikvall K, Miller WL. Human cytochromes P450 in health and disease. Philos Trans R Soc Lond B Biol Sci. 2013 Feb 19;368(1612):20120431.
145. Ander BP, Dupasquier CM, Prociuk MA, et al. Polyunsaturated fatty acids and their effects on cardiovascular disease. Exp Clin Cardiol. 2003 Winter;8(4):164-72.
146. Ostermann AI, Schebb NH. Effects of omega-3 fatty acid supplementation on the pattern of oxylipins: a short review about the modulation of hydroxy-, dihydroxy-, and epoxy-fatty acids. Food Funct. 2017 Jul 19;8(7):2355-2367.
147. Jamieson KL, Endo T, Darwesh AM, et al. Cytochrome P450-derived eicosanoids and heart function. Pharmacol Ther. 2017 Nov;179:47-83.
148. Arnold C, Markovic M, Blossey K, et al. Arachidonic acid-metabolizing cytochrome P450 enzymes are targets of omega-3 fatty acids. J Biol Chem. 2010 Oct 22;285(43):32720-32733.
149. Enayetallah AE, French RA, Thibodeau MS, et al. Distribution of soluble epoxide hydrolase and of cytochrome P450 2C8, 2C9, and 2J2 in human tissues. J Histochem Cytochem. 2004 Apr;52(4):447-54.
150. Valencia R, Bassiouni W, Darwesh AM, et al. Cardiomyocyte-specific CYP2J2 and its therapeutic implications. Expert Opin Drug Metab Toxicol. 2022 Jul-Aug;18(7-8):423-439.
151. Schunck WH, Konkel A, Fischer R, et al. Therapeutic potential of omega-3 fatty acid-derived epoxyeicosanoids in cardiovascular and inflammatory diseases. Pharmacol Ther. 2018 Mar;183:177-204.
152. Darwesh AM, Jamieson KL, Wang C, et al. Cardioprotective effects of CYP-derived epoxy metabolites of docosahexaenoic acid involve limiting NLRP3 inflammasome activation (1). Can J Physiol Pharmacol. 2019 Jun;97(6):544-556.

153. Seubert JM, Zeldin DC, Nithipatikom K, et al. Role of epoxyeicosatrienoic acids in protecting the myocardium following ischemia/reperfusion injury. Prostaglandins Other Lipid Mediat. 2007 Jan;82(1-4):50-9.
154. Panigrahy D, Edin ML, Lee CR, et al. Epoxyeicosanoids stimulate multiorgan metastasis and tumor dormancy escape in mice. J Clin Invest. 2012 Jan;122(1):178-91.
155. Lu T, VanRollins M, Lee HC. Stereospecific activation of cardiac ATP-sensitive K(+) channels by epoxyeicosatrienoic acids: a structural determinant study. Mol Pharmacol. 2002 Nov;62(5):1076-83.
156. Zhang G, Panigrahy D, Mahakian LM, et al. Epoxy metabolites of docosahexaenoic acid (DHA) inhibit angiogenesis, tumor growth, and metastasis. Proc Natl Acad Sci U S A. 2013 Apr 16;110(16):6530-5.
157. Cui PH, Petrovic N, Murray M. The omega-3 epoxide of eicosapentaenoic acid inhibits endothelial cell proliferation by p38 MAP kinase activation and cyclin D1/CDK4 down-regulation. Br J Pharmacol. 2011 Mar;162(5):1143-55.
158. Hildreth K, Kodani SD, Hammock BD, et al. Cytochrome P450-derived linoleic acid metabolites EpOMEs and DiHOMEs: a review of recent studies. J Nutr Biochem. 2020 Dec;86:108484.
159. Samokhvalov V, Jamieson KL, Darwesh AM, et al. Deficiency of Soluble Epoxide Hydrolase Protects Cardiac Function Impaired by LPS-Induced Acute Inflammation. Front Pharmacol. 2018;9:1572.
160. Motoki A, Merkel MJ, Packwood WH, et al. Soluble epoxide hydrolase inhibition and gene deletion are protective against myocardial ischemia-reperfusion injury in vivo. Am J Physiol Heart Circ Physiol. 2008 Nov;295(5):H2128-34.
161. Whelan J, Fritsche K. Linoleic acid. Adv Nutr. 2013 May 1;4(3):311-2.
162. Edin ML, Wang Z, Bradbury JA, et al. Endothelial expression of human cytochrome P450 epoxygenase CYP2C8 increases susceptibility to ischemia-reperfusion injury in isolated mouse heart. FASEB J. 2011 Oct;25(10):3436-47.
163. Moran JH, Mitchell LA, Bradbury JA, et al. Analysis of the cytotoxic properties of linoleic acid metabolites produced by renal and hepatic P450s. Toxicol Appl Pharmacol. 2000 Nov 1;168(3):268-79.
164. Hayakawa M, Ogawa T, Sugiyama S, et al. Hydroxyl radical and leukotoxin biosynthesis in neutrophil plasma membrane. Biochem Biophys Res Commun. 1989 Jun 30;161(3):1077-85.
165. Moghaddam MF, Grant DF, Cheek JM, et al. Bioactivation of leukotoxins to their toxic diols by epoxide hydrolase. Nat Med. 1997 May;3(5):562-6.
166. Yokoo K, Hayakawa M, Sugiyama S, et al. A Novel Uncoupler of Mitochondrial Respiration, 9, 10-Epoxy-12-octadecenoate, Exists in Human Burned Skin. Journal of Clinical Biochemistry and Nutrition. 1986;1(2):121-127.
167. Ozawa T, Hayakawa M, Takamura T, et al. Biosynthesis of leukotoxin, 9,10-epoxy-12 octadecenoate, by leukocytes in lung lavages of rat after exposure to hyperoxia. Biochem Biophys Res Commun. 1986 Feb 13;134(3):1071-8.
168. Hayakawa M, Sugiyama S, Takamura T, et al. Neutrophils biosynthesize leukotoxin, 9, 10-epoxy-12-octadecenoate. Biochem Biophys Res Commun. 1986 May 29;137(1):424-30.

169. Hayakawa M, Kosaka K, Sugiyama S, et al. Proposal of leukotoxin, 9,10-epoxy-12-octadecenoate, as a burn toxin. Biochem Int. 1990;21(3):573-9.
170. Hanaki Y, Kamiya H, Ohno M, et al. Leukotoxin, 9, 10-epoxy-12-octadecenoate: a possible responsible factor in circulatory shock and disseminated intravascular coagulation. Jpn J Med. 1991 May-Jun;30(3):224-8.
171. Ozawa T, Nishikimi M, Sugiyama S, et al. Cytotoxic activity of leukotoxin, a neutrophil-derived fatty acid epoxide, on cultured human cells. Biochem Int. 1988 Feb;16(2):369-73.
172. Hu JN, Taki F, Sugiyama S, et al. Neutrophil-derived epoxide, 9,10-epoxy-12-octadecenoate, induces pulmonary edema. Lung. 1988;166(6):327-37.
173. Sugiyama S, Hayakawa M, Nagai S, et al. Leukotoxin, 9, 10-epoxy-12-octadecenoate, causes cardiac failure in dogs. Life Sci. 1987 Jan 19;40(3):225-31.
174. Sugiyama S, Hayakawa M, Hanaki Y, et al. The role of leukotoxin (9,10-epoxy-12-octadecenoate) in the genesis of coagulation abnormalities. Life Sci. 1988;43(3):221-7.
175. Zheng J, Plopper CG, Lakritz J, et al. Leukotoxin-diol: a putative toxic mediator involved in acute respiratory distress syndrome. Am J Respir Cell Mol Biol. 2001 Oct;25(4):434-8.
176. Totani Y, Saito Y, Ishizaki T, et al. Leukotoxin and its diol induce neutrophil chemotaxis through signal transduction different from that of fMLP. Eur Respir J. 2000 Jan;15(1):75-9.
177. Thompson DA, Hammock BD. Dihydroxyoctadecamonoenoate esters inhibit the neutrophil respiratory burst. J Biosci. 2007 Mar;32(2):279-91.
178. Moran JH, Weise R, Schnellmann RG, et al. Cytotoxicity of linoleic acid diols to renal proximal tubular cells. Toxicol Appl Pharmacol. 1997 Sep;146(1):53-9.
179. Sakai T, Ishizaki T, Ohnishi T, et al. Leukotoxin, 9,10-epoxy-12-octadecenoate inhibits mitochondrial respiration of isolated perfused rat lung. Am J Physiol. 1995 Sep;269(3 Pt 1):L326-31.
180. Sisemore MF, Zheng J, Yang JC, et al. Cellular characterization of leukotoxin diol-induced mitochondrial dysfunction. Arch Biochem Biophys. 2001 Aug 1;392(1):32-7.
181. Moran JH, Mon T, Hendrickson TL, et al. Defining mechanisms of toxicity for linoleic acid monoepoxides and diols in Sf-21 cells. Chem Res Toxicol. 2001 Apr;14(4):431-7.
182. Nowak G, Grant DF, Moran JH. Linoleic acid epoxide promotes the maintenance of mitochondrial function and active Na+ transport following hypoxia. Toxicol Lett. 2004 Mar 1;147(2):161-75.
183. Tam VC, Quehenberger O, Oshansky CM, et al. Lipidomic profiling of influenza infection identifies mediators that induce and resolve inflammation. Cell. 2013 Jul 3;154(1):213-27.
184. Levan SR, Stamnes KA, Lin DL, et al. Elevated faecal 12,13-diHOME concentration in neonates at high risk for asthma is produced by gut bacteria and impedes immune tolerance. Nat Microbiol. 2019 Nov;4(11):1851-1861.
185. Lin DIN, Rackaityte E, Magnaye K, et al. Gut bacterial-derived 12,13-diHOME promotes inflammatory macrophage polarization and epigenetic modifications. Journal of Allergy and Clinical Immunology. 2022;149(2):AB231.

186. Bergmann CB, McReynolds CB, Wan D, et al. sEH-derived metabolites of linoleic acid drive pathologic inflammation while impairing key innate immune cell function in burn injury. Proc Natl Acad Sci U S A. 2022 Mar 29;119(13):e2120691119.
187. Sosnowski DK, Jamieson KL, Darwesh AM, et al. Changes in the Left Ventricular Eicosanoid Profile in Human Dilated Cardiomyopathy. Front Cardiovasc Med. 2022;9:879209.
188. Chaudhary KR, Zordoky BN, Edin ML, et al. Differential effects of soluble epoxide hydrolase inhibition and CYP2J2 overexpression on postischemic cardiac function in aged mice. Prostaglandins Other Lipid Mediat. 2013 Jul-Aug;104-105:8-17.
189. Pinckard KM, Shettigar VK, Wright KR, et al. A Novel Endocrine Role for the BAT-Released Lipokine 12,13-diHOME to Mediate Cardiac Function. Circulation. 2021 Jan 12;143(2):145-159.
190. Mitchell LA, Grant DF, Melchert RB, et al. Linoleic acid metabolites act to increase contractility in isolated rat heart. Cardiovasc Toxicol. 2002;2(3):219-30.
191. Bannehr M, Lohr L, Gelep J, et al. Linoleic Acid Metabolite DiHOME Decreases Post-ischemic Cardiac Recovery in Murine Hearts. Cardiovasc Toxicol. 2019 Aug;19(4):365-371.
192. Edin ML, Gruzdev A, Bradbury JA, et al. Disruption of Ephx2 in cardiomyocytes but not endothelial cells improves functional recovery after ischemia-reperfusion in isolated mouse hearts. J Biol Chem. 2023 Apr;299(4):103049.
193. Stimers JR, Dobretsov M, Hastings SL, et al. Effects of linoleic acid metabolites on electrical activity in adult rat ventricular myocytes. Biochim Biophys Acta. 1999 Jun 10;1438(3):359-68.
194. Ha J, Dobretsov M, Kurten RC, et al. Effect of linoleic acid metabolites on Na(+)/K(+) pump current in N20.1 oligodendrocytes: role of membrane fluidity. Toxicol Appl Pharmacol. 2002 Jul 1;182(1):76-83.
195. Green D, Ruparel S, Gao X, et al. Central activation of TRPV1 and TRPA1 by novel endogenous agonists contributes to mechanical allodynia and thermal hyperalgesia after burn injury. Mol Pain. 2016;12.
196. Zimmer B, Angioni C, Osthues T, et al. The oxidized linoleic acid metabolite 12,13-DiHOME mediates thermal hyperalgesia during inflammatory pain. Biochim Biophys Acta Mol Cell Biol Lipids. 2018 Jul;1863(7):669-678.
197. da Costa Souza F, Grodzki ACG, Morgan RK, et al. Oxidized linoleic acid metabolites regulate neuronal morphogenesis in vitro. Neurochem Int. 2023 Mar;164:105506.
198. Anita NZ, Forkan N, Kamal R, et al. Serum soluble epoxide hydrolase related oxylipins and major depression in patients with type 2 diabetes. Psychoneuroendocrinology. 2021 Apr;126:105149.
199. Lynes MD, Leiria LO, Lundh M, et al. The cold-induced lipokine 12,13-diHOME promotes fatty acid transport into brown adipose tissue. Nat Med. 2017 May;23(5):631-637.
200. Stanford KI, Lynes MD, Takahashi H, et al. 12,13-diHOME: An Exercise-Induced Lipokine that Increases Skeletal Muscle Fatty Acid Uptake. Cell Metab. 2018 May 1;27(5):1111-1120 e3.

201. Vasan SK, Noordam R, Gowri MS, et al. The proposed systemic thermogenic metabolites succinate and 12,13-diHOME are inversely associated with adiposity and related metabolic traits: evidence from a large human cross-sectional study. Diabetologia. 2019 Nov;62(11):2079-2087.
202. Wolfs D, Lynes MD, Tseng YH, et al. Brown Fat-Activating Lipokine 12,13-diHOME in Human Milk Is Associated With Infant Adiposity. J Clin Endocrinol Metab. 2021 Jan 23;106(2):e943-e956.
203. Hamaguchi M, Wu HN, Tanaka M, et al. A case series of the dynamics of lipid mediators in patients with sepsis. Acute Med Surg. 2019 Oct;6(4):413-418.
204. McReynolds CB, Cortes-Puch I, Ravindran R, et al. Plasma Linoleate Diols Are Potential Biomarkers for Severe COVID-19 Infections. Front Physiol. 2021;12:663869.
205. Levy RJ, Piel DA, Acton PD, et al. Evidence of myocardial hibernation in the septic heart. Crit Care Med. 2005 Dec;33(12):2752-6.
206. Durand A, Duburcq T, Dekeyser T, et al. Involvement of Mitochondrial Disorders in Septic Cardiomyopathy. Oxid Med Cell Longev. 2017;2017:4076348.
207. Yang L, Chen C, Lv B, et al. Epoxyeicosatrienoic acids prevent cardiomyocytes against sepsis by A(2A)R-induced activation of PI3K and PPARgamma. Prostaglandins Other Lipid Mediat. 2021 Dec;157:106595.
208. Dai M, Wu L, He Z, et al. Epoxyeicosatrienoic acids regulate macrophage polarization and prevent LPS-induced cardiac dysfunction. J Cell Physiol. 2015 Sep;230(9):2108-19.
209. Piotrowski J, Jedrzejewski T, Pawlikowska M, et al. The weakening effect of soluble epoxide hydrolase inhibitor AUDA on febrile response to lipopolysaccharide and turpentine in rat. J Physiol Biochem. 2017 Nov;73(4):551-560.
210. Dong R, Hu D, Yang Y, et al. EETs reduces LPS-induced hyperpermeability by targeting GRP78 mediated Src activation and subsequent Rho/ROCK signaling pathway. Oncotarget. 2017 Aug 1;8(31):50958-50971.
211. Zhang J, Zhang M, Huo XK, et al. Macrophage Inactivation by Small Molecule Wedelolactone via Targeting sEH for the Treatment of LPS-Induced Acute Lung Injury. ACS Cent Sci. 2023 Mar 22;9(3):440-456.
212. Chen Z, Tang Y, Yu J, et al. sEH Inhibitor Tppu Ameliorates Cecal Ligation and Puncture-Induced Sepsis by Regulating Macrophage Functions. Shock. 2020 Jun;53(6):761-771.
213. Luo XQ, Duan JX, Yang HH, et al. Epoxyeicosatrienoic acids inhibit the activation of NLRP3 inflammasome in murine macrophages. J Cell Physiol. 2020 Dec;235(12):9910-9921.
214. Laskin DL, Sunil VR, Gardner CR, et al. Macrophages and tissue injury: agents of defense or destruction? Annu Rev Pharmacol Toxicol. 2011;51:267-88.
215. Novorolsky RJ, Nichols M, Kim JS, et al. The cell-permeable mitochondrial calcium uniporter inhibitor Ru265 preserves cortical neuron respiration after lethal oxygen glucose deprivation and reduces hypoxic/ischemic brain injury. J Cereb Blood Flow Metab. 2020 Jun;40(6):1172-1181.

216. Ye J, Coulouris G, Zaretskaya I, et al. Primer-BLAST: a tool to design target-specific primers for polymerase chain reaction. BMC Bioinformatics. 2012 Jun 18;13:134.
217. Gnaiger E. Mitochondrial pathways and respiratory control: an introduction to OXPHOS analysis. Bioenergetics Communications. 2020;2020:2-2.
218. Lemieux H, Blier PU, Gnaiger E. Remodeling pathway control of mitochondrial respiratory capacity by temperature in mouse heart: electron flow through the Q-junction in permeabilized fibers. Sci Rep. 2017 Jun 6;7(1):2840.
219. Jakobs C, Bartok E, Kubarenko A, et al. Immunoblotting for active caspase-1. Methods Mol Biol. 2013;1040:103-15.
220. Lund ME, To J, O'Brien BA, et al. The choice of phorbol 12-myristate 13-acetate differentiation protocol influences the response of THP-1 macrophages to a pro-inflammatory stimulus. J Immunol Methods. 2016 Mar;430:64-70.
221. Forrester MA, Wassall HJ, Hall LS, et al. Similarities and differences in surface receptor expression by THP-1 monocytes and differentiated macrophages polarized using seven different conditioning regimens. Cell Immunol. 2018 Oct;332:58-76.
222. Awad F, Assrawi E, Jumeau C, et al. Impact of human monocyte and macrophage polarization on NLR expression and NLRP3 inflammasome activation. PLoS One. 2017;12(4):e0175336.
223. Tedesco S, De Majo F, Kim J, et al. Convenience versus Biological Significance: Are PMA-Differentiated THP-1 Cells a Reliable Substitute for Blood-Derived Macrophages When Studying in Vitro Polarization? Front Pharmacol. 2018;9:71.
224. L'Homme L, Esser N, Riva L, et al. Unsaturated fatty acids prevent activation of NLRP3 inflammasome in human monocytes/macrophages. J Lipid Res. 2013 Nov;54(11):2998-3008.
225. Zhao W, Ma L, Cai C, et al. Caffeine Inhibits NLRP3 Inflammasome Activation by Suppressing MAPK/NF-kappaB and A2aR Signaling in LPS-Induced THP-1 Macrophages. Int J Biol Sci. 2019;15(8):1571-1581.
226. Luther JM, Ray J, Wei D, et al. GSK2256294 Decreases sEH (Soluble Epoxide Hydrolase) Activity in Plasma, Muscle, and Adipose and Reduces F2-Isoprostanes but Does Not Alter Insulin Sensitivity in Humans. Hypertension. 2021 Sep;78(4):1092-1102.
227. Viola A, Munari F, Sanchez-Rodriguez R, et al. The Metabolic Signature of Macrophage Responses. Front Immunol. 2019;10:1462.
228. Widdrington JD, Gomez-Duran A, Pyle A, et al. Exposure of Monocytic Cells to Lipopolysaccharide Induces Coordinated Endotoxin Tolerance, Mitochondrial Biogenesis, Mitophagy, and Antioxidant Defenses. Front Immunol. 2018;9:2217.
229. Sun N, Yun J, Liu J, et al. Measuring In Vivo Mitophagy. Mol Cell. 2015 Nov 19;60(4):685-96.
230. Horng T. Calcium signaling and mitochondrial destabilization in the triggering of the NLRP3 inflammasome. Trends Immunol. 2014 Jun;35(6):253-61.
231. Rizzuto R, Marchi S, Bonora M, et al. Ca(2+) transfer from the ER to mitochondria: when, how and why. Biochim Biophys Acta. 2009 Nov;1787(11):1342-51.
232. Zhang Z, Meszaros G, He WT, et al. Protein kinase D at the Golgi controls NLRP3 inflammasome activation. J Exp Med. 2017 Sep 4;214(9):2671-2693.

233. Woods JJ, Nemani N, Shanmughapriya S, et al. A Selective and Cell-Permeable Mitochondrial Calcium Uniporter (MCU) Inhibitor Preserves Mitochondrial Bioenergetics after Hypoxia/Reoxygenation Injury. ACS Cent Sci. 2019 Jan 23;5(1):153-166.
234. Chanput W, Mes JJ, Wichers HJ. THP-1 cell line: an in vitro cell model for immune modulation approach. Int Immunopharmacol. 2014 Nov;23(1):37-45.
235. Park EK, Jung HS, Yang HI, et al. Optimized THP-1 differentiation is required for the detection of responses to weak stimuli. Inflamm Res. 2007 Jan;56(1):45-50.
236. Baxter EW, Graham AE, Re NA, et al. Standardized protocols for differentiation of THP-1 cells to macrophages with distinct M(IFNgamma+LPS), M(IL-4) and M(IL-10) phenotypes. J Immunol Methods. 2020 Mar;478:112721.
237. Genin M, Clement F, Fattaccioli A, et al. M1 and M2 macrophages derived from THP-1 cells differentially modulate the response of cancer cells to etoposide. BMC Cancer. 2015 Aug 8;15:577.
238. Qin Z. The use of THP-1 cells as a model for mimicking the function and regulation of monocytes and macrophages in the vasculature. Atherosclerosis. 2012 Mar;221(1):2-11.
239. Keuper M, Dzyakanchuk A, Amrein KE, et al. THP-1 Macrophages and SGBS Adipocytes - A New Human in vitro Model System of Inflamed Adipose Tissue. Front Endocrinol (Lausanne). 2011;2:89.
240. Wiatrak B, Balon K. Protective Activity of Abeta on Cell Cultures (PC12 and THP-1 after Differentiation) Preincubated with Lipopolysaccharide (LPS). Mol Neurobiol. 2021 Apr;58(4):1453-1464.
241. Giambelluca S, Ochs M, Lopez-Rodriguez E. Resting time after phorbol 12-myristate 13-acetate in THP-1 derived macrophages provides a non-biased model for the study of NLRP3 inflammasome. Front Immunol. 2022;13:958098.
242. Madhvi A, Mishra H, Leisching GR, et al. Comparison of human monocyte derived macrophages and THP1-like macrophages as in vitro models for M. tuberculosis infection. Comp Immunol Microbiol Infect Dis. 2019 Dec;67:101355.
243. Chanput W, Mes J, Vreeburg RA, et al. Transcription profiles of LPS-stimulated THP-1 monocytes and macrophages: a tool to study inflammation modulating effects of food-derived compounds. Food Funct. 2010 Dec;1(3):254-61.
244. Pick N, Cameron S, Arad D, et al. Screening of Compounds Toxicity against Human Monocytic cell line-THP-1 by Flow Cytometry. Biol Proced Online. 2004;6:220-225.
245. Tsuchiya S, Yamabe M, Yamaguchi Y, et al. Establishment and characterization of a human acute monocytic leukemia cell line (THP-1). Int J Cancer. 1980 Aug;26(2):171-6.
246. Shiratori H, Feinweber C, Luckhardt S, et al. THP-1 and human peripheral blood mononuclear cell-derived macrophages differ in their capacity to polarize in vitro. Mol Immunol. 2017 Aug;88:58-68.
247. Schildberger A, Rossmanith E, Eichhorn T, et al. Monocytes, peripheral blood mononuclear cells, and THP-1 cells exhibit different cytokine expression patterns following stimulation with lipopolysaccharide. Mediators Inflamm. 2013;2013:697972.

248. Kohro T, Tanaka T, Murakami T, et al. A comparison of differences in the gene expression profiles of phorbol 12-myristate 13-acetate differentiated THP-1 cells and human monocyte-derived macrophage. J Atheroscler Thromb. 2004;11(2):88-97.
249. Riddy DM, Goy E, Delerive P, et al. Comparative genotypic and phenotypic analysis of human peripheral blood monocytes and surrogate monocyte-like cell lines commonly used in metabolic disease research. PLoS One. 2018;13(5):e0197177.
250. Hijiya N, Miyake K, Akashi S, et al. Possible involvement of toll-like receptor 4 in endothelial cell activation of larger vessels in response to lipopolysaccharide. Pathobiology. 2002;70(1):18-25.
251. Maess MB, Wittig B, Cignarella A, et al. Reduced PMA enhances the responsiveness of transfected THP-1 macrophages to polarizing stimuli. J Immunol Methods. 2014 Jan 15;402(1-2):76-81.
252. Aldo PB, Craveiro V, Guller S, et al. Effect of culture conditions on the phenotype of THP-1 monocyte cell line. Am J Reprod Immunol. 2013 Jul;70(1):80-6.
253. Zhou L, Shen LH, Hu LH, et al. Retinoid X receptor agonists inhibit phorbol-12-myristate-13-acetate (PMA)-induced differentiation of monocytic THP-1 cells into macrophages. Mol Cell Biochem. 2010 Feb;335(1-2):283-9.
254. Kepp O, Galluzzi L, Lipinski M, et al. Cell death assays for drug discovery. Nat Rev Drug Discov. 2011 Mar;10(3):221-37.
255. Tugal D, Liao X, Jain MK. Transcriptional control of macrophage polarization. Arterioscler Thromb Vasc Biol. 2013 Jun;33(6):1135-44.
256. Ricote M, Li AC, Willson TM, et al. The peroxisome proliferator-activated receptor-gamma is a negative regulator of macrophage activation. Nature. 1998 Jan 1;391(6662):79-82.
257. Wang Q, Chen K, Zhang F, et al. TRPA1 regulates macrophages phenotype plasticity and atherosclerosis progression. Atherosclerosis. 2020 May;301:44-53.
258. Lv Z, Xu X, Sun Z, et al. TRPV1 alleviates osteoarthritis by inhibiting M1 macrophage polarization via Ca(2+)/CaMKII/Nrf2 signaling pathway. Cell Death Dis. 2021 May 18;12(6):504.
259. Liu Y, Xu R, Gu H, et al. Metabolic reprogramming in macrophage responses. Biomark Res. 2021 Jan 6;9(1):1.
260. Chen X, Jiang J, Liu H, et al. MSR1 characterized by chromatin accessibility mediates M2 macrophage polarization to promote gastric cancer progression. Int Immunopharmacol. 2022 Nov;112:109217.
261. Govaere O, Petersen SK, Martinez-Lopez N, et al. Macrophage scavenger receptor 1 mediates lipid-induced inflammation in non-alcoholic fatty liver disease. J Hepatol. 2022 May;76(5):1001-1012.
262. Jin Z, Wei W, Yang M, et al. Mitochondrial complex I activity suppresses inflammation and enhances bone resorption by shifting macrophage-osteoclast polarization. Cell Metab. 2014 Sep 2;20(3):483-98.
263. Cai S, Zhao M, Zhou B, et al. Mitochondrial dysfunction in macrophages promotes inflammation and suppresses repair after myocardial infarction. J Clin Invest. 2023 Feb 15;133(4).

264. Yuan Y, Chen Y, Peng T, et al. Mitochondrial ROS-induced lysosomal dysfunction impairs autophagic flux and contributes to M1 macrophage polarization in a diabetic condition. Clin Sci (Lond). 2019 Aug 15;133(15):1759-1777.
265. Ouimet M, Ediriweera HN, Gundra UM, et al. MicroRNA-33-dependent regulation of macrophage metabolism directs immune cell polarization in atherosclerosis. J Clin Invest. 2015 Oct 26;125(12):4334-48.
266. Van den Bossche J, Baardman J, Otto NA, et al. Mitochondrial Dysfunction Prevents Repolarization of Inflammatory Macrophages. Cell Rep. 2016 Oct 11;17(3):684-696.
267. Xing Y, Yao X, Li H, et al. Cutting Edge: TRAF6 Mediates TLR/IL-1R Signaling-Induced Nontranscriptional Priming of the NLRP3 Inflammasome. J Immunol. 2017 Sep 1;199(5):1561-1566.
268. Perregaux D, Gabel CA. Interleukin-1 beta maturation and release in response to ATP and nigericin. Evidence that potassium depletion mediated by these agents is a necessary and common feature of their activity. J Biol Chem. 1994 May 27;269(21):15195-203.
269. Hornung V, Bauernfeind F, Halle A, et al. Silica crystals and aluminum salts activate the NALP3 inflammasome through phagosomal destabilization. Nat Immunol. 2008 Aug;9(8):847-56.
270. Martinon F, Petrilli V, Mayor A, et al. Gout-associated uric acid crystals activate the NALP3 inflammasome. Nature. 2006 Mar 9;440(7081):237-41.
271. Franchi L, Eigenbrod T, Munoz-Planillo R, et al. Cytosolic double-stranded RNA activates the NLRP3 inflammasome via MAVS-induced membrane permeabilization and K+ efflux. J Immunol. 2014 Oct 15;193(8):4214-4222.
272. Yi YS. Functional crosstalk between non-canonical caspase-11 and canonical NLRP3 inflammasomes during infection-mediated inflammation. Immunology. 2020 Feb;159(2):142-155.
273. Rivers-Auty J, Brough D. Potassium efflux fires the canon: Potassium efflux as a common trigger for canonical and noncanonical NLRP3 pathways. Eur J Immunol. 2015 Oct;45(10):2758-61.
274. Kayagaki N, Stowe IB, Lee BL, et al. Caspase-11 cleaves gasdermin D for non-canonical inflammasome signalling. Nature. 2015 Oct 29;526(7575):666-71.
275. Baker PJ, Boucher D, Bierschenk D, et al. NLRP3 inflammasome activation downstream of cytoplasmic LPS recognition by both caspase-4 and caspase-5. Eur J Immunol. 2015 Oct;45(10):2918-26.
276. Schmid-Burgk JL, Gaidt MM, Schmidt T, et al. Caspase-4 mediates non-canonical activation of the NLRP3 inflammasome in human myeloid cells. Eur J Immunol. 2015 Oct;45(10):2911-7.
277. Ruhl S, Broz P. Caspase-11 activates a canonical NLRP3 inflammasome by promoting K(+) efflux. Eur J Immunol. 2015 Oct;45(10):2927-36.
278. Vigano E, Diamond CE, Spreafico R, et al. Human caspase-4 and caspase-5 regulate the one-step non-canonical inflammasome activation in monocytes. Nat Commun. 2015 Oct 28;6:8761.
279. Rathinam VA, Jiang Z, Waggoner SN, et al. The AIM2 inflammasome is essential for host defense against cytosolic bacteria and DNA viruses. Nat Immunol. 2010 May;11(5):395-402.

280. Broz P, Dixit VM. Inflammasomes: mechanism of assembly, regulation and signalling. Nat Rev Immunol. 2016 Jul;16(7):407-20.
281. Cunha LD, Silva ALN, Ribeiro JM, et al. AIM2 Engages Active but Unprocessed Caspase-1 to Induce Noncanonical Activation of the NLRP3 Inflammasome. Cell Rep. 2017 Jul 25;20(4):794-805.
282. Bae JH, Jo SI, Kim SJ, et al. Circulating Cell-Free mtDNA Contributes to AIM2 Inflammasome-Mediated Chronic Inflammation in Patients with Type 2 Diabetes. Cells. 2019 Apr 8;8(4).
283. Wang Y, Kanneganti TD. From pyroptosis, apoptosis and necroptosis to PANoptosis: A mechanistic compendium of programmed cell death pathways. Comput Struct Biotechnol J. 2021;19:4641-4657.
284. Xaus J, Comalada M, Valledor AF, et al. LPS induces apoptosis in macrophages mostly through the autocrine production of TNF-alpha. Blood. 2000 Jun 15;95(12):3823-31.
285. He S, Liang Y, Shao F, et al. Toll-like receptors activate programmed necrosis in macrophages through a receptor-interacting kinase-3-mediated pathway. Proc Natl Acad Sci U S A. 2011 Dec 13;108(50):20054-9.
286. Lamkanfi M, Kanneganti TD, Van Damme P, et al. Targeted peptidecentric proteomics reveals caspase-7 as a substrate of the caspase-1 inflammasomes. Mol Cell Proteomics. 2008 Dec;7(12):2350-63.
287. Tsuchiya K, Nakajima S, Hosojima S, et al. Caspase-1 initiates apoptosis in the absence of gasdermin D. Nat Commun. 2019 May 7;10(1):2091.
288. Sagulenko V, Thygesen SJ, Sester DP, et al. AIM2 and NLRP3 inflammasomes activate both apoptotic and pyroptotic death pathways via ASC. Cell Death Differ. 2013 Sep;20(9):1149-60.
289. Gurung P, Anand PK, Malireddi RK, et al. FADD and caspase-8 mediate priming and activation of the canonical and noncanonical Nlrp3 inflammasomes. J Immunol. 2014 Feb 15;192(4):1835-46.
290. Moran JH, Nowak G, Grant DF. Analysis of the toxic effects of linoleic acid, 12,13-cis-epoxyoctadecenoic acid, and 12,13-dihydroxyoctadecenoic acid in rabbit renal cortical mitochondria. Toxicol Appl Pharmacol. 2001 Apr 15;172(2):150-61.
291. Gu X, Ma Y, Liu Y, et al. Measurement of mitochondrial respiration in adherent cells by Seahorse XF96 Cell Mito Stress Test. STAR Protoc. 2021 Mar 19;2(1):100245.
292. Medeiros DM. Assessing mitochondria biogenesis. Methods. 2008 Dec;46(4):288-94.
293. Onishi M, Yamano K, Sato M, et al. Molecular mechanisms and physiological functions of mitophagy. EMBO J. 2021 Feb 1;40(3):e104705.
294. Zhu J, Dagda RK, Chu CT. Monitoring mitophagy in neuronal cell cultures. Methods Mol Biol. 2011;793:325-39.
295. Twig G, Elorza A, Molina AJ, et al. Fission and selective fusion govern mitochondrial segregation and elimination by autophagy. EMBO J. 2008 Jan 23;27(2):433-46.
296. Priault M, Salin B, Schaeffer J, et al. Impairing the bioenergetic status and the biogenesis of mitochondria triggers mitophagy in yeast. Cell Death Differ. 2005 Dec;12(12):1613-21.

297. Twig G, Shirihai OS. The interplay between mitochondrial dynamics and mitophagy. Antioxid Redox Signal. 2011 May 15;14(10):1939-51.
298. Yu Z, Wang H, Tang W, et al. Mitochondrial Ca(2+) oscillation induces mitophagy initiation through the PINK1-Parkin pathway. Cell Death Dis. 2021 Jun 19;12(7):632.
299. Liu C, Li HJ, Duan WX, et al. MCU Upregulation Overactivates Mitophagy by Promoting VDAC1 Dimerization and Ubiquitination in the Hepatotoxicity of Cadmium. Adv Sci (Weinh). 2023 Mar;10(7):e2203869.
300. Chen Z, Zhou Q, Chen J, et al. MCU-dependent mitochondrial calcium uptake-induced mitophagy contributes to apelin-13-stimulated VSMCs proliferation. Vascul Pharmacol. 2022 Jun;144:106979.
301. West MA, Clair L, Bellingham J. Role of calcium in lipopolysaccharide-stimulated tumor necrosis factor and interleukin-1 signal transduction in naive and endotoxin-tolerant murine macrophages. J Trauma. 1996 Oct;41(4):647-52.
302. Hoffmann A, Kann O, Ohlemeyer C, et al. Elevation of basal intracellular calcium as a central element in the activation of brain macrophages (microglia): suppression of receptor-evoked calcium signaling and control of release function. J Neurosci. 2003 Jun 1;23(11):4410-9.
303. Schappe MS, Szteyn K, Stremska ME, et al. Chanzyme TRPM7 Mediates the Ca(2+) Influx Essential for Lipopolysaccharide-Induced Toll-Like Receptor 4 Endocytosis and Macrophage Activation. Immunity. 2018 Jan 16;48(1):59-74 e5.
304. Balderas E, Eberhardt DR, Lee S, et al. Mitochondrial calcium uniporter stabilization preserves energetic homeostasis during Complex I impairment. Nat Commun. 2022 May 19;13(1):2769.
305. Pressman BC, Fahim M. Pharmacology and toxicology of the monovalent carboxylic ionophores. Annu Rev Pharmacol Toxicol. 1982;22:465-90.
306. Deryabin PI, Shatrova AN, Borodkina AV. Targeting Multiple Homeostasis-Maintaining Systems by Ionophore Nigericin Is a Novel Approach for Senolysis. Int J Mol Sci. 2022 Nov 17;23(22).
307. Selivanov VA, Zeak JA, Roca J, et al. The role of external and matrix pH in mitochondrial reactive oxygen species generation. J Biol Chem. 2008 Oct 24;283(43):29292-300.
308. Zhang H, Huang HM, Carson RC, et al. Assessment of membrane potentials of mitochondrial populations in living cells. Anal Biochem. 2001 Nov 15;298(2):170-80.
309. Wang Y, Shi P, Chen Q, et al. Mitochondrial ROS promote macrophage pyroptosis by inducing GSDMD oxidation. J Mol Cell Biol. 2019 Dec 19;11(12):1069-1082.
310. Allam R, Lawlor KE, Yu EC, et al. Mitochondrial apoptosis is dispensable for NLRP3 inflammasome activation but non-apoptotic caspase-8 is required for inflammasome priming. EMBO Rep. 2014 Sep;15(9):982-90.
311. Lee GS, Subramanian N, Kim AI, et al. The calcium-sensing receptor regulates the NLRP3 inflammasome through Ca2+ and cAMP. Nature. 2012 Dec 6;492(7427):123-7.
312. Tomar D, Elrod JW. Metabolite regulation of the mitochondrial calcium uniporter channel. Cell Calcium. 2020 Dec;92:102288.

313. Peng TI, Jou MJ. Oxidative stress caused by mitochondrial calcium overload. Ann N Y Acad Sci. 2010 Jul;1201:183-8.
314. Baumgartner HK, Gerasimenko JV, Thorne C, et al. Calcium elevation in mitochondria is the main Ca2+ requirement for mitochondrial permeability transition pore (mPTP) opening. J Biol Chem. 2009 Jul 31;284(31):20796-803.
315. Baughman JM, Perocchi F, Girgis HS, et al. Integrative genomics identifies MCU as an essential component of the mitochondrial calcium uniporter. Nature. 2011 Jun 19;476(7360):341-5.
316. De Stefani D, Raffaello A, Teardo E, et al. A forty-kilodalton protein of the inner membrane is the mitochondrial calcium uniporter. Nature. 2011 Jun 19;476(7360):336-40.
317. Wacquier B, Combettes L, Dupont G. Cytoplasmic and Mitochondrial Calcium Signaling: A Two-Way Relationship. Cold Spring Harb Perspect Biol. 2019 Oct 1;11(10).
318. Kirichok Y, Krapivinsky G, Clapham DE. The mitochondrial calcium uniporter is a highly selective ion channel. Nature. 2004 Jan 22;427(6972):360-4.
319. Broekemeier KM, Krebsbach RJ, Pfeiffer DR. Inhibition of the mitochondrial Ca2+ uniporter by pure and impure ruthenium red. Mol Cell Biochem. 1994 Oct 12;139(1):33-40.
320. Alevriadou BR, Patel A, Noble M, et al. Molecular nature and physiological role of the mitochondrial calcium uniporter channel. Am J Physiol Cell Physiol. 2021 Apr 1;320(4):C465-C482.
321. Murgia M, Rizzuto R. Molecular diversity and pleiotropic role of the mitochondrial calcium uniporter. Cell Calcium. 2015 Jul;58(1):11-7.
322. Patergnani S, Suski JM, Agnoletto C, et al. Calcium signaling around Mitochondria Associated Membranes (MAMs). Cell Commun Signal. 2011 Sep 22;9:19.
323. Rizzuto R, Brini M, Murgia M, et al. Microdomains with high Ca2+ close to IP3-sensitive channels that are sensed by neighboring mitochondria. Science. 1993 Oct 29;262(5134):744-7.
324. Rizzuto R, Pinton P, Carrington W, et al. Close contacts with the endoplasmic reticulum as determinants of mitochondrial Ca2+ responses. Science. 1998 Jun 12;280(5370):1763-6.
325. Dong Z, Shanmughapriya S, Tomar D, et al. Mitochondrial Ca(2+) Uniporter Is a Mitochondrial Luminal Redox Sensor that Augments MCU Channel Activity. Mol Cell. 2017 Mar 16;65(6):1014-1028 e7.
326. Ghosh S, Basu Ball W, Madaris TR, et al. An essential role for cardiolipin in the stability and function of the mitochondrial calcium uniporter. Proc Natl Acad Sci U S A. 2020 Jul 14;117(28):16383-16390.
327. Wishart DS, Guo A, Oler E, et al. HMDB 5.0: the Human Metabolome Database for 2022. Nucleic Acids Res. 2022 Jan 7;50(D1):D622-D631.
328. Schwenk RW, Holloway GP, Luiken JJ, et al. Fatty acid transport across the cell membrane: regulation by fatty acid transporters. Prostaglandins Leukot Essent Fatty Acids. 2010 Apr-Jun;82(4-6):149-54.
329. Caires R, Sierra-Valdez FJ, Millet JRM, et al. Omega-3 Fatty Acids Modulate TRPV4 Function through Plasma Membrane Remodeling. Cell Rep. 2017 Oct 3;21(1):246-258.

330. Bok E, Chung YC, Kim KS, et al. Modulation of M1/M2 polarization by capsaicin contributes to the survival of dopaminergic neurons in the lipopolysaccharide-lesioned substantia nigra in vivo. Exp Mol Med. 2018 Jul 3;50(7):1-14.
331. Zhang Y, Hou B, Liang P, et al. TRPV1 channel mediates NLRP3 inflammasome-dependent neuroinflammation in microglia. Cell Death Dis. 2021 Dec 14;12(12):1159.
332. Yang CC, Wu CH, Lin TC, et al. Inhibitory effect of PPARgamma on NLRP3 inflammasome activation. Theranostics. 2021;11(5):2424-2441.
333. Chen Y, Falck JR, Manthati VL, et al. 20-Iodo-14,15-epoxyeicosa-8(Z)-enoyl-3-azidophenylsulfonamide: photoaffinity labeling of a 14,15-epoxyeicosatrienoic acid receptor. Biochemistry. 2011 May 10;50(18):3840-8.
334. Yan Y, Jiang W, Spinetti T, et al. Omega-3 fatty acids prevent inflammation and metabolic disorder through inhibition of NLRP3 inflammasome activation. Immunity. 2013 Jun 27;38(6):1154-63.
335. Jung SH, Hwang BH, Shin S, et al. Spatiotemporal dynamics of macrophage heterogeneity and a potential function of Trem2(hi) macrophages in infarcted hearts. Nat Commun. 2022 Aug 6;13(1):4580.
336. Bystrom J, Wray JA, Sugden MC, et al. Endogenous epoxygenases are modulators of monocyte/macrophage activity. PLoS One. 2011;6(10):e26591.
337. Behmoaras J, Diaz AG, Venda L, et al. Macrophage epoxygenase determines a profibrotic transcriptome signature. J Immunol. 2015 May 15;194(10):4705-4716.
338. Li H, Bradbury JA, Edin ML, et al. sEH promotes macrophage phagocytosis and lung clearance of Streptococcus pneumoniae. J Clin Invest. 2021 Nov 15;131(22).
339. Jia C, Zhang J, Chen H, et al. Endothelial cell pyroptosis plays an important role in Kawasaki disease via HMGB1/RAGE/cathespin B signaling pathway and NLRP3 inflammasome activation. Cell Death Dis. 2019 Oct 14;10(10):778.
340. Ghiringhelli F, Apetoh L, Tesniere A, et al. Activation of the NLRP3 inflammasome in dendritic cells induces IL-1beta-dependent adaptive immunity against tumors. Nat Med. 2009 Oct;15(10):1170-8.
341. Fan R, Kim J, You M, et al. alpha-Linolenic acid-enriched butter attenuated high fat diet-induced insulin resistance and inflammation by promoting bioconversion of n-3 PUFA and subsequent oxylipin formation. J Nutr Biochem. 2020 Feb;76:108285.
342. Liu PY, Li YH, Chao TH, et al. Synergistic effect of cytochrome P450 epoxygenase CYP2J2*7 polymorphism with smoking on the onset of premature myocardial infarction. Atherosclerosis. 2007 Nov;195(1):199-206.
343. Tagetti A, Ericson U, Montagnana M, et al. Intakes of omega-3 polyunsaturated fatty acids and blood pressure change over time: Possible interaction with genes involved in 20-HETE and EETs metabolism. Prostaglandins Other Lipid Mediat. 2015 Jul;120:126-33.
344. Dick SA, Macklin JA, Nejat S, et al. Self-renewing resident cardiac macrophages limit adverse remodeling following myocardial infarction. Nat Immunol. 2019 Jan;20(1):29-39.

APPENDIX

Raw immunoblot replicate images for figures (red rectangle represents target bands):

(Figure 3.4)

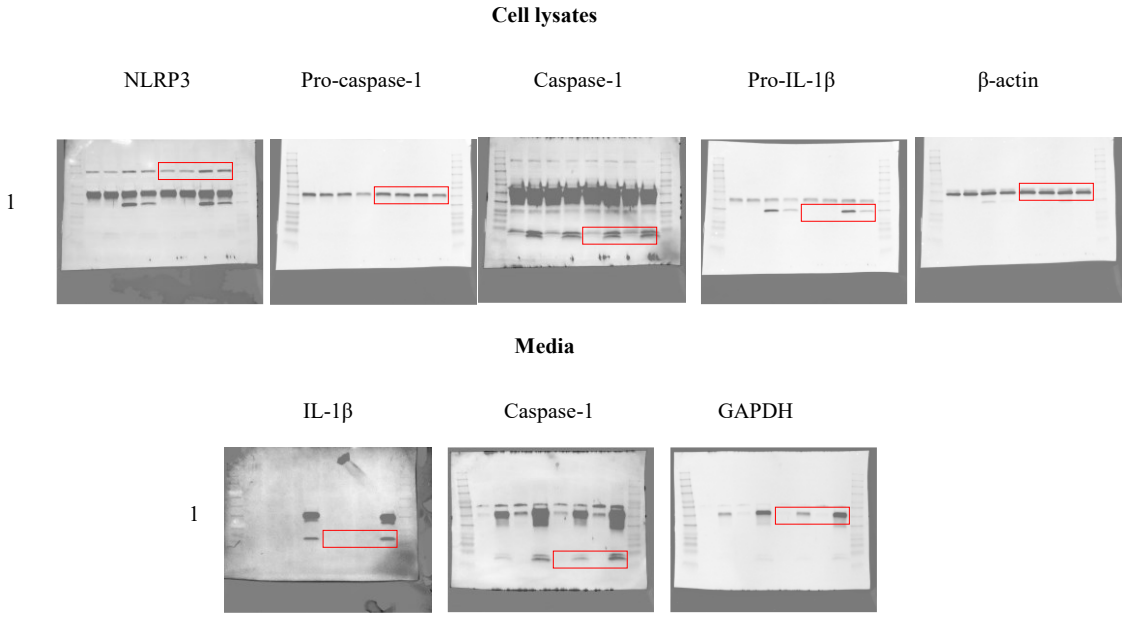

(Figure 3.5.1)

Cell lysates

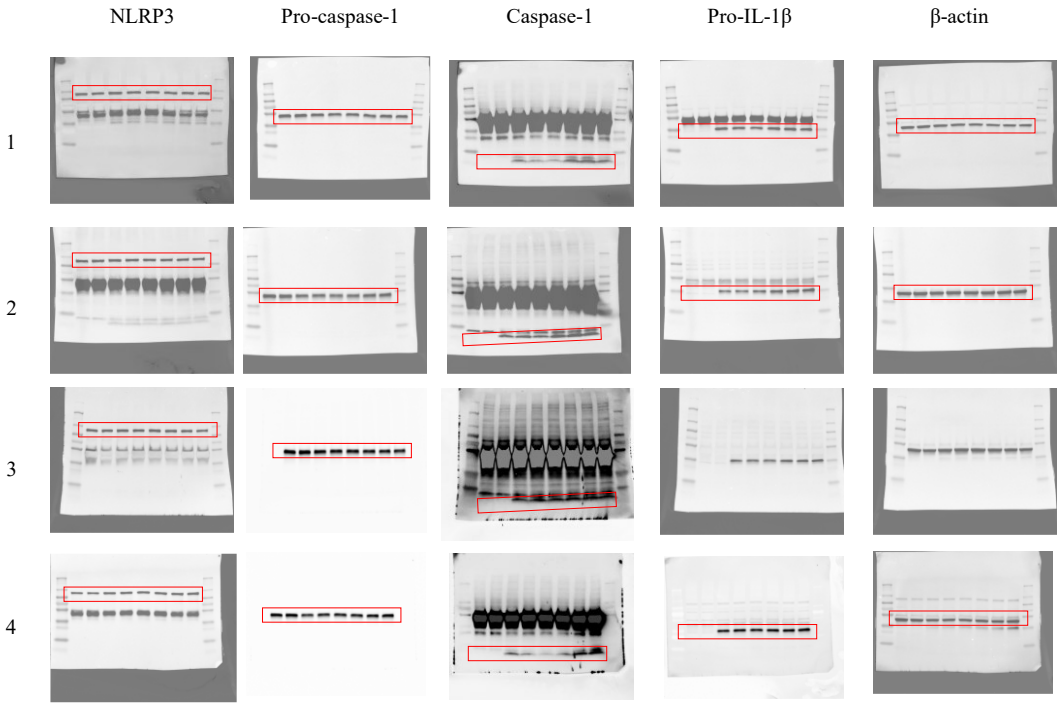

Media

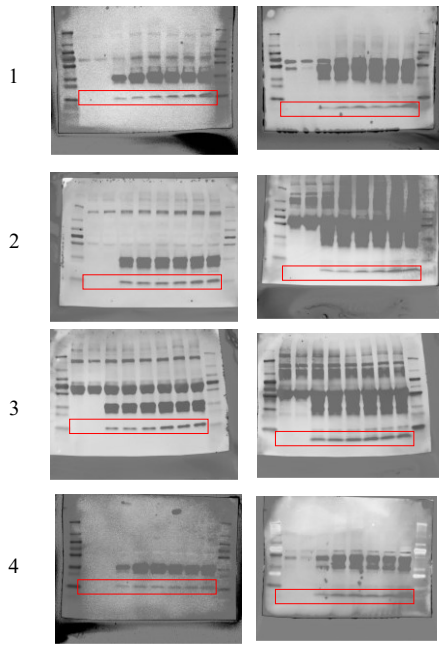

(Figure 3.5.3)

Cell debris

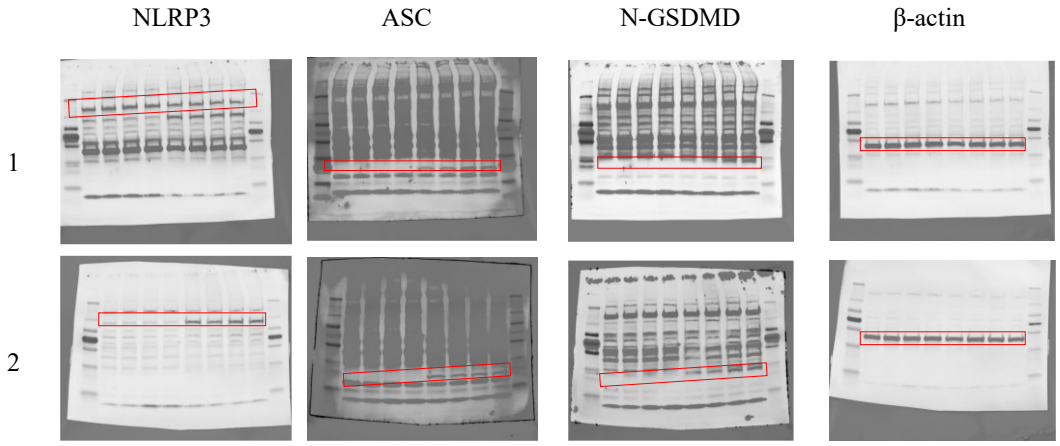

(Figure 3.5.4)

Cell lysates

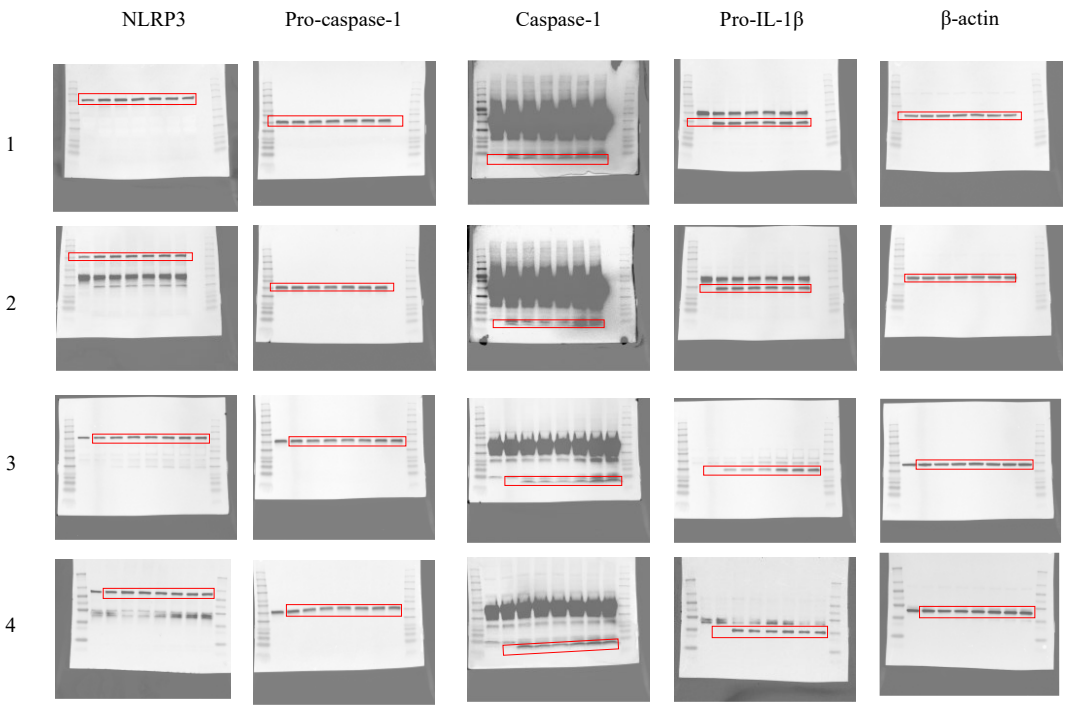

Media

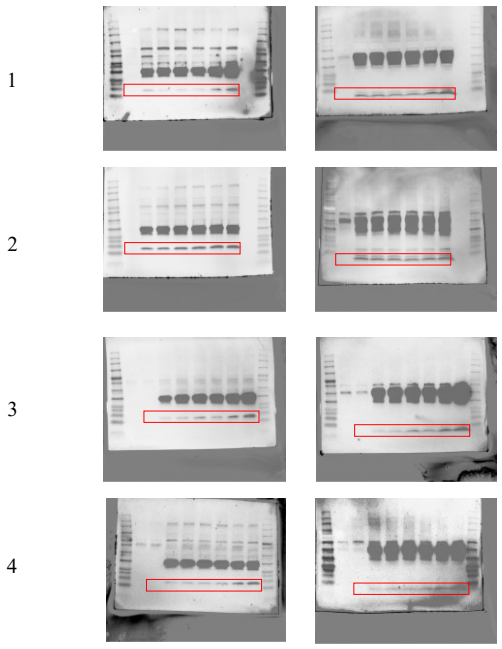

(Figure 3.6.1)

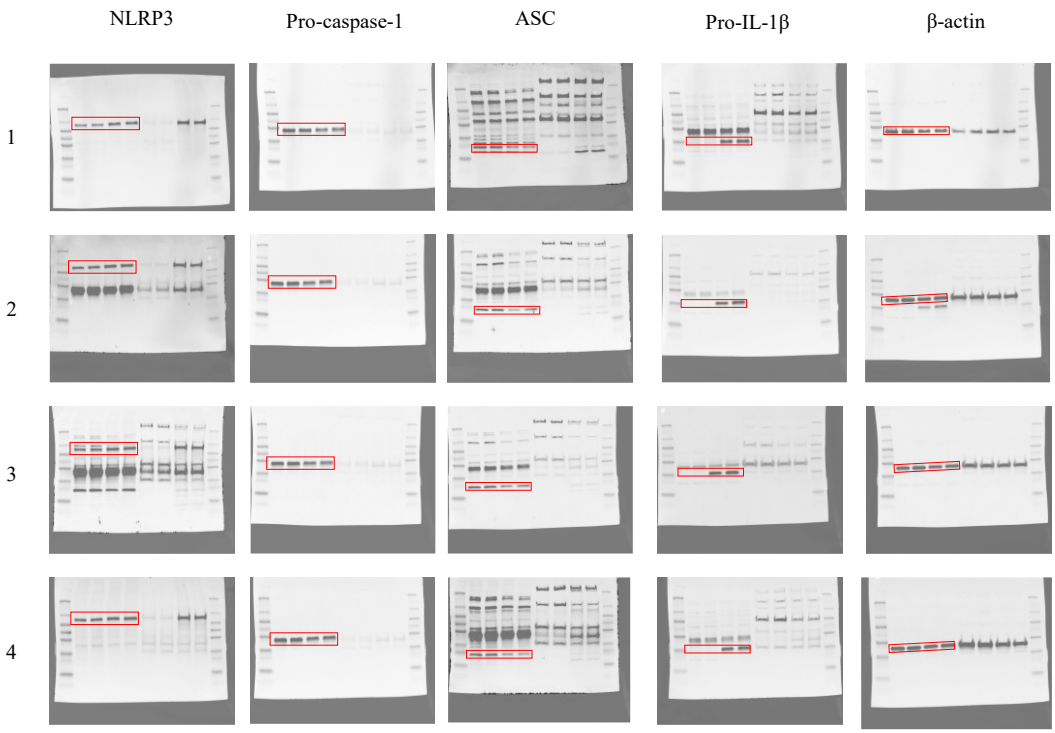

(Figure 3.9)

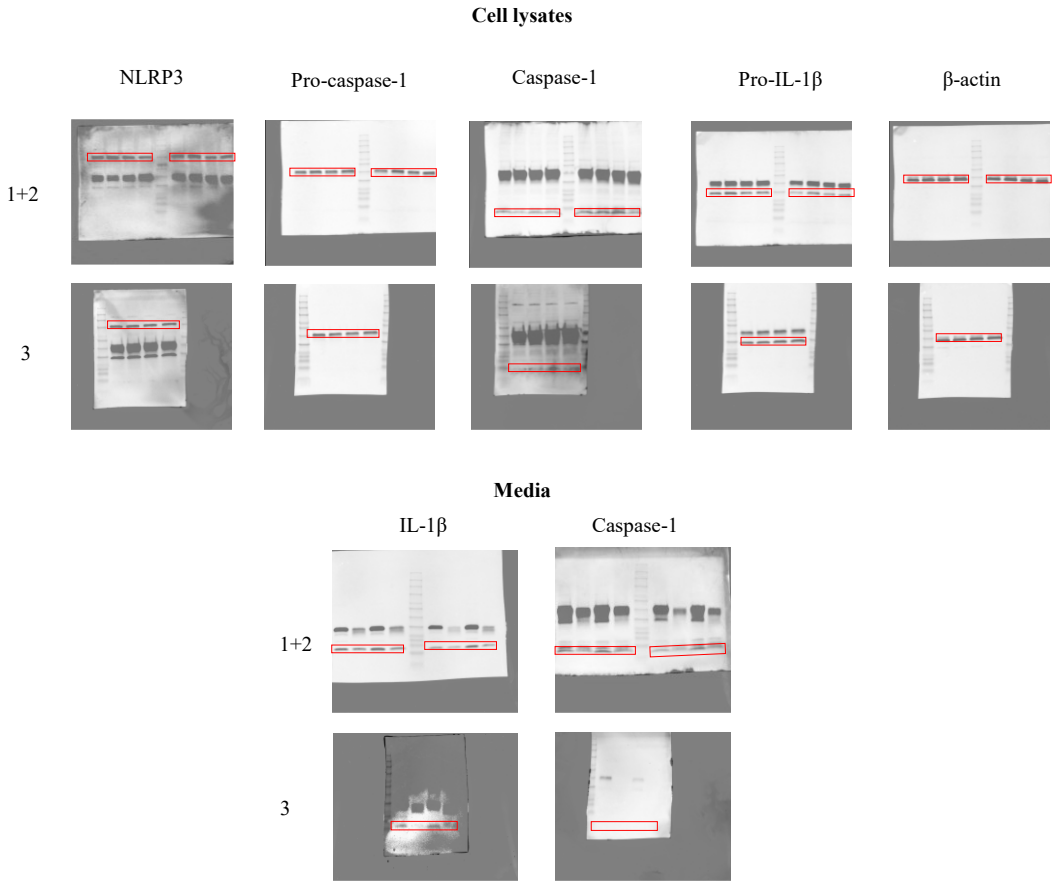
Cell lysates
NLRP3
Pro-caspase-1
Caspase-1
Pro-IL-1β
β-actin
1+2
3
Media
IL-1β
Caspase-1
1+2
3